

**Alma Mater Studiorum – Università di Bologna**

**DOTTORATO DI RICERCA IN**

**CHIMICA**

**Ciclo XXXI**

**Settore Concorsuale: 03/C2**

**Settore Scientifico Disciplinare: CHIM/04**

***Oxidative cleavage of glycols derived  
from unsaturated fatty acids***

**Presentata da:** Andrea Vassoi

**Coordinatore Dottorato**

**Prof. Aldo Roda**

**Supervisore**

**Prof. Fabrizio Cavani**

**Esame finale anno 2019**



*I would like to dedicate this Thesis to my mother,  
the one who allowed me to start my journey.*

*To my sweetheart, Irene.*





## ***Key words***

*Bio-industries*

*Bio-based economy*

*Bio-refinery*

*Heterogeneous catalyst*

*Green chemistry*

*Triglycerides*

*Oleic acid*

*Glycol*

*Azelaic acid*

*Pelargonic acid*

*Oxidative cleavage*

*Supported catalyst*

*Copper oxide*

*Co-precipitation catalysts*

*Copper ferros spinels*



# Abstract

The PhD project presented in this thesis was carried out in the framework of the European Flagship project First2Run and it was focused on the development and improvement of a new sustainable catalytic process for the valorization of unsaturated fatty acids.

Specifically, the present study was focused on the oxidative cleavage of oleic acid (or the corresponding triglyceride) into shorter mono- and di- carboxylic acids.

In particular, the oxidative scission was performed in order to produce azelaic acid and pelargonic acid starting from the vicinal glycol obtained by means of the dihydroxylation of the oleic acid contained in cardoon flower oil.

The oxidative scission process is currently carried out in industry by using ozone as the oxidant the use of which, however, implies hazardous process conditions. A more sustainable alternative oxidant proposed in the literature is oxygen, which requires specific catalysts.

Aim of this research was to investigate various heterogeneous catalysts for the oxidative cleavage of 9,10-dihydroxystearic acid by means of oxygen.

Moreover, the most promising catalysts were used for the investigation of the influence of several reaction parameters, such as temperature, time of reaction, stirring rate, oxidant gas pressure, amount of catalyst.

Finally, the stability and reusability of the best catalysts were conducted by means of leaching-tests and the development of a regeneration step.

Thanks to this research work, it was possible to discover a very promising heterogeneous catalytic system alternative to that one currently used in industry.



## **Table of Contents**

Acknowledgments	7
1. INTRODUCTION	9
1.1. General introduction	9
1.2. From Fossil-oil refinery to Bio-refinery	12
1.2.1. Biomass& Bio-refinery	13
1.2.2. Integrated Bio-refinery	17
1.2.3. The (possible) Future of bio-refineries	18
1.3. Oleochemical Bio-refinery	22
1.3.1. Potentials for Oleochemistry <sup>11</sup>	24
1.3.2. Value chain for Oleochemistry	25
1.3.3. Oleochemical substances	27
1.3.3.1. Triglycerides	30
1.3.3.2. Fatty acids	31
1.3.3.3. Glycerol	33
1.3.3.4. Carboxylic acids	34
2. First2run project	35
2.1. Objectives of the project	36
2.1.1. Agronomic objectives	36
2.1.2. Industrial objectives	36
2.1.3. Energetic objectives	36
2.1.4. Social objectives	37
2.1.5. Environmental objectives	37
2.2. The Work Packages	38
2.2.1. WP1 – Feedstock oil crops	38

2.2.2.	WP2 - Chemical and biochemical conversion of vegetable oils into bio-degradable esters	39
2.2.3.	WP3 - Scale-up	40
2.2.4.	WP4 – Bio-based products formulation and validation	40
2.2.5.	WP5 – By-products and co-products valorization and exploitation	41
2.2.6.	WP6 – Sustainability and Standardization	41
2.2.7.	WP7 – Dissemination and exploitation	41
2.3.	Project partners	42
2.3.1.	Novamont S.p.A.	42
2.3.2.	Matrica S.p.A.	43
2.3.3.	SoliQz BV	43
2.3.4.	SIP Ltd	43
2.3.5.	Roelmi HPC S.r.l.	43
2.3.6.	Alma Mater Studiorum – University di Bologna	43
2.4.	Exploitation	44
3.	Oxidative cleavage of vicinal glycols	46
3.1.	Sustainable Catalytic Oxidation	46
3.2.	Oxidative cleavage of Unsaturated Fatty Acids	48
3.2.1.	Literature	51
3.2.1.1.	Ozonolysis	53
3.2.1.2.	Oxidation with Strong Oxidants	55
3.2.1.3.	Catalytic Oxidation with Molecular Oxygen	56
3.2.2.	Patents	60
4.	Aim of the work	63
5.	Materials and Methods	64
5.1.	Preparation of the catalytic systems	64
5.1.1.	Metal-modified ferros spinels	64

5.1.1.1. Co-precipitation	64
5.1.1.2. Thermal treatments	66
5.1.2. Metal nanoparticles	68
5.1.3. Iron-substituted polyoxometalate	71
5.1.4. Copper based catalysts	72
5.1.4.1. Commercial Copper Oxide based materials	72
5.1.4.2. Copper Oxide over different supports	73
5.2. Characterization techniques	76
5.2.1. Structural properties	76
5.2.1.1. Specific surface area	76
5.2.1.2. X-ray diffraction of powder (powder-X.R.D.)	77
5.2.1.3. Attenuated total reflectance IR-spectroscopy (A.T.R.-IR)	79
5.2.1.4. Dynamic Light Scattering (D.L.S.)	80
5.2.2. Composition	81
5.2.2.1. X-ray fluorescence (X.R.F.)	81
5.2.2.2. Diffusive reflectance UV-spectroscopy (DR-UV)	82
5.2.2.3. Thermogravimetric/differential thermal analysis (T.G.A./D.T.A.)	83
5.2.3. Surface properties	84
5.2.3.1. Transmission electron microscopy/Scanning electron microscopy (T.E.M./S.E.M.) - Energy dispersive spectroscopy E.D.X.	84
5.2.4. Bulk and Redox proprieties	86
5.2.4.1. Temperature programmed reduction/oxidation (TPR <sub>1</sub> /O/R <sub>2</sub> )	86
5.3. Catalytic tests	88
5.3.1. Bench scale high-pressure reaction vessels	88
5.3.1.1. Multiple reactor system	88
5.3.1.2. Batch reactor	90
5.3.2. Derivatization of the products	92

5.3.3.	Gas Chromatography (GC) analysis	94
5.3.4.	Gas Chromatography – Mass Spectrometer (GC-MS) analysis	96
5.3.5.	Expression of the results	97
5.3.5.1.	Catalysts screening	97
5.3.5.2.	Further reactivity tests	97
6.	Results and Discussion	101
6.1.	Oxidative cleavage of glycols derived from unsaturated fatty acids	101
6.1.1.	Introduction	101
6.1.2.	Characterization of the starting material	104
6.2.	Catalysts screening	107
6.2.1.	Catalysts Characterization	107
6.2.1.1.	Mixed metal oxides with spinel structure	107
	The effect of thermal annealing on bulk characteristics	107
	Characterization of the M-modified ferros spinels	109
6.2.1.2.	Gold nanoparticles	111
6.2.1.3.	Iron-substituted polyoxometalate	114
6.2.2.	Screening results	115
6.2.3.	Conclusions about catalysts screening	120
6.3.	Copper oxide	122
6.3.1.	Effect of the support	122
6.3.2.	Catalyst characterization	124
6.3.3.	Catalytic tests with CuO/Al <sub>2</sub> O <sub>3</sub>	130
6.3.3.1.	On the effect of reaction time	130
6.3.3.2.	On the effect of reaction temperature	133
6.3.3.3.	On the effect of stirring rate	136
6.3.3.4.	On the effect of catalyst amount	138
6.3.3.5.	On the effect of oxidant gas pressure	139



6.3.3.6.	On the reusability of the catalyst	141
6.3.3.7.	Conclusions on Catalytic tests with CuO over alumina	147
6.3.4.	Copper oxide over different supports	148
6.3.4.1.	Characterization of catalysts	148
6.3.4.2.	Catalysts screening with multiple reactor system	158
6.3.4.3.	Conclusions about supported catalysts screening	160
6.3.5.	Catalyst tests with copper oxide supported over silica	161
6.3.5.1.	On the effect of reaction time	164
6.3.5.2.	On the effect of reaction temperature	167
6.3.5.3.	On the effect of stirring rate	170
6.3.5.4.	On the effect of catalyst amount	172
6.3.5.5.	On the effect of type of oxidant	174
6.3.5.6.	Conclusions on the catalytic test with CuO/SiO <sub>2</sub>	175
6.4.	Copper – ferrites	177
6.4.1.	Copper ferrites with different Cu/Fe ratio	177
6.4.1.1.	Synthesis	177
6.4.1.2.	Characterization	178
6.4.1.3.	Reactivity tests using Cu/Fe/O ferros spinels	185
6.4.2.	Cu/Fe/O (Cu/Fe = ¼) ferros spinel catalyst	188
6.4.2.1.	Effect on thermal annealing on catalytic performance	188
6.4.2.2.	On the effect of reaction time	190
6.4.2.3.	On the effect of reaction temperature	192
6.4.2.4.	On the effect of stirring rate	195
6.4.2.5.	On the effect of catalyst amount	196
6.4.2.6.	On the effect of oxidant pressure	197
6.4.2.7.	On the reusability of the catalyst	199

## *Table of Contents*

---

6.4.2.8. Conclusions on the reactivity tests with copper ferrite with Cu/Fe ratio =1/4	201
6.5. Leaching experiments	202
7. Conclusions	205
Appendix I - Nomenclature	207
Appendix II - Fatty acids	208
Saturated fat	208
Unsaturated fat	209
8. References	212

# Acknowledgments

This project has received funding from the Bio Based Industries Joint Undertaking under the *European Union's Horizon 2020* research and innovation programme under grant agreement No 669029.

---

First and foremost, I would like to express my sincere gratitude to my Professor Fabrizio Cavani for the great opportunity that he gave me; he consistently allowed this Thesis to be my own work, but he always helped me out whenever I was struggling.

Besides my advisor, my sincere thanks also goes to the two external referees, Prof. Antonio Proto and Prof. Jean-Marc Millet, for their review and very valuable comments.

I thank Dr. Olena Vozniuk, who took me as intern, and gave me the first access to the laboratory and research facilities.

I must express my very profound gratitude to my fellow lab mates for all the fun we have had in the last three years: it was a great sharing laboratory with all of you. Without their precious support it would not be possible to conduct this research.

Last but not the least, I would like to thank my parents, Rosa & Adri, Paolo & Silvia, my brother Alessio and sister Giulia for supporting me spiritually throughout my years of study and globally during my life. In particular, I am grateful to my girlfriend Irene with her unfailing support and continuous encouragement throughout writing this thesis.

This accomplishment would not have been possible without them, thank you all!



# 1. INTRODUCTION

## 1.1. General introduction

Over the course of the past decades, due to the rapid increase of world population, the fast explosion of energy demand and its consumption were registered.

The increasing public awareness of the environmental problems linked to the anthropogenic activities is motivating the governments to take more restrictive measure and binding laws in terms of emissions of pollutants so as to preserve both the environment and human safety for the present and future generations. Another worrying effect of the increase of human activities concerns plastic pollution: 8,3 billion metric tons (9,1 billion US tons) of plastic have been produced since plastic was introduced in the 1950s<sup>1</sup>. The amount of plastic produced in a year is roughly the same as the entire weight of humanity<sup>2</sup>. For this reason, on April 30<sup>th</sup> 2018, the UN Environment Programme (UNEP, or UN Environment) has tackled the single-use plastics and asked for a reduction of micro-plastics in cosmetics and toiletries. According to UNEP, raising awareness on the impact of plastic pollution has helped to build up a global momentum to tackle pollution<sup>3</sup>.

These reasons pushed the research of both chemical industries and academia to play a key role in the development of new and cleaner technologies, to plan and design new chemical products and processes able to reduce or eliminate the use and generation of hazardous substances and pollution; all this without forgetting the economic sustainability.

This concept, expressed in the term “*Green Chemistry*”, was initially developed as a response to the Pollution Prevention Act in 1990. This Act declared that the U.S. National policy should eliminate pollution by improving the design of chemical products and paying attention to the cost-effective changes of their production; moreover, this policy should enhance the use of renewable raw materials and recycling instead of the treatment and disposal of harmful wastes. As reported in the preface of “*Green Chemistry – Theory and practice*” written by Paul T. Anastas and John C. Warner:

“Green chemistry is not different from the traditional chemistry in as much as it embraces the same creativity, and innovation that has always been central to classical chemistry. Green chemistry merely pursues those same ideals and implementation of chemistry historically [...] in the most creative, innovative, and responsible manner possible”<sup>4</sup>.

During the latest years, green chemistry has concretely demonstrated how it could be essential the role of chemists in the modification of the existing technologies with the aim of protecting both human health and environment in an economically beneficial manner.

Noteworthy, the most relevant improvements are being made in several key research areas, for instance the development of new and more efficient catalysts, the progressive abandon of the more toxic and harmful reagents by replacing them with safer chemicals or the use of environmentally benign solvents. This trend also corresponds to an exponential increase of the studies on new platform molecules, no longer derived from fossil fuels, but based on renewable feedstocks (i.e. biomass or oilseeds).

In this way, current and future chemists are striving to work at molecular level to achieve the sustainability of the future processes and products, with an increased awareness for problems related to environmental impact<sup>5</sup>.

It is therefore evident that the chemical industry plays a key role in creating a sustainable and resource-efficient economy and society.

The guiding framework of Green Chemistry is summarized in the *Twelve Principles*, which were introduced for the first time in 1998 by P. Anastas and J. Warner.

They can be applied to all the aspects of chemical processes; moreover, the complete life-cycle of every product should be taken into account, from the raw materials used and their transformation efficiency until the toxicity and biodegradability of products and reagents employed.









The *twelve principles of Green Chemistry* are reported below<sup>6</sup>:



1. Waste Prevention: it is better to prevent waste than to treat or clean up waste after it has been created.



2. Atom Economy: synthetic methods should be designed to maximize the incorporation of all materials used in the process into the final product.

-  3. Less Hazardous Chemical Syntheses: wherever practicable, synthetic methods should be designed to use and generate substances that possess little or no toxicity to human health and the environment.
-  4. Designing Safer Chemicals: chemical products should be designed to affect their desired function while minimizing their toxicity.
-  5. Safer Solvents and Auxiliaries: the use of auxiliary substances (e.g., solvents, separation agents, etc.) should be made unnecessary wherever possible and innocuous when used.
-  6. Design for Energy Efficiency: energy requirements of chemical processes should be recognized for their environmental and economic impacts and should be minimized. If possible, synthetic methods should be conducted at ambient temperature and pressure.
-  7. Use of Renewable Feedstocks: a raw material or feedstock should be renewable rather than depleting whenever technically and economically practicable.
-  8. Reduce Derivatives: unnecessary derivatization (use of blocking groups, protection/de-protection, temporary modification of physical/chemical processes) should be minimized or avoided if possible, because such steps require additional reagents and can generate waste.
-  9. Catalysts (vs Stoichiometric): catalytic reagents (as selective as possible) are superior to stoichiometric reagents.
-  10. Design for Degradation: chemical products should be designed so that at the end of their function they break down into innocuous degradation products and do not persist in the environment.
-  11. Real-time analysis for Pollution Prevention: analytical methodologies need to be further developed to allow for real-time, in-process monitoring and control prior to the formation of hazardous substances.



12. Inherently Safer Chemistry for Accident Prevention: substances and the form of a substance used in a chemical process should be chosen to minimize the potential for chemical accidents, including releases, explosions, and fires.

After the publication of these milestones, there was a general international awareness that led to the creation of hundreds of programs and governmental initiatives on Green Chemistry around the world, with leading programs located in the U.S., United Kingdom, and also in Italy<sup>7</sup>.

All the concepts and guidelines laid down by the green chemistry were taken into account during the overall research activity conducted for this Thesis work.

## ***1.2. From Fossil-oil refinery to Bio-refinery***

The large use of petroleum, coal and natural gas in the XX century allowed our society to achieve a high level of economic wealth and technological development never reached before.

At the same time, this massive exploitation has led to environmental problems, such as pollution and greenhouse effect. Moreover, the uneven distribution of non-renewable resources on Earth caused dramatic social-political issues due to the need of supply of fossil raw materials.

In the last years these problems, together with the concern for the gradual depletion of the fossil resources, have stimulated the research and the use of alternative renewable feedstocks for the production of energy, fuel and chemicals. In the last period, this pulse has obtained a renewed force thanks to the influence of the public opinion on governments as demonstrated by the ratification of important agreements signed to stop the climate change<sup>8</sup>.

Nowadays, the processing of renewable raw materials is often associated to the term bio-refinery. Several definitions and explanations of this concept have been developed over the last few years, but the core of this expression could be generally resumed as follow: "Bio-refining is the sustainable processing of biomass into a spectrum of marketable products and energy"<sup>9</sup>.



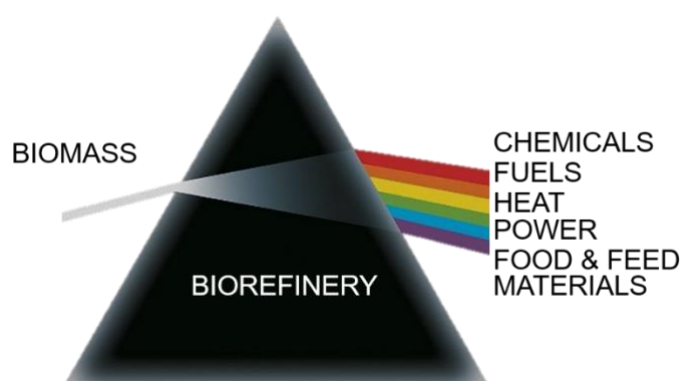


Figure 1.1. Schematic representation of the bio-refinery concept. (Adapted from ref. 9)

### 1.2.1. *Biomass& Bio-refinery*

Among the various types of renewable resources, today biomass appears to be an highly suitable alternative raw material for the chemical industry: it represents the main resource of renewable organic carbon on Earth, and for this reason, it is the principal candidate to replace fossil feedstocks in the production of fuels and chemicals, based on the model of bio-refinery<sup>10, 11, 12, 13, 14</sup>.

The term biomass indicates any organic and bio-organic material derived from a photosynthesis process, except fossil fuels; in other words, biomass represents every element that is part of the biosphere life cycle.

At present, the world production of biomasses is about 180'000 millions of tons per annum<sup>10,12</sup>, and they are classified in function of their production: the biomass of first generation derived by dedicated culture which, however, presents ethical issues caused by the competition in the use of resources used to satisfy food demand; the biomass of second generation, that is collected by agricultural, forestry, industrial and urban waste and by non-food crops grown on unusable soil for human supply.

The use of biomass as raw material is closely related to the bio-refinery concept. Despite the fact that the term bio-refinery has been increasingly used during the last years, its concept is not easy to define. However, it is commonly accepted that this new concept aims to develop a new production chain based on the direct transformation of renewable materials into fuels and/or value-added products. This new value-chain is

supposed to be able to replace the classical production model based on fossil resources in the traditional refinery (Figure 1.2)<sup>15</sup>.

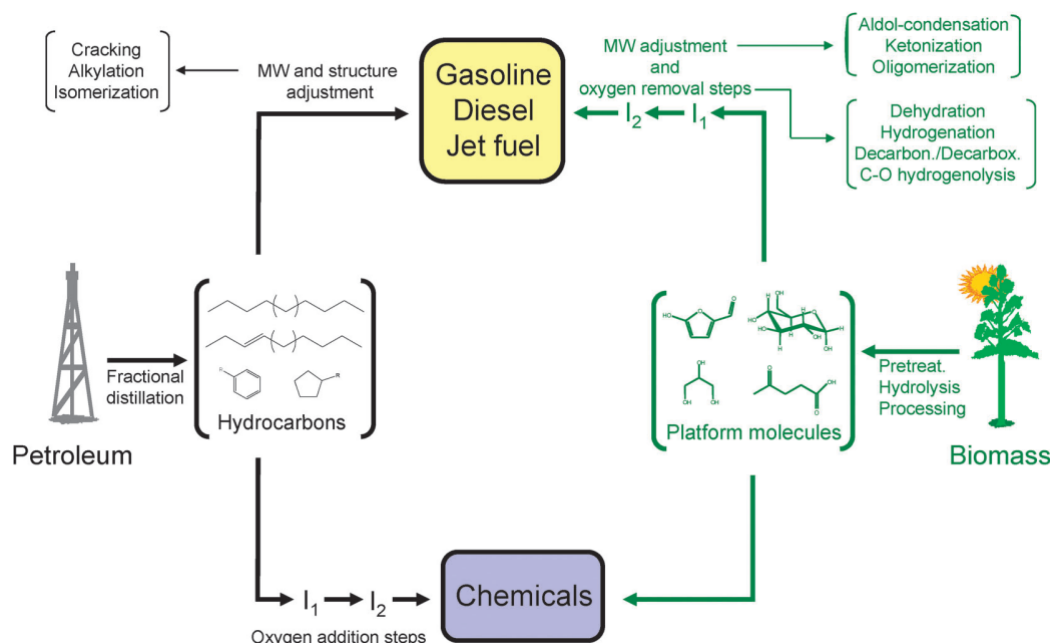


**Figure 1.2. Comparison between “traditional” and “bio” refinery<sup>12</sup>.**

As represented in Figure 1.2, in the bio-refinery model the theoretical production pathway is comparable to the traditional one starting from fossil resources: from raw materials to platform molecules, and subsequent transformation into fuels and chemicals.

Actually, the approach to the transformation into the desired product must be necessarily different compared to the traditional refinery because of the complex chemical structure and the variable composition of biomass, often due to the seasonal nature of the material. Therefore, the bio-refinery model is based on an alternative concept of production: chemical plants have to use different technologies, and especially have to be more flexible in production, in order to be suitable for the transformation of the different types of biomass<sup>11, 12, 16, 17</sup>.

As already mentioned before, each type of biomass substrate requires different procedures and technologies. As a consequence, many different models and concepts of bio-refinery can be foreseen, with a large variety of technologies that have to be necessarily developed. Moreover, the development of an industrial chemistry based on biomass requires an important phase of study and improvement of the technologies,

which includes engineering and chemical aspects, such as the design of operative conditions and catalysts: hence the need of important financial investments for the realization of new plants or the adjustment (revamping) of the old technologies to the alternative ones. A different choice could dramatically affect the fixed costs of the overall process and the profitability of the various specific routes.

Therefore, only a small number of the bio-refinery concepts designed for several biomass feedstock will be effectively implemented on commercial scale. Furthermore, sustainability is another critical element which will drive the effective implementation on a large scale of the different bio-refinery concepts<sup>18</sup>.

As remarked before, the commercial implementation of bio-routes of production appears today less promising than few years ago, for a number of reasons from economics to environmental sustainability<sup>19, 20</sup>. It is thus necessary to revise the existing concept of bio-refineries in order to identify priority paths and technologies.

Although the presence of these critical issues, the European commission has compiled two important documents outlying the potential and prospective of the European bio-refinery and the establishment of a fruitful Bio-economy: “The Joint European Biorefinery Vision for 2030” and “European Biorefinery Joint Strategic Research Roadmap”<sup>21</sup>.

“The European Biorefinery 2030 Vision” is a document created by the collaborative effort between European commission and Star-COLIBRI team involving five European Technology Platforms and five major European research organisations. This document provides the information and tools to enable policy makers to build a framework for the development of a sustainable “Knowledge-Based European Bio-economy”, with a network of bio-refineries playing an essential role.

As predicted by the document, a significant proportion of the overall European demand for chemicals, energy, materials and fibres will be fulfilled by 2030 using biomass as a feedstock for bio-refining technologies:

- 30% of overall chemical production will be bio-based. For high added-value chemicals and polymers (specialities and fine chemicals) the proportion will be

more than 50%, whilst less than 10% of bulk commodity chemicals will be derived from renewable feedstocks.

- 25% of Europe's transport energy needs will be supplied by biofuels, with advanced fuels – especially bio-based jet fuels – taking an increasing share.
- The European market for bio-based fibres and polymers such as viscose, carbon fibres, nano-cellulose derivatives and bioplastics will continue to grow rapidly. Traditional fibre products such as paper remain 100% bio-based.
- A new generation of bio-based materials and composites produced in bio-refineries allows the production of lightweight, better-performing components for industries including automotive and construction.
- 30% of Europe's heat and power generation will be from biomass.

The economic aspect is probably the most important factor that has limited the development of the bio-refinery model, especially if we make a comparison between the investments which are still made in traditional refineries.

The possible solution to overcome this economic gap is the model of bio-refinery that is being developed in recent time, which is differentiated from the traditional one by the amount of compounds annually produced and the relatively smaller scale. This new model will be further described in this Thesis, and it has allowed the bio-refinery to improve and become competitive.

## 1.2.2. *Integrated Bio-refinery*

As mentioned above, the use of natural and agricultural feedstock for the production of chemicals has grown rapidly in recent years and has led to the development of integrated bio-refinery concepts as the way to achieve the scale and economics needed to compete with current mineral and petrochemical routes<sup>22</sup>.

This concept is related to the integration of further conversion steps on the intermediates produced by the first transformation (see Figure 1.4), so moving towards sustainable optimisation (maximising profit and minimising waste).

Bio-refining is in its early days and is currently facing the same challenges that traditional refining solved many years ago. At the very beginning, oil refining aimed at the production of only a small series of products mainly used as fuels. Only afterwards refining began to produce other basic chemicals, such as hydrogen, olefins (ethane, propene, butenes and butadiene), methyl-*tert*-butyl ether (MTBE), aromatics (benzene, toluene and xylenes) and so on.

Analogously, in a bio-refinery the raw material undergoes a number of separations into valuable fractions that are then processed and transformed to produce fuels, and also chemical intermediates, including polymers or their monomers. In order to extract the highest possible value from bio-refining, it will be necessary to take advantage from the whole biomass as well as preserving the molecular complexity given by nature, rather than from just one or few of its fractions. As still often occurs, most of the technologies for the exploitation of the whole biomass (including lignin, its most recalcitrant fraction) still as to be developed or proven at an industrial scale. Thus it can be safely held that bio-refinery profitability can only increase in the next few years.

In the case of vegetable oil refining, the target products (i.e. acid oil, fatty acid distillates and similar) are typically about 5% of the total output. However, some by-products obtained from this type of refining have a higher value than the incoming crude oil and thus positively contribute to the economics of the refinery. By-products are generally indexed in value to the crude vegetable oil, which they may substitute when the difference in price is sufficient to overcome the extra costs needed to purify or process them further.

Another important aspect is that bio-economy must be integrated within the territory hosting the new production sites, that is, the bio-refineries, and with the local agricultural system.

### **1.2.3. *The (possible) Future of bio-refineries***

Recently, the concept of bio-refinery has become quite popular, but controversial at the same time.

Biorefinery concept is not driven by economy, at least in the traditional sense of possibility to produce at lower costs, but from an ensemble of factors, such as:

- geopolitics and security of supplies;
- preservation of rural developments and recently also employment in otherwise dismissing traditional refineries;
- lower impact on environment of mobility and reduced greenhouse gases (GHGs);
- sustainability.

These driving forces have been translated into a mix of actions such as legislation for fuel mix, subsidies, renewable targets, and carbon targets.

Only in few cases, such as the bioethanol for Brazil, the economic factor is relevant but cannot explain alone the fast expansion of the production.

There is, thus, the demand to reconsider the model of bio-refineries and analyze the new directions and scenario to evaluate possibilities and anticipate needs for research considering also how the socio-political drivers (SPDs) could determine the evolution in this sector.

Nowadays, a transitional economy is occurring (e.g. as during the transition from an economic cycle to another one). This transition is typically characterized in process industry by different pushing (for example new raw materials, technologies and processes) and pulling forces (new social demands, environmental forces, sustainability)<sup>23</sup>.

One of the key elements characterizing this transition is the emergence of new companies looking at the new technologies/processes as a mechanism to gain market

positions through innovation. This is well evident in the area of bio-refineries, with the fast explosion of new models and technologies/processes.

Because of these elements, there are converging ideas that the future of bio-refineries will be centred on four elements of evolution:

- From big size to smaller size plants in order to enhance the adaptation at regional level and minimize biomass transport, and lower capital investments with short-time amortization.
- More flexible production, for example, possibility to switch the production between chemicals and fuels, with the aim to better fit into the market request.
- Production of higher added value products but in an integrated, full biomass use.
- Value chain integration and symbiosis.

This new model is preferably indicated with the term bio-factory<sup>24</sup> rather than bio-refinery, which is strongly linked with oil refinery concept, that is, large scale production and relatively limited range of products.

The model of bio-factory remarks the aspect that chemical production is becoming the main target, with energy products (mainly higher-value additives rather than direct components for fuel blending) as side element.

This model focuses at integrating within current oil-centred refinery and chemical production, rather than substitute it, as hidden in many current models and discussion of bio-refinery and bio-based economy. Oil will be still abundant in the next half century, and a successful transition to a more sustainable economy is possible only when the barrier to change (e.g. the necessary economic investments, but also other elements which delay the introduction of new market products) is reduced. This requires that the new processes/technologies can be inserted readily within the current infrastructure (drop-in products and processes/technologies). The new bio-refinery, or bio-factory, has to aim to a better integration of these realities at regional level and to develop a production more suited to follow a fast evolving scenario, low capital investment, more efficient intensification of the processes and overall lower impact on environment.



The process design should allow a flexible switch between chemical and energy products, in order to adapt better to the fast-changing market opportunities. The new model is thus not only different in terms of targets, but also in size, plant design, and reference market. It is likely that old and new models will coexist, as well as a number of other bio-refinery concepts (indicated as integrated bio-refineries<sup>12, 25</sup>).

Basically, there are two interesting new models of advanced bio-refinery/bio-factory models, which are emerging as a new opportunity<sup>29, 24</sup>:

- bio-production of olefins and other base raw materials;
- development of flexible production of chemicals and fuels.

The first one is centred on the production of base raw materials for chemicals production. The second one focuses on intermediates and high added-value chemical products, including monomers for polymerization, but with a flexible production for a rapid switch to produce eventually fuel additives, depending on market opportunities. Two of the elements characterizing both models are the full use of the biomass and the process intensification (for efficient small-scale productions).

For example, a new model of bio-refineries is presented by Matrícia S.p.A.<sup>26</sup>, a 50/50 joint venture established in 2011 between Novamont S.p.A. and Versalis S.p.A. (Eni group). The plant located in Porto Torres (Sardinia, Italy) produces chemicals starting from an up-stream process of transformation of cardoon flower oil since 2014.

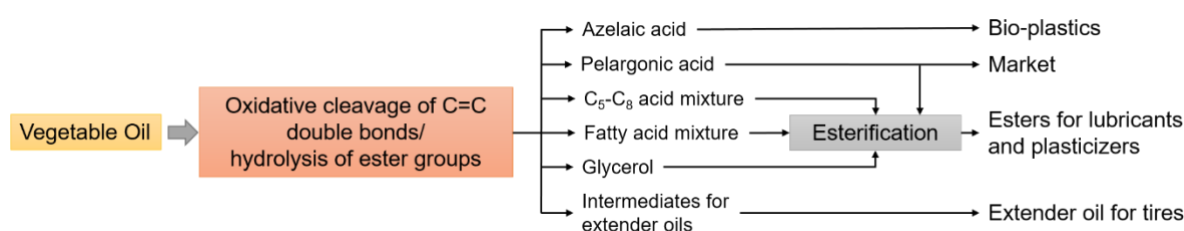


**Figure 1.3. Matrícia (jv Novamont S.p.A. and Versalis S.p.A.) biorefinery based on vegetable oils. (Adapted from ref. 26).**

This plant has a nominal production capacity of 35 ktons per years, with the driving element of the initiative being to decommission an old petrochemical site in order to develop a cleaner and with better market perspective production.

The social factor is thus driving the creation of the new bio-refinery model strongly linked to the territory and as a recovery strategy for local economy. In fact, the production is



integrated with the agricultural supply chain of local crops, developed on purpose by Novamont.

The same concept could be applied in other similar situations in Italy. This is certainly a positive element, which can also raise governmental or international funds to help the start of new projects. This example shows two key questions about the future of bio-refineries: (a) the mixing of different driving elements that do not allow a clear identification of the long-term sustainability and (b) when the proposed models have a general validity or depend strongly on local situations.

### 1.3. Oleochemical Bio-refinery

The increasing demand for renewable and sustainable chemicals and energy feedstocks has led to consider the use of fats and oils as one of the most prominent alternative to carbon fossil resources. The use of renewable fats and oils to obtain standard products and specialities is based on triglycerides and the corresponding derivatives. The use of these raw materials not only faces the challenge of an efficient use of available renewable sources, but also it ensures a continuous, economic and sustainable supply of fats and oils as the basis to provide high-quality products<sup>27, 28</sup>. The use of oils and fats for industrial applications has been growing steadily over recent years, at a faster rate than for human nutrition. Furthermore, vegetable oils experience a growing share of the industrial and chemicals sector as a sustainable source of hydrocarbon-rich feedstock, by means of the substitution of traditional mineral oil-based chemicals and products.

The comparison between the “general” and the oleochemical bio-refinery concepts is schematically shown in Figure 1.4.

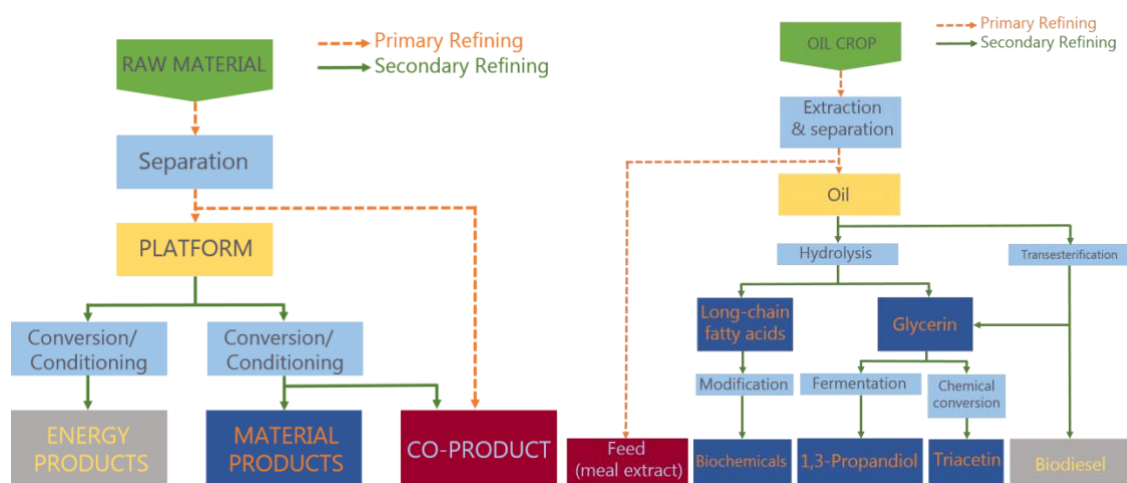


**Figure 1.4. Scheme of a “general” bio-refinery and oleochemical bio-refinery. (Adapted from ref. 29); green box = raw material, yellow box = intermediate, light-blue box = technologies, blue box = chemicals, red box = , grey box = energy products.**

The simplified scheme reported in the figure above indicates the main raw materials, the intermediates, and the final products (chemical and energy products), as well as the type of technologies exploited. Additionally, the scheme differentiates between the

primary and the secondary refining: most conventional biomass processing plants (e.g. oil crushing, starch extraction and cellulose pulp extraction) carry out the primary refining and, in some case, a first conversion step. For the maximization of the process sustainability, the intermediates produced by the primary refining are further converted into high-added value products in order to increase the profit and minimise the waste.

Although these are general schemes, they clearly evidence the complexity of the treatment necessary to convert the renewable raw materials into valuable products. This complexity is much higher compared to fossil oil, which is composed by several thousands of chemicals, but which can be lumped into a limited number of classes of chemicals.

The development of green chemistry and the environmental regulatory constrains also gives a new impetus to the field of oleochemistry, and its growth is not only confined to the academia's world, indeed several important industrial developments have been seen in the last decade. For instance in Europe, Novamont S.p.A.<sup>30</sup> is combining both oleochemistry and carbohydrate chemistry in the development of bio-degradable polymers for packaging materials, within a broad and highly integrated bio-refinery concept. In this value-chain, the vegetable feedstock is represented by unsaturated vegetable oils, which are subjected to a catalysed oxidative cleavage in the presence of hydrogen peroxide. The products formed during the process comprise mono- and di-functional acids, which can be considered basic (lipid-derived) platform chemicals.

Therefore, one of the most important issues that oleochemistry has to rapidly solve is the independence from classical fat and oil sources that could compete with the food and feed chain. Moreover, the most common oil seed plants used in this sector, such as plant oil, are usually locally restricted, and they are already facing peak consumptions with consequent environmental problem.

### **1.3.1. Potentials for Oleochemistry<sup>11</sup>**

Oleochemistry has been studied for a very long time and developed before mineral oil chemistry, but now it represents a niche industry sector due to the fossil oil price. It is considered the most versatile bio-based chemistry and a huge number of reactions concerning these compounds are very well known. Moreover, oils/fats contain a lot of oxygen inside their molecular structure, so they are potentially capable to replace mineral oil in a huge number of applications.

As oleochemistry is mostly based on renewable raw materials, it is clearly a sustainable chemistry, with the potential to represent a prototype for the integration of bio-economy concepts and industrial chemistry.

In this context, the access to the starting materials is the key point: industrial projects are to be favoured only in the case that raw material availability is satisfied without repeating the mistakes that EU made with bio-fuels. European farmers, thanks to the new agricultural policy, are looking for solutions in order to be able to face international markets. A new deal between industry and agriculture is necessary to cope the needs of fighting climate changes and, at the same time, finding local raw materials to feed local value chains. All without forgetting to preserve the rural development.

Oils and fats prices are now strictly related to mineral oil price, due to their use in bio-fuels. In case no mandatory rules are put in place, the future development of oleochemistry will depend, beside on oil/fat availability, on the delta price between mineral oil and natural oils/fats.

### 1.3.2. Value chain for Oleochemistry

Generally, oleochemistry has always used renewable fats and oils to obtain standard products and specialities. Nowadays, oilseed bio-refinery produces mainly food and feed ingredients, biodiesel and oleochemicals from oleaginous plant such as rape, sunflower and soybean. Conversely from other bio-refinery concepts, oleochemical bio-refineries are based on already well-established technologies, which potentially makes this solution a concrete alternative to fossil refinery.

Independently from the source and origin of the raw materials used, the value-chain based on oleochemistry comprises the processing steps shown in Figure 1.5.<sup>31</sup>

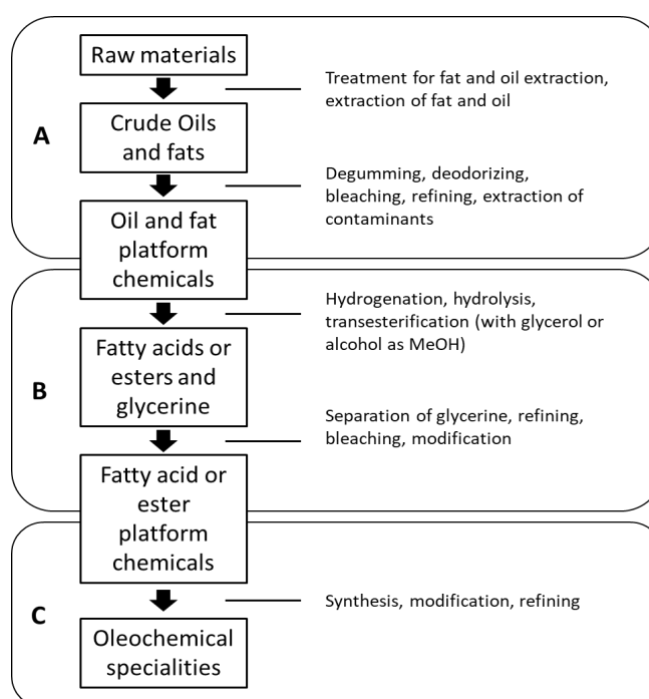


**Figure 1.5. Oleochemistry value chain: section (A) corresponds to the isolation of oils and fats from raw materials in order to obtain primary platform chemicals for further processing; section (B) sum up the conversion of oils and fats to fatty acids and their esters as secondary platform chemicals; section (C) shows the transformation to oleochemical specialities. (Adapted from ref. 11)**

The classical value chain of oleochemistry processes triglycerides as the main raw material, that is, esters of glycerine with fatty acids<sup>32, 33</sup>. These compounds are naturally occurring in oils and fats that are extracted from vegetable biomasses, or produced as a side-stream of animal processing (food and feed industries).

The first technologies used at the very beginning of the value-chain is the extraction of

crude oils/fats: the oil- and fat- containing biomass is pre-treated, then they are extracted by a variety of techniques (e.g. solvent extraction) that depend on the source and targeted quality of the final fat or oil. For example, in the case of fruit oils (e.g. olive and palm oil), the fruits are firstly sterilized, separated from residues, grinded or milled and then pressed in order to extract oil. On the other hand, the seeds (e.g. soybean or sunflower), are previously shucked, or flaked, before the real extraction by pressing.

Independently from the type of oil, the process of solvent extraction may be eventually used with the aim to enhance yields by further extracting the remaining oil quantities in the filter cake from pressing operation.

Considering that in the extracted crude there are a variety of substances together with the triglycerides of interest, further refining of the crude oil/fats is necessary to obtain raw materials with the proper grade of purity for further processing. The degumming is an example of refining step; it is used for the removal of phospholipids (residue of cell content). Other possible refining steps are bleaching by adsorption over particular clays, deodorizing by stripping or steam distillation, and winterization by waxes elimination<sup>34</sup>.

Once the proper raw materials are obtained, they are processed in order to obtain the main building blocks for oleochemistry, that are fatty acids or their short chain alcohol esters and glycerol. There are two core process typically used by oleochemical companies:

- **hydrogenation** in the presence of a catalyst (Ni, Pd) at approximately 160°C and 12 bar hydrogen pressure at least 20 minutes in order to get to the desired degree of saturation;
- **splitting process**, which is the hydrolysis of fats/oils yielding fatty acids and crude glycerol in water as products, carried out in a splitting column heated at 250°C by high pressure steam, resulting in a column pressure of about 50 bar, without any catalyst.

The resulting products might either be further processed or can be directly commercialized for a huge variety of applications.

### 1.3.3. *Oleochemical substances*

Nature is generous about the number of oil plants available for humankind and their importance as a source of food is substantial. Recently, their industrial application as raw materials for the preparation of bio-diesel, chemicals and polymers, as partial replacements of fossil feedstock have become equally relevant.

The total world production of the major oils and fats in 2014 was estimated at around 207 million metric tons<sup>35</sup>, and palm, soybean (production amounts to more than 42 million tons per year), sunflower (more than 13 million per year) and rapeseed (more than 24 million per year) oil account for two-thirds of the production<sup>36</sup>. Animal fats (tallow, lard, butter and fish) contribute approximately for the 12,5% of the total and specialty vegetable oils, such as corn, linseed, and castor oil constitute the 2,6%. The annual growth of the major vegetable oils production, over the period 2010-2014 was around 4,2%.

In 2011, it was estimated that about 70-75% of the global production of oils and fats would have been consumed in human nutrition, with the remainder going into animal feed, biofuels and oleochemicals<sup>37</sup>.

The worldwide leading source of natural oils is represented by palm oil. The global production of palm oil is more than 55 million tons to which about 6 million tons of palm kernel oil has to be added<sup>38</sup>.

In recent years, the increase of bio-fuels production demand has caused a tremendous increase in palm oil production that has driven to rainforest depletion. It is therefore expected that in a close future some mandatory requirements for the production of biofuels and chemicals through oleochemistry will be issued.

Moreover, biodiesel production and co-generation of energy in power stations have increased the non-food demand for vegetable oils. The large-scale use of renewable oils for fuel and energy is, however, generally non-economic in the absence of financial incentives. The ongoing debate on the use of food-grade vegetable oils in both industrial applications and fuel production has an impact on the assessment of the net environmental and sustainability benefits from the use of bio-based raw materials. The

focal point of these discussions has been bio-diesel and power generation since, compared to chemical and industrial uses, these have the potential to consume vast amount of natural resources.

The possibility of using oils/fats as starting materials for the production of several chemicals is related to their chemical composition (see Figure 1.6). They are all triglycerides in which the fatty acid structures vary as a function of the resource from which they are extracted. This fact is responsible of the final features of the oil and it determines the different applications as renewable feedstock. The number of double bonds, as well as their positions within the aliphatic chain of the fatty acids, and the presence of other reactive moieties such as hydroxyl groups, strongly affect the oil properties. Indeed, the pleasure and pain of the oils/fats chemistry is the heterogeneity and variability of the triglycerides which they are composed of, due to the statistical distribution of the fatty acids per triglyceride.

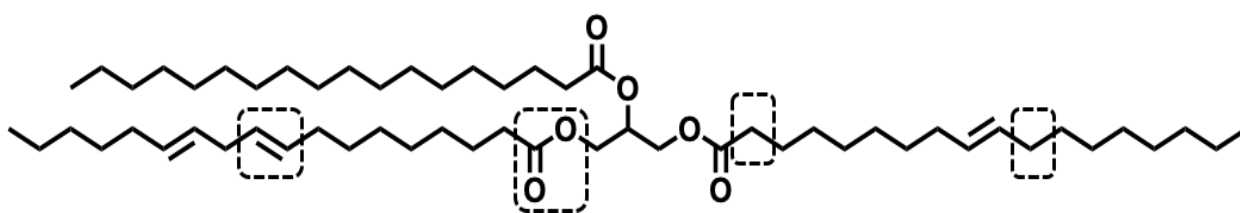


**Figure 1.6. Reactive sites present into a general unsaturated triglyceride.**

Figure 1.6 illustrates a generic structure of an unsaturated triglyceride highlighting the specific sites that can undergo reactions or chemical modifications.



It is possible to find a list of the common fatty acids present in various vegetable oil in the Appendix II - Fatty acids, while in Table 1-1 the typical composition of several vegetable oils are shown.

**Table 1-1. Common vegetable oils and their fatty acid composition. (Adapted from ref. 39)**

FATTY ACID		VEGETABLE OILS											
	CN/DB*	Palm	Soybean	Coconut	Sunflower	Rapeseed	Castor	Linseed	Corn	Olive	Sesame	Safflower	Cardoon
Caprylic ac.	8:0	-	-	6,2	-	-	-	-	-	-	-	-	-
Capric ac.	10:0	-	-	6,2	-	-	-	-	-	-	-	-	-
Lauric ac.	12:0	-	-	51,0	-	-	-	-	-	-	-	-	-
Myristic ac.	14:0	1,2	-	18,9	-	-	-	-	-	-	0,1	0,1	1,0
Palmitic ac.	16:0	41,8	14,0	8,6	6,5	4,0	1,5	5,0	10,0	6,0	8,2	6,8	10,9
Stearic ac.	18:0	3,4	4,0	1,9	2,0	2,0	0,5	4,0	4,0	4,0	3,6	2,3	3,3
Arachidic ac.	20:0	-	-	-	-	-	-	-	-	-	-	0,3	-
Oleic ac.	18:1	41,9	23,3	5,8	45,4	56,0	5,0	22,0	34,0	83,0	42,1	12,0	23,1
Linoleic ac.	18:2	11,0	52,2	1,3	46,0	26,0	4,0	17,0	48,0	7,0	43,4	7,0	61,2
$\alpha$ -linolenic ac.	18:3	-	5,6	-	0,1	10,0	0,5	52,0	-	-	-	0,4	1,0
Ricinoleic ac.	18:1	-	-	-	-	-	87,5	-	-	-	-	-	-

\*CN/DB = number of carbon atom in the chain vs. number of double bonds.

Note that the contents listed in Table 1-1 can be different as a consequence of the type of crop breeding or genetic modifications<sup>40</sup>. For example, the toxicity for the humans caused by the high content of erucic acid in rapeseed oil could be reduced to zero thanks to their genetic modification<sup>41</sup>. Furthermore, developments in crop breeding technology have a growing importance in industrial oleochemistry, opening up the possibility for new and improved oilseed varieties with more tailored compositions in an economically viable way.

Indeed, starting from the conventional oleochemicals derived from oilseed raw materials, such as fatty acids and its esters, it is possible to obtain very versatile compounds that are important for a huge number of industries and applications (Figure 1.7).

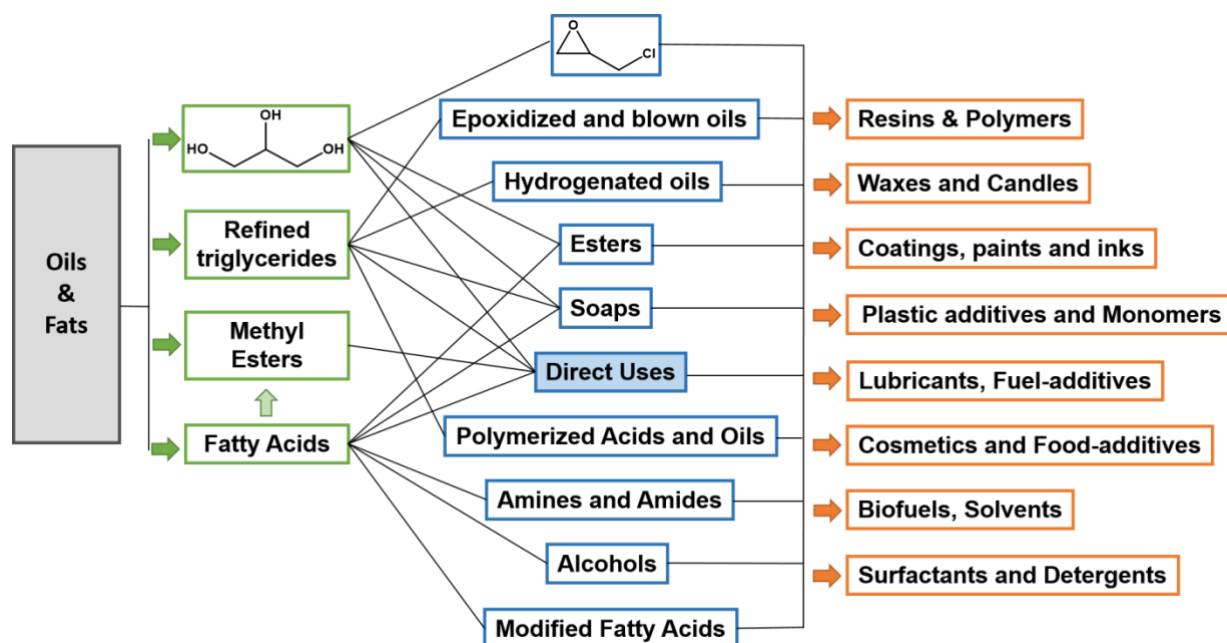


**Figure 1.7. Schematic overview of the different value-chains of oleochemical bio-refinery: starting from oils and fats it is possible to obtain several products usable in different industries. (Modified fatty acid includes conjugated, branched, hydroxylated and hydrogenated fatty acids).**

### 1.3.3.1. Triglycerides

Triacylglycerides can be used as starting point to obtain renewable-based materials by means of the direct modification of oils/fats, including epoxidation or polymerization to obtain designed properties. In addition, triglycerides can be used in food and nutrition, as well as pharmaceutical industries, biodegradable base fluids for lubricants or fracturing fluids, usage in coatings, or application as hydrophobic agents in a variety of products<sup>42 43 44 45 46</sup>.

Another approach is represented by the transesterifications of fats and oils with glycerol in order to obtain mono- or di- glycerides, widely used as emulsifier, or biofuels by using methanol. The last one represents also an interesting route to produce glycerol that could be directly used in health care applications or for the synthesis of a wide variety of derivatives by further processing<sup>47, 48</sup>

### 1.3.3.2. *Fatty acids*

Whereas food and food-production uses predominantly refined oils and fats, fatty acids are the major raw materials for the production of chemicals and industrial products (excluding direct fuel and bio-diesel uses).

World consumption and production of fatty acids in 2011 were estimated at 6,0 million tons (excluding production of fatty alcohols), expected to rise to 7,0 million tons by 2016<sup>49</sup>. In general, the growth of the production of fatty acids follows the Gross Domestic Product (GDP) growth in the region of consumption, reflecting the broad range of end-use industries.

As far as fatty acids are concerned, they could be directly used as a nutritional supplements, for candles, as bio-lubricants and in the production of textiles or polymers. From their modifications it is possible to obtain specialities, for example branched fatty acids, polymer fatty acids and estolides, which find application as lubricants, greases or coatings<sup>50, 51</sup>.

It also possible to modify the carboxylic group present in fatty acids for the production of biodegradable high-performance surfactants used in health care sectors. Such fatty acids can be used also for the formation of salts with selected metal cations (i.e. Zinc, Calcium and Magnesium) in order to make soaps, or stabilizers in polymer industries and as an acid scavenger.

A large number of industry sectors are affected by oleochemistry, that is, soaps and detergents, additives for plastic materials, resins and coatings, rubber and tires, paper, drilling, food and feed, lubricants, candles, personal care, cosmetics, pharmaceutical, medical devices, building textiles, leather, fibres, firefighting and agricultural products.

In addition, fatty acids are one of the major oleochemical compounds. In particular, unsaturated fatty acids (UFAs) represent the most versatile starting material for the production of several valuable compounds, such as carboxylic acids and their derivate.

Generally, UFAs obtained from vegetable oils have 16–18 carbon atoms and 1–3 double bonds, while oil and fats from animal lipids can also give unsaturated fatty acids with a longer carbon chain. The most common unsaturated fatty acids derived from vegetable oils and fats are summarized in Table 1-2.

Table 1-2. Conventional Unsaturated fatty acids (UFAs) derived from common oil and fats

Common name	Systematic name	Lipid number	Naturally Occurring in
<b>Palmitoleic ac.</b>	cis-9-hexadecenoic ac.	C16:1	Macadamia nuts <sup>52</sup>
<b>trans-Vaccenic ac.</b>	cis-11-octaecenoic ac.	C18:1	Dairy products such as milk, butter, and yogurt <sup>53</sup>
<b>Oleic ac.</b>	cis-9-octaecenoic ac.	C18:1	Olive oil, pecan oil <sup>54</sup> , canola oil <sup>55</sup> , cardoon oil <sup>56</sup> , sunflower oil <sup>57</sup>
<b>Petroselinic ac.</b>	cis-6-octaecenoic ac.	C18:1	Apiaceae, Araliaceae <sup>58</sup> , Griselinia <sup>59</sup> and in Garryaceae <sup>60</sup>
<b>Linoleic ac.</b>	9,12-octaecenoic ac.	C18:2	Peanut oil <sup>61</sup> , chicken fat <sup>62</sup> , olive oil <sup>63, 64</sup>
<b><math>\alpha</math>-linolenic ac.</b>	9,12,15-octaecenoic ac.	C18:3	Flaxseeds, chia seeds, walnuts <sup>65</sup>
<b><math>\gamma</math>-linolenic ac.</b>	6,9,12-octaecenoic ac.	C18:3	Borage oil, black currant oil, evening primrose oil <sup>66</sup> and safflower oil <sup>67</sup>

Among the UFAs listed in the table above, oleic acid (OA) is one of the most abundant unsaturated fatty acids present in nature. It has numerous applications such as food and ingredients for soaps and detergents in chemical industry.

### 1.3.3.3. Glycerol

Glycerol (1,2,3-trihydroxypropane) is one of the simplest polyol compound. It has three hydroxyl groups and its backbone is found in all lipids (triglycerides).

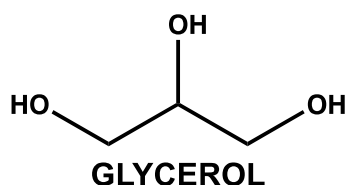


**Figure 1.8. Chemical structure of glycerol.**

It was accidentally discovered in 1779 by K.W. Scheele, the Swedish chemist, while he was heating a mixture of olive oil and litharge (lead monoxide). Scheele called glycerine the "sweet principle of fat"<sup>68</sup>.

Indeed, nowadays it is mainly generated as a co-product in processes which involve the production of fatty acids by hydrolysis of triglycerides or by trans-esterification with methanol, which leads to the production of fatty acid methyl esters (FAME), also called biodiesel<sup>69</sup>.

Every year about 20 Mt of fats and oils are processed by the chemical industries; this leads to a great abundance of glycerol on the market; about 1,54 Mt in 2015 and it is expected to rise to 2,5 Mt in 2020<sup>70</sup>.

These data underline the importance of glycerol as a low-priced molecule with a ready availability and strong potential to become a primary building block for the biorefinery.

For these reasons, glycerol chemical and physical properties have been widely investigated and several technologies have emerged as candidates for the conversion of glycerol into other useful chemicals<sup>71</sup>.

Indeed, glycerol is an extremely versatile compound, which can be used as a feedstock for the synthesis of a high number of molecules (e.g. ethers, esters, carboxylic acids, ethylene glycol, epichlorohydrin, syngas, oligomers, polymers, etc.)<sup>72</sup>.

#### **1.3.3.4. Carboxylic acids**

The use of biomass as source of chemicals alternative to fossil resources has developed rapidly in recent years and several valuable chemicals could be produced starting from these renewable starting materials. Although biomass is annually regenerated and abundant, it is extremely important to process it in the most efficient way. Thereby, it is necessary to consider which chemicals are reasonably and economically obtained from biomass.

Considering the high oxygen content of renewable feedstocks, it is reasonable to convert the biomass into valuable oxygen-containing fine chemicals, among which organic acids are one of the most important classes and widely used chemicals.

One of most important routes for the production of carboxylic acids starting from biomass is the oxidative cleavage of unsaturated fatty acids. The dicarboxylic acids arising from the oxidative cleavage of UFAs find application in a wide range of industrial areas such as plastics, cosmetics, coatings, or lubricants.

Moreover, carboxylic acids derived from vegetable oils can be used to prepare important polymers like polyesters and poly-amides<sup>73</sup>. For example, azelaic acid or brassylic acid with 9 or 13 carbon atoms respectively, are important bio-monomers for the synthesis of advanced Nylon-6,9 and Nylon-13,13<sup>74</sup>. These polymers can be synthesized from biomass feedstock other than petroleum route, which can reduce the dependence on fossil resources<sup>75, 76</sup>.

## 2. *FIRST2RUN PROJECT*

The FIRST2RUN project aims at demonstrating the technical, economic, environmental and social sustainability at industrial scale of a first-of-kind value chain where low input and underutilized oil crops (i.e. cardoon) grown in arid and/or marginal lands and not in competition with food or feed, are exploited for the extraction of vegetable oils to be further converted into bio-monomers (mainly pelargonic and azelaic acids) as building blocks for high added value bio-products, bio-lubricants, cosmetics, bioplastics and additives, through the integration of chemical and biotechnological processes.



**Figure 2.1. Representation of the concept behind the First2Run project: demonstrating the feasibility of the production of high-valued bio-products starting from renewable sources thanks to the development of innovative technologies.**

By- and co-products from the process will be valorised for energy, feed for animals and added value chemicals productions in order to increase the sustainability of the value chain. Standardization, certification and dissemination activities will support the project in relation to increased marketability as well as social acceptability of developed bio-based products in view of their penetration in the market.



## **2.1. Objectives of the project**

The main objectives of the project can be summarized as followed.

### **2.1.1. Agronomic objectives**

1. Large scale cultivation, thanks to strong involvement and support of local farmers, of cardoon crop (up to 3,5 kha) through the application of low input optimized technical/agronomic protocols;
2. Implementation of innovative mechanical oil extraction techniques.

### **2.1.2. Industrial objectives**

1. Application of sustainable, cost-effective and innovative catalytic and biocatalytic processes for the production of bio-building blocks from high oleic oils (such as azelaic acid, pelargonic acid and glycerol);
2. Demonstration of bio-based azelaic and pelargonic acid production using a continuous production plant up to 10 ktons/year each and demonstration of biodegradable esters batch production up to 20 ktons/year;
3. Integration of chemical and biotech processes for the developed bio-based materials, in the formulation of bio-products with improved technical performance, biodegradability and compostability, such as bio-lubricants for various applications, bio-plastics and bio-cosmetics;
4. Valorization of downstream process by- and co-products, such as panels for feed application as well as for compost.

### **2.1.3. Energetic objectives**

1. Increase of the energy independency of the bio-refinery from fossil energy sources through the implementation of industrial systems for the production of energy from lignocellulosic biomass.



2. Reduction of thermal and electric energy consumption of chemical processes up to 50% and 20%, respectively.

### **2.1.4. Social objectives**

1. Creation of new employment opportunities;
2. Social Life Cycle Assessment aimed at evaluating the social impact of the consequential scenario of having such a low impact cultivation and production of bio-based products, able to avoid resources depletion and pollution generation, with a contemporary increase of agro-industry workplaces and land protection;
3. Adoption of new models of collaboration that could make the relationships among the different key players of the whole value chain more effective. Promotion of communication activities that could not only foster an appropriate culture and level of knowledge, but also the implementation of stakeholder engagements awareness for social and market acceptability of sustainable chemical products from renewable resources.

### **2.1.5. Environmental objectives**

1. Development of products with sustainable environmental profiles with a reduction in GHG emission by the 35%;
2. Assessment of the environmental and economic impact (LCA, LCC) of the whole process allowing to identify the critical aspects along the demonstrated value chain and to define adequate strategies for improvement, demonstrating the sustainability of the validated bio-based products;
3. Definition of a strategy and measures to be undertaken towards the standardization and certification of the developed and validated bioprocesses and bio-products for the removal of market barriers, assuring safety, increasing the compatibility and promoting common technical understanding.

## 2.2. The Work Packages

The project has been broken down into 8 WORK PACKAGES (six technical and two non-technical WPs, see Figure 2.2), each targeting partial developments concurring as a whole to the achievement of the project targets previously described .

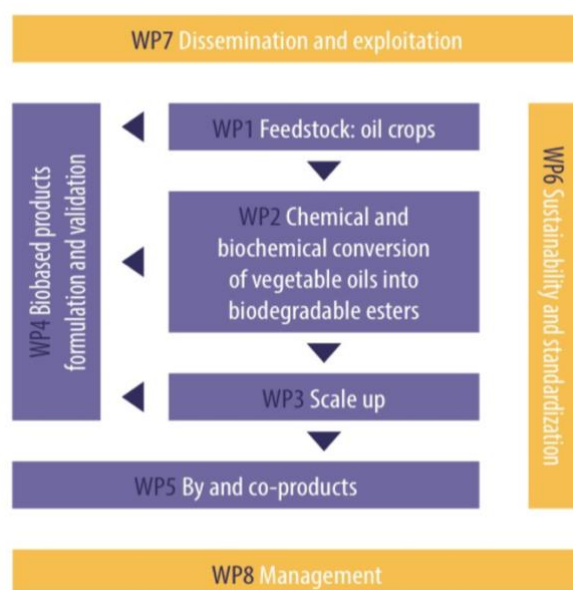


**Figure 2.2. First2Run's work packages.**

Every WP has specific objectives, described below.

### 2.2.1. WP1 – Feedstock oil crops

Main objective: to demonstrate at large scale the cultivation of cardoon crops in identified marginal lands through the implementation of sustainable agronomic protocols for fields cultivation management aimed at reducing inputs and increasing seed yield as well as to demonstrate the implementation of innovative oil extraction techniques towards the obtainment of sufficient oil quality, reduction of waste streams and improved energetic performances.

Specific objectives:

- large scale cultivation of cardoon crop in identified marginal lands;

- implementation of sustainable agronomic protocols for the reduction of required inputs for crops cultivation;
- optimization of harvesting, separation, storage and transportation of the collected fractions;
- implementation of innovative mechanical treatment for oil extraction with reduced energy requirement, decreased loss and improved oil yield.

## **2.2.2. WP2 - Chemical and biochemical conversion of vegetable oils into bio-degradable esters**

Main objective: to develop and optimize at pilot scale chemical processes for the vegetable oil conversion into the targeted building blocks (bio-based carboxylic acids), i.e., pelargonic and azelaic acid and the subsequent catalytic and bio-catalytic esterification processes in order to collect the key parameters for the subsequent scale-up at demonstration size in WP3.

Specific objectives:

- to develop optimized catalytic systems for the oxidative cleavage process with improved yields and increased sustainability;
- to set up the optimal conditions for the oxidative cleavage process at intermediate scale;
- to develop and optimize high performance and low cost separation and purification of the targeted bio-based monomers;
- to set up the optimal conditions for the improved catalytic and bio-catalytic esterification processes of the carboxylic acids with polyols.

The commitment of the University of Bologna in the FIRST2RUN project is precisely in this WP.

### **2.2.3. WP3 - Scale-up**

Main objective: to validate and demonstrate the feasibility of the processes developed in WP2 for the production of Building Blocks and Biodegradable oils from vegetable oils obtained in WP1.

Specific objectives:

- adaptation and improvement of the existing production facility, to be exploited in order to reach the targeted productivity of BBs and biodegradable oils;
- validation and demonstration of biobased BBs production from vegetable oils up to 20,000 tons/year;
- validation and demonstration of biodegradable oils (complex esters of pelargonic acid) production up to 10,000 tons/year;
- polymerization of di-carboxylic acids and further compounding for the bio-based materials production up to 50,000 tons/year.

### **2.2.4. WP4 – Bio-based products formulation and validation**

Main objective: to validate the bio-based materials produced in WP2 (biodegradable esters – Matríca) and WP3 (scale-up of WP2 - Novamont) within the formulation of bio-based products, i.e. bio-lubricants, bio-plastics and cosmetics.

Specific objectives:

- validation and demonstration of at least one bio-based polymer able to be used in the formulation of a biodegradable and compostable bio-plastic for mulch films and hand bags.
- validation and demonstration of at least one formulation of bio-lubricants for agriculture applications.
- validation and demonstration of at least one formulation of oil palm-free constituents for cosmetic applications.

### **2.2.5. WP5 – By-products and co-products valorization and exploitation**

Main objective: to implement industrial processes to recover and valorise by- and co-products, deriving from the different processes, both for energy recovery and for added value compounds production, in order to increase the environmental and economic sustainability of the whole value chain.

Specific objective is to implement a novel industrial system for the production of energy from lignocellulosic residues from cardoon crops as well as from by-products from oil extraction process (i.e., panel).

### **2.2.6. WP6 – Sustainability and Standardization**

Main objectives: to evaluate technical-economical, environmental and social sustainability of the demonstrated bio-based materials and products.

Second goal is to define strategies and measures to be undertaken towards the standardization of the developed and validated products.

### **2.2.7. WP7 – Dissemination and exploitation**

Main objective: to promote the project's results as widely as possible and the dissemination of the most relevant results to all relevant stakeholders.

Secondly, WP7 plan to ensure the proper handling of Intellectual Property within the Consortium.

## 2.3. Project partners

The F2R project brings together five partners from industry and one partner from academia, the University of Bologna (Figure 2.3). The partnership between various industrial and academic institutions is a clear indication of the multidisciplinary nature of the project.

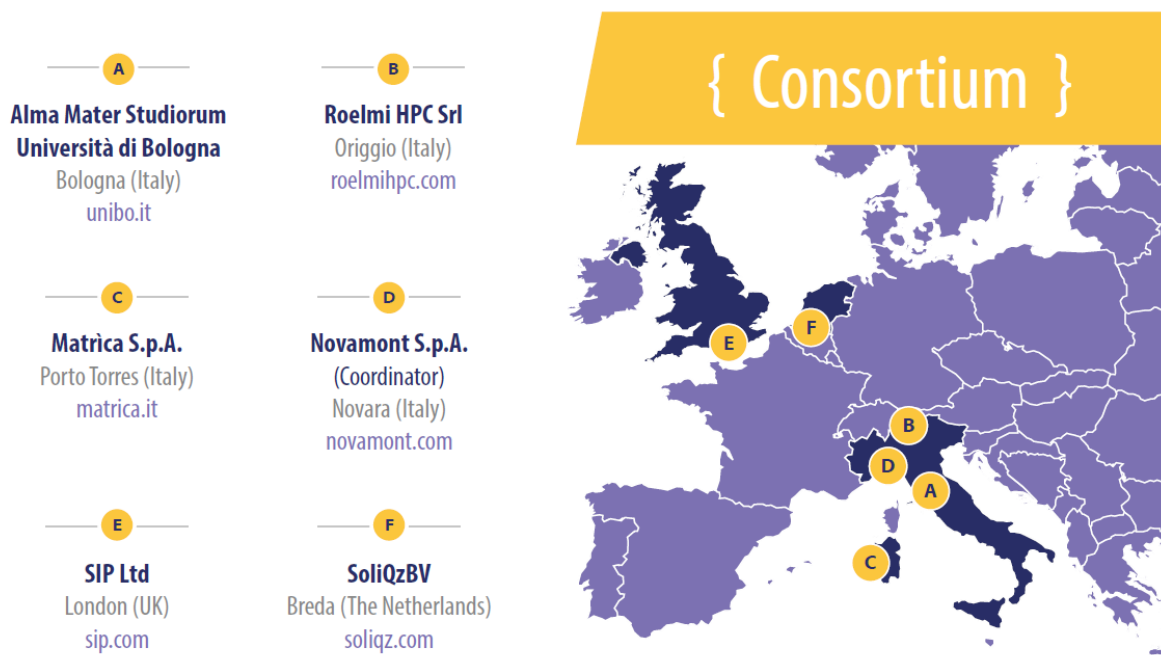


**Figure 2.3. First2Run's partners.**

Each partner plays a fundamental role in the work packages in which the project was structured, thanks to their experience. Here are summarized the different roles of each partner in the project.

### 2.3.1. Novamont S.p.A.

- Management and Coordination;
- Field management;
- Implementation of catalytic and bio-catalytic conversion of vegetable oil;
- Demonstration activities at the bio-refinery site;
- Bio-based materials formulation;

- Conversion of by- and co-products;
- Standardization and Dissemination & Exploitation.

### **2.3.2. *Matrica S.p.A.***

- Catalytic and bio-catalytic esterification of carboxylic acids with polyols;
- Demonstration of bio-based monomers production up to 20,000 tons/year;
- Demonstration of biodegradable esters of pelargonic acid production up to 10,000 tons/year;
- Recovery and valorisation of residual lignocellulosic biomass.

### **2.3.3. *SoliQz BV***

- Products recovery: feasibility tests, standards and industrial scale evaluation.

### **2.3.4. *SIP Ltd***

- Formulation and validation of bio-based lubricants.

### **2.3.5. *Roelmi HPC S.r.l.***

- Formulation and validation of bio-based cosmetics.

### **2.3.6. *Alma Mater Studiorum – University di Bologna***

- Development of catalyst for oxidative cleavage.

## **2.4.    *Exploitation***

In Figure 2.4 are shown the key exploitable routes identified for the complete valorisation of the cardoon crops.

The figure also shows which is the part of the value-chain where the commitment of the University of Bologna is focussed (see the red rectangle in the Figure 2.4).



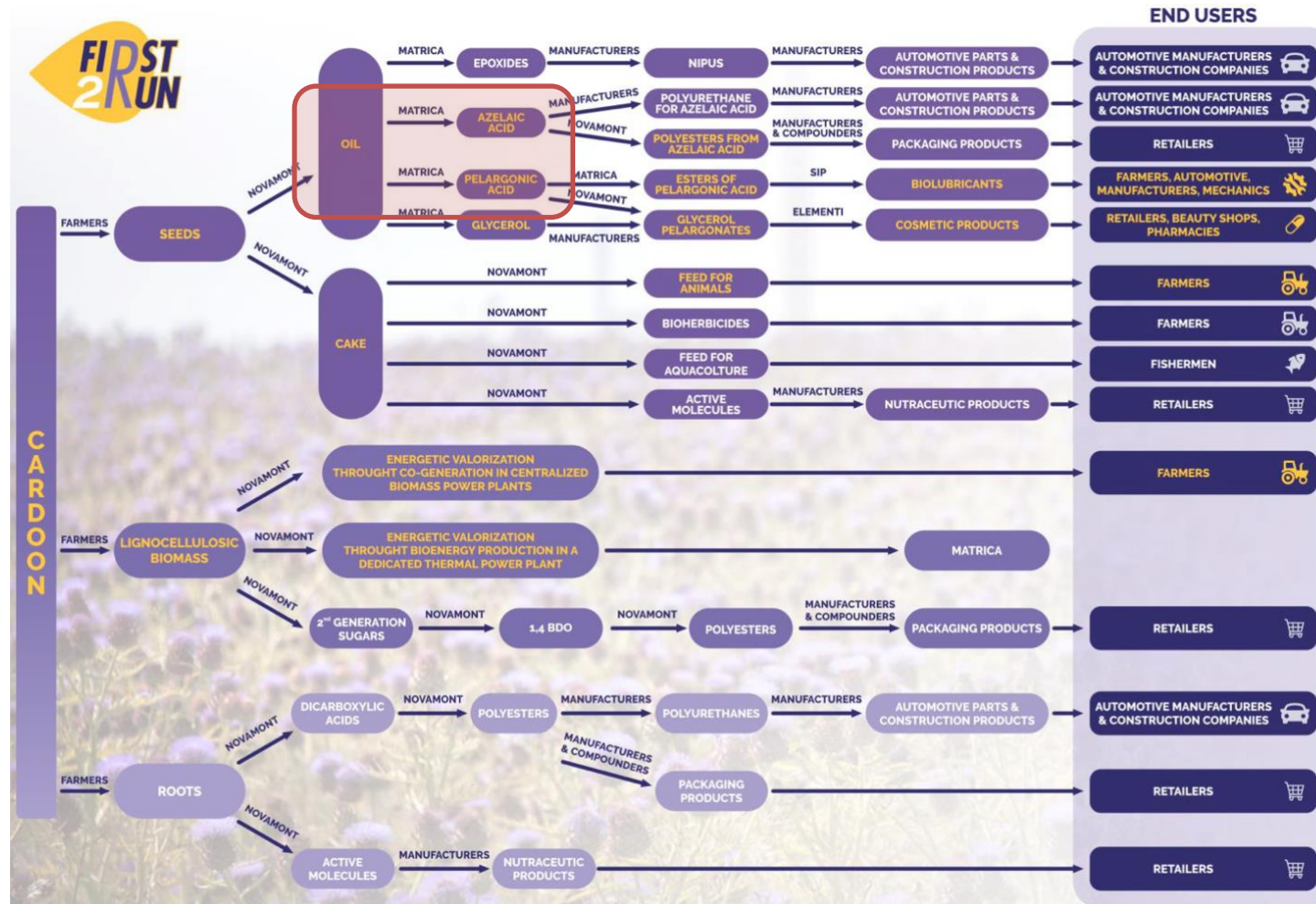


Figure 2.4. Exploitation routes identified in the perspective of the integrated biorefinery starting from Cardoon oil. (In the red rectangle is highlighted the role of the University of Bologna inside the project)

### **3. OXIDATIVE CLEAVAGE OF VICINAL GLYCOLS**

In this chapter the main topic of this research is described, highlighting the state of art concerning the oxidative scission of glycols.

Specifically, the whole landscape of the different catalytic oxidation processes nowadays used in industry will be briefly described. Then, the oxidative cleavage of vicinal glycols obtained from unsaturated fatty acids will be described in detail, emphasizing the different catalytic systems reported in literature.

#### **3.1. Sustainable Catalytic Oxidation**

Catalytic oxidations are extremely important from the scientific, technological and commercial point of view since they allow obtaining important intermediates for the chemical industry. More than half of the products synthesized using catalytic processes are obtained by selective oxidation, and nearly all the monomers used in the production of fibres and plastics are prepared in this way<sup>77</sup>.

These oxidation processes involve amounts of products in the order of million tons per year<sup>78</sup>, therefore their industrial sustainability, which comprises economic, social and environmental aspects, is of paramount importance. The industrial sustainability involves continuous innovation, improvement and use of clean and safer technologies to reduce pollution levels and consumption of resources. At the same time, it has to improve both safety and quality of work, while maintaining industrial competitiveness and responding to social and legislation questions<sup>77</sup>.

Catalysis is the key for the development of a more sustainable chemistry, since over 90% of chemical industrial processes make use of a catalyst. A catalyst is a substance that can help a reaction to proceed faster or under different conditions than otherwise possible, using less resources and generating less waste. In complex reactions with several possible products, it can favour a reaction pathway and improve selectivity<sup>77, 79</sup>. In this perspective, oxidation catalysis is playing a primary role for the development of sustainable processes by pursuing the following targets<sup>77</sup>:

- develop of “greener” catalytic systems and processes by means of new heterogeneous, rather than homogeneous, catalysts;
- replace traditional petrochemical building-blocks with alternative raw materials, such as renewable bio-platform molecules;
- replace stoichiometric metallic oxidants with greener ones such as hydrogen peroxide, air or oxygen, so reducing waste and solvents;
- apply the concept of process intensification, by using smaller reactors, often with continuous instead of discontinuous feed, and under less severe reaction conditions, thus decreasing energy consumption;
- maximize selectivity and yield to the desired product, reducing costs and environmental impacts associated to its separation and purification.

Oxidation of organic substrates can be carried out either in vapour or in liquid phase<sup>80</sup>. Liquid phase oxidations may involve problems with catalysts recovery, if homogeneous, because they could be difficult to separate; on the other hand, if heterogeneous, they could lose the active phase that may be released into the reaction mixture. For these reasons, a multiphase system that might allow avoiding difficulties in catalyst separation and recycle, while maintaining the advantages of homogeneous over heterogeneous catalysis (typically higher specific activity related to metal content, higher selectivity, possibility of fine tuning and better understanding at a molecular level) is a subject of great relevance for a more sustainable industrial chemistry. Despite this, liquid phase oxidations are more selective than vapour-phase ones and are sometimes used in large-scale productions when products can be easily separated from the reaction medium (e.g., in terephthalic acid production), or they are thermally unstable (such as hydroperoxides), or very reactive at high temperature (such as epoxides, aldehydes, ketones). Moreover, the liquid phase has a higher density compared to the liquid phase, which may imply both an improved productivity, and an easier control of the reaction with lower possibility of thermal runaways<sup>80</sup>.

The cheapest and more easily available oxidant is air, since all the others, for example,  $\text{HNO}_3$ ,  $\text{H}_2\text{SO}_4$ ,  $\text{Cl}_2$ ,  $\text{MnO}_2$ ,  $\text{CrO}_3$ ,  $\text{KMnO}_4$ , as well as  $\text{H}_2\text{O}_2$  and the organic hydroperoxides, have to be produced using oxygen or electric current. Moreover, often

their use co-produces molecules that have to be separated from the desired product in the downstream effluents. Moreover, the use of oxygen instead of air allows having the same partial pressure with a much lower total pressure, decreasing the amount of polluting emissions released<sup>35</sup>. On the other hand, oxidation with molecular oxygen usually needs much more complex catalysts and process development to reach the high selectivity shown by those processes where, for instance,  $\text{Cl}_2$  or  $\text{HNO}_3$  are used<sup>81</sup>.

Considering the several problems associated to the development of more sustainable industrial processes, someone could argue that it makes no sense to replace old and well-known technologies, carried out in plants that are now completely depreciated, and reactions that have been fully optimized in terms of resource utilization, energy consumption and emissions abatement. Nevertheless, a more rational use of raw materials, with environmentally friendlier oxidants, would not only meet the sustainability criteria, but also bring economic advantages<sup>82</sup>.

## **3.2.      *Oxidative cleavage of Unsaturated Fatty Acids***

The first step to take into account for chemicals production starting from biomass are the structural properties and economics of the overall process.

Oxygen-containing products are of great significance in our daily life. Organic acids and their derivatives, such as esters and anhydrides, are value-added fine chemicals. They are widely employed as solvents, cosmetics, polymer monomers and food additives.

Presently, organic acids are mainly produced from fossil resources, but the hydrocarbons constituting these raw materials are oxygen-deficient. Thus, the production of organic acids from fossil feedstocks requires the destruction of the relatively inert C-H or C-C bonds of the hydrocarbons and the formation of C-O bonds via insertion of oxygen atoms.

As remarked in chap. 1.3.3.4, biomass is oxygen-enriched with abundant C-O bonds. Retaining oxygen atoms to produce organic acids is economically feasible. Moreover, the C-C or C-H bonds of biomass are activated by oxygen atoms and are more susceptible to oxidation than hydrocarbons.

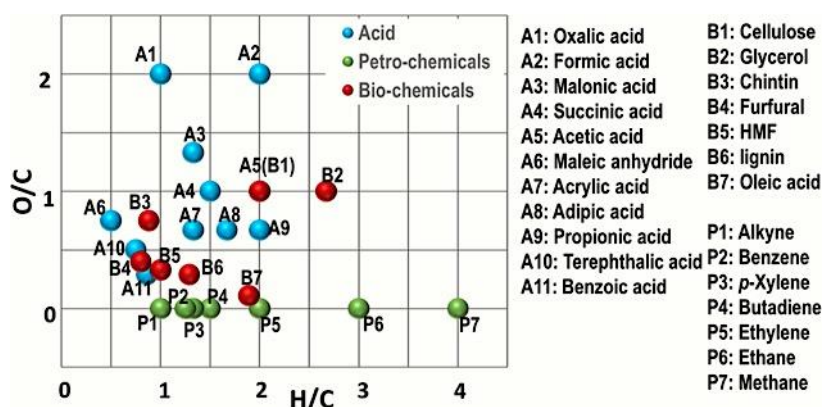


Figure 3.1. O/C and H/C ratio of acids, biomass resource and fossil resource<sup>83</sup>.

Figure 3.1 shows the O/C and H/C ratio of the acids, biomass resources, and fossil resources. The O/C and H/C ratio of acids is more similar to that of biomass resources. Thus, the direct conversion of biomass to the valuable organic acids is a very promising avenue and may be competitive to the present petroleum routes<sup>83</sup>.

Recently, many achievements have been obtained in the oxidative cleavage of biomass-derived building blocks both in the academia and industrial research. This process is conveniently exploitable for breaking the C-C bond of biomass in order to produce small molecules and introduce acid functionality at the same time.

Between the different type of biomass, oils and fats represent one of the most promising alternative for the production of organic acids available for the market, as reported in chapter 1.3.3.2.

UFAs could be depicted as one of the most promising renewable feedstock for the reliable production of valuable bio-building blocks, such as mono- and di-carboxylic acids.

Among the UFAs, oleic acid is certainly one the most abundant in nature. This acid is currently used in numerous industrial applications such as food and ingredients for soaps and detergents. The oxidation network of OA comprises three main transformations involving the double bond (Figure 3.2): epoxidation, dihydroxylation and the direct C=C double bond cleavage.

These pathways were intensively investigated using several alternative catalysts and the corresponding mono (pelargonic acid) or dicarboxylic acid (azelaic acid) can be



generated from the direct cleavage process, as well as the tandem multistep method with the epoxide or the 1,2-diol as intermediates<sup>84, 85, 86</sup>.

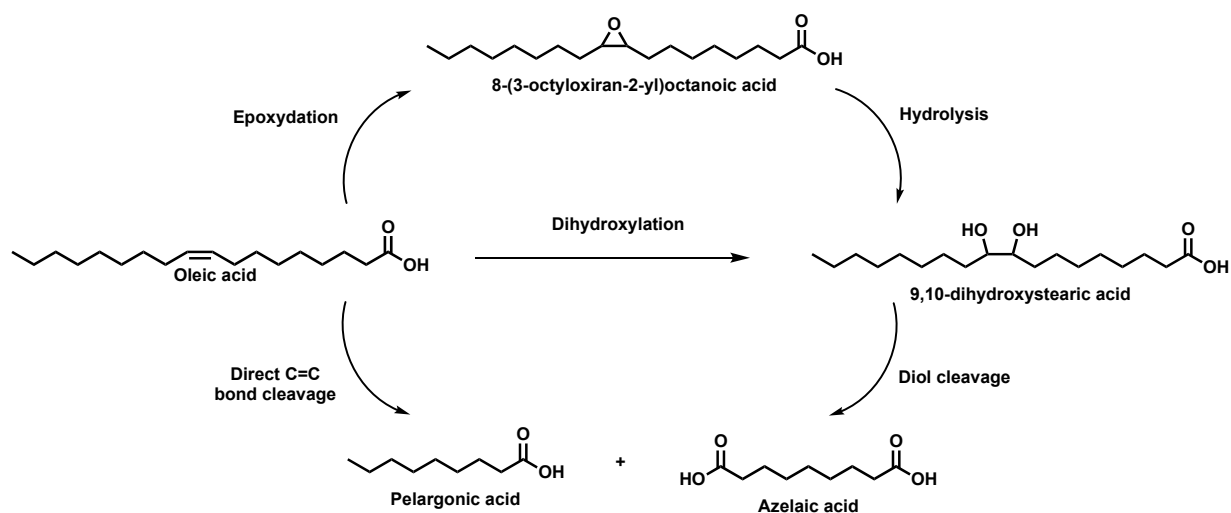


**Figure 3.2. Different pathways for the oxidative cleavage of oleic acid for the production of carboxylic acids.**

### 3.2.1. Literature

In this section, the advances in the oxidative cleavage of unsaturated fatty acids to carboxylic acids, especially for the transformation of oleic acid to pelargonic and azelaic acids, are described. Table 3-1 compiles the most relevant catalytic systems developed during the past decades.

**Table 3-1. Different catalytic systems and the relative oxidants for the oxidative cleavage of UFAs into carboxylic acids; (RT = room temperature, A: pelargonic acid, AA: azelaic acid, NL: nonanal, OA: oleic acid, MO: methyl oleate, MA: methyl azelate, MB: methyl brassylate, and MEA: methyl azelate. SAA and SPA mean the selectivity of AA and PA, respectively).**

Substrate	Catalytic System/Oxidant	Reaction conditions	Yield	Reference
Oleic ac.	Oxone/periodate in MeCN:H <sub>2</sub> O	reflux, 6 h	PA: 99%	87
Oleic ac.	RuCl <sub>3</sub> /NaIO <sub>4</sub> in cosolvents	2 h, RT	AA: 73% PA: 65%	88
Oleic ac.	RuCl <sub>3</sub> /NaIO <sub>4</sub>	0.75 h, RT, ultrasonic radiation	AA: 81%	89
Oleic ac.	RuCl <sub>3</sub> /NaIO <sub>4</sub>	8 h, RT, ultrasonic radiation, organic solvent- free	AA: 62%	90
Oleic ac.	[MoO(O <sub>2</sub> )-2,6-dipicolinate)](H <sub>2</sub> O)/H <sub>2</sub> O <sub>2</sub>	5 h, 90 °C	AA: 82%	91
Oleic ac.	[Fe(OTf) <sub>2</sub> (6-Me-PyTACN)]/NaIO <sub>4</sub>	H <sub>2</sub> SO <sub>4</sub> , 48 h, RT	PA: 85%	92
Oleic ac.	H <sub>6</sub> CoW <sub>12</sub> O <sub>40</sub> /H <sub>2</sub> O <sub>2</sub> -O <sub>2</sub>	4.5 h, 70 °C	AA: 52.5%	93
Oleic ac.	[Ru(2,6-dipicolinate) <sub>2</sub> ]/H <sub>2</sub> O <sub>2</sub>	24 h, 80 °C	PA: 59%	94
Oleic ac.	H <sub>2</sub> WO <sub>4</sub> and Co(acac) <sub>3</sub> /H <sub>2</sub> O <sub>2</sub> and NHPI in O <sub>2</sub>	5 h, 70–75 °C	AA: 15% PA: 15%	95
Oleic ac.	PCWP/H <sub>2</sub> O <sub>2</sub>	5 h, 90 °C organic solvent-free	AA: 57%	96
Oleic ac.	PCWP/H <sub>2</sub> O <sub>2</sub>	4 h, 80 °C	AA: 86% PA: 82%	97
Oleic ac.	Peroxo-tungsten complex with Aliquat 336 as PTA/ H <sub>2</sub> O <sub>2</sub>	5 h, 80 °C	AA: 79% PA: 82%	98

Oleic ac.	PCWP/H <sub>2</sub> O <sub>2</sub>	5 h, 85 °C, organic solvent-free	AA: 81% PA: 86%	99
Oleic ac.	Tungsten oxide supported on silica/H <sub>2</sub> O <sub>2</sub>	1 h, 130 °C	AA: 25% PA: 28%	100
Oleic ac.	Tungsten oxide/H <sub>2</sub> O <sub>2</sub>	1 h, 130 °C	AA: 16% PA: 17%	100
Oleic ac.	CTAB-molybdenum oxide/H <sub>2</sub> O <sub>2</sub>	3.5 h, 85 °C	AA: 83% PA: 68%	101
Oleic ac.	Chromium supported on MCM-41/O <sub>2</sub>	8 h, 80 °C in scCO <sub>2</sub>	AA: 31% PA: 30%	102
Oleic ac.	OsO <sub>4</sub> /O <sub>2</sub> /aldehyde/AIBN	5 h, 90 °C	AA: 43% PA: 36%	103
DEE mixture of industrial oleic ac.	Co(OAc) <sub>2</sub> -Mn(OAc) <sub>2</sub> -HBr/O <sub>2</sub>	8 h, 100 °C	Conv.: 88% DA <sub>9+8</sub> : 84%	104
Methyl oleate	OsO <sub>4</sub> /oxone in DMF	3 h, RT	PA: 93%	105
Methyl oleate	Oxone/periodate in MeCN:H <sub>2</sub> O	reflux, 6 h	PA: 70%	106
Methyl oleate	[Fe(OTf) <sub>2</sub> (6-Me-PyTACN)]/H <sub>2</sub> O <sub>2</sub> and NaIO <sub>4</sub>	36 h, 0 °C	PA: 55%	87
Methyl oleate	Ruthenium-based POM: [Ru(2,6-dipicolinate) <sub>2</sub> ]/H <sub>2</sub> O <sub>2</sub>	24 h, 80 °C	PA: 81%	107
Methyl oleate	Peroxo-tungsten complex with Aliquat 336 as PTA/ H <sub>2</sub> O <sub>2</sub>	4 h, 85 °C organic solvent-free	MEA: 83% PA: 84%	108
Methyl oleate	H <sub>2</sub> WO <sub>4</sub> and Co(acac) <sub>3</sub> /H <sub>2</sub> O <sub>2</sub> and NHPI in O <sub>2</sub>	5 h, 70–75 °C	MEA: 19% PA: 20%	109
9,10-dihydroxystearic acid	Au supported on Al <sub>2</sub> O <sub>3</sub> /O <sub>2</sub>	260 min, 80 °C	AA: 86% PA: 99%	110
9,10-dihydroxystearic acid	Co(OAc) <sub>2</sub> -Mn(OAc) <sub>2</sub> -HBr/O <sub>2</sub>	8 h, 100 °C	AA: 89% PA: 85%	111
Methyl erucate	H <sub>2</sub> WO <sub>4</sub> and Co(acac) <sub>3</sub> /H <sub>2</sub> O <sub>2</sub> and NHPI in O <sub>2</sub>	5 h, 70–75 °C	MB: 41% PA: 54%	112
Methyl ricinoleate	A peroxo-tungsten complex with Aliquat336 as PTA/ H <sub>2</sub> O <sub>2</sub>	4 h, 85 °C, organic solvent-free	MA: 85%	113



The table also reports the most important catalytic systems for the direct cleavage of either the UFAs or the corresponding esters. However, these systems are far from the topic of this research work and they were not described in detail.

In the following sections, the different catalytic systems reported so far for the oxidative cleavage of unsaturated fatty acids, and their corresponding glycols, are classified and divided into several groups according to the oxidant used: from the traditional and strong oxidants to much greener and sustainable ones, such as hydrogen peroxide and oxygen.

In particular, the most significant industrial process and catalytic systems developed for the oxidative cleavage of glycols derived from UFAs by using benign oxidants, such as oxygen, are described in detail.

### 3.2.1.1. Ozonolysis

Nowadays, the most common industrial technology for the oxidative cleavage of fatty acids is ozonolysis, which for several years has been used for the production of azelaic acid from oleic acid, as the sole commercial process<sup>114</sup>. This method was initially patented in 1957 by Goebel and it was able to achieve 78% yield of azelaic acid since the early stage of development<sup>115</sup>.

Ozone is an allotrope of oxygen and it is a symmetrical bent molecule with a central positively charged oxygen atom and two terminal oxygen atoms that share a negative charge. Thanks to its 1,3-dipole nature it can be inserted rapidly into the C=C double bonds of alkenes via 1,3-dipolar cycloadditions without using any metal catalyst, in order to further generate aldehydes or carboxylic acids.

The reaction steps of the ozonolysis process are reported in Figure 3.3. In the first step, OA reacts with ozone (1%<sub>vol.</sub> in air) at 20 - 40°C via 1,3-dipolar cycloaddition, generating 1,2,3-trioxolane. This product is very unstable because of the presence of two very weak O-O single bond (140 kJ/mol) and it immediately decomposes by a *reverse* 1,3-dipolar cycloaddition. The products are an aldehyde and a new, rather unstable molecule: a 1,3-dipole known as carbonyl oxide. These two compounds react together *via* a third cycloaddition step with the nucleophilic oxyanion attacking the carbon atom of the

carbonyl group. The final product is a 1,2,4-trioxolane, known as an ozonide. It is still not stable and is quite explosive, so it needs decomposing.

Indeed, in the second step of the process, the ozonide is cleaved to carboxylic acids by oxidation with  $O_2$  at 70-110 °C without any catalyst<sup>114</sup>.

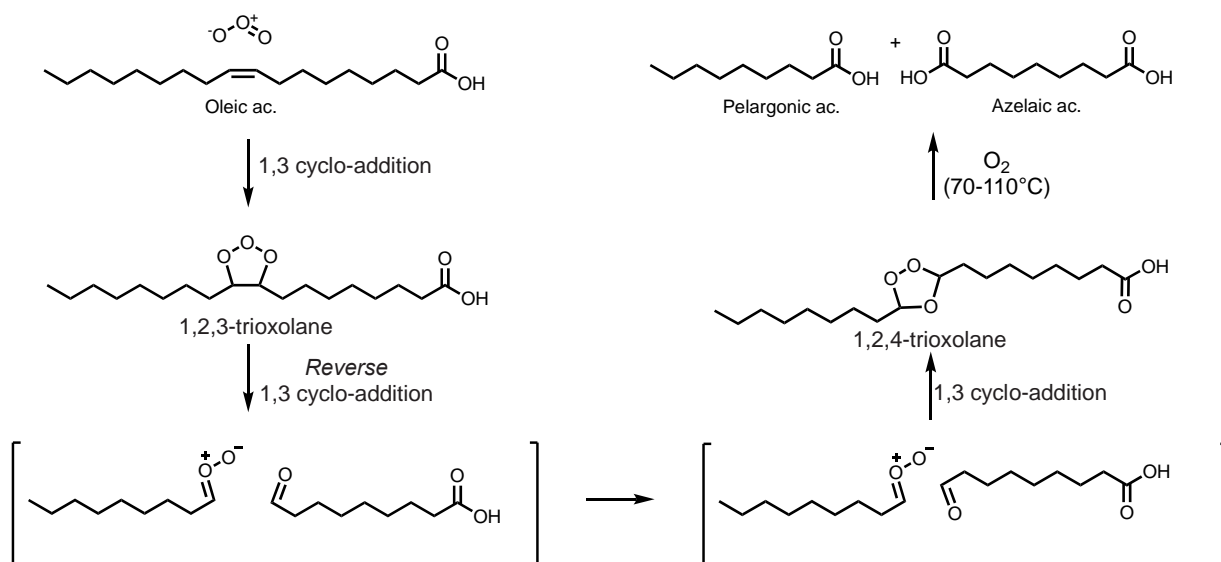


**Figure 3.3. Reaction network of ozonolysis of oleic acid (adapted from ref.114).**

Other important dicarboxylic acids or acid mixtures also have been produced through ozonolysis from some natural raw materials. For example, brassylic acid (72 – 82% yield) of high purity, was produced by means of a two-stage cleavage of erucic acid with ozone and oxygen, with pelargonic acid as a co-product, and this method was also translated to a small pilot-scale operation<sup>116, 117</sup>.

Tremendous efforts have been done to modify the ozonolysis process in order to improve the azelaic acid yield, which did not exceed the 80%<sup>118, 119, 120, 121, 122, 123, 124</sup>. The use of acetic acid or other solvents was described for the ozonolysis of both oleic acid and methyl oleate<sup>125</sup>.

Also the second step of the reaction was investigated by using different strategies, for example the application of phase transfer catalysts as well as oxidation catalysts in the oxidative work-up of the secondary ozonide. Thus, Shi et al. combined ozonolysis with oxidation using  $H_2O_2$ , phosphotungstic acid, or tungstic acid as catalyst precursor and quaternary ammonium salts as phase-transfer catalysts and obtained 71% yield of azelaic acid<sup>126</sup>.

A similar process was claimed by Sun *et al.* who developed a method comprising the oxidation of the ozonide with molecular oxygen, and catalysts based on supported by Mo–, V–, Mn–, Co–, Fe–, and Pb-containing oxides or salts and tungstic acid as oxidation catalysts. The obtained yield of azelaic acid ranged from 70% to 87%<sup>127, 128</sup>.

The decomposition of the secondary ozonide was investigated also with microwaves without a catalyst. The obtained azelaic acid yields amounted to about 70–80% and the reaction time could be shortened<sup>129, 130</sup>.

Despite the use of these “exotic” systems, the best result was achieved by Ackman *et al.* thanks to the in-situ formation of performic acid from H<sub>2</sub>O<sub>2</sub> and formic acid. This catalytic system was employed in combination with ozonolysis of OA in methanol. Azelaic acid yields up to 95% were observed<sup>131</sup>. This procedure was also proposed as a method for the determination of the C=C position in long-chain fatty acids.

In conclusion, ozonolysis is a relatively well developed process with apparent advantages like good selectivity, the absence of waste derived from the oxidant and the simple reprocessing. However, hazardous and environmental problems associated with ozone utilization hampered it to be widely used. Alternatives which are more economical and environmentally friendly are needed for the production of carboxylic acids.

### 3.2.1.2. Oxidation with Strong Oxidants

Cleavage reactions with stoichiometric use of oxidants in the absence of catalyst are only of historical interest and should be discussed shortly.

Several strong oxidants, such as K<sub>2</sub>Cr<sub>2</sub>O<sub>7</sub>, HNO<sub>3</sub>, KMnO<sub>4</sub>, and NaIO<sub>4</sub>, were used as stoichiometric reactants for the oxidation of the double bond<sup>132</sup>.

The yield of azelaic acid obtained with these unsustainable oxidants and using different seed oils was increased up to 60–87%, also employing phase transfer catalysts, emulsifiers alone, or in combination with ultrasonic treatment due to an improved mass transfer through phase boundaries<sup>133, 134</sup>.

Two-stage methods were also described: oleic acid was converted to DSA by Cl<sub>2</sub>/NaOH and then cleaved to azelaic acid using chromic acid<sup>135, 136</sup>. Diepoxy- and

tetrahydroxystearic acids were cleaved under strongly alkaline conditions to achieve 29 and 43% azelaic acid yield, respectively<sup>137</sup>. Furthermore, these strong oxidants used in excess, showed an insufficient product selectivity. Products of chain degradation were often found. Thus, yields of the desired products azelaic acid and pelargonic acid are not competitive.

Concluding, the use of stoichiometric oxidants is not economic and causes environmental problems; therefore, it is only marginally used for scientific interest, but not suitable for an industrial application.

### **3.2.1.3. Catalytic Oxidation with Molecular Oxygen**

Molecular oxygen ( $O_2$ ) is quite abundant in nature and 21%<sub>vol.</sub> percentage of air is oxygen. Molecular oxygen is an ideal oxidant for oxidation reactions considering the availability and price. Moreover, it is also one of the most “greener” oxidants because its use doesn’t cause the formation of hazardous waste from the process.

Molecular oxygen is widely used in oxidation reactions, such as hydrocarbon oxygenation, alcohols oxidation and amine oxidation<sup>138, 139, 140</sup>. However, molecular oxygen is naturally inert due to its triplet state, which prevents the direct reaction with many other molecules, which are often in the singlet state<sup>141</sup>.

Therefore, only a few works have been reported for the oxidative cleavage with  $O_2$ . Utilization of oxygen as terminal oxidant showed low selectivity due to several side reactions, such as decarboxylation and over-oxidation. The latter leads to the formation of keto groups that subsequently degrade to a mixture of acids with different carbon chains (Figure 3.4)<sup>142</sup>.

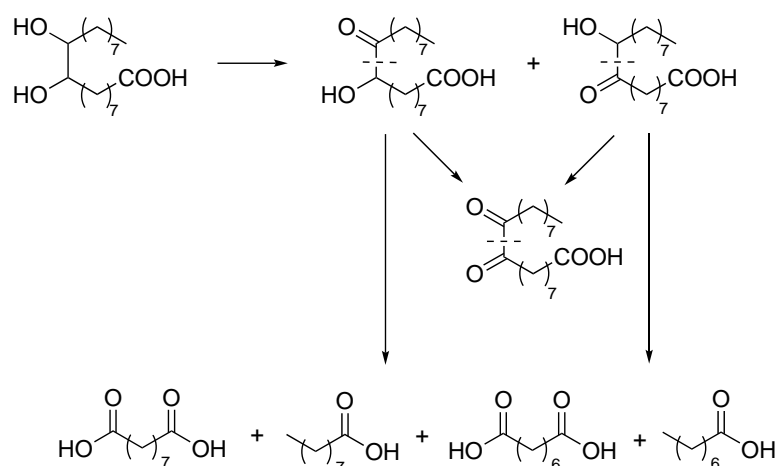


**Figure 3.4. Degradation of keto-intermediates during the oxidation of diol with oxygen. (Adapted from ref. 142)**

Generally, the use of  $O_2$  as the oxidant for the cleavage of UFAs was reported in conjunction with two-step methods, where it was used for the oxidative cleavage of the diol intermediate (see Figure 3.2).

In the first step, the C-C double bond was converted into diols by oxidants other than oxygen, usually with  $H_2WO_4/H_2O_2$ . Then the diols underwent C-C bond oxidative cleavage to acids with  $O_2$ .

Although the conversion of UFAs to dihydroxy-derivatives was well developed<sup>107, 143, 144, 145</sup>, the oxidative cleavage of this intermediate stimulated much attention.

Woodward developed a  $H_2WO_4/Co(acac)_3/N$ -hydroxyphthalimide (NHPI) catalytic system for the oxidation of UFAs with  $H_2O_2/O_2$  as oxidants. Oleic acid, methyl oleate, and methyl erucate were dihydroxylated by  $H_2O_2$  in the presence of  $H_2WO_4$ , while  $Co(acac)_3/NHPI$  was used for the oxidative cleavage of the diols intermediate to carboxylic acids. This system used a limited amount of  $H_2O_2$ , but the yield was very low.

Similarly, Santacesaria and co-workers<sup>86, 146, 147</sup> reported a cobalt polyoxometalate for the oxidative cleavage of the diols. The oxidative cleavage of UFAs was obtained with a two-step process: firstly, the C=C bond was oxidized to diols with  $H_2O_2$ . Secondly, the oxidative cleavage of the diols with  $O_2$  was presumably catalysed by the in-situ formed  $H_6CoW_{12}O_{40}$ . However, using this catalytic system, the yield of azelaic acid production from 9,10-dihydroxystearic acid was not high (53%, temperature 70 °C, time 270 min).

In order to improve the efficiency of the diols cleavage and address the problem of catalyst recycle, heterogeneous catalysts have been explored for this transformation. Kulik and co-workers<sup>110,148</sup> reported the oxidative cleavage of diols from oleic acid, methyl oleate, and erucic acid using a supported gold catalyst with O<sub>2</sub> as the oxidant. Among the investigated supports Al<sub>2</sub>O<sub>3</sub>, CeO<sub>2</sub>, TiO<sub>2</sub>, and ZrO<sub>2</sub>, Au/Al<sub>2</sub>O<sub>3</sub> showed the best results. Azelaic acid and pelargonic acid were obtained in 86% and 99% yields, respectively, from 9,10-dihydroxystearic acid. However, catalytic activity significantly decreased after repeated uses: after the first recycle, the conversion declined from 94% to 77%, as well as the yields of azelaic and pelargonic acids were decreased by approximately the 30%. Moreover, a large amount of NaOH was needed in order to activate the substrate.

A mechanistic study indicated that the hydroxyketone and diketone might be the reactive intermediates: the diols were first oxidatively dehydrogenated to hydroxyketone or diketone which were then cleaved to a mixture of acid products (see Figure 3.4)<sup>148</sup>.

Another approach reported in literature is the use of sacrificial aldehydes in order to improve the efficiency of the reaction carried out with O<sub>2</sub>.

Aldehydes are easily oxidized to the peracid even in the absence of catalyst<sup>149, 150, 151</sup>; the peracid is more active than O<sub>2</sub> and widely used for the epoxidation of olefins<sup>152,153</sup>. Köckritz and co-workers<sup>103</sup> used O<sub>2</sub>/isobutyraldehyde in the oxidation of methyl oleate and oleic acid. Monomethyl azelate and pelargonic acid with 50–70% yields were obtained from methyl oleate with OsO<sub>4</sub> catalyst. The oxidation of the aldehyde by O<sub>2</sub> generated a peracid which was the active oxidant for the cleavage of C–C bond. 2,2-Azobis(isobutyronitrile) (AIBN) was used as the radical initiator to promote the oxidation of isobutyraldehyde to the peracid.

Fujitani and co-workers<sup>111</sup> employed a Co–Mn–Br catalytic system in the oxidation of UFAs. Co–Mn–Br is widely used in the oxidation of hydrocarbons to acids. It is also effective in the preparation of dicarboxylic acids from UFAs. For example, industrial oleic acid, containing oleic acid, palmitoleic acid, linoleic acid, and linolenic acid, was converted into azelaic acid and suberic acid. Soybean acid and tall acid majorly consisting of linoleic acid and linolenic acid were also oxidized to the related dicarboxylic acids.

Ikushima and co-workers<sup>102</sup> investigated mesoporous silicas (Cr-MCM-41, Mn-MCM-41, Co-MCM-41) and microporous zeolites (Cr-APO-5, Co-MFI, Mn-MFI) as catalysts for the oxidation of oleic acid with O<sub>2</sub>. Chromium-containing catalysts showed the best performance with 95% conversion. The catalyst was recycled without obvious decrease of catalytic activity. Although this catalyst was highly active, the selectivity was low (32% for azelaic acid and 32% for pelargonic acid) because of the degradation to C<sub>6</sub>–C<sub>10</sub> acids. Furthermore, the use of a chromium-based catalyst is not in accordance with the green chemistry principles.

### **3.2.2. *Patents***

The catalytic oxidative cleavage of UFAs contained in vegetable oils has received considerable attention also from the industrial world. Many catalytic systems able to catalyse the reaction in the presence of green oxidants, i.e. oxygen or air, have been patented. Table 3-2 summarizes the different technologies showing the reaction conditions and results in terms of yield into the desired product.



Table 3-2. Catalytic systems for the oxidative cleavage of UFAs reported in patents.

Patent Name	Number of Publication/Year	Type of Process	Substrate	(Preferred) Catalytic System	Oxidant	Reaction conditions	Yield
<i>Process for preparing a carboxylic acid from a diol or from an epoxide by oxidative</i>	US20150210623/2015	Batch	Oleic ac./ 9,10-dihydroxystearic acid	$\text{Ru}(\text{OH})_x/\text{Al}_2\text{O}_3$	$\text{O}_2$	90-110 °C, 15 h, 8 bar	Carboxylic acids: > 40%
<i>Continuous process for the production of derivatives of saturated carboxylic acids</i>	US20150073162A1/2015	Jeet - loop (Batch)	Unsaturated fatty acids	$\text{Co}(\text{OCOCH}_3)_2$ O $\text{CoCl}_2$	Oxygen-enriched Air	60-70 °C, 2-8 h, $\leq 25 \cdot 10^5$ Pa	AA: 77,3% PA: 79,8%
<i>Continuous process of oxidative cleavage of vegetable oils</i>	US8835662B2/2014	Jeet-loop (Batch)	Vegetable oils	$\text{Co}(\text{OCOCH}_3)_2$ or $\text{CoCl}_2$	$\text{O}_2$ or Air	60-70°C, 2-8h, $\leq 25 \cdot 10^5$ Pa	AA: 79,2% PA: 80,1%
<i>Process for the catalytic cleavage of vegetable oils</i>	US20120226060/2012	Not specified	Vegetable oils	$\text{Co}(\text{OCOCH}_3)_2$ or $\text{CoCl}_2$	$\text{O}_2$	60-70 °C, 3-12 h, 15 atm	AA: >80%
<i>Improved Process for the Production of Derivatives of Saturated Carboxylic Acids</i>	US20080245995A1/2008	Not specified	Vegetable oils (containing unsaturated fatty acids)	$\text{Co}(\text{OCOCH}_3)_2$ or $\text{CoCl}_2$	$\text{O}_2$	60-70°C, 3-12h, $\leq 10$ atm	AA: 65-70% PA: 65-70%
<i>Process for the preparation of carboxylic acids and esters thereof by oxidative cleavage of unsaturated fatty acids and esters thereof</i>	US5714623/1994	Not specified	Vegetable oils or mixture of vegetable oils (containing unsaturated fatty acids)	$\text{Co}(\text{OCOCH}_3)_2$ or $\text{CoCl}_2$ or $\text{Co}(\text{SO}_4)_2$	$\text{O}_2$ or Air	50-90°C, 5-12h, $\leq 10$ atm	AA: 70,2-75% PA: 70-75,4%
<i>Process for preparing carboxylic acid</i>	US4606863A/1986	Not specified	Unsaturated carboxylic acid or their esters	Oxide/Hydroxides/Complex of Co, Mn, Ce, Ni or as it	$\text{O}_2$ or Air	80-140°C, 5-12h, $\text{P}_{\text{O}_2}=0,1-10\text{Kg/cm}^2$	AA: 22-72% PA: 21-71%
<i>Oxidation of vicinal glycols in the presence of organic peroxides and cobaltous compounds</i>	US3711523A/1973	Not specified	Vicinal diol	Cobalt (II) salts	$\text{O}_2$ or Air and peroxide compounds	70-100°C, 30min-4h	-

Noteworthy, a recent Japanese patent claimed an interesting approach and an environmentally benign alternative to heavy metal oxidants. Methyl oleate was cleaved in  $\text{H}_2\text{O}_2/\text{H}_2\text{O}$  under subcritical conditions at 180–370 °C and 1–25 MPa<sup>154</sup>. The obtained azelaic acid yield of 31% needs to be improved. A high-energy consumption and corrosion problems are the main disadvantages of the process.

## 4. AIM OF THE WORK

The aim of the present study was to develop the optimal catalyst system for the conversion of unsaturated fatty acids into shorter chain, mono and di-carboxylic acids.

Specifically, the project presented in this thesis was aimed at the study of the catalytic process for the oxidative scission of the vicinal glycol derived from oleic acid into azelaic acid and pelargonic acid (see Figure 4.1). This is also the objective of the work package 2 of the F2R project, already mentioned in paragraph 2.2.2, in which the Unibo is involved.

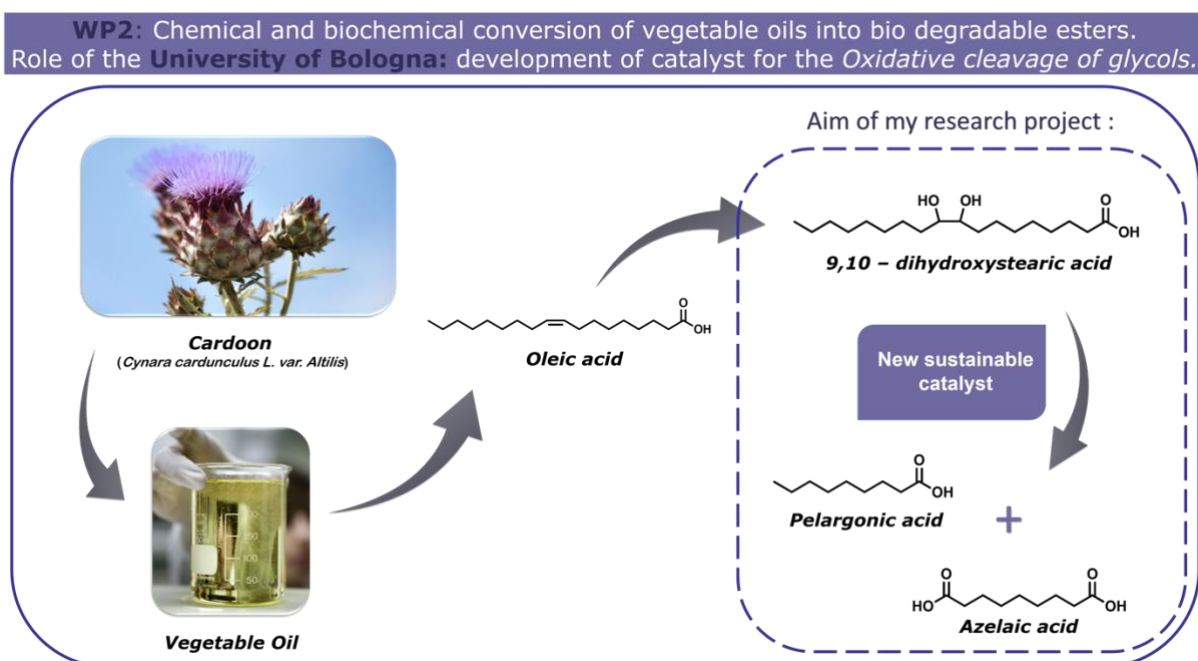


**Figure 4.1. Schematization of the aim of this Thesis in the context of the F2R project.**

Several catalytic systems alternative to those proposed in literature were synthesized, characterized, and screened in the oxidative cleavage using oxygen as the oxidant.

The preliminary screening allowed to identify three different catalysts, which were then used for the investigation of the effect of reaction parameters, such as temperature, time of reaction, stirring rate, oxidant pressure, amount of catalyst, on catalyst performance.

Finally, the stability of these catalysts was studied together with the possibility to re-use them, thanks to the development of an economic and efficient regeneration procedure.

## **5. MATERIALS AND METHODS**

This chapter describes, the methods used for catalysts preparation and the techniques used to characterize them. These materials were chosen as possible candidates for the oxidative cleavage of oleic acid to pelargonic and azelaic acids. Moreover, the operating conditions used for reactivity experiments and the methods used to analyse the reaction mixtures are outlined.

### **5.1. Preparation of the catalytic systems**

Herein, the complete description of the synthesis procedures adopted for catalysts preparation is reported.

For the sake of convenience, the presentation has been divided according to the type of materials.

#### **5.1.1. Metal-modified ferros spinels**

Typically, M-modified ferrites are synthesized by solid - state reaction at 1000 °C<sup>155</sup>. In this way, it is possible to obtain very crystalline materials, but with a very low surface area. Thus, in terms of reactivity, too stable materials are obtained. For this reason, all the ferros spinels employed were prepared using the co-precipitation method (Figure 5.1), extensively described in the literature<sup>156</sup>.

##### **5.1.1.1. Co-precipitation**

The materials synthesized belong to the type  $A_x^{2+}Fe_{3-x}^{3+}O_y^{2-}$ , where  $A^{2+}$  was either  $Fe^{2+}$ ,  $Co^{2+}$ ,  $Ni^{2+}$  or  $Cu^{2+}$  (the first one corresponds to the unmodified magnetite). The list of the chemicals used for the preparations is shown in Table 5-1.

The procedure used for the synthesis can be summarized as follows: the mixed solutions of metal precursors containing 50 mL of 1M  $Fe(NO_3)_3$  and 50 mL of 0,5M  $M^{II}(NO_3)_2$  (where M = Co, Ni, Mn or Cu) were put into a separation funnel and then drop-

by-drop added into the reaction vessel containing 500 mL of NaOH aqueous solution (2M) at the temperature of 45°C, under vigorous stirring, with continuous monitoring of the pH (maintained at above 13).

For the synthesis of magnetite ( $\text{Fe}_3\text{O}_4$ ),  $\text{Fe}^{\text{II}}(\text{SO}_4) \cdot 7\text{H}_2\text{O}$  was preferred as precursor instead of the nitrate salt.

Finally, the suspension was digested for 2 h at 45°C. The precipitate was recovered by vacuum filtration and washed with at least 1,5 L of demineralized water at room temperature (RT), in order to remove the sodium and nitrate/sulphate ions.

**Table 5-1. Chemicals used for the synthesis of the M-modified ferrites.**

COMPOUNDS	REFERENCES	PURITY
$\text{Fe}(\text{NO}_3)_3 \cdot 9 \text{H}_2\text{O}$	SIGMA-ALDRICH	98%
$\text{Cu}(\text{NO}_3)_2 \cdot 2,5 \text{H}_2\text{O}$	SIGMA-ALDRICH	98%
$\text{Mg}(\text{NO}_3)_2 \cdot 6 \text{H}_2\text{O}$	SIGMA-ALDRICH	99%
$\text{Fe}^{\text{II}}(\text{SO}_4)$	MERK	99,50%
NaOH	SIGMA-ALDRICH	>99 %

From the table of chemicals used during catalysts synthesis, it is possible to note that nitrate salts (as sources for the cations), NaOH and water were handled. With the exception of water, all the other products showed some dangerous issues, so all the operations were carried out using the necessary individual protective systems.

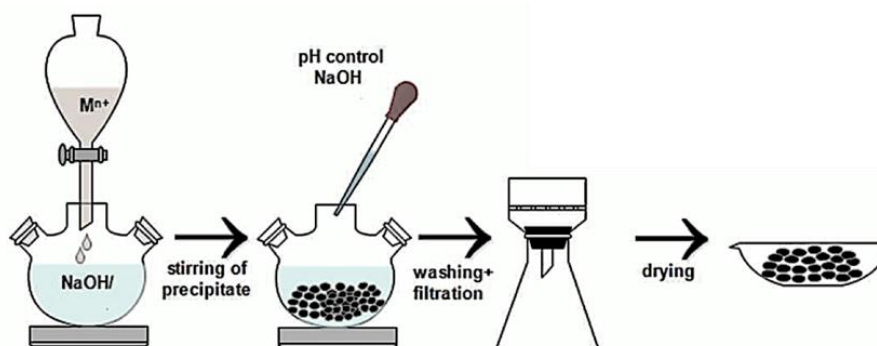


**Figure 5.1. Scheme of the synthesis of iron oxides with spinel structure.**

### 5.1.1.2. Thermal treatments

The washed samples obtained by co-precipitation were dried at 120°C in air for 2 hours; for magnetite, the drying temperature was kept at 80°C in order to avoid the easy oxidation of  $\text{Fe}^{2+}$  to  $\text{Fe}^{3+}$ . These compounds represented the “precursors” of the desired mixed oxides.

Considering that co-precipitation was used rather than solid-state reaction at high temperature, further thermal treatments required for the formation of the desired spinel phase were carried out at moderate temperature.

Accordingly, after the drying process, the solids were milled in an agate mortar and then annealed in static air at 450°C for 8 hours by using a temperature ramp of 10 °C/min. As far as the magnetite is concerned, it was thermally treated in inert atmosphere by heating under  $\text{N}_2$  flow at 450°C for 8h, so as to prevent the complete oxidation of  $\text{Fe}_3\text{O}_4$  into hematite ( $\text{Fe}_2\text{O}_3$ ).

Mixed oxides with the spinel structure were formed with the procedure outlined above. The unit cell of the obtained materials is shown in Figure 5.2. The crystallographic structure of spinel oxides includes a nearly closed-packed face centered cubic (*fcc*) of the anions (Figure 5.2.) with two inequivalent sites for the cations, which differ in oxygen coordination<sup>157</sup>. A tetrahedral site,  $\text{AO}_4$ , with the cation at the centre of a cube and four oxygen atoms in the nonadjacent corners. The octahedral site,  $\text{BO}_6$ , consists of a cation surrounded by six oxygen atoms, two along each dimensional axis, to form an octahedron<sup>158</sup>. The preference of the individual ions for the two types of lattice sites ( $\text{O}_h$  vs  $\text{T}_d$ ) is determined by:

- the ionic radii of the specific ions;
- the size of the interstices;
- the temperature of treatment;
- the orbital preference for a specific coordination.

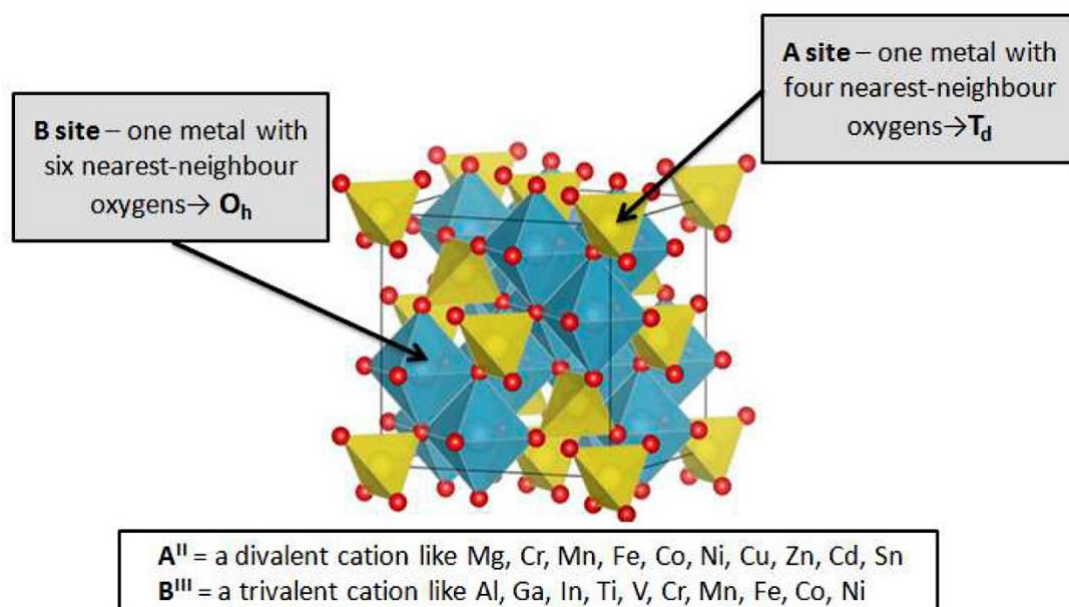


**Figure 5.2. Spinel oxide unit cell.**

According to the distribution of A and B cations between  $T_d$  and  $O_h$  sites, there are two types of spinel oxides: normal and inverse spinels. In the normal spinel, the A cations (divalent) occupy all the tetrahedral sites, and the B cations (trivalent) fill the octahedral sites. Since tetrahedral holes are smaller than octahedral holes, A ions should be smaller than B ions. However, this condition is not always fulfilled, in fact there is another type of spinel, which is more common in nature, called the inverse spinel to indicate that it is the opposite of what has already been described. In the inverse spinel, the B cations occupy the tetrahedral sites, and the octahedral sites contains a mixture of B and A cations<sup>159</sup>.



### 5.1.2. Metal nanoparticles

Gold nanoparticles supported on titania were synthesized and studied in the reaction of oxidative cleavage with molecular oxygen.

The catalysts were prepared by incipient wetness impregnation of a suspension of gold nanoparticles on the support.

First, the synthesis of the suspension of gold nanoparticles were performed. The choice of the method for nanoparticles synthesis is very important because it allows to modulate their characteristics such as shape, size and its distribution, composition and degree of agglomeration (in the case of colloidal systems). For this reason, it is important to carefully follow the recipe, in order to ensure the reproducibility of the results.

The suspension of gold nanoparticles was prepared by synthesis in water according to the modified *Turkevich method* described in the literature and patented<sup>160</sup>.

The synthesis was conducted in water and it consists in the reduction of Au(III) by glucose in a basic environment of NaOH using PVP (polyvinylpyrrolidone, Figure 5.3) as stabilising agent for the nanoparticles.

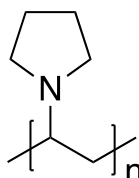


**Figure 5.3. Structure of the repeating unit that constitutes the PVP polymer.**

The molar ratio used for the synthesis were the following:

$$Au : glucose : NaOH : PVP = 1 : 2 : 8 : 2.75.$$

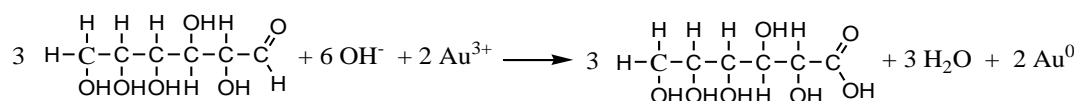


**Figure 5.4. Stoichiometric reaction of Au<sub>NP</sub> synthesis.**

The final suspension concentration was about  $5 \cdot 10^{-3}$  M with a volume of 100 mL.



The synthesis was conducted as described in the general scheme shown in Figure 5.5.

The synthesis started with the dissolution of the right amount of  $\text{HAuCl}_4$  in 10 mL of distilled water. PVP and sodium hydroxide were dissolved in 90 mL of distilled water in a three necked round bottom flask provided with magnetic stirrer (600 rpm), thermometer and vapour condenser, and heated up to 95 °C in a glycol bath. When the desired temperature was reached, glucose was added to the solution and the mixture was warmed up for no more than 30 seconds to avoid excessive sugar degradation. Then the gold solution was added and after 2,5 minutes, the reaction was quenched by fast cooling of the flask in ice and water. The final gold suspension showed a dark red colour. In order to preliminarily check the quality of gold nanoparticles, it was essential to measure the hydrodynamic diameter by D.L.S. (Dynamic light scattering, see paragraph 5.2.1) analysis.

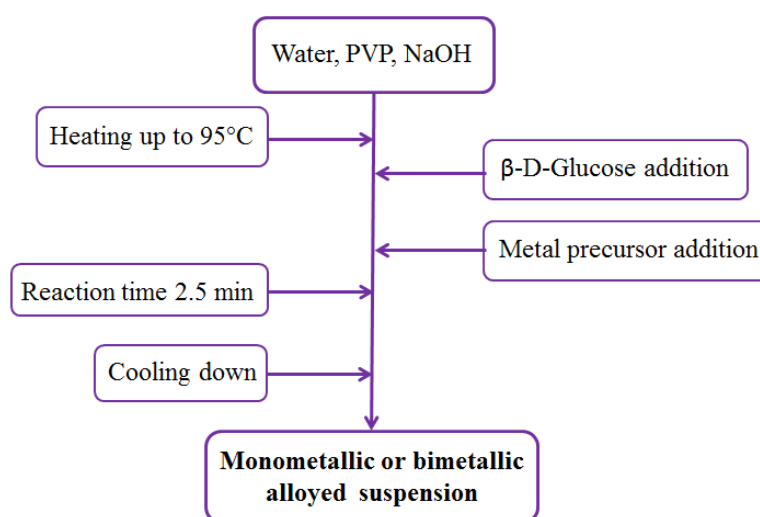


**Figure 5.5. General scheme for the synthesis of monometallic nanoparticles.**

The list of the chemicals used for the preparations is given in Table 5-2:

Table 5-2. Chemicals used for the synthesis Au<sub>NP</sub> - based catalyst.

COMPOUNDS	REFERENCES	PURITY
<b>TiO<sub>2</sub> – DT51</b>	CristalACTiV	> 98 %
<b>Glucose</b>	Sigma-Aldrich	> 99 %
<b>HAICl<sub>4</sub></b>	Sigma-Aldrich	> 99 %
<b>NaOH</b>	Sigma-Aldrich	>99 %
<b>PVP</b>	Sigma-Aldrich	-

The synthesis of the final catalyst is described in details below:

#### **Au/TiO<sub>2</sub> 1,5%<sub>wt.</sub>**

The catalysts were prepared by impregnating the support (in this case, TiO<sub>2</sub>) with a suspension of gold nanoparticles. Based on the required weight percentage of gold on the support, the precise amount of gold nanoparticles suspension was weighted and concentrated by centrifugation in tubes fitted with filters of cellulose (50 kDa *Amicon Ultra Filters*, Millipore) at 1700 rpm for no more than 25 minutes.

The Incipient Wetness Impregnation method provides the solution of the metal to drip on the support until reaching the “point of mud”: the volume of the used liquid is equal to that of the pores of the support. After the incipient wetness impregnation of the concentrated suspension, the catalyst was dried for a night at 120 °C in order to remove the imbibed liquid; then it was washed with boiling water for 30 minutes with the aim of removing the adsorbed PVP, it was dried ad night at 120 °C and finally calcined in static air at 300 °C for 3 hours. This treatment is also necessary to prevent the leaching of the catalyst during its use in the reaction.

Following this procedure, Au/TiO<sub>2</sub> with metal loading of 1,5%<sub>wt.</sub> was obtained and the final catalyst colour was a light violet powder.

### 5.1.3. Iron-substituted polyoxometalate

The next catalysts tested for the oxidative cleavage of unsaturated fatty acids with oxygen were polyoxometalates, in particular Keggin-type P/W/Fe heteropolyacids.

Polyoxometalates (POMs) are polyatomic ions with general formula  $[M_mO_y]^{p-}$ . The ion consists of oxygen and transition metals, usually of group 5 and 6 at their highest oxidation states. Also POMs can contain different heteroatoms such as P, Si, B, and in this case they belong to the heteropolyanions with the general formula of  $[X_xM_mO_y]^{q-}$  ( $x \leq m$ ). The most known structural form for heteropolyacids is the Keggin structure. It has the general formula  $[XM_{12}O_{40}]^{n-}$ , where M is the addenda atom (usually Mo or W) and X is the heteroatom, such as  $P^{5+}$ , or  $B^{3+}$ . The structure (Figure 5.6) is made of a heteroatom bounded to four oxygen atoms forming a tetrahedron, surrounded by 12 octahedral  $MO_6$ -units. The tetrahedron is linked to each octahedron through the oxygen atoms, and each octahedron is linked to four adjacent octahedra via an edge and corners forming a bridge  $-M-O-M-$ <sup>161</sup>.

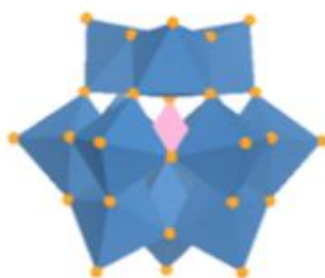


**Figure 5.6. Structure of heteropolyacids with Keggin structure.**

In P/W/Fe heteropolyacids one atom of W was replaced by Fe atoms and had the formula  $H_4[PW_{11}Fe(H_2O)O_{39}]$ .

The Iron-substituted Keggin-type heteropolyacid was synthesized according to the available procedure described by Matveev and co-workers<sup>162</sup>.

First, 0,86 g of  $H_3PO_4$  and 2,5 g of  $Fe(NO_3)_3$  were dissolved separately in 10 mL and 15 mL of deionized water, respectively. Subsequently, the two solutions were mixed

together in a separating funnel and then added drop-by-drop into an aqueous solution of  $\text{Na}_2\text{WO}_4$  (22,5 g in 25 mL of  $\text{H}_2\text{O}$ ), kept under continuous stirring.

After 5 minutes from the complete addition of the solution, a beige-yellowish precipitate formed, which was stirred at room temperature for 15 min. At this point, about 10 mL of an aqueous solution of  $\text{H}_2\text{SO}_4$  was added dropwise to the mixture and the yellowish solid disappeared. In the acid environment, the formation of  $4\text{H}^+ [\text{PW}_{11}\text{Fe}(\text{H}_2\text{O})\text{O}_{39}]^{4-}$  was promoted.

After 10-15 min of continuous stirring, a new yellow-precipitate was formed. The final precipitate was separated by filtration on a Büchner funnel and dried at  $120^\circ\text{C}$  overnight.

## **5.1.4. Copper based catalysts**

### **5.1.4.1. Commercial Copper Oxide based materials**

The copper (II) oxide and copper oxide supported over alumina ( $\text{CuO}/\text{Al}_2\text{O}_3$ , pellets 14-20 mesh, with nominal CuO loading of 13 % by weight) were initially purchased respectively from Merck and Sigma-Aldrich in order to check the possibility of using these materials as catalysts for the desired reaction. After their successful use for the oxidative scission, the synthesis of this material was reproduced in our lab using the method described later in this chapter.



**Figure 5.7. Commercial copper (II) oxide supported over  $\text{Al}_2\text{O}_3$  (nominal CuO loading = 13 %<sub>wt.</sub>) as 14-20 mesh pellets.**

#### 5.1.4.2. Copper Oxide over different supports

The materials below were chosen as supports, in order to investigate a possible synergic effect between the active phase and the support itself:

- **Al<sub>2</sub>O<sub>3</sub>** (Sigma Aldrich)
- **TiO<sub>2</sub>** (DT-51)
- **SiO<sub>2</sub>** (360 - Grace<sup>®</sup>)
- **CeO<sub>2</sub>** (delivered from Solvay S.p.A.)

Alumina and silica are probably the materials most widely employed as catalysts and catalyst supports in many chemical processes<sup>163, 164</sup>. The usefulness of these oxides can be traced back to a favourable combination of their textural properties, such as surface area, pore volume, and pore-size distribution, and their acid/base characteristics, which are mainly related to surface chemical composition, local microstructure, and phase composition.

Likewise alumina and silica, titania is extensively used as catalyst or support<sup>165</sup>. In contrast to SiO<sub>2</sub>, whose normal role is to ensure that the supported phase has a large surface area, titania typically interacts with the deposited active phase conferring new properties to the material<sup>166</sup>.

As far as ceria is concerned, it was chosen as support because of its superior ability to increase reaction rates involving redox steps compared to “inert”, non-reducible supports such as alumina<sup>167</sup>.

Catalysts were prepared by the impregnation of the active phase over the desired support. The used method is the so-called *incipient wetness impregnation* (IWI) which guarantees a lower amount and a better dispersion of the active metal precursor than *wet impregnation*.

In this procedure, a certain volume of solution containing the precursor of the active phase is contacted with the solid support which, in a subsequent step, is dried to remove the imbibed solvent.

Differently from *wet impregnation*, the volume of the precursor solution used is equal or slightly less than the total pore volume of the support. Control of the operation must be rather precise and repeated applications of the solution may be necessary. The maximum loading is limited by the solubility of the precursor in the solution.

The most important operating variable is temperature, which influences both the precursor solubility and the solution viscosity and, as a consequence, the wetting time as well. The concentration profile of the impregnated compound depends on the mass transfer conditions within the pores during impregnation and drying<sup>168</sup>.

In this case  $\text{Cu}(\text{NO}_3)_2 \cdot 2.5\text{H}_2\text{O}$ , the active metal precursor, was dissolved in an aqueous solution and then added drop-by-drop to the support. Finally, the obtained material was dried at 85 °C for 12 h and calcined at 300 °C for 3 hours (temperature ramp: 3°C/min) in order to drive off the volatile components and develop the active phase (see Figure 5.8).



**Figure 5.8. Example of incipient wetness impregnation of CuO over  $\text{SiO}_2$  (360-Grace) employing  $\text{Cu}(\text{NO}_3)_2 \cdot 2.5\text{H}_2\text{O}$  as precursor.**

The materials with alumina as the support were synthesized in order to reproduce the commercial catalyst used for the initial study.

Alumina was purchased at Sigma – Aldrich and the synthesis was performed using this oxide as such or after a calcination treatment at 500 °C for 5 h (temperature ramp of 10 °C/min). In Figure 5.9, it is possible to observe the pictures of the two catalysts synthesized together with the commercial catalyst.

From the picture of the three samples, it is clear that the appearance of the catalyst made of CuO supported over alumina and calcined at 500 °C was very similar to the commercial catalyst, whereas the material synthesized with the untreated support shows a brighter green colour.

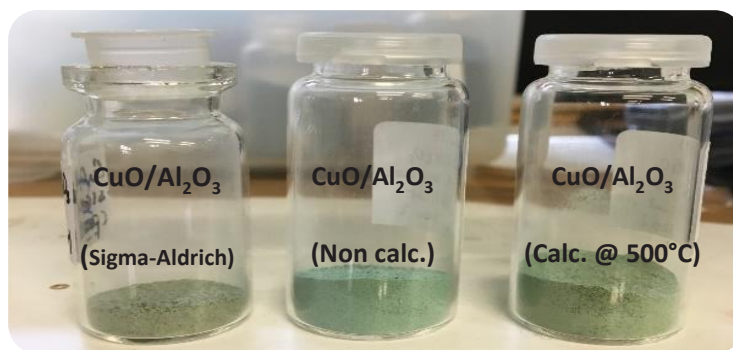


**Figure 5.9.** Pictures representing the results of the IWI synthesis using alumina as support: (from left to right) commercial  $\text{CuO}/\text{Al}_2\text{O}_3$ ,  $\text{CuO}$  over non-calcined alumina (Sigma-Aldrich), copper oxide over  $\text{Al}_2\text{O}_3$  calcined at  $500^\circ\text{C}$  for 5h ( $10^\circ\text{C}/\text{min}$ ).

As far as the other supports are concerned, three sets of catalysts were synthesized with the *IWI method* by changing the final amount of active phase:

- $\text{CuO}$  loading 5 %wt.;
- $\text{CuO}$  loading 10 %wt.;
- $\text{CuO}$  loading 15 %wt.

The results of the synthesis are presented in Figure 5.10.



**Figure 5.10.** Results of the incipient wetness impregnation using  $\text{TiO}_2$ ,  $\text{SiO}_2$  and  $\text{CeO}_2$  as supports.

As expected, the three sets of catalyst showed different colours due to the different interaction between the active phase and the support itself.



## 5.2. Characterization techniques

In this chapter, the principles of the physical and chemical techniques used to characterise the materials synthesized and, in some cases, spent after the oxidative cleavage reaction, are described.

For each technique, the general principle, the apparatus and the detailed method used are reported.

The description of the techniques is divided according to the nature of the physical-chemical property investigated.

### 5.2.1. Structural properties

#### 5.2.1.1. Specific surface area

N<sub>2</sub> adsorption/desorption was used to characterize the textural properties of the solids. The specific surface area and total pore volume of the catalysts were measured by physisorption of liquid nitrogen at -196 °C using a *MICROMERITICS ASAP 2020* instrument.

The specific surface area of catalysts was determined using the multi-layer physical adsorption in single point (simplified as B.E.T. model). This model was applied directly by the instrument.

The method calculates the surface area of the sample from the volume of the gas corresponding to the monolayer adsorption. Therefore, the gas volume for the monolayer adsorption was measured from the analysis.

The single-point approximation is based on only one measurement of the pressure of adsorption and the corresponding gas volume adsorbed; the formula used is here reported:

$$\frac{P}{V(P_S - P)} = \frac{c - 1}{V_m \cdot c} \cdot \frac{P}{P_S} + \frac{1}{V_m \cdot c}$$

Where:

- *P* is the pressure;



- $P_S$  is the surface tension of the adsorbed gas (in this case nitrogen);
- $V$  is the adsorbed gas volume;
- $V_m$  is the mono-layer gas volume;
- $c$  is a constant related to the gas-surface interaction.

A second approximation made by the software concerns the constant  $c$  which is very high compared to the other variables and so the final equation is:

$$\frac{P}{V(P_S - P)} = \frac{1}{V_m} \cdot \frac{P}{P_S}$$

The error that derives from these approximations is about 7% on values over 3 m<sup>2</sup>; below this limit, the surface area calculated cannot be considered reliable.

In a typical analysis, 0,5 g of catalyst are loaded in the sample holder, and heated up to 150 °C under vacuum, in order to desorb water molecules and the impurities adsorbed on catalyst surface; after this pre-treatment, the catalyst is temperature-controlled in a bath of liquid nitrogen, at -196 °C, and a flow of gaseous nitrogen is adsorbed on the surface and in the pores of the solid sample. The instrument measures the volume of the adsorbed nitrogen and, using the equation of the B.E.T model, provides the value of the specific surface area.

### 5.2.1.2. X-ray diffraction of powder (powder-X.R.D.)

X-ray diffraction is a technique used to identify the nature of the crystalline phases and to measure the size, shape and internal stress of small crystalline regions. The information on the sample is given by the position, intensity, sharpness and width of the diffraction lines. The diffraction angle  $2\theta$  and the spacing between two planes ( $h,k,l$ )  $d$  are related by the Bragg's law<sup>169</sup>:

$$2d \cdot \sin\theta = n \lambda$$

Where:

- $\lambda$  is the wavelength of incident X-ray beam;
- $n$  is the diffraction order.

The X-ray diffraction allows to obtain information about crystalline properties of the catalysts, such as nature of the crystalline phase, crystal size and possible distortions of the lattice.

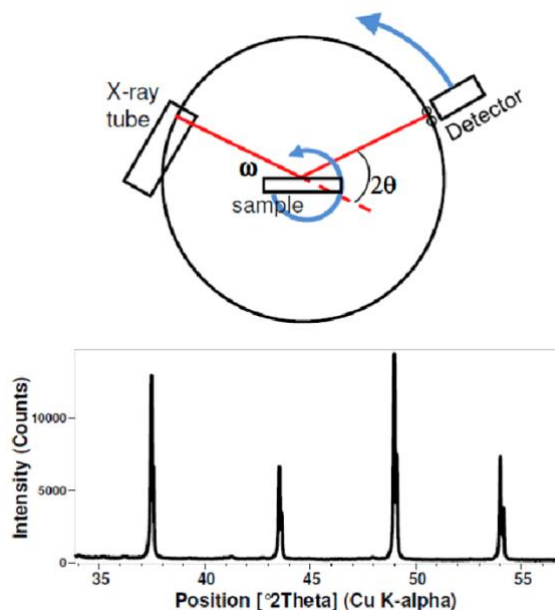


**Figure 5.11. Scheme of the X-ray diffraction experimental setup (Bragg – Brentano geometry) and pattern obtained from the analysis.**

The instrument used for X.R.D. analysis is a vertical goniometric diffractometer (Bragg – Brentano geometry) *Philips PW 1050/81* with a *PW 1710* chain counting, and the powder method has been chosen to collect diffraction patterns. The Cu K $\alpha$  radiation, made monochromatic by means of a nickel filter with  $\lambda$  of 0.15418 nm, is used for analysis; the acquisition region is  $5^{\circ} < 2\theta < 80^{\circ}$ , with steps of  $0.1^{\circ}$  and count of intensity every 2 seconds. The range of analysis is  $20^{\circ} < 2\theta < 80^{\circ}$  with a scanning rate of  $0.05^{\circ}/s$  and time-per-step = 1 s.

The interpretation of the patterns and phase identification is made by using a software from PANalytical Company and the —ICSD Database FIZ Karlsruhe library.

The *Debye-Scherrer equation* is used for the calculation of crystallite dimensions, which is related to the FWHM (Full Width at Half Maximum) through the formula:

$$\tau = \frac{K \lambda}{\beta \cos \theta}$$

Where:

- $\tau$  is the mean size of the ordered (crystalline) domains, which may be smaller or equal to the grain size;
- $K$  is a dimensionless shape factor; the shape factor has a typical value of about 0,9 but varies with the actual shape of the crystallite;
- $\lambda$  is the X-ray wavelength;
- $\beta$  is the line broadening at half the maximum intensity (*FWHM*), after subtracting the instrumental line broadening, in radians;
- $\theta$  is the Bragg angle.

### 5.2.1.3. Attenuated total reflectance IR-spectroscopy (A.T.R.-IR)

The A.T.R. spectroscopy is an IR technique used to collect information about binding force and molecular geometry of the catalyst; this method is based on attenuated total internal reflectance phenomena of IR radiation, which is transmitted through a high refractive index material, diamond crystal in this case, placed closely to the sample (described in Figure 5.12). *Brucker Alpha Platinum* IR spectrometer is used for these analysis, and no pre-treatment of the sample is necessary. IR spectra were taken with an average of 64 scan per sample at a resolution of  $2\text{ cm}^{-1}$ .

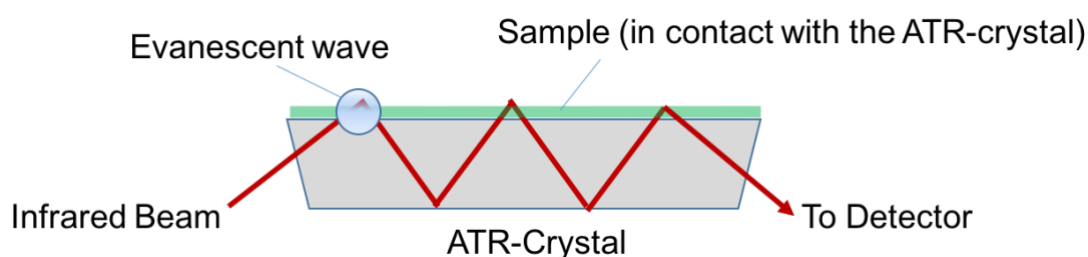


Figure 5.12. Scheme of the A.T.R. analysis.

#### **5.2.1.4. Dynamic Light Scattering (D.L.S.)**

This technique is based on the scattering by a laser beam ( $\lambda = 633 \text{ nm}$ ) that invests a colloidal suspension with a particles size between 0,6 nm and 6 m. The Brownian motion of particles occurs with a speed inversely proportional to their size. The intensity of the scattered light after interaction with the particles has a frequency of fluctuation that depends on their rate of diffusion; therefore, it is possible to derive the size of particles from the analysis of fluctuations.

The instrument is able to provide a statistical distribution of the nanoparticles size based on the intensity of scattering. It is possible to obtain two types of size distributions with respect:

- to the volume occupied by the particles;
- to the number of particles.

During the measurement, a curve showing the distribution of the particle size and the index of polydispersity of the particle size in the suspension (P.D.I.) is obtained.

The value of P.D.I. is between 0 and 1: index closer to zero means more mono-disperse size distribution:

- for the mono-dispersed suspension it is  $\leq 0,2$ ;
- if the index is between 0,2 and 0,5, the suspension is in average poly-dispersed;
- for values greater than 0,6 the distribution is definitely poly-dispersed.

The measurement of the hydrodynamic diameter of the particles in the suspension, was performed with a *Zetasizer Nanoseries* (Malvern Instruments) schematized in Figure 5.13.

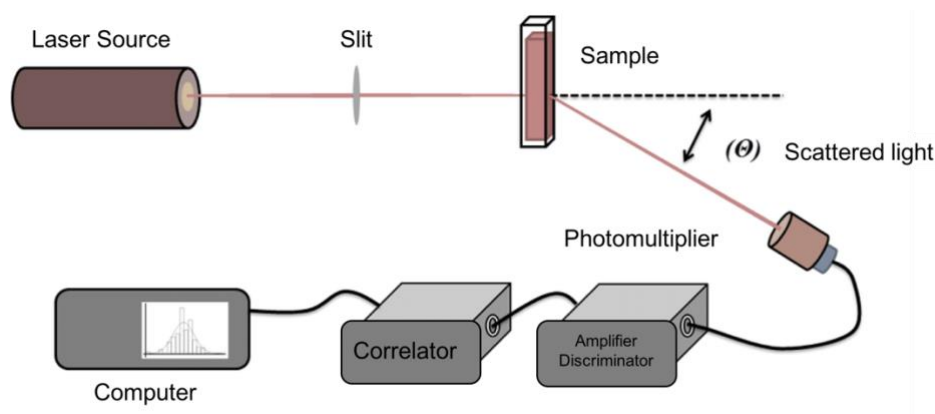


**Figure 5.13. Scheme of D.L.S. analyser.**

Before each analysis, 10 drops of samples were diluted in 10 mL of water to avoid the interactions between particles that may change the rate of diffusion and therefore the estimation of the size.

## 5.2.2. Composition

### 5.2.2.1. X-ray fluorescence (X.R.F.)

X-ray fluorescence permits to obtain information about the amount of each element present in the materials.

The instrument used for this type of analysis was a *PANalytical Axios Advanced* dispersive wavelength spectrometer; this instrument is equipped with rhodium tube of 4 kW power, and usually uses radiation in the keV order that involves exclusively the core electrons (as is possible to see from Figure 5.14).

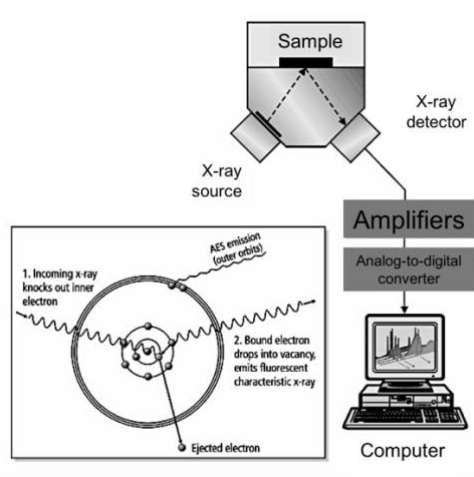


**Figure 5.14. X-ray fluorescence apparatus and scheme of the physical principle.**

The measurements were performed under vacuum. The samples were grinded and mixed with an organic wax (300 mg sample, 100 mg wax) before being pelletized.

#### **5.2.2.2. Diffusive reflectance UV-spectroscopy (DR-UV)**

DR-UV spectroscopy measures the reflected fraction of the analytical radiation which results attenuated after the interaction with the sample; this technique, which is complementary to molecular adsorption spectroscopy, allows to determine the different chemical species of an element (oxidation state, coordination).

*Perkin Elmer Lambda 19* spectrometer, equipped with a calcium sulphate integrating sphere (see Figure 5.15), was used for the analysis; the band of analysis is  $190 \text{ nm} < \lambda < 450 \text{ nm}$ , and no pre-treatment of the sample was necessary.

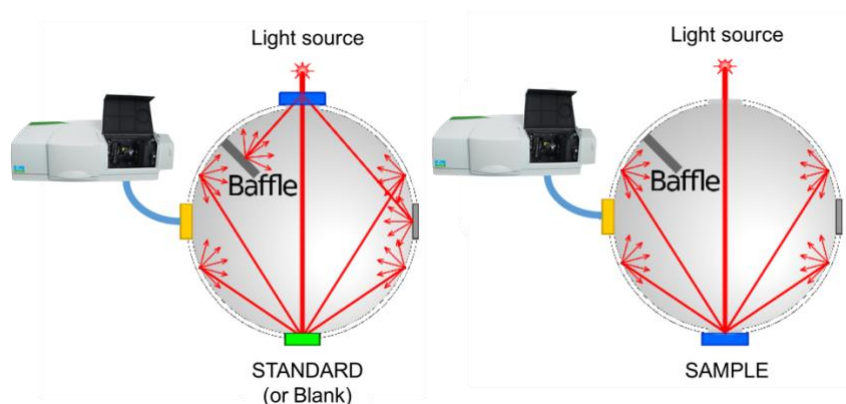


**Figure 5.15. UV-Vis instrument coupled with the integrating sphere.**

### 5.2.2.3. Thermogravimetric/differential thermal analysis (T.G.A./D.T.A.)

T.G./D.T. – analysis was used to quantify the loss of weight of samples as a function of the time/temperature. These techniques provided important physical-chemical - information, for instance the adsorption or chemisorption of molecules over the solids.

TA SDT Q600 instrument was used for the analysis of “fresh” catalysts and, in some cases, of the materials recovered at the end of the reaction (the so-called “spent” catalyst).

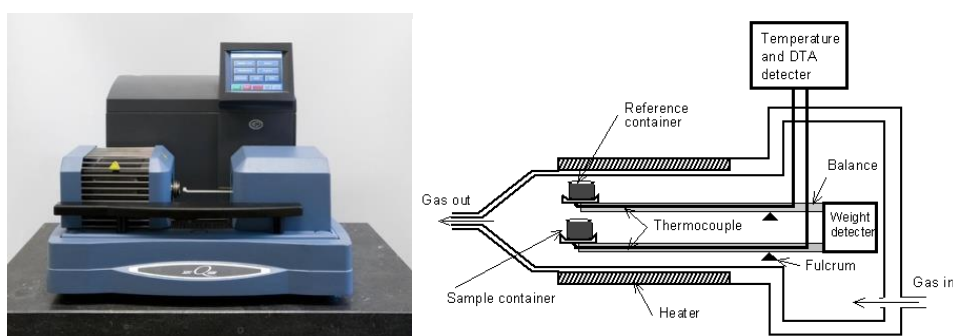


Figure 5.16. (On the left) TA SDT Q600 and (on the right) thermogravimetric analysis scheme.

In a typical analysis 20 mg of sample was loaded in an  $\text{Al}_2\text{O}_3$  – pan (container) heated up to 900 °C with a ramp of 10 °C/min while 100 mL/min of nitrogen was continuously fed.

### **5.2.3. Surface properties**

#### **5.2.3.1. Transmission electron microscopy/Scanning electron microscopy (T.E.M./S.E.M.) - Energy dispersive spectroscopy E.D.X.**

In T.E.M./E.D.X. characterization, an electronic beam of electrons was transmitted through a thin specimen interacting with it as it passes through. An image is formed from the interaction of the electrons transmitted through the sample; the image is magnified and focused onto an imaging device. Before each analysis, the samples were crushed, suspended in ethanol and homogenized using ultra-sonication (for 5 min). The suspension was deposited on a holey-carbon film Cu-grid for TEM analysis, then dried at 100 °C. The analyses were carried out by means of a microscope TEM/STEM FEI TECNAI F20 at 200 keV.

Differently from T.E.M., in the S.E.M. analysis the image is produced directly by scanning the surface through the detection of secondary electrons emitted by sample's atoms excited by the electron beam. The analyses were performed by using a *SEM Zeiss EP EVO 50* with a tungsten electron source, secondary and backscattered electrons detectors. The E.D.X. system is an *Oxford Instruments INCA ENERGY 350* including a Si(Li) detector equipped with an ultrathin window ( $Z > 4$  (Be)). The images were collected in a high vacuum mode at EHT = 20 keV and the spectra were registered for a 60 s collection time.



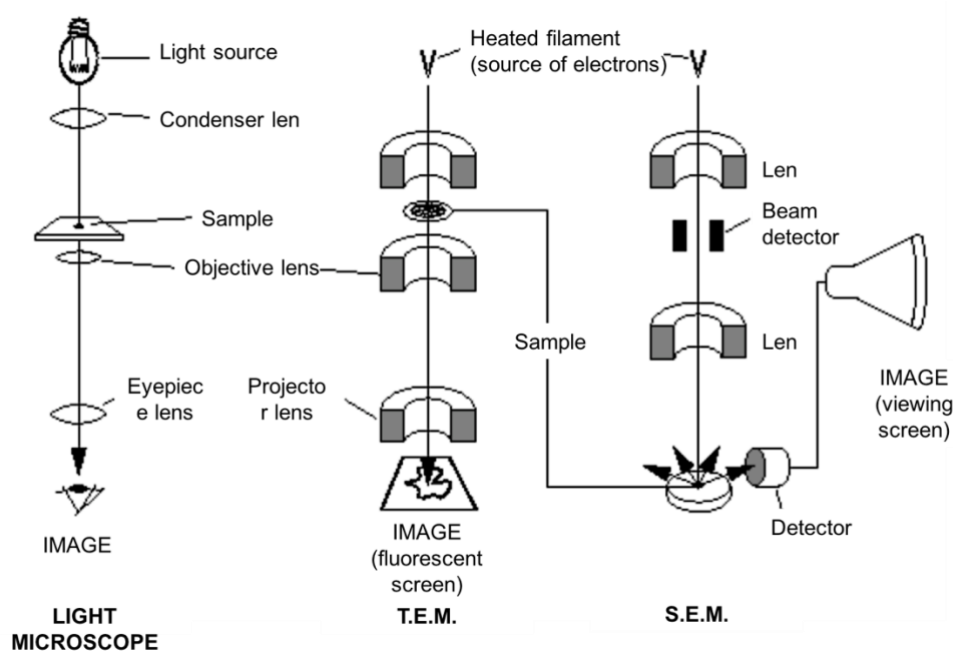


**Figure 5.17. Key differences between light microscope, transmission electron microscope (T.E.M.), and scanning electron microscope (S.E.M.).**

T.E.M. offers invaluable information on the inner structure of the sample, such as crystal structure and morphology, while S.E.M. provides information on the sample's surface and composition. Furthermore, the most pronounced differences between the two methods is the optimal spatial resolution that they can achieve: S.E.M. resolution is limited to  $\sim 0,5 \text{ nm}$ , while images with spatial resolution of less than  $50 \text{ pm}$  ( $10^{-12} \text{ m}$ ) can be achieved with T.E.M.

The energy dispersive spectroscopy E.D.X. is an additional characterization technique used for the elemental analysis or chemical characterization of the samples (the overall analytical accuracy is app.  $\pm 2\%$ ). It is worth noting, that the E.D.X. is a surface analysis technique, however it can be assimilated to a bulk analysis for nanoparticles smaller than the penetration depth of the incident beam  $x \sim 0.1 \cdot E^{1.5} / \rho^{104}$  where  $x$  is in  $\mu\text{m}$ ,  $E$  in  $\text{keV}$  and  $\rho$  in  $\text{kg m}^{-3}$ . For  $E$  15  $\text{keV}$  and  $\rho \sim 6$  the penetration depth is about  $1 \mu\text{m}$ , so the E.D.X. analysis of particles up to  $2 \mu\text{m}$  can be considered representative of the bulk composition.

## 5.2.4. Bulk and Redox proprieties

### 5.2.4.1. Temperature programmed reduction/oxidation (TPR<sub>1</sub>/O/R<sub>2</sub>)

The temperature programmed reduction-oxidation-reduction (TPR<sub>1</sub>-O-R<sub>2</sub>) analysis was used in order to characterize the materials synthesized highlighting the redox properties of each component. This analysis could be very informative because the reducibility/oxidability of the catalyst strongly depends on the particles dimension of the active phase, its metal oxidation state and its interaction with the support.

The instrument used for these analysis is a *Micromeritics Autochem 2 2920V 4.05 Chemisorption Analyzer* (Figure 5.18). In a typical analysis, 0,1 g of sample are pre-treated with an inert gas flow in order to desorb water molecules and impurities; then, the sample is heated up under controlled temperature programmed and H<sub>2</sub>/O<sub>2</sub> concentration flows. The desorbed species from the materials were measured by means of a TCD detector and a quadrupole MS. The H<sub>2</sub>/O<sub>2</sub> consumed by reduction/oxidation of the material generates a difference in TCD signal compared to the unaltered analysis gas sent directly through the detector (see left scheme in Figure 5.18). The difference is shown in a graph and peaks represent the presence of a redox species in the catalyst.

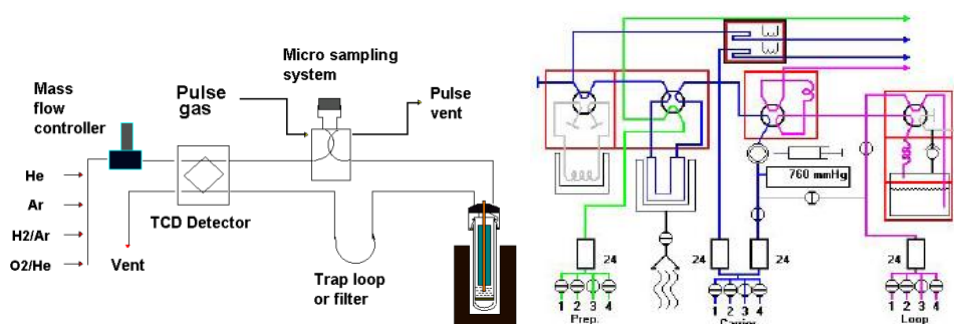


Figure 5.18. Temperature programmed reduction/oxidation instrument scheme.

Usually, TPR/O cycles are executed in order to analyse the possible recovery of the original state after the first reduction; in this thesis, for instance, a three-cycle analysis has been performed with the following analysis conditions:

1. Sample pre-treatment:
  - Gas: He;

- flow: 30 mL/min;
  - temperature ramp: 150 °C for 10 min (10 °C/min);
2. Temperature programmed reduction-1 (TPR<sub>1</sub>):
- Gas: 5%H<sub>2</sub>/Ar;
  - flow: 30 mL/min;
  - temperature ramp: 750 °C for 30 min (10 °C/min).
3. Temperature programmed oxidation (TPO):
- Gas: 5%O<sub>2</sub>/Ar;
  - flow: 30 mL/min;
  - temperature ramp: 750 °C for 30 min (10 °C/min).
4. Temperature programmed reduction-2 (TPR<sub>2</sub>):
- 5%H<sub>2</sub>/Ar;
  - flow: 30 mL/min;
  - temperature ramp: 750 °C for 30 min (10 °C/min).

## **5.3. Catalytic tests**

This chapter describes the operating procedures and apparatus used to carry out catalytic tests and the analytical techniques for the determination of the products concentration.

### **5.3.1. Bench scale high-pressure reaction vessels**

The reaction studied in this thesis was carried out in high pressures vessels using different bench - scale reactors. The apparatus employed are described below.

#### **5.3.1.1. Multiple reactor system**

The AmAr equipment Pvt. Ltd. Eco catalyst screening 6-25 was used for high throughput reactivity tests. It is generally used for conducting faster screening of catalysts by running six autoclaves in similar conditions. The standard specifications of the apparatus used are summarized below:

- six independent vessel of 25 mL with common lid;
- design pressure 100 bar (Max. Working pressure around 80% of the design pressure);
- stirring rate and heating are common for all the vessels with a bottom magnetic stirrer and Teflon bit;
- common valve for inlet and vent.

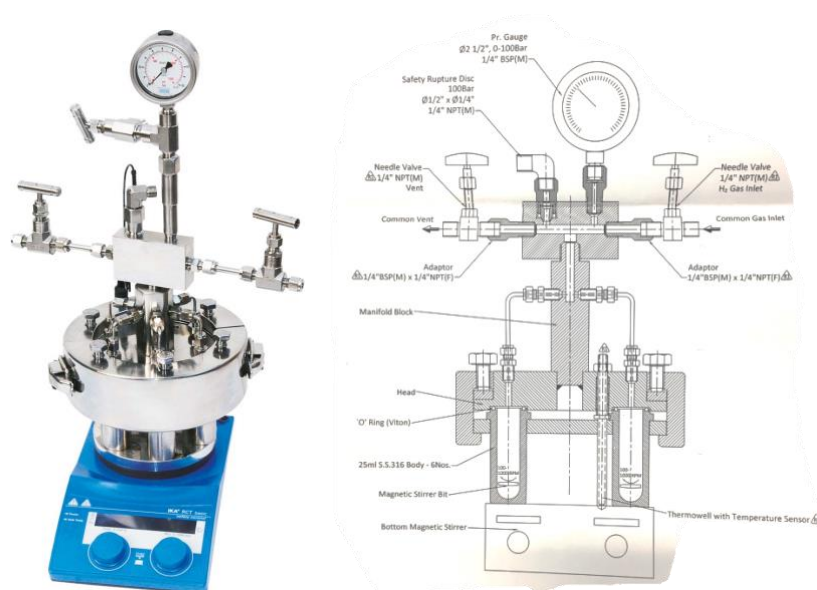


**Figure 5.19. Multiple system used for high throughput reactivity experiments; picture of the AmAr equipment used (on the left) and its schematic diagram (on the right).**

Although this apparatus shows several advantages in terms of high-throughput screening, it presents some limitations. The most important one is represented by the fact that the six vessels are connected. This aspect could be crucial in reactivity experiments with gaseous reactants because more efficient catalyst in a vessel may consume much more gas than the other ones.

In a typical test, 10 g of the starting diol was charged in every vessel with the desired catalyst (~ 1 %wt. compared to the starting material).

The apparatus was sealed, vented with nitrogen and finally pressurized with the required gas (usually oxygen) at the desired pressure. The system was heated and stirred during the reaction; the “time zero” of the reaction was taken when the reactor reached the desired reaction temperature.

At the end of the reaction time, the heating was stopped and the autoclave was cooled down without stopping the stirring. At more or less 50 °C, the multiple system was opened and the reaction mixtures were transferred into Falcon centrifuge tubes for catalyst recovery. Catalysts were then separated from the reaction mixture by means of centrifugation (4500 rpm for 15 min).

Gas chromatographic analyses of unconverted DSA and reaction products were carried out after derivatization (described in paragraph 5.3.2).

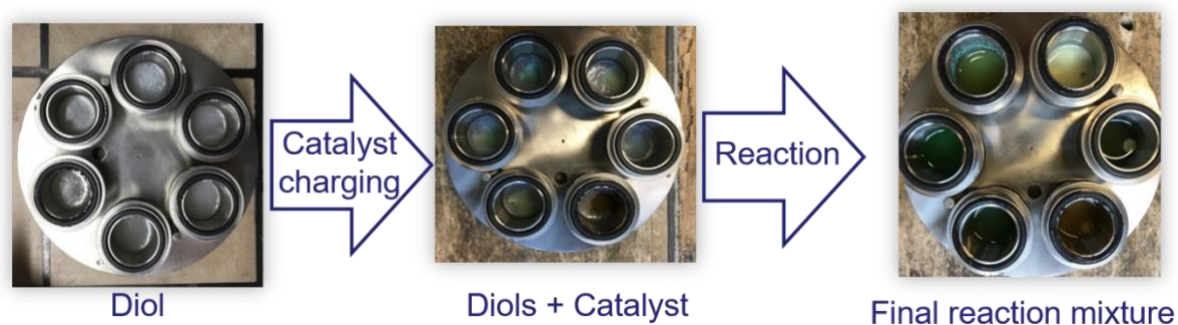


**Figure 5.20. Typical procedure implemented for the conduction of the reactivity tests in the multiple reactor system.**

### **5.3.1.2. Batch reactor**

The oxidative cleavage of DSA was conducted in a stainless steel autoclave manufactured by *AmAr equipment Pvt. Ltd.* (see the picture on the left in Figure 5.21) with a magnetic drive stirrer. Additionally, the instrument was equipped with a Teflon (PTFE) vessel with internal volume about 100mL, in order to prevent the corrosion of the steel caused by the carboxylic acids produced during the reaction.

The range of temperature was between 60 °C and 140 °C, while the time of reaction investigated was in the range between 2h and 8h.

The oxidative scission was performed without any addition of solvent, neither aqueous nor organic, with pure oxygen or air as oxidant in a pressure range between 5 and 30 bar.

The reaction apparatus is shown in the following pictures (Figure 5.21):



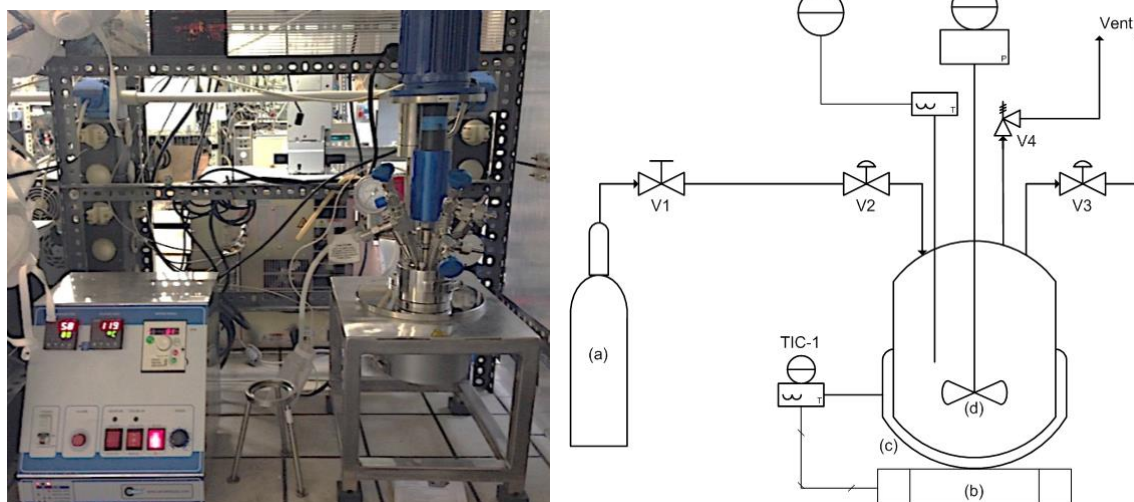


**Figure 5.21.** (On the left) *AmAr equipment* autoclave; (on the right) schematization of the high-pressure batch reactor, stainless steel autoclave: (a) O<sub>2</sub>/Air cylinder or in some cases nitrogen cylinder, V1 shut-off valve, V2 high-pressure needle valve (IN), (b) heating plate controlled by a PID (TIC-1), in order to obtain the desired reaction temperature of the oven (c), and (d) impeller with a magnetic drive stirring; V3 high-pressure needle valve (OUT) and V4 safety valve (with a nominal pressure limit of 100 bar at 500 °C) . PI-1 motor (stir).

In a standard reaction procedure, about 15 g of the starting reactant (DSA) and the catalyst (often in the amount of 1%<sub>wt.</sub> compared to the diol) were charged inside the PFTE vessel located inside the autoclave. Then, the system was sealed and purged with the desired gas (O<sub>2</sub> or Air). Subsequently, the reactor was pressurized at the desired starting pressure with the same gas and the heating was started.

At the end of the reaction time, the gas still presented was vented out while the heating was stopped. The autoclave was cooled down without stopping the stirring until the temperature of 50 °C was reached. At this point, the stirring was stopped and the autoclave was opened.

The final reaction mixture was transferred into a Falcon 50 mL conical centrifuge tubes. Catalyst was recovered by means of centrifugation (4500 rpm for 15 min). Gas chromatographic analyses of unconverted DSA and reaction products were carried out after derivatization (detail in paragraph 5.3.2).

**Note:** considering that no solvent was added to the reaction mixture, the diol had to be previously melt at roughly 50 °C.

### 5.3.2. Derivatization of the products

GC analysis was used to analyse fatty acids either as free fatty acids or as the corresponding fatty acid methyl esters (the so-called FAMES).

Nevertheless, the analysis of FAMES instead of free fatty acids presents some advantages. First of all, in their free, not derivatized form, fatty acids may be difficult to analyse because these highly polar compounds tend to form hydrogen bonds with the column's phase, leading to adsorption issues. Reducing their polarity and increasing their volatility may make them more amenable for analysis.

Secondly, to distinguish between the very slight differences exhibited by unsaturated fatty acids, the polar carboxylic groups must first be neutralized. This allows the column to perform separation by boiling point elution, degree of unsaturation and also cis/trans configuration.

Therefore, the products obtained from the reaction were derivatized in order to produce the corresponding methyl esters. These compounds offer excellent stability and provide quick and quantitative samples for GC analysis.

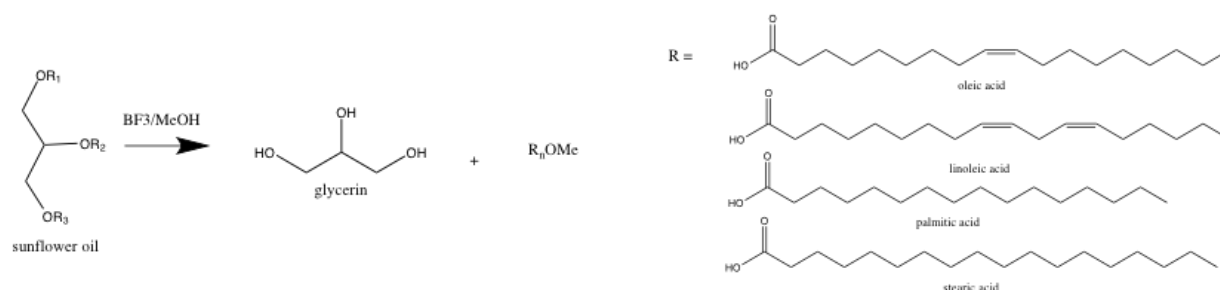


**Figure 5.22. Reaction involved during the derivatization of the oxidative cleavage products by means  $\text{BF}_3$  in  $\text{MeOH}$ .**

The procedure described in Figure 5.22 involved an acid-catalysed transesterification with methanol in order to produce fatty acid methyl esters (FAMES). As shown in the reaction mechanism reported below, the transesterification involves the condensation of the  $-\text{OR}$  group of the ester and the hydroxyl group of an alcohol (here, methanol). The reaction is best done in the presence of a catalyst, such as boron trifluoride.



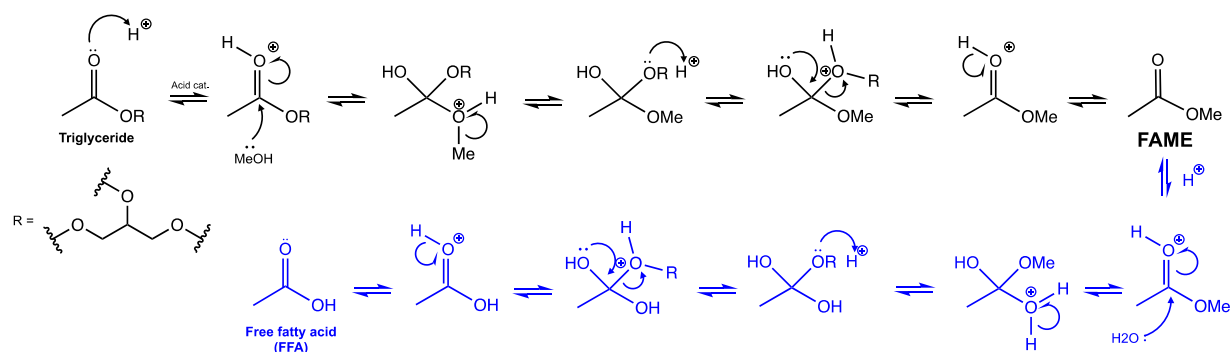


**Figure 5.23. Reaction pathways of the derivatization of the products obtained from the oxidative cleavage of triglycerides: acid-catalysed transmethylation of the triglyceride (black pathway) and the competitive acid-catalysed hydrolysis of the fatty acid methylester (blue pathway).**

As it is possible to note from the reaction scheme, water has to be removed from the reaction environment in order to prevent the side - reaction of hydrolysis (blue pathway in Figure 5.23); for this reason, 2,2' – dimethoxy propane was added to the transmethylation mixture as water-scavenger. Furthermore, this strategy was also useful for the formation of the corresponding FAME of the free fatty acids (for instance pelargonic acid) that were formed during the oxidative scission of the diol used as starting material (look at the blue pathway in Figure 5.23 from left to right).

Moreover, the derivatization process permitted also to analyze the 9,10 – dihydroxystearic acid thanks to the formation of an adduct between the scavenger (i.e. 2,2' – dimethoxypropane) and the DSA itself (see Figure 5.24).

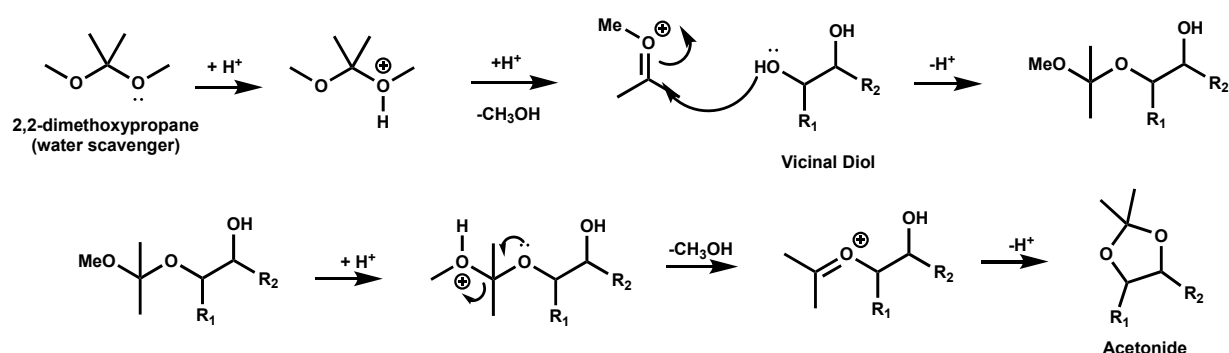


**Figure 5.24. Acid-catalysed reaction mechanism of acetonide formation from a vicinal diol and 2,2' – dimethoxy propane.**

During this reaction, water is generated and could be a problem for the transmethylation reaction (shown in Figure 5.23), favouring the hydrolysis of FAMEs.

This issue may produce an error in the quantitative evaluation of the reaction products, especially when the amount of the diol is greater (i.e. at low conversion).

The typical derivatization protocol used for the qualitative and quantitative evaluation of the reaction products is described below:

1. dissolution of 0,1 g of the reaction mixture ( $m_{\text{sample}}$ ), previously dried with  $\text{Na}_2\text{SO}_4$ , in 1 mL toluene;
2. addition of 450  $\mu\text{L}$  of internal STD (solution prepared by dissolving 1%<sub>wt.</sub> of 10-undecenoic acid and 0,8%<sub>wt.</sub> of nonadecanoic acid in 10 mL of MeOH);
3. addition of 2,8 mL  $\text{BF}_3$ /methanol (10%<sub>wt.</sub>) and 150  $\mu\text{L}$  2,2-dimethoxypropane;
4. heating of the solution at 80 °C for 1h; cooling down, then addition of 1mL of water and 1 mL of  $\text{CHCl}_3$ ;
5. careful removal of the lower (organic) layer, and drying with anhydrous  $\text{Na}_2\text{SO}_4$ .

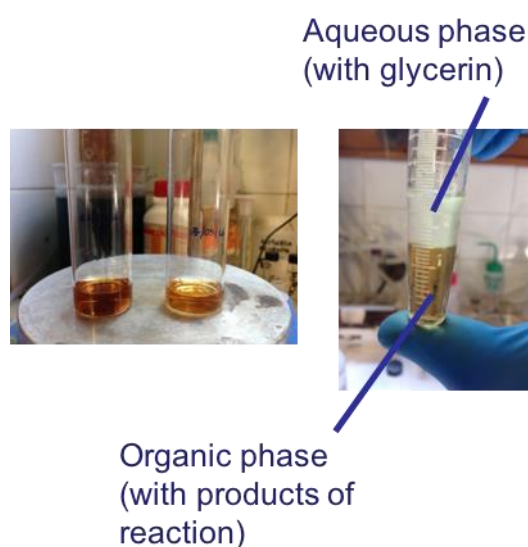


**Figure 5.25.** Final reaction mixture after derivatization (image on the left) and after extraction with water and chloroform (image on the right).

### 5.3.3. Gas Chromatography (GC) analysis

The compounds of interest were analysed and quantified using a gas-chromatograph Shimadzu GC-2025AF model equipped with auto-injector AOC-20i with syringe (Figure 5-26). A capillary column Agilent J&W DB-23 used for the analysis was specifically designed for the high-quality separation of fatty acid methyl esters (FAMES). DB-23

column is made of a highly polar phase formed of (50%-cyanopropyl)-methylpolysiloxane. The column dimensions were 60m x (ID) 0,250 mm x 0,25  $\mu$ m (thickness of the active layer).



**Figure 5-26.**  
Shimadzu GC-  
2025AF

The injector temperature was kept at 523 K (250 °C) with a split ratio of 40:1, while the carrier gas was Helium (3,8 mL/min in column). The volume of the solution injected for each analysis was about 1 $\mu$ L. The standard programmed temperature used was: the oven temperature was held at 50 °C for 5 min, then increased until 180°C at 15 °C/min, finally increased until 240 °C at 20 °C/min and kept at 240 °C for 15 min.

Below, a typical chromatogram is shown (Figure 5.27); for each compound (after derivatization, described in paragraph 5.3.2) its retention time is highlighted.

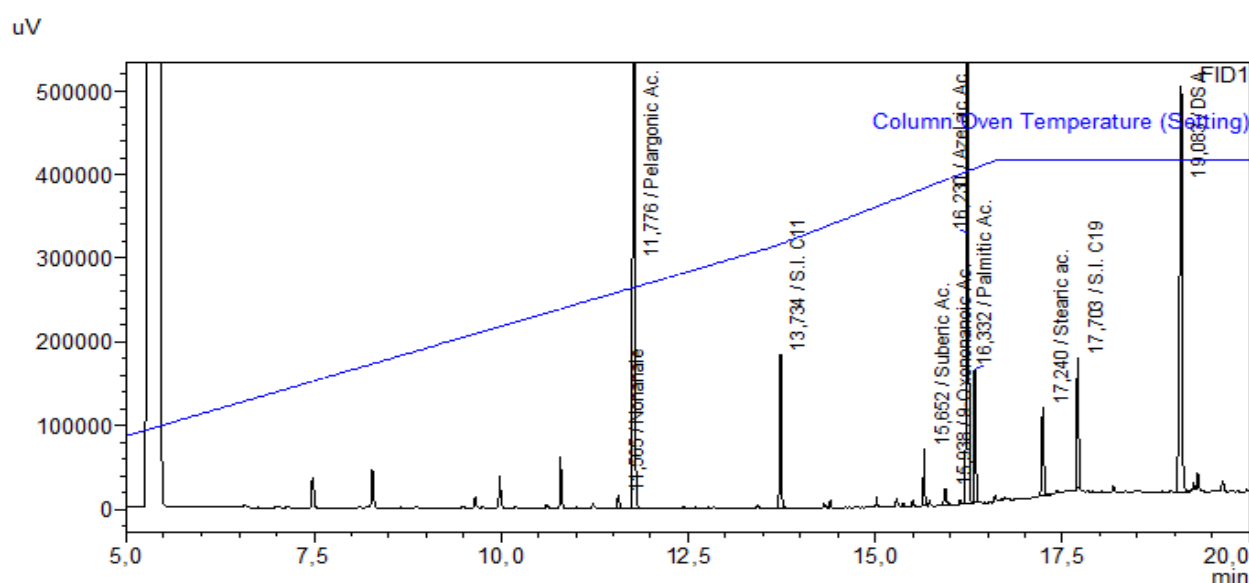


**Figure 5.27. Typical Chromatogram of reaction products obtained by Gas Chromatography analysis with DB-23 column (after derivatization with BF<sub>3</sub>/MeOH).**

Each compound was calibrated by using the reference standard compound (see Figure 5.28) in an appropriate range of concentrations. In this way, it was possible to obtain a specific response factor ( $f_i$ ), using the appropriate internal standard mixture formed by

1%<sub>wt.</sub> of 10-undecenoic acid (STD\_C11) and 0,8%<sub>wt.</sub> of nonadecanoic acid (STD\_C19) in methanol, according to the formula:

$$(1) \quad \frac{A_i}{A_{STD}} = f_i \cdot \frac{m_i(g)}{m(g)_{STD}}$$

Considering that the compounds analysed in this study were in the range of C5 to C18 atoms, the use of two standards was required in order to enhance the accuracy of the analysis.

### **5.3.4. Gas Chromatography – Mass Spectrometer (GC-MS) analysis**

The unknown products were also analysed by means of gas chromatography combined with a mass spectrometer detector.

The GC-MS used was an *Agilent Technologies 6890N* GC coupled with a mass spectrometer *Agilent Technologies 5973 Inert system* with ionization filament EI (electron impact) and quadrupole mass analyser-photomultiplier (MSD).

The capillary column installed on this instrument was a non-polar column *Agilent J&W HP-5MS* (5% Phenyl - 95% methylsiloxane), 30m x (ID) 0,250 mm x 1,05 µm.

Helium was used as carrier gas at a flow rate equal to 1mL/min; the injector was maintained at a temperature of 250 ° C in the split mode (40:1); total flow was 23,9 mL/min. The volume of solution injected was about 0,5 µL.

The separation of the compounds took place according to the following program: 5 min at 50 °C, then ramp 15 °C/min until 180 °C and finally 20 °C/min until 240 °C and kept at this temperature for 15 min.

Note that the temperature program was the same used for products analyses with GC (see paragraph 5.3.3.). In this way, a rough comparison of the retention time obtained with the two instruments was possible.

## 5.3.5. Expression of the results

### 5.3.5.1. Catalysts screening

During the first part of this research, particularly during the initial catalysts screening, it was assumed that the starting material used for reactivity tests contained only DSA and no other compounds formed during the previous hydroxylation step (see chapter 6.1.2 for details). This strategy was used to speed up the research of a new catalytic system. Furthermore, only the two products of interest, i.e. pelargonic and azelaic acids, and the diol were quantitatively evaluated at the beginning. These compounds were calibrated with commercial standards (see Figure 5.28 for an example of calibration curve) after the derivatization procedure described in chapter 5.3.2.

Therefore, due to the approximations described above, the conversion of 9,10-dihydroxystearic acid and yields of azelaic and pelargonic acids were calculated with the equations shown below:

$$(2) X_{DSA}^{screen} = \frac{m_{DSA}^i - m_{DSA}^f}{m_{DSA}^i}$$

$$(3) Y_{i,DSA}^{screen} = \frac{m_i^f}{m_{DSA}^i}$$

(with  $i$  = Pelargonic Acid or Azelaic Ac.)

Values of  $m_i^f$  were obtained directly from the GC area of each compound using the response factor derived from the calibration and equation (1).

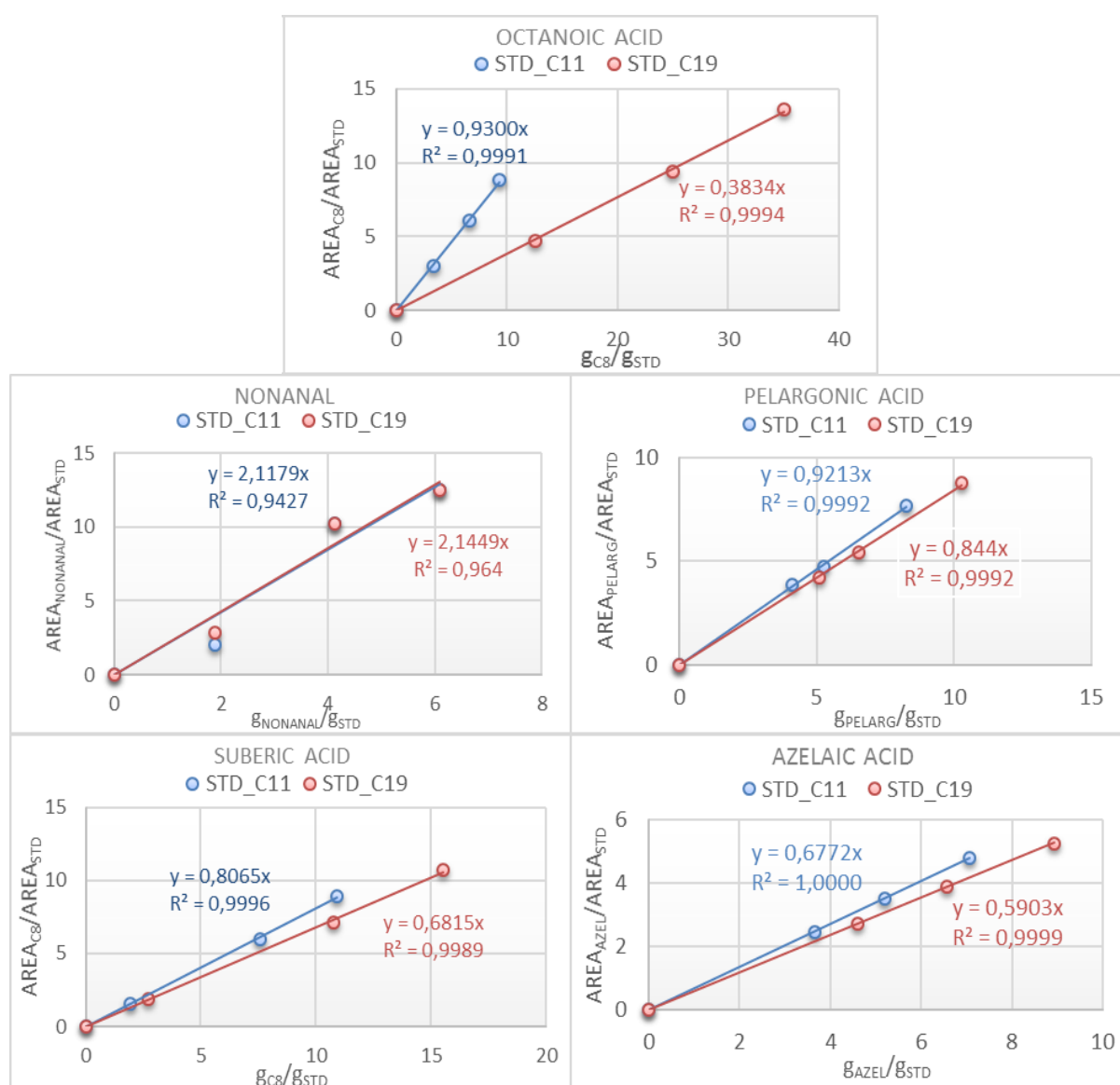
Notice that with these approximations the  $m_{DSA}^i$  corresponded to the mass of the derivatized sample. Therefore, the conversion of the diol was overestimated during the catalysts screening.

### 5.3.5.2. Further reactivity tests

After the initial screening, the analytical method used for the quantitative determination of reaction products was refined.

First of all, the formation and determination of the by- and co-products of the reaction were investigated more in detail; therefore, the calibration of the other species formed during the reaction was carried out by using reference standard compounds, in order to calculate each GC response factor.

Figure 5.28 shows an example of calibration curves for each product, after the transmethylation with  $\text{BF}_3/\text{MeOH}$ .



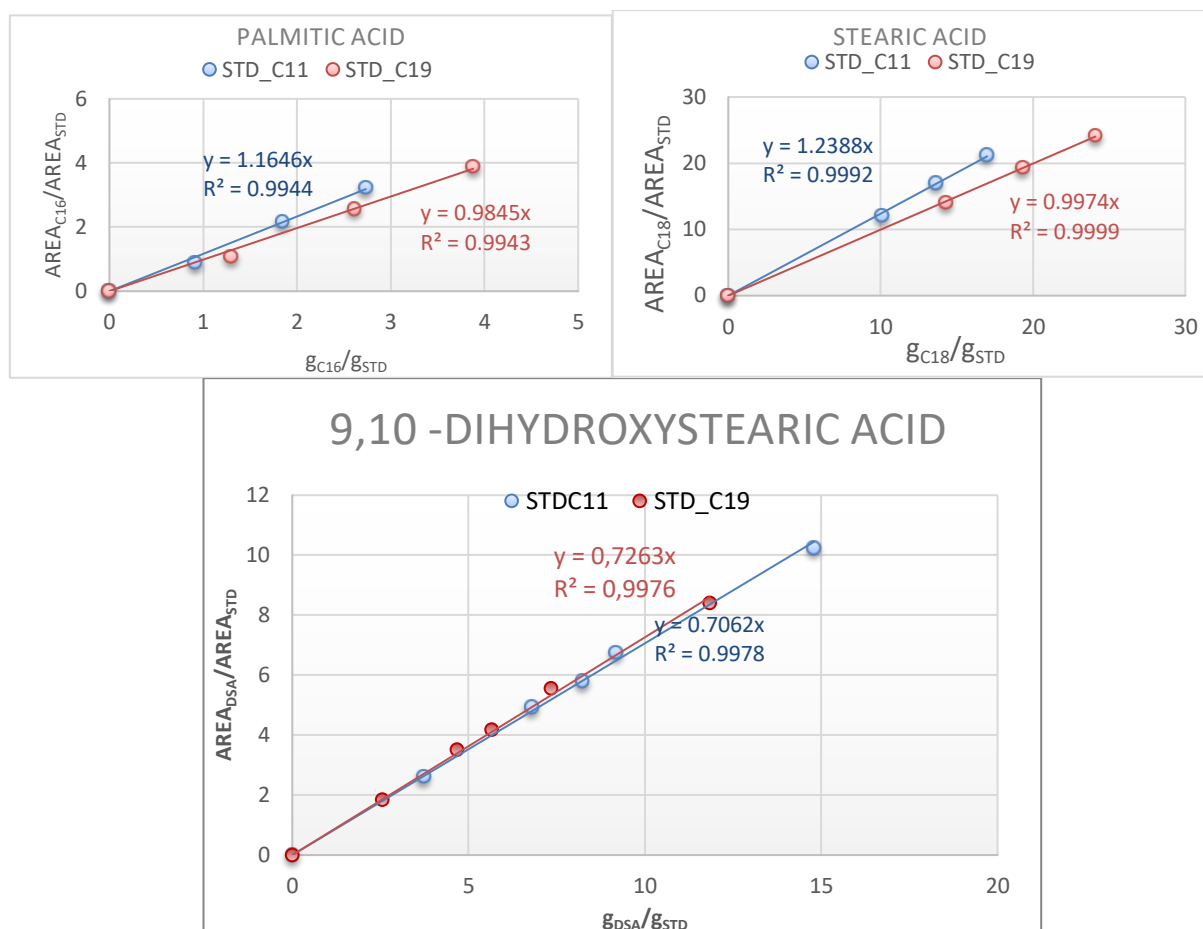


**Figure 5.28. GC Calibration curves for products and main by-products formed in DSA oxidative cleavage (in the form of methyl esters).**

Moreover, it was discovered that some compounds were already inside the starting material (chapter 6.1.2); among them, also the two desired acids (PA and AA) were already present in the raw diol.

For these reasons, the conversion of DSA and yields of the main products obtained from the oxidative cleavage were calculated using the formulas shown below:

$$(4) X_{DSA} = \frac{\%p_{DSA}^0 - \%p_{DSA}}{\%p_{DSA}^0}$$

$$(5) Y_{i, DSA} = \frac{\%p_i - \%p_i^0}{\%p_{DSA}^0}$$

(Where  $\%p_i^0$  represents the amount of the  
(i – esim compound already present in the starting material)).

The  $\%p_i$  was derived from the equation (1) as follows:

$$(6) \%p_i = \frac{\frac{AREA_i}{AREA_{STD}} \cdot m_{STD}}{m_{sample}}$$

(With  $m_{sample}$  = weight of the sample used for the derivatization step, see step(1) *paragraph 5.3.2*).

In order to have an idea of the sustainability of the whole value chain, the overall PA and AA yields were also evaluated, as calculated based on the original oil used for the hydroxylation step (see *paragraph 6.1.2*):

$$(7) Y_{i, Starting\ oil} = \frac{\%p_i}{\%p_i^{MAX}} \times 100$$

Where  $\%p_i^{MAX}$  is the weight percentage potentially obtainable from the starting oil if all the components were cleaved. For instance, considering the complete conversion of the mono-unsaturated oleic acid (and di-unsaturated linoleic acid), the maximum wt. percentage obtainable was 37 %wt. for PA and 48 % wt. for AA.

Additionally, equation (7) was also commonly used for the comparison of different catalytic systems.



## 6. RESULTS AND DISCUSSION

In this Chapter, the results of catalysts characterization and of reactivity experiments will be presented.

The following chapters describe step by step how the results have been achieved. The first milestone of the study was the screening of several heterogeneous catalysts commonly employed as oxidation catalysts. Then, the research was focused on the best catalysts discovered and the influence of several reaction parameters was investigated. For each class of catalysts, the relationship between the results of the experiments and their physical-chemical properties was searched for and discussed in detail.

### 6.1. Oxidative cleavage of glycols derived from unsaturated fatty acids

#### 6.1.1. Introduction

The oxidative cleavage of vicinal diols is an important reaction for the synthesis of ketones, aldehydes and carboxylic acids (Figure 6.1). This reaction can be performed using stoichiometric oxidants which, however, cause the formation of a large amount of inorganic waste; therefore, the research on this reaction with greener oxidants, such as hydrogen peroxide (HP) and oxygen, was carried out in depth<sup>170</sup>.

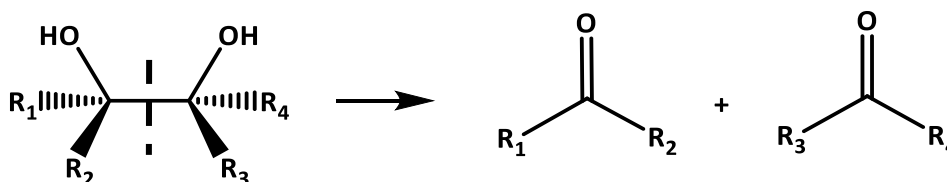
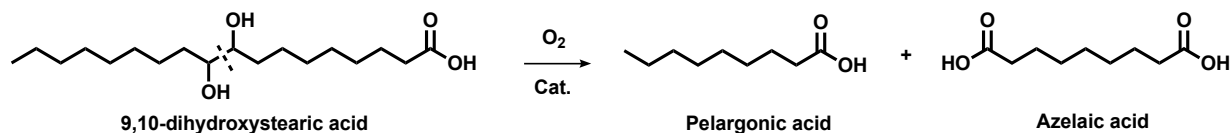


Figure 6.1. Possible products of the oxidative cleavage of vicinal diols.

This work was focussed on the study of the oxidative cleavage of 9,10-dihydroxystearic acid (DSA) into azelaic and pelargonic acids with molecular oxygen as the oxidant (see Figure 6.2).



**Figure 6.2. Products of the catalytic oxidative cleavage of 9,10-dihydroxystearic acid with oxygen.**

In this study, the role of different catalysts was investigated. Several alternative systems were proposed for the screening in order to find a suitable catalyst for the oxidative cleavage. Systems selected for testing were:

- iron oxide based catalysts, e.g. *ferrites*;
- supported gold nanoparticle;
- iron-substituted Keggin-type polyoxometalate;
- copper-based catalysts.

Firstly, various classes of iron oxide-based catalysts were investigated; these systems have been studied for oxidation reactions with molecular oxygen for years. For instance, spinel-type mixed oxides (e.g.  $NiFe_2O_4$ ,  $CoFe_2O_4$ , etc.) were used for the aerobic oxidation of cyclohexane to cyclohexanol/cyclohexanone<sup>171</sup>, or the oxidation of benzyl alcohol to benzaldehyde<sup>172</sup>.

Furthermore, Mn/Fe/O was reported for the oxidation of 2-hydroxymethylfurfural to 2,5-furandicarboxylic acid<sup>173</sup>.

In literature, ferrites have been already shown to be good catalysts for the oxidation of cyclohexene into adipic acid (used for the synthesis of nylon 6,6)<sup>174, 175</sup>.

Another catalyst used for the oxidative cleavage of DSA was based on supported gold nanoparticle.

A third interesting class of catalysts are the Keggin polyoxometalates<sup>176</sup>. A polyoxometalate substituted with iron was also prepared and used for DSA cleavage. Indeed, it is well-known that mixed Mo-V Keggin-type catalytic systems have interesting applications as oxidation catalysts in reactions carried out with air or molecular oxygen.

In fact, their redox potential is such that they can establish catalytic cycles where the mixed POM is first reduced while oxidizing the substrate, and then is re-oxidized with oxygen, as proposed by Weinstock<sup>177</sup>:

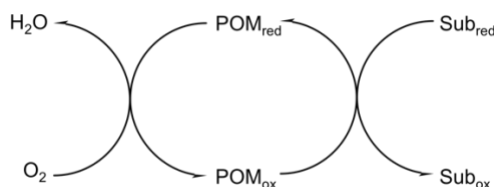


**Figure 6.3. Catalytic cycle promoted by polyoxometalates.**

However, a big practical disadvantage of this class of compounds is that POMs are generally soluble in most solvents and the separation from the reaction mixture is very difficult. The catalytic activity of POMs in oxidation reactions and oxidative cleavage is already known and this type of catalyst is amongst the most active ones<sup>178 179 180</sup>. For instance, Brégeault et al performed the oxidative cleavage of 1,2-cyclohexanediol using a P/Mo/V heteropolyacid catalyst in ethanol at 75 °C, and obtained 90% selectivity to the diethyl ester of AA with 62% reactant conversion<sup>181</sup>.

Finally, copper-based catalysts were prepared and used for DSA oxidation. These systems are also reported in literature as efficient catalysts for the oxidation of CO to CO<sub>2</sub><sup>182</sup>.

### 6.1.2. Characterization of the starting material

The starting reactant was kindly provided by Matr ca S.p.A. and Novamont S.p.A., and it was obtained from the *hydroperoxidation* of a specific vegetable oil in the Matr ca's pilot plant.

The vegetable oil chosen as feedstock for the production of the vicinal glycol is a high-oleic oil. An example of fatty acids composition is reported in Table 6-1.

**Table 6-1. Example of fatty acids distribution of a high-oleic vegetable oil exploitable for the oxidative cleavage process.**

Component	CN/DB	%p <sub>i</sub>
Palmitic acid	C 16:0	4,2
Palmitoleic acid	C 16:2	0,1
Stearic acid	C 18:0	2,8
<b>Oleic acid*</b>	<b>C 18:1</b>	<b>83,8</b>
Linoleic acid*	C 18:2	7,9
Linolenic acid	C 18:3	0,1
Arachidic acid	C 20:0	0,1
Behenic acid	C 20:0	0,1

\*unsaturated fatty acids suitable for the production of AA and PA

The vegetable oil described above is only an example of the starting feedstock for the process; many other vegetable oils can be used, as long as they possess unsaturated fatty acids.

In the dihydroxylation process the unsaturated fatty acids present in the starting triglyceride are converted to vicinal glycols as follows:

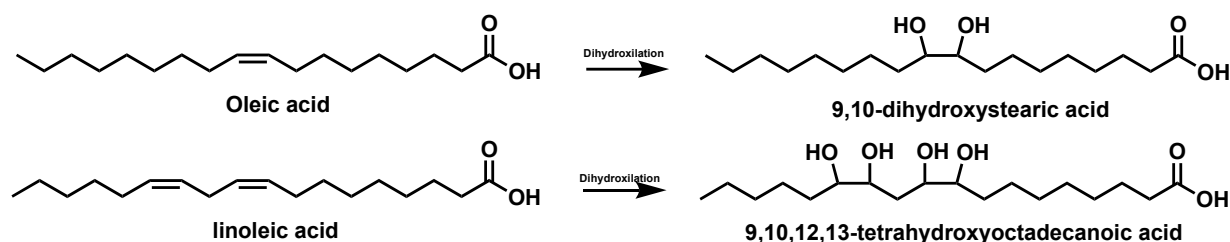


**Figure 6.4. Products of the dihydroxylation process of mono- and di-unsaturated fatty acids.**

These compounds represent the reagents that have to be converted by oxidative scission into saturated shorter-chain mono- and dicarboxylic acids.

The dihydroxylated vegetable oil used as starting material appeared as a sticky whitish wax (melting point about 57 °C) and in its fluid form it acted as a medium in which the reaction takes place. Its composition is presented in Table 6-2:

**Table 6-2. Composition of the dihydroxylated vegetable oil used as reagent for the oxidative cleavage.**

Compounds:	%p <sup>0</sup> <sub>i</sub>	σ
Octanoic Ac.	0,2%	0,1%
Nonanale	1,7%	0,3%
Pelargonic Ac.	4,6%	0,7%
9-oxononanoic Ac.	2,2%	0,2%
Azelaic Ac.	9,0%	1,3%
Palmitic Ac.	3,9%	0,5%
Stearic ac.	2,5%	0,4%
DSA	70,6%	3,0%

As highlighted in the table above, the two target compounds (i.e. azelaic and pelargonic acids) were already present in the DSA.

Nevertheless, it is very important to know exactly the compounds contained in the starting reagent for the correct evaluation of the yields of the scission products and conversion of the diol (see paragraph 5.3.5.2).

Additionally, the diol produced exhibits a certain degree of uneven composition, as shown in Figure 6.5 and Table 6-3.

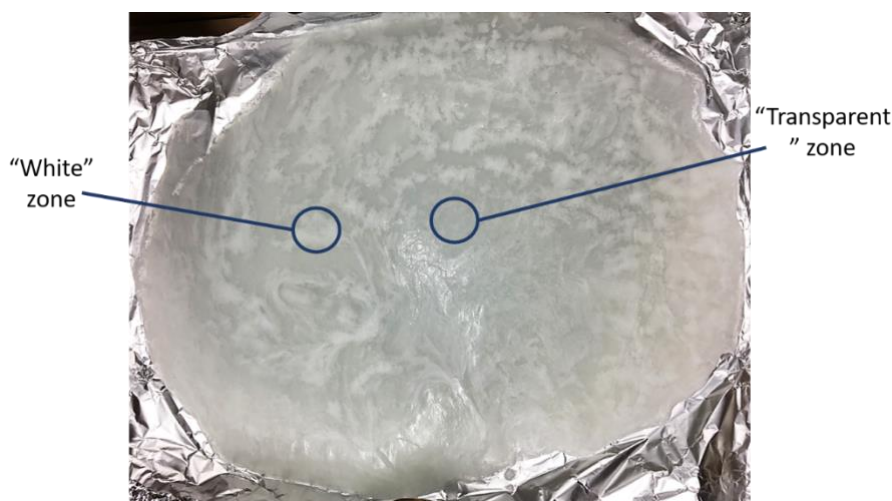


**Figure 6.5. Uneven composition of the starting material used for the catalytic tests.**

From Table 6-3, it is clear that the major variance in composition is related to the 9,10-dihydroxystearic acid itself (DSA). This could be a source of analytical errors, especially at low conversion of the glycol.

**Table 6-3. Percent difference for each compound in “white” and “transparent” zones (see Figure 6.5) of the starting material used for the catalytic tests.**

COMPOUNDS	$\Delta$ composition
Octanoic Ac.	0,3%
Nonanale	0,7%
Pelargonic Ac.	0,9%
Aldehyde Azel.	0,6%
Azelaic Ac.	0,8%
Palmitic Ac.	1,1%
Stearic ac.	0,9%
DSA	11,5%

Therefore, the starting material used in this work was quite difficult to employ without incurring in some reproducibility problems.

## **6.2. Catalysts screening**

The first part of this work was aimed at the investigation of a possible alternative to the conventional catalyst already used in industry (i.e. toxic metal salts or ozonolysis).

In this chapter, the results of catalysts screening and characterization are reported and discussed.

### **6.2.1. Catalysts Characterization**

Here, the physical and chemical characterization of materials used are briefly described.

#### **6.2.1.1. Mixed metal oxides with spinel structure**

##### **The effect of thermal annealing on bulk characteristics**

A sample having Cu/Fe atomic ratio equal to 1/4 was prepared (code of the sample: CuFeO14). In previous studies carried out in our laboratory<sup>183 184</sup>, it was shown that the annealing temperature significantly affects the structure of the materials, as it can be seen in Figure 6.6, where the X-ray diffraction patterns of the copper ferrite both as synthesized and annealed at 250 °C, 450 °C and 750 °C (temp. ramp. 10 °C/min), are shown.

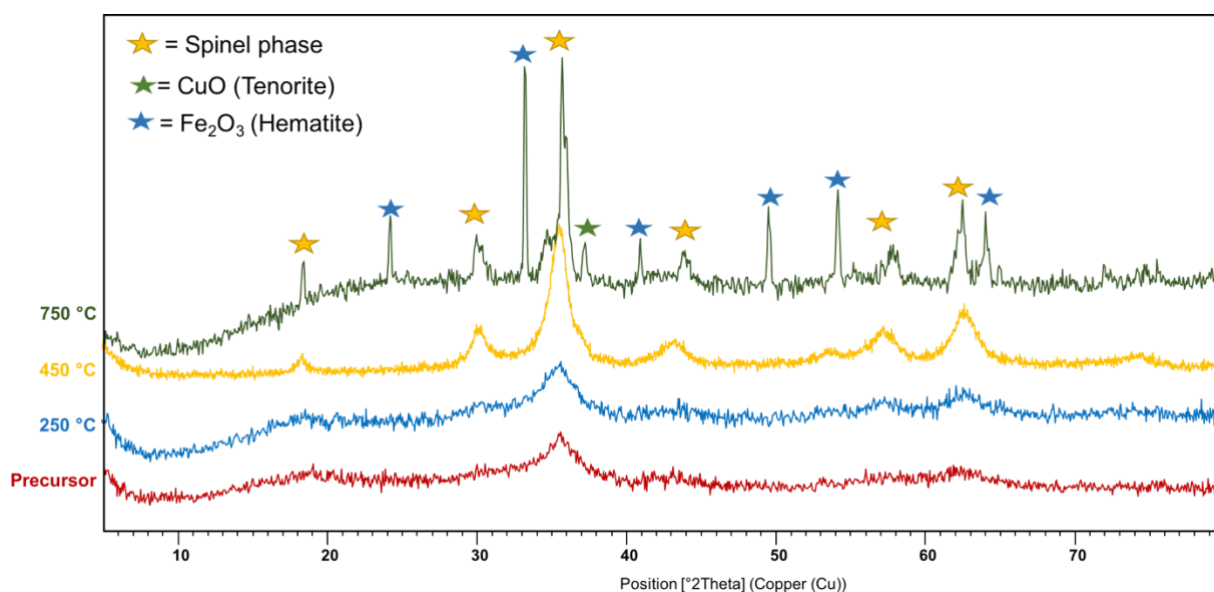


**Figure 6.6. (From the top) X.R.D. pattern of CuFeO<sub>14</sub> calcined at 750 °C, 450 °C, 250 °C and of the corresponding precursor.**

The pattern shown corresponds to that one typical of the spinel structure, with reflections at 18°, 30°, 36°, 43°, 57°, 63° 2 $\theta$ . It is possible to note that on increasing the annealing temperature, reflections became narrower. This indicates the presence of larger particles caused by sintering phenomena promoted by the high temperature. Moreover, the sample calcined at 750 °C showed the presence of several additional peaks highlighting the formation of different crystalline phases. These features could be reasonably caused by the segregation of copper from the spinel structure of magnetite. This segregation can be favoured by the higher ionic radii of Cu<sup>2+</sup> (0,73 nm) compared to Fe<sup>2+</sup> (0,70nm). Furthermore, the segregation of copper facilitates the formation of iron oxide, for instance hematite, rather than magnetite.

A further confirmation of the particle size increase was obtained from the results of the B.E.T. specific surface area measurement, reported in Table 6-4.



**Table 6-4. B.E.T. surface area obtained with copper ferrosipinel annealed at different temperature.**

SAMPLE	Thermal treatment	ASS <sub>B.E.T.</sub> m <sup>2</sup> /g
<i>CuFeO14 precursor</i>	Dried 120°C overnight	241
<i>CuFeO14</i>	Calc. 250°C for 8h (10°C/min)	231
<i>CuFeO14</i>	Calc. 450°C for 8h (10°C/min)	86
<i>CuFeO14</i>	Calc. 750°C for 8h (10°C/min)	3

It was possible to conclude that an increase of the calcination temperature led to a decrease of the specific surface area from values close to 240 m<sup>2</sup>/g for the precursor down to 3 m<sup>2</sup>/g for the sample annealed at 750 °C.

According to these results and to reactivity results (described later in this thesis), the preferred calcination temperature for all the M-modified ferrosipinels was 450 °C, for 8 hours (10 °C/min) in static air.

### **Characterization of the M-modified ferrosipinels**

As described in chapter 5.2, the characterization techniques used were powder-X.R.D., B.E.T. and T.P.R./O. analysis which allowed us to investigate the structural and redox properties of the mixed oxides.

Metal-modified ferrosipinels (with M/Fe ratio 1/2) were initially analysed by means of X-ray Powder Diffraction (X.R.D.), in order to confirm the formation of the spinel structure. X.R.D. patterns of the co-precipitated solids were registered after annealing at 450 °C for 8 hours. Results are reported in Figure 6.7.

Patterns demonstrated the successful development of the spinel phase for all the materials synthetized. In the case of magnetite, Co-, Ni- and Cu- ferrites, the spinel

phase was formed after the thermal treatment at 450 °C, as evident from reflections at 2θ: 18°, 31°, 36°, 44°, 54°, 58°, 63°, 75°<sup>185</sup>.

Nevertheless, the synthesized magnetite appeared poorly crystalline, since its reflections were quite broad.

Both cobalt-ferrite and nickel-ferrite showed the same diffractograms of the magnetite. However, comparing the two patterns, NiFe<sub>2</sub>O<sub>4</sub> seemed to be less crystalline than CoFe<sub>2</sub>O<sub>4</sub> since its reflections were broader. This was also confirmed by B.E.T. results shown in Table 6-6: Ni-ferrite had higher surface area compared to Co-ferrite.

In the case of copper ferrite, the cuprospinel was still the main crystalline compound; however, the presence of several spurious peaks pointed out that a part of Cu did not enter the pattern of the ferrite but remained segregated in the form of copper oxide (CuO) (Table 6-7). As already mentioned in this chapter, M<sup>2+</sup> segregation, which did not occur with the other materials, can be linked to the higher ionic radii of Cu<sup>2+</sup> compared to Fe<sup>2+</sup>. In fact, as shown in Table 6-5, copper has significantly higher size and mass compared to the other metals.

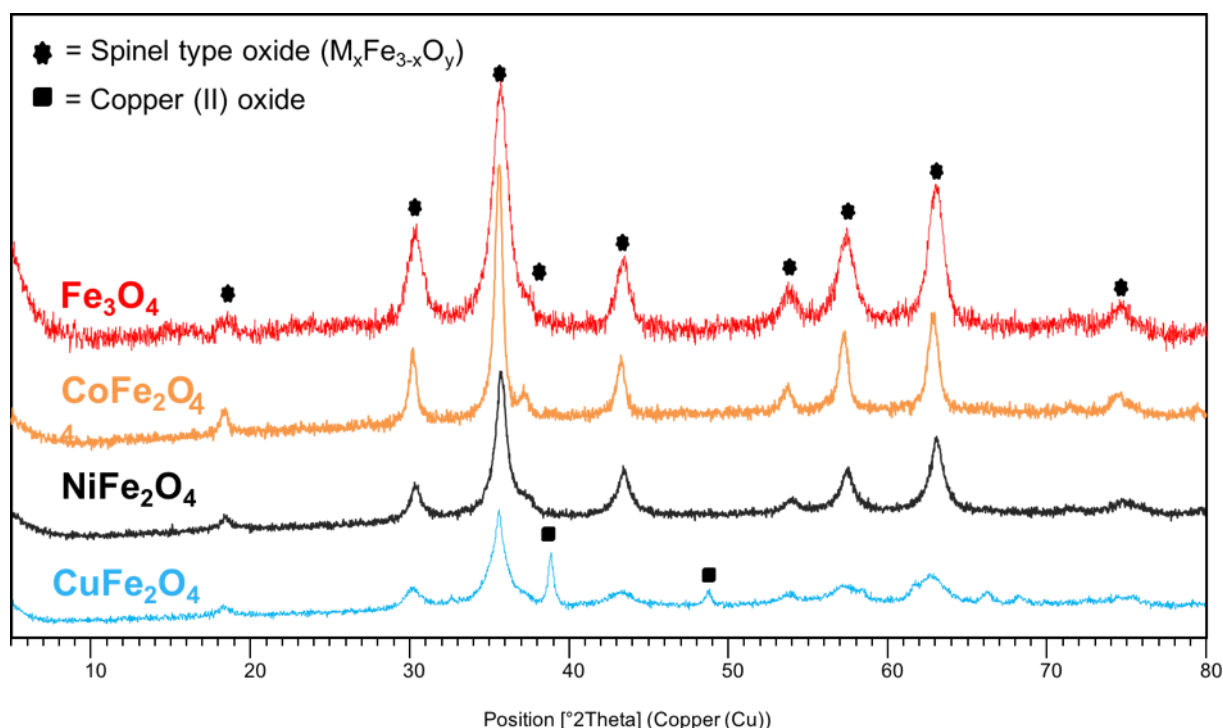


Figure 6.7. X.R.D. patterns of the “fresh” materials calcined at 450 °C for 8h (10 °C/min).

**Table 6-5. Ionic radii and masses of the different divalent ions.**

Compound	Oh ionic radii (nm) <sup>1</sup>	Atomic mass
$Fe_3O_4$	0,61	55,8
$CoFe_2O_4$	0,65	58,9
$NiFe_2O_4$	0,69	58,7
$CuFe_2O_4$	0,73	63,5

<sup>1</sup>For the divalent ion into the inverse-spinel structure:  $A_{Oh}^{2+}B_{(Oh,Th)}^{3+}_4O_4^{2-}$ .

The specific surface area of the co-precipitated materials is reported in Table 6-6; it is possible to note that although the surface area values were similar for all materials, small differences exist. These results allowed us to rank the surface area of the different solids annealed at 450 °C in the order:  $NiFe_2O_4 > Fe_3O_4 > CuFe_2O_4 \geq CoFe_2O_4$ .

**Table 6-6. specific surface area of M-modified ferrosinels calcined in static air at 450 °C for 8h (10 °C/min).**

CATALYST (annealed @ 450°C)	ASS <sub>B.E.T.</sub> (m <sup>2</sup> /g)
$Fe_3O_4$	85
$CoFe_2O_4$	72
$NiFe_2O_4$	94
$CuFe_2O_4$	74

### 6.2.1.2. Gold nanoparticles

The measurement of the hydrodynamic diameter of the nanoparticle suspension obtained by the synthesis reported in paragraph 5.1.2. was performed with the Dynamic Light Scattering. Figure 6.8. displays the distribution of the nanoparticles size. It is possible to conclude that the average hydrodynamic diameter of the particles was 11,7 nm. The P.D.I. was about 0,2 confirming that the synthesis of a mono-dispersed suspension was achieved.

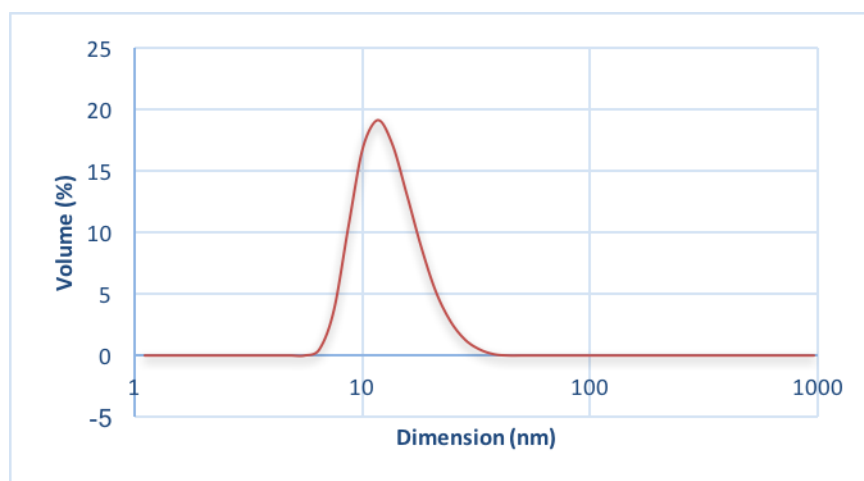


**Figure 6.8. D.L.S. analysis of Au particle dynamic size for the suspension used for Au/TiO<sub>2</sub> catalysts preparation; average particle size is 11,7 nm.**

Supported catalysts were examined by high resolution transmission electron microscopy (HR-T.E.M.) for gold particles size distribution and dispersion. Figure 6.9 shows the T.E.M. images of Au<sub>NP</sub>/TiO<sub>2</sub> catalyst at three different enlargements, while Figure 6.10 reports the size distribution.

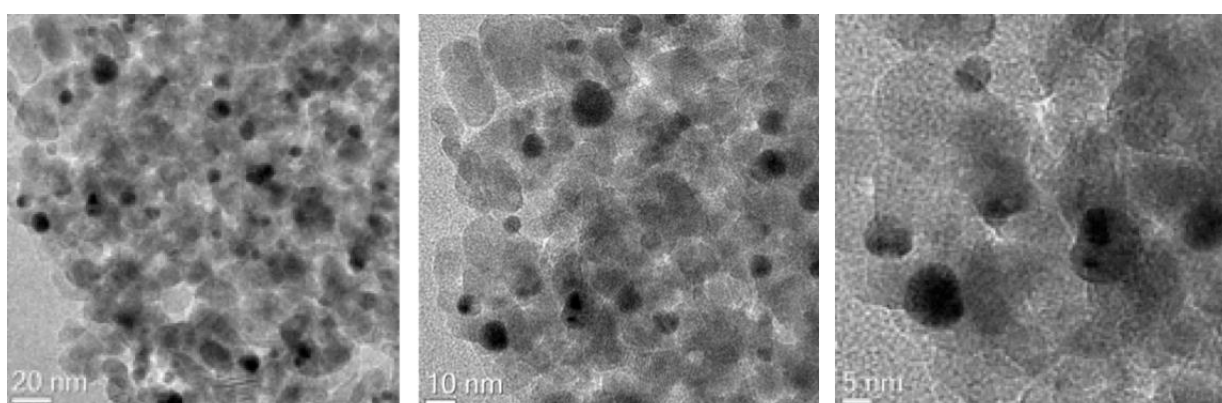


**Figure 6.9. HR-T.E.M. images of Au/TiO<sub>2</sub> (Au loading = 1,5 %wt.) catalyst.**

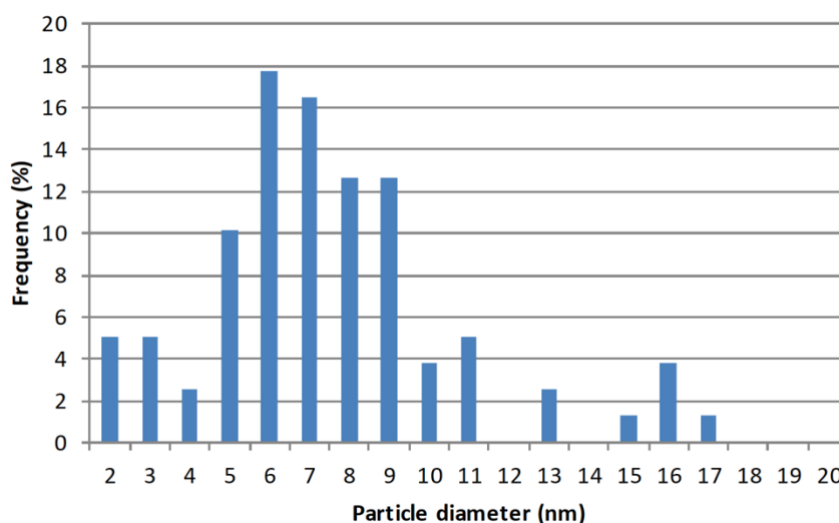


**Figure 6.10.** Size distribution calculated from T.E.M. analysis over  $\text{Au}_{\text{NP}}/\text{TiO}_2$  (Au loading = 1,5 %wt.).

The average nanoparticles size was about 7,4 nm and the dispersion was 15,7%.

The X.R.D. pattern of gold nanoparticle supported on  $\text{TiO}_2$  is shown in Figure 6.11.

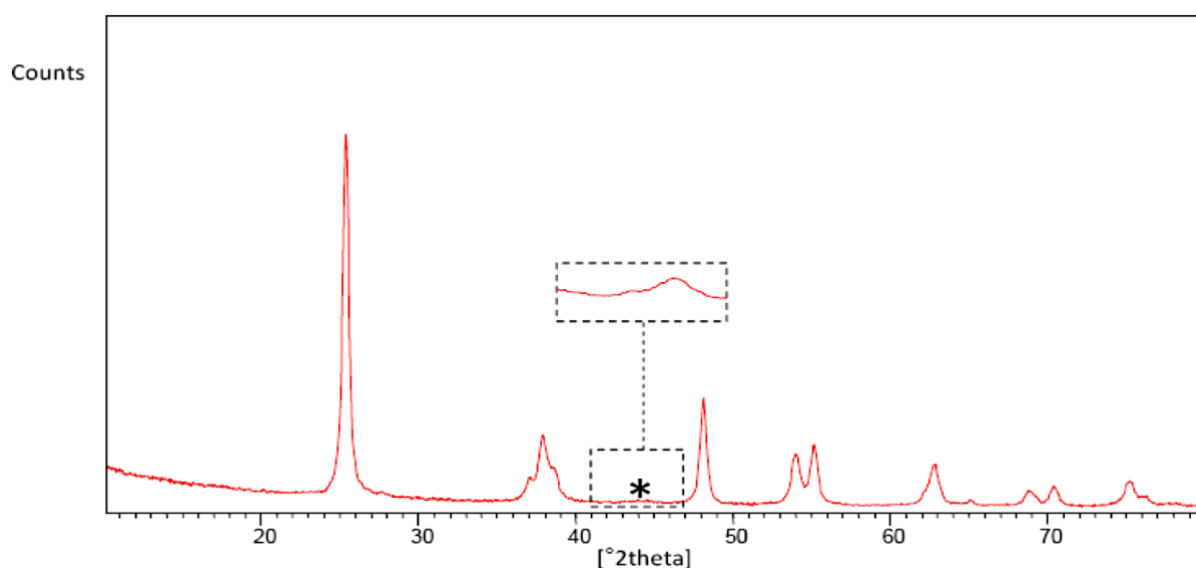


**Figure 6.11.** X.R.D. pattern of  $\text{Au}_{\text{NP}}/\text{TiO}_2$  (metal loading = 1,5%wt.).

The reflections in the pattern are attributed to the support with the exception of the weak reflection at  $44^\circ 2\theta$ . The latter, as expected, was almost imperceptible due to the fact that the X.R.D. signals were more enlarged and flattened when the size of the crystallites was close to the detection limit of 2-3 nm. In this case, the accumulation

every  $0,1^{\circ} 2\theta$ , in the range  $42$  to  $46^{\circ} 2\theta$ , was performed in order to increase the intensity of the signal at  $44^{\circ} 2\theta$ .

The Debye-Scherrer equation was used to calculate the size of the crystallites (see paragraph 5.2.1); an average particle diameter of 6 nm was obtained.

In conclusion, it can be stated that the synthesis of the catalyst led to Au nanoparticles well dispersed on the surface of titania.

### 6.2.1.3. Iron-substituted polyoxometalate

The Fe-polyoxometalate was characterized by means of attenuated total reflection (A.T.R.) infrared spectroscopy in order to confirm the formation of the Keggin-type structure (as also shown in Figure 5.6).

The IR spectrum of  $H_4[PW_{11}Fe(H_2O)O_{39}]$  is reported in Figure 6.12.

According to the literature, the most characteristic IR bands in the spectrum of Fe-containing tungstophosphate are attributed to the  $[PW_{12}O_{40}]^{3-}$  anion. From literature, it is possible to assign bands at 1080, 985, 890 and  $800\text{ cm}^{-1}$  to vibrations of the Keggin structure and are assigned to (P-O), (W-O), corner-sharing (W-O-W), and edge-sharing (W-O-W) groups, respectively<sup>186, 187</sup>.

The broad band at around  $3500\text{ cm}^{-1}$  may be attributed to surface silanols and adsorbed water molecules, while vibrations of adsorbed molecules cause the absorption bands at  $1623\text{--}1640\text{ cm}^{-1}$ <sup>188</sup>.

In the synthesized sample, the  $1080\text{ cm}^{-1}$  band was splitted into two components ( $1077\text{--}1038\text{ cm}^{-1}$ ), due to the decrease in the symmetry of the  $PO_4$  tetrahedron.

The other bands found are 969 (as (W-O<sub>d</sub>)), 854 (as(W-O<sub>b</sub>-W)),  $768\text{ cm}^{-1}$  (as(W-O<sub>c</sub>-W)), and differ from those typical of  $[PW_{12}O_{40}]^{3-}$ <sup>187</sup>.

These results, coupled with the splitting of the P-O band frequency and a slight shifting toward lower frequency compared to bulk lacunary unit indicated that Fe was introduced into the Keggin anion. The slight shifting of bands in FT-IR spectra of iron-substituted phosphotungstate anion compared to the phosphotungstate may be due to formation of a pseudo-symmetric environment resulting from the replacement of a W atom with a Fe atom<sup>189</sup>.

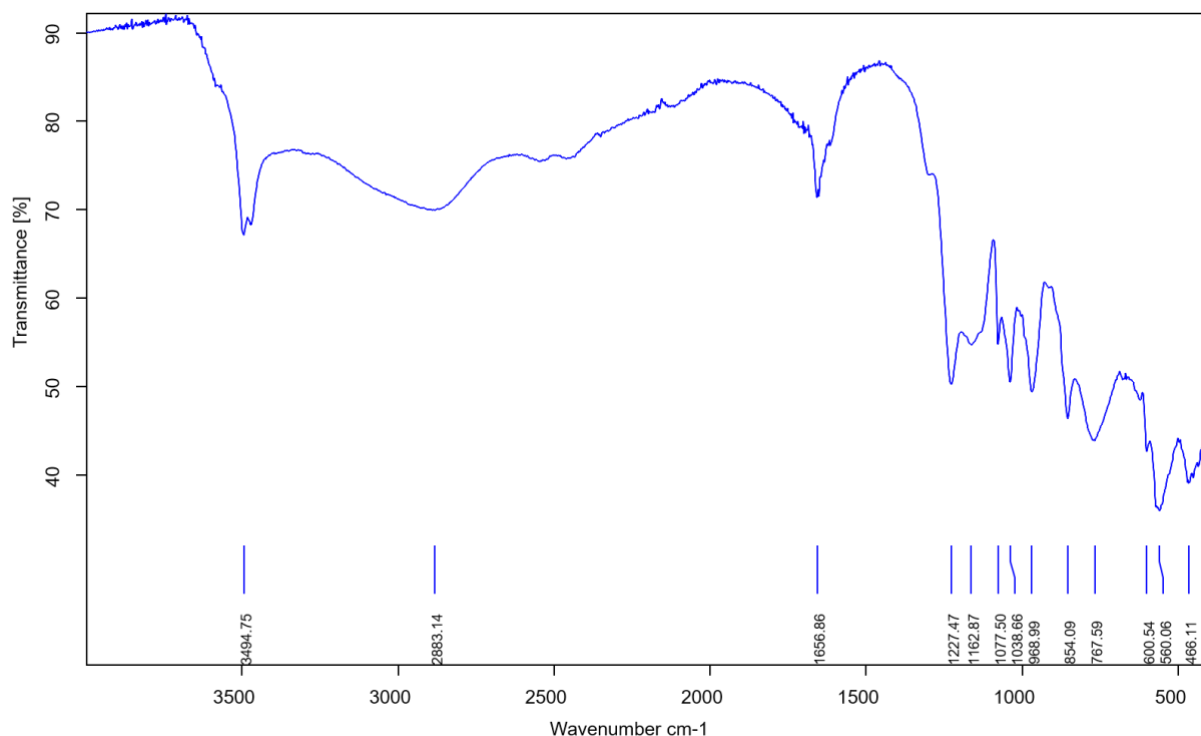


**Figure 6.12.** The FT-IR spectra obtained with A.T.R. analysis of  $H_4[PW_{11}Fe(H_2O)O_{39}]$ .

In conclusion, the spectrum shows the presence of the typical bands of the Keggin-type structures based on tungsten. The presence of Fe embedded in the structure is confirmed by the IR spectrum and by the intense yellow colour of the solid obtained, typical of these compounds.

## 6.2.2. Screening results

In this section, the results obtained by testing the catalytic activity of materials described in the previous chapter are presented.

In summary, the materials initially tested were:

- blank test (no catalyst);
- $AuNP/TiO_2$  (metal loading = 1,5 %wt.);
- M-modified ferrites:
  - $Fe_3O_4$ ;
  - $CoFe_2O_4$ ;



- $\text{NiFe}_2\text{O}_4$ ;
- $\text{CuFe}_2\text{O}_4$ ;
- $\text{H}_4[\text{PW}_{11}\text{Fe}(\text{H}_2\text{O})\text{O}_{39}]$  (code POM4).

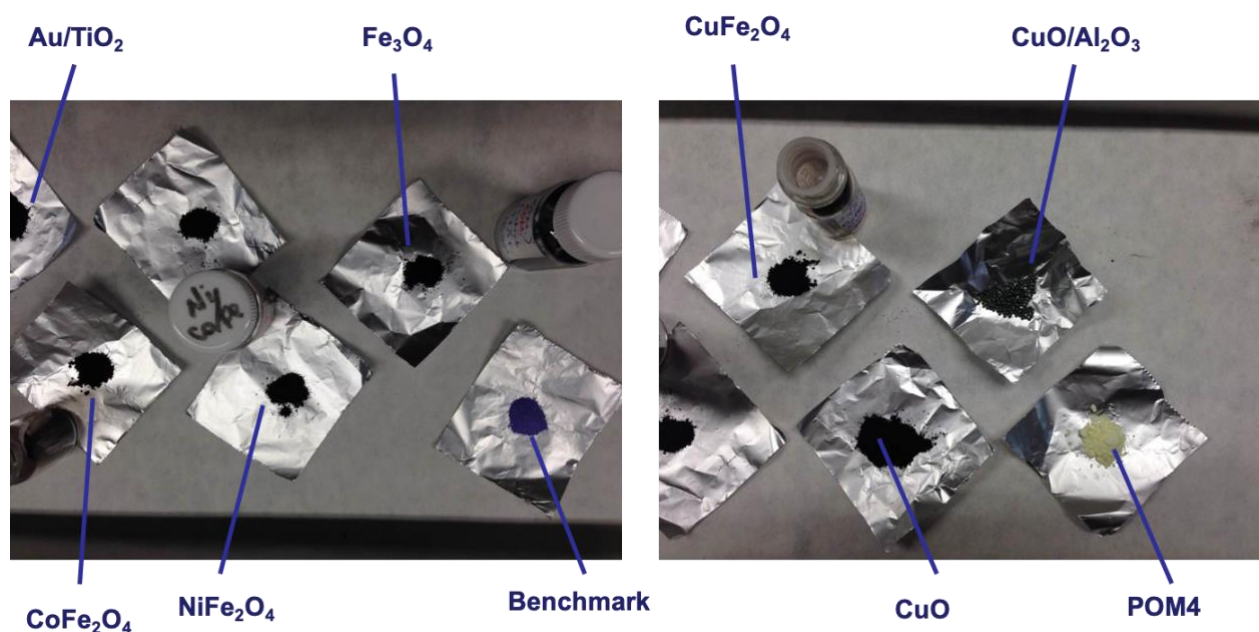


**Figure 6.13. Materials screened as possible heterogeneous catalysts for the oxidative cleavage of vicinal diol obtained from unsaturated fatty acid.**

The catalytic tests were carried out with the modality described in chapter 5.3.1.2 with the following conditions:

- 100 mL autoclave with magnetic drive and PTFE vessel;
- 15 g of starting material and 0,15 g of catalyst (1%<sub>wt.</sub> of catalyst with respect to the amount of the initial starting material);
- temperature of reaction = 80 °C;
- stirring rate = 500 rpm;
- pure molecular oxygen as oxidant;
- pressure of oxidant = 25 bar;
- reaction time = 5 h.

These parameters were initially chosen on the basis of the literature and patents.



At the end of the reaction, the products were analysed by means of GC-FID after derivatization (described in chapter 5.3.2); the catalyst was recovered by means of centrifugation.

Table 6-7 compares the results of experiments carried out with the various catalysts prepared, including the industrial homogeneous catalyst chosen as benchmark. A blank test was also performed in order to check a possible thermal contribution on the scission of the diol.

As already mentioned in chapter 6.1.2, the starting material already contained small amounts of pelargonic and azelaic acids. In this first part of the study the system was simplified by assuming that the starting material only contained the diol, without taking into account the two acids (see paragraph 5.3.5.1 for more details on the equations used).

**Table 6-7. Oxidative cleavage of 9,10-dihydroxystearic acid (DSA) at 80 °C, 5 h, 25 bar O<sub>2</sub>.**

CATALYST	X <sup>screen</sup> <sub>DSA</sub> (%)	Y <sup>screen</sup> <sub>PELARG, DSA</sub> (%)	Y <sup>screen</sup> <sub>AZEL, DSA</sub> (%)
<b>Blank test</b>	24%	4%	9%
<b>Benchmark</b>	95%	15%	19%
<b>AuNP/TiO<sub>2</sub></b>	43%	6%	9%
<b>POM4</b>	50%	3%	6%
<b>Fe<sub>3</sub>O<sub>4</sub></b>	20%	4%	6%
<b>CoFe<sub>2</sub>O<sub>4</sub></b>	27%	8%	12%
<b>NiFe<sub>2</sub>O<sub>4</sub></b>	27%	12%	14%
<b>CuFe<sub>2</sub>O<sub>4</sub></b>	96%	23%	36%

9,10-Dihydroxystearic acid conversion and yields (calculated with eq. (2) and (3), chapter 5.3.5.1) of the two acids also compared in Figure 6.14:

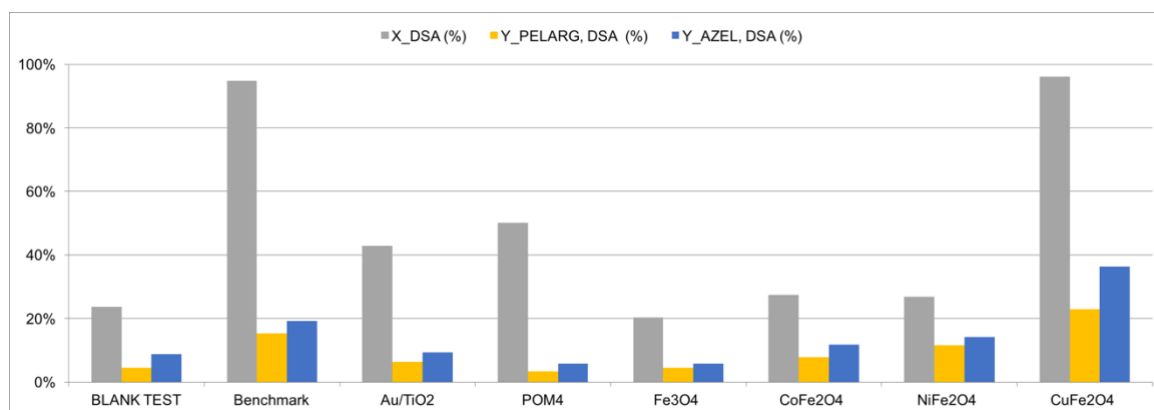


**Figure 6.14.** Conversion of 9,10-dihydroxystearic acid (X\_DSA), yield of Pelargonic acid (Y\_PELARG, DSA) and yield of Azelaic acid (Y\_AZEL, DSA), for the various catalysts prepared; T 80 °C, 5 h, 25 bar O<sub>2</sub>, stirring rate 500 rpm.

An unexpected finding was that the Cu ferrite was able to catalyse the reaction with performance even better than the benchmark catalyst.

It is also important to remember that the benchmark was a homogenous catalyst, while the system discovered was heterogeneous.

Besides this good outcome, we investigated on the reasons why the other catalysts did not work. AUNP over titania was already reported as catalyst for this reaction, but under reaction conditions different from those used in this study. Very importantly, we added no base to the reaction mixture in order to activate the substrate, as instead reported in literature on these systems. Secondly, the concentration of the reagent could play a crucial role; the reaction was conducted without any solvent, therefore the concentration of the diol was much higher than that one reported in literature.

Although the cobalt-based catalyst worked under homogeneous conditions, Cobalt-ferrite did not show any catalytic effect. The reason may be that cobalt promotes the reaction only when sequestered by the tungstate anions, with in-situ formation of polyoxometalate.

Therefore, some experiments were carried out in the presence of tungstate anion as co-catalyst in order to check whether a synergic effect is necessary for the conduction of the reaction, as reported by Santacesaria *et al.*<sup>147</sup>. The tests were performed at the same reaction conditions reported above with aqueous solution of WO<sub>4</sub><sup>2-</sup> (tungsten = 1%<sub>wt.</sub>).

Table 6-8 compiles the results obtained while Figure 6.15 compares the results with and without tungstate co-catalyst.

**Table 6-8. Results of oxidative cleavage of DSA (9,10-dihydroxystearic acid) with catalyst + WO<sub>4</sub><sup>2-</sup>(aq.) at 80 °C, 5 h, 25 bar O<sub>2</sub>, stirring 500 rpm.**

CATALYST	X <sup>screen</sup> <sub>DSA</sub> (%)	Y <sup>screen</sup> <sub>PELARG, DSA</sub> (%)	Y <sup>screen</sup> <sub>AZEL, DSA</sub> (%)
Benchmark	95%	15%	19%
Fe <sub>3</sub> O <sub>4</sub> + Na <sub>2</sub> WO <sub>4</sub> (aq)	21%	5%	6%
NiFe <sub>2</sub> O <sub>4</sub> + Na <sub>2</sub> WO <sub>4</sub> (aq)	27%	12%	14%
CuFe <sub>2</sub> O <sub>4</sub> + Na <sub>2</sub> WO <sub>4</sub> (aq)	90%	13%	20%

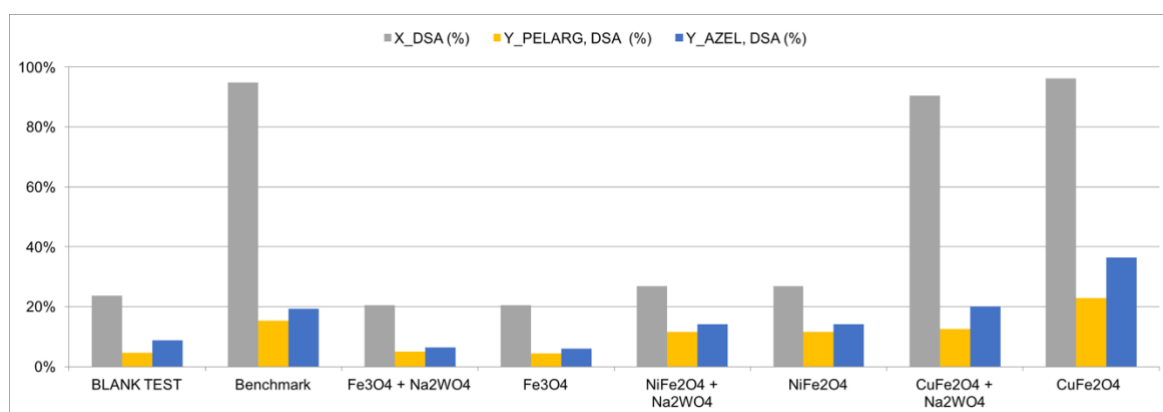


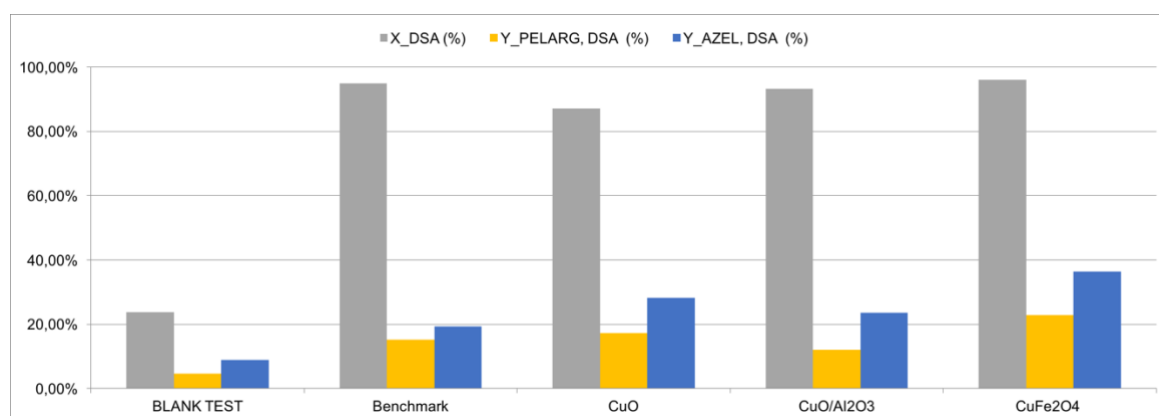
**Figure 6.15. Catalytic performance with and without WO<sub>4</sub><sup>2-</sup>(aq.), in terms of: conversion of 9,10-dihydroxystearic acid (X\_DSA), yield of Pelargonic acid (Y\_PELARG, DSA) and yield of Azelaic acid (Y\_AZEL, DSA), at 80 °C, 5h, 25 bar O<sub>2</sub>, stirring 500 rpm.**

From these tests it was clear that no synergic effect occurred since results obtained adding the WO<sub>4</sub><sup>2-</sup> were similar (or even worse) to those without tungstate.

Encouraged by the good results obtained with copper ferrosinels, we made some experiments aimed at finding a possible activity of the copper oxide impurities in the Cu ferrite. Indeed, the catalytic activity of other commercial Cu oxide-based materials was tested at the same reaction conditions reported for the preliminary screening. Results are compiled in Table 6-9 and Figure 6.16.

**Table 6-9. Oxidative cleavage of DSA (9,10-dihydroxystearic acid) at 80 °C, 5 h, 25 bar O<sub>2</sub>, stirring 500 rpm, with Cu-based catalysts.**

CATALYST	X <sup>screen</sup> <sub>DSA</sub> (%)	Y <sup>screen</sup> <sub>PELARG, DSA</sub> (%)	Y <sup>screen</sup> <sub>AZEL, DSA</sub> (%)
Benchmark	95%	15%	19%
CuO (Merck)	87%	17%	28%
CuO/Al <sub>2</sub> O <sub>3</sub> (Sigma-Aldrich)	93%	12%	23%
CuFe <sub>2</sub> O <sub>4</sub>	96%	23%	36%

**Figure 6.16. Catalytic performance of CuO catalysts in terms of: conversion of 9,10-dihydroxystearic acid (X\_DSA), yield of Pelargonic acid (Y\_PELARG,DSA) and yield of Azelaic acid (Y\_AZEL), at 80 °C, 5h, 25 bar O<sub>2</sub>, stirring 500 rpm.**

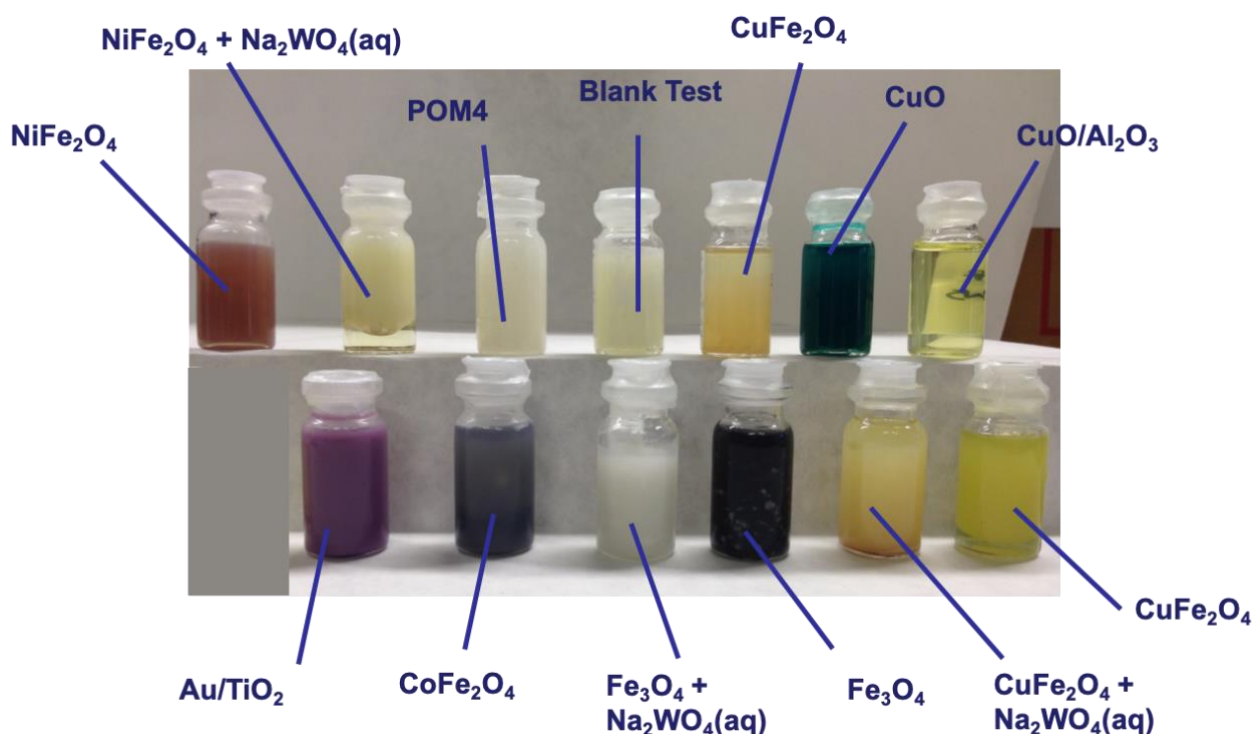
### 6.2.3. Conclusions about catalysts screening

Figure 6.17 displays the pictures of the vials containing the reaction mixture after reactivity experiments.

The reaction mixtures obtained with the least active catalysts were solid as a consequence of the low DSA conversion. Conversely, active catalysts produced a fluid reaction mixture with a viscosity more or less inversely proportional to the degree of conversion.

Moreover, the final reaction mixture after use of the copper oxide catalyst was green, because of the dissolution of Cu<sup>2+</sup>. This phenomenon was not observed with the catalyst

made of CuO supported on Al<sub>2</sub>O<sub>3</sub>; with the latter catalyst, at the end of the reaction the organic phase appeared clearer and more transparent.



**Figure 6.17.** Reaction mixtures obtained with catalysts tested at 80 °C, 5h, 25 bar O<sub>2</sub>, stirring 500 rpm.

In conclusion, some interesting results were achieved in this preliminary catalytic screening: the heterogeneous catalyst developed in our laboratory reached similar performance to the homogeneous system used in industry.

Therefore, the study was then focused on the improvement of the catalytic performance of copper based catalysts, both copper spinel and CuO based materials.

## 6.3. *Copper oxide*

The initial catalytic screening showed that copper represents an alternative active phase to the conventional homogeneous catalyst. For this reason, the focus of this research was put on the study of copper oxide based materials as catalysts for the oxidative cleavage of unsaturated fatty acids. In particular, the relationship between the results of catalytic experiments and catalyst physical-chemical properties are discussed.

### 6.3.1. *Effect of the support*

As previously shown in chapter 6.2.3, by supporting the active phase, for instance CuO, over a support it was possible to achieve a good catalyst stability in the reaction conditions. This is clearly shown in Figure 6.18, which compares the final reaction mixture obtained with bulk and supported materials after catalyst recovery.

Figure 6.18 highlights the dissolution of Cu<sup>2+</sup> into the reaction mixture with bulk catalyst, while the mixture produced with the supported copper oxide did not show any leaching.



**Figure 6.18. Final reaction mixtures obtained with copper oxide (on the left) and copper oxide supported over alumina (on the right).**

Moreover, by supporting the active phase over alumina, it was possible to improve the specific surface area of the active phase, as shown in Table 6-10.

Table 6-10. B.E.T. specific surface area of commercial copper oxide based materials.

CATALYST	ASS <sub>B.E.T.</sub> (m <sup>2</sup> /g)
CuO (Merck)	30
CuO/Al <sub>2</sub> O <sub>3</sub> (Sigma-Aldrich) (14-20 mesh pellets)	170
CuO/Al <sub>2</sub> O <sub>3</sub> (Sigma-Aldrich) (powder from pellets)	179

A possible effect of the bare support was verified; results in Figure 6.19 suggested that support contribution on catalytic activity was negligible.

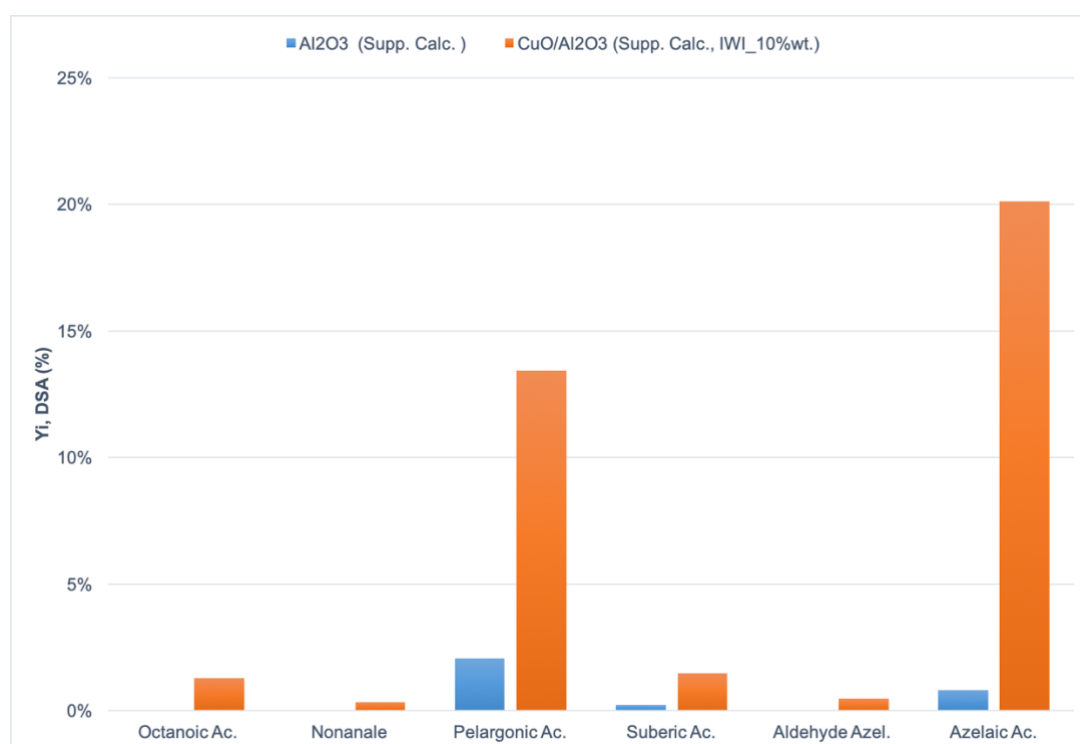
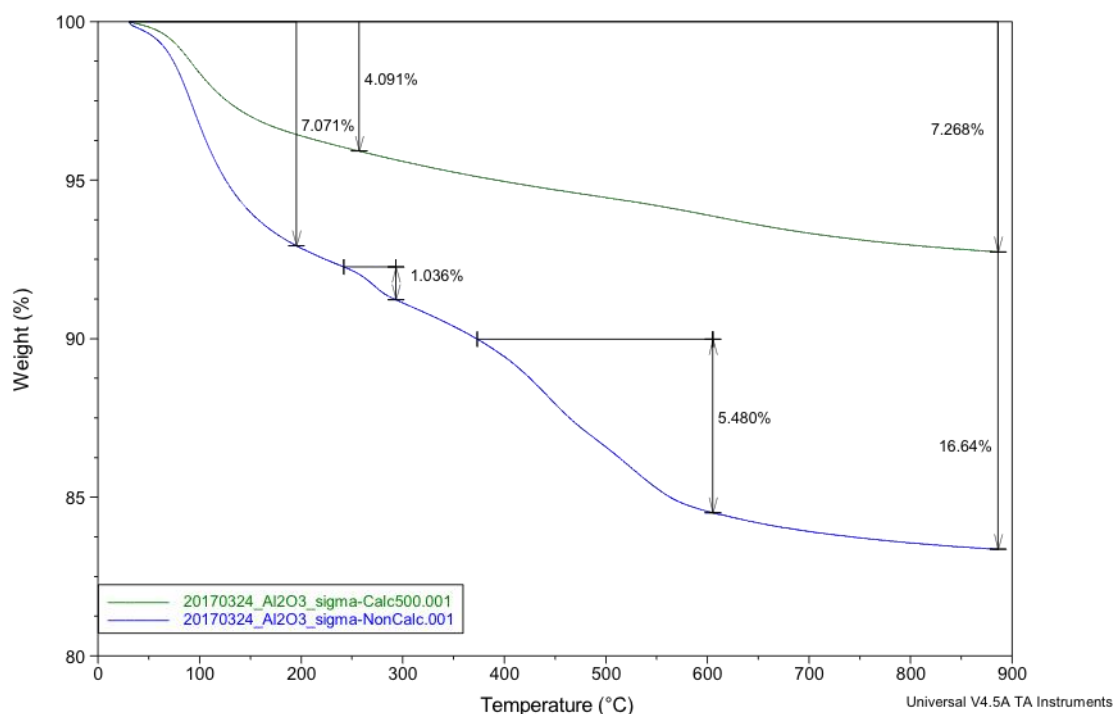


Figure 6.19. Yields of the main products in the oxidative cleavage of DSA with CuO supported over alumina and alumina.

### 6.3.2. Catalyst characterization

Commercial alumina was purchased in pellets (3 mm) form by Sigma –Aldrich and it was milled and used either as such or after calcination at 500 °C for 5 h (10 °C/min). The two samples of alumina showed a common weight loss at about 100 °C due to water desorption. In contrast with the calcined sample, the alumina as such showed another significant weight loss at more or less 500 °C, that may be caused by release of OH groups in the form of water during the phase transition from *boehmite* to  $\gamma$ - $\text{Al}_2\text{O}_3$ <sup>190</sup>.



**Figure 6.20. T.G.A. analysis of commercial alumina (powder from crushed pellets) as such and after calcination at 500°C for 5 h (10°C/min).**

Indeed, from X.R.D. patterns (Figure 6.21) of catalysts prepared by *incipient wetness impregnation* (described in chapter 5.1.4), it is possible to note that catalysts made with the calcined support showed the same pattern of the commercial one, while the catalyst prepared with the non-calcined support showed the pattern of a different alumina structure, i.e. *boehmite*.



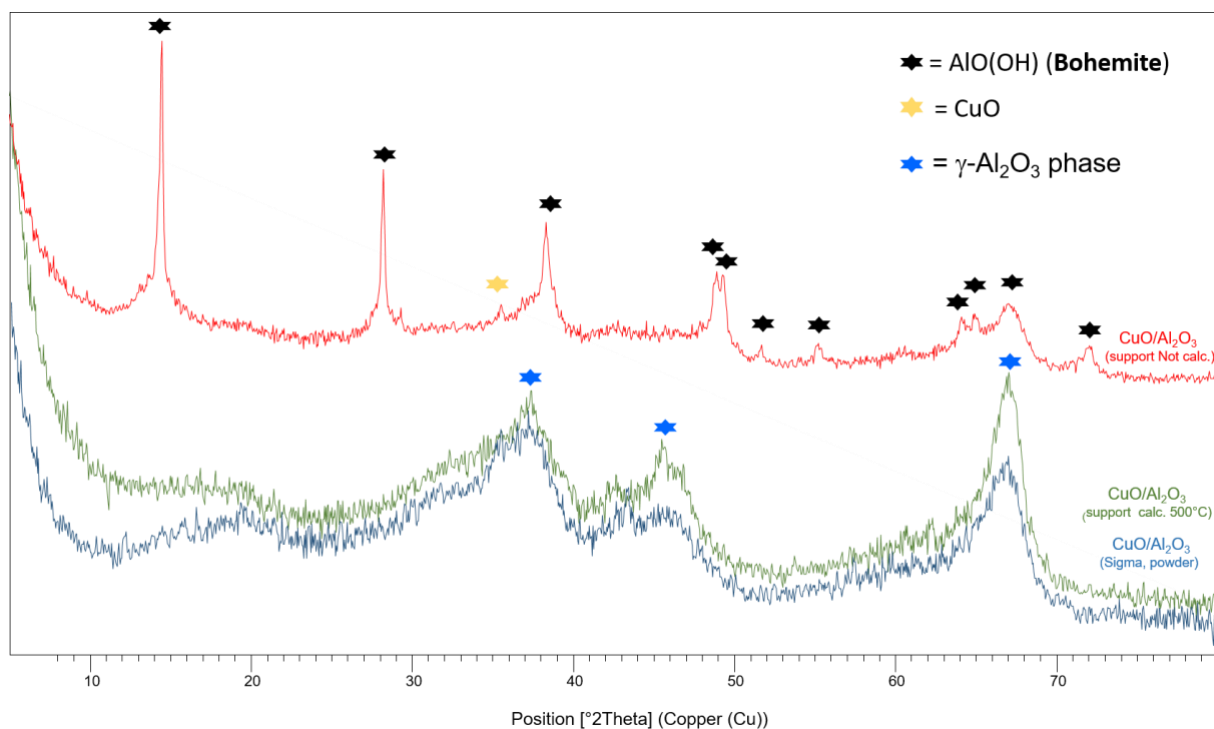


**Figure 6.21.** X.R.D. pattern of CuO over Al<sub>2</sub>O<sub>3</sub>; (from top to bottom) CuO supported over non-calcined alumina, CuO over alumina calcined at 500°C and commercial catalyst (powder from crushed pellets).

The X-ray fluorescence spectroscopy (X.R.F.) analysis was done in order to evaluate the amount of the active phase actually present on the support. Results are reported in Table 6-11.

**Table 6-11.** X.R.F. results related to copper oxide supported over alumina.

Sample	% <sub>wt.</sub> CuO
CuO/Al <sub>2</sub> O <sub>3</sub> (Sigma)	18,8
CuO/Al <sub>2</sub> O <sub>3</sub> (Supp. Calc. @500°C)	17,6
CuO/Al <sub>2</sub> O <sub>3</sub> (Supp. Not Calc.)	16,9

The analysis evidenced that *IWI method* made possible to obtain materials with comparable amount of active phase.

S.E.M.–E.D.X. analysis was also performed in order to corroborate the results achieved with the other techniques. The images below show the morphology of CuO over alumina

calcined at 500 °C and of the commercial catalyst in the form of powder obtained by milling the pellets. The attention was focussed only on these two systems because of the X.R.D. patterns: only one of the two systems synthesized reproduced the commercial catalyst.

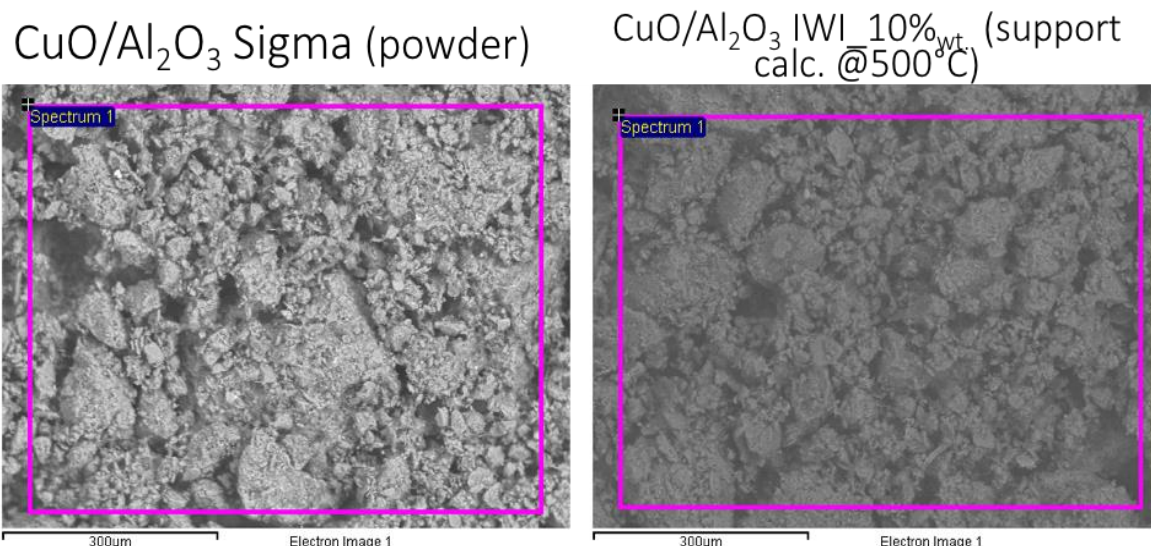


Figure 6.22. Images obtained with (from left to right) CuO/Al<sub>2</sub>O<sub>3</sub> (commercial) and CuO/Al<sub>2</sub>O<sub>3</sub> prepared with IWI of the calcined support.

Table 6-12. Results obtained with E.D.X. analysis of CuO over different supports.

Catalyst	Cu % <sub>wt.</sub>	Al % <sub>wt.</sub>	O % <sub>wt.</sub>	Calculated CuO % <sub>wt.</sub>
<b>CuO/Al<sub>2</sub>O<sub>3</sub> Sigma</b> (powder from pellets)	14,1	43,4	42,5	17,6
<b>CuO/ Al<sub>2</sub>O<sub>3</sub></b> <b>IWI_10%<sub>wt.</sub></b> (support calcined @500°C)	16,0	40,2	43,8	20,0

The weight content of CuO from E.D.X. analysis was 17,6% and 20,0% for CuO/Al<sub>2</sub>O<sub>3</sub> Sigma (powder) and CuO/Al<sub>2</sub>O<sub>3</sub> (supported calc.), respectively. These results are in line with those obtained by means of X-ray fluorescence technique.

Finally, results of the porosity analysis are reported in Table 6-13. The surface area of the synthesized sample was higher than that one of the commercial catalyst. However, the main pores features were similar.

**Table 6-13. Results of the surface area and porosity analysis of CuO over alumina support.**

SAMPLE	S <sub>B.E.T.</sub>	V <sub>pore</sub>	Pore average diameter
	m <sup>2</sup> /g	cm <sup>3</sup> /g	nm
CuO/Al <sub>2</sub> O <sub>3</sub> Sigma (powder from pellets)	171	0,37	8,5
CuO/Al <sub>2</sub> O <sub>3</sub> (support calc. @500°C)	218	0,38	7,0
CuO/Al <sub>2</sub> O <sub>3</sub> (support not calc.)	256	0,40	5,5

The redox properties of catalysts were investigated with temperature programmed reduction/oxidation. These analysis were conducted as described in chapter 5.2.4 and could be very informative because the reducibility/oxidability properties of the catalyst strongly depends on the particles dimension of the active phase, its metal oxidation state and its interaction with the support. Figure 6.23 shows the profiles obtained with the cycle TPR<sub>1</sub>-O-R<sub>2</sub>.

Many parameters were evaluated from these profiles:

- the number of the peaks, that represent the number of reducible/oxidizable species;
- the temperature at which the peak maximum occurs;
- the shape of the peaks.

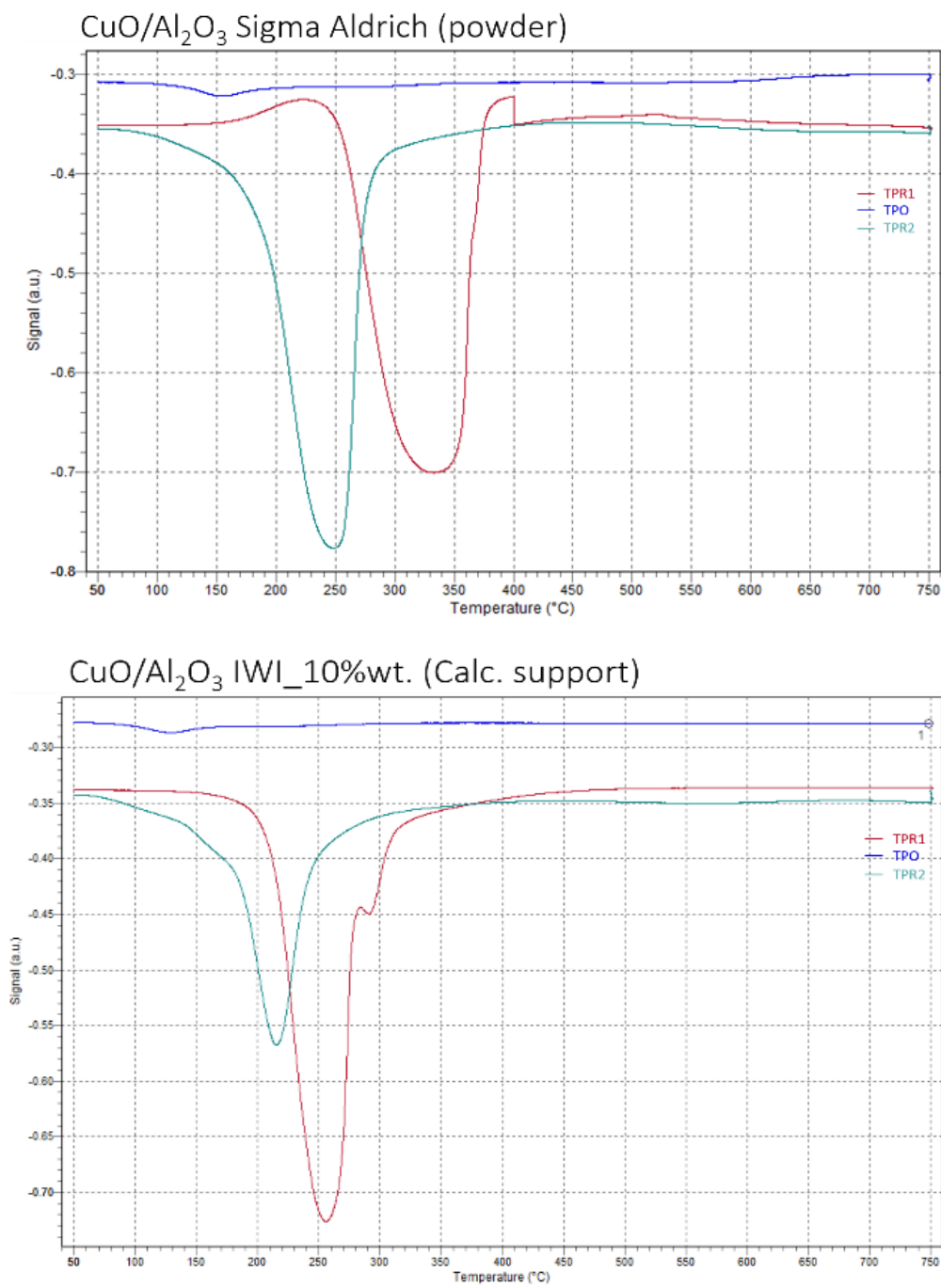


**Figure 6.23.** TPR-O-R profile of CuO supported on alumina; (from left to right) CuO/Al<sub>2</sub>O<sub>3</sub> Sigma-Aldrich (powder from pellets) and CuO/Al<sub>2</sub>O<sub>3</sub> (support calc.@500°C).

The temperature at which the peaks occur may vary from sample to sample depending on several materials features, for example the particle size of reducible/oxidizable species.

For both sample, TPR<sub>1</sub> presents a peak that can be attributed to the reduction of CuO into Cu<sup>(0)</sup><sup>191, 192</sup>.

From Figure 6.23, it is clear that CuO/Al<sub>2</sub>O<sub>3</sub> synthesized with the calcined support showed very sharp peaks compared to the commercial material. This could be related to the high dispersion and sharp distribution of the particles size. In fact, high copper loading samples are usually reported to have a broad peak due to the low dispersion and uniformity of the supported particles<sup>193</sup>. Moreover, the commercial sample presented a reduction peak at higher temperature, with a maximum centered at 330 °C due to a much lower dispersion compared to those prepared by means of the *IWI* technique.

CuO/Al<sub>2</sub>O<sub>3</sub> (calc. support) showed also a different TPR<sub>1</sub> profile compared to the commercial catalyst; probably, this was caused by the presence of CuO particles with different size which are reduced at two different temperatures.

In the second reduction carried out after TPO analysis, the two catalysts presented similar TPR<sub>2</sub> profiles and the most remarkable difference was the value of temperature at which the maximum is shown: the synthesized material was reduced at lower temperature (210 °C) compared to the commercial catalyst (250 °C). This result may also be due to a different active phase particle size that affects the reduction profile. In addition, the TPR<sub>2</sub> profile of the two samples were shifted compared to TPR<sub>1</sub> because of the sintering of the reducible species.

Table 6-14 compiles the temperature maxima of all peaks registered by TPR<sub>1</sub>-O-R<sub>2</sub> analysis related to the unsupported CuO (purchased by Merck) and CuO supported over alumina.

**Table 6-14. Temperature maxima of the peaks obtained from the TPR<sub>1</sub>-O-R<sub>2</sub> analysis over CuO over alumina as supports.**

CATALYST	Temperature of (First) Reduction peak maxima (°C)	Temperature of Oxidation peak maxima (°C)		Temperature of (Second) Reduction peak maxima (°C)
	$\alpha 1$	$\beta 1$	$\beta 2$	$\gamma 1$
CuO (Merck)	300		690	350
CuO/Al <sub>2</sub> O <sub>3</sub> SIGMA (powder)	330	155		250
CuO/Al <sub>2</sub> O <sub>3</sub> IWI_10% <sub>wt.</sub>	275	135	250	210

Overall, it is possible to conclude that *incipient wetness impregnation* was a suitable method for the reproduction of the commercial copper oxide over alumina catalyst, which showed high activity in the oxidative scission of fatty glycols.

### **6.3.3. Catalytic tests with $\text{CuO}/\text{Al}_2\text{O}_3$**

In this section, reaction parameters were investigated by using CuO over alumina as catalyst. The aim of these experiments was to find conditions at which the best yield is achieved.

The catalyst chosen for these tests was the commercial  $\text{CuO}/\text{Al}_2\text{O}_3$  catalyst because (a) it was an available commercial catalyst, (b) it gave very good yields to PA and AA and (c) the final reaction mixture was very clear with no apparent metal dissolution.

#### **6.3.3.1. On the effect of reaction time**

The commercial copper oxide over alumina (pellets) was employed for the kinetics investigation of DSA oxidative cleavage. The experiments were carried out by changing the reaction time from 0 to 8 hours.

The catalytic tests were carried out as described in chapter 5.3.1.2, using the following conditions:

- 100 mL autoclave with magnetic drive and PTFE vessel;
- 15 g of starting material (dihydroxylated oil) and 0,15 g of catalyst (1%<sub>wt.</sub> of catalyst with respect to the amount of s.m.);
- temperature of reaction = 80 °C;
- stirring rate = 500 rpm;
- pure molecular oxygen as oxidant;
- pressure of oxidant = 25 bar;
- time of reaction = 0, 2, 4, 6, 8 h.

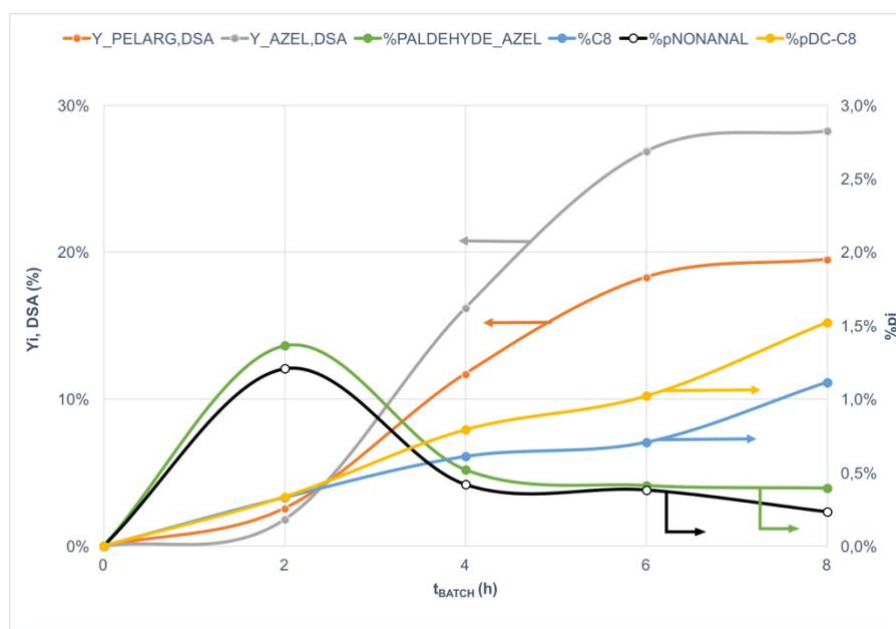
The reaction products were analysed by GC-FID after a derivatization process (described in chapter 5.3.2) and the catalyst was recovered by means of centrifugation.



The results concerning DSA conversion and yields to AA and PA are compiled in Table 6-15. In this case, results were obtained by applying equations (4) and (5).

**Table 6-15. Oxidative cleavage of DSA (9,10-dihydroxystearic acid) catalysed by CuO/Al<sub>2</sub>O<sub>3</sub> (Sigma-Aldrich) in function of reaction time.**

Catalyst	t (h)	pO <sub>2</sub> (bar)	T (°C)	% <sub>wt.</sub> Cat.	X <sub>DSA</sub> (%)	Y <sub>PELARG,DSA</sub> (%)	Y <sub>AZEL,DSA</sub> (%)
CuO/Al <sub>2</sub> O <sub>3</sub> (Sigma-Aldrich)	2	25	80	1,0%	40%	3%	2%
	4	25	80	1,0%	73%	12%	16%
	6	25	80	1,0%	75%	18%	27%
	8	25	80	1,0%	79%	19%	28%

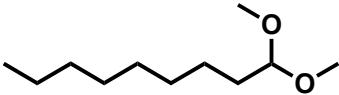
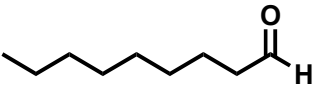
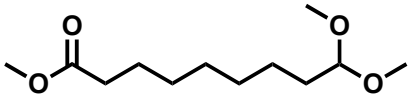
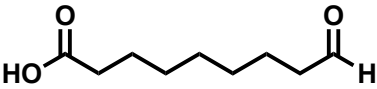
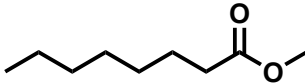
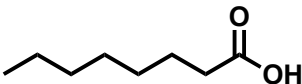
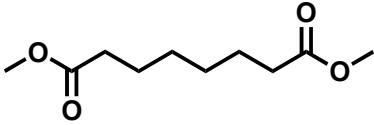
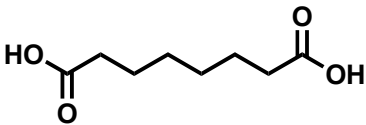


**Figure 6.24. Oxidative cleavage of DSA in function of reaction time. Yields of pelargonic acid (Y<sub>PELARG,DSA</sub>) and azelaic acid (Y<sub>AZEL,DSA</sub>) registered at 80 °C, 25 bar O<sub>2</sub>, stirring 500 rpm; the weight percentage of octanoic ac. (%pC8), nonanal (%pNONANAL), suberic ac. (%pDC-C8) and 9-oxononanoic acid (%pALDEHYDE\_AZEL) are also reported.**

In the figure, the %p<sub>i</sub> (see eq. (6)) of several products are reported.

These molecules were identified by GC-MS analysis of the derivatized products. Table 6-16 shows the molecular structure of compounds identified by means of CG-MS and the corresponding non-derivatized molecules which were produced during the oxidative scission.

Table 6-16. Main by- and co- products of DSA oxidative cleavage identified by means of GC-MS (after derivatization with  $\text{BF}_3/\text{MeOH}$ )

GC-MS molecules (derivatized with $\text{BF}_3/\text{MeOH}$ )	Corresponding molecule (not derivatized molecule)
 1,1-dimethoxynonane	 nonanal
 methyl 9,9-dimethoxynonanoate	 9-oxononanoic acid
 methyl octanoate	 octanoic acid
 dimethyl octanedioate	 suberic acid

The C8 products showed the typical trend of kinetically parallel reactions. Conversely, the two aldehydes were formed at the beginning of the reaction and their yields decreased during the progress of the reaction, a behaviour typical of intermediate products. Moreover, AA and PA apparently formed by conversion of the two aldehydes.

In literature, it was already reported the parallel formation of  $\text{C}_{n-1}$  products (i.e. octanoic and suberic acid) during the oxidative cleavage of DSA. These by-products indicate the formation of an intermediate containing a keto-group, as proposed by S. Warwel *et al.*<sup>153</sup>.

As highlighted by A. Köckritz *et al.*<sup>84</sup>, the formation of shorter chain by-products should be found if the reaction pathway includes an over-oxidation or oxidative degradation, following a radical reaction pathway. The formation of products with only C8 and C9 atoms in the chain might be explained with keto group-containing intermediates such



as 9(10)-hydroxy-10(9)-oxostearic acid (hydroxyketone, HK) and 9,10-dioxostearic acid (diketone, DK)<sup>194</sup>.

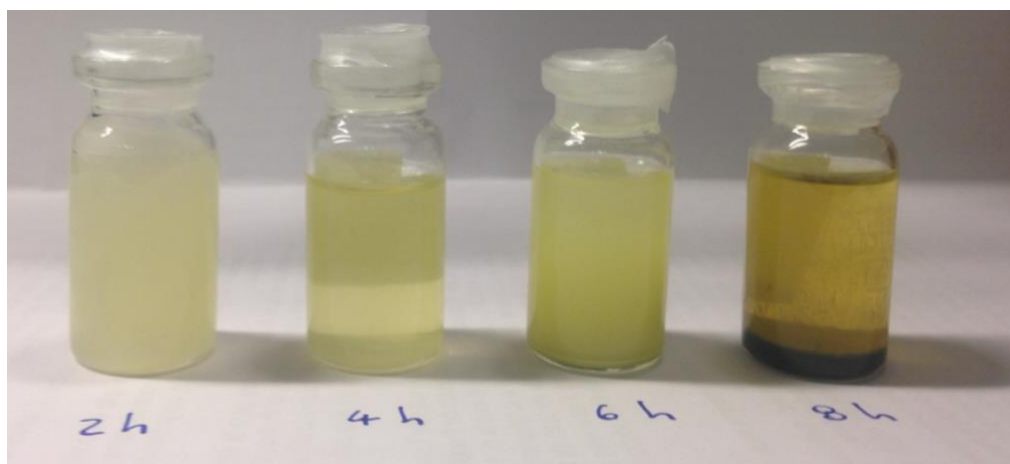


**Figure 6.25.** Pictures of reaction mixtures obtained from experiments in function of reaction time with CuO/Al<sub>2</sub>O<sub>3</sub> catalyst: (in order from left to right) 2 h, 4 h, 6 h, 8 h, at 80 °C, 25 bar O<sub>2</sub>, stirring 500 rpm.

To conclude, an increase of reaction time allowed to achieve yields to AA of 28%, and to PA of 17%, after 8 h reaction time at 80°C. The mixture appeared quite clear and pale yellow after 4 hours of reaction, while increasing the reaction time the yellow colour became more intense. This phenomenon could be attributed to the degradation of some compounds.

### 6.3.3.2. On the effect of reaction temperature

Oxidative scission of DSA was carried out in function of temperature by using commercial copper oxide over alumina (pellets). The experiments were carried out by changing the temperature from 60 °C to 140 °C; 60 °C represented the lower T limit because under this temperature the starting diol is solid, while 140 °C was the upper T limit for PTFE vessel exploitation.

The catalytic tests were carried out as described in the chapter 5.3.1.2 using the following conditions:

- 100mL autoclave with magnetic drive and PTFE vessel;
- 15 g of starting material (dihydroxylated oil) and 0,15 g of catalyst (1%<sub>wt.</sub> of catalyst with respect to the amount of s.m.);

- temperature of reaction = 60, 80, 100, 120, 140 °C;
- stirring rate = 500 rpm;
- pure molecular oxygen as oxidant gas;
- pressure of oxidant gas = 25 bar;
- time of reaction = 5 h.

The reaction products were analysed by GC-FID after a derivatization process (described in chapter 5.3.2) and the catalyst was recovered by means of centrifugation.

The results are summarized in Table 6-17 and Figure 6.26.

Figure 6.27 displays the pictures of the final reaction mixtures.

**Table 6-17. Oxidative cleavage of DSA (9,10-dihydroxystearic acid) catalysed by CuO/Al<sub>2</sub>O<sub>3</sub> (Sigma-Aldrich) in function of the reaction temperature.**

Catalyst	T (°C)	pO <sub>2</sub> (bar)	t (h)	% <sub>wt.</sub> Cat.	X <sub>DSA</sub> (%)	Y <sub>PELARG,DSA</sub> (%)	Y <sub>AZEL,DSA</sub> (%)
CuO/Al <sub>2</sub> O <sub>3</sub> (Sigma-Aldrich) (Pellets)	60	25	5	1,0%	0%	0%	0%
	80	25	5	1,0%	80%	13%	19%
	100	25	5	1,0%	83%	13%	20%
	120	25	5	1,0%	82%	11%	17%
	140	25	5	1,0%	72%	7%	10%

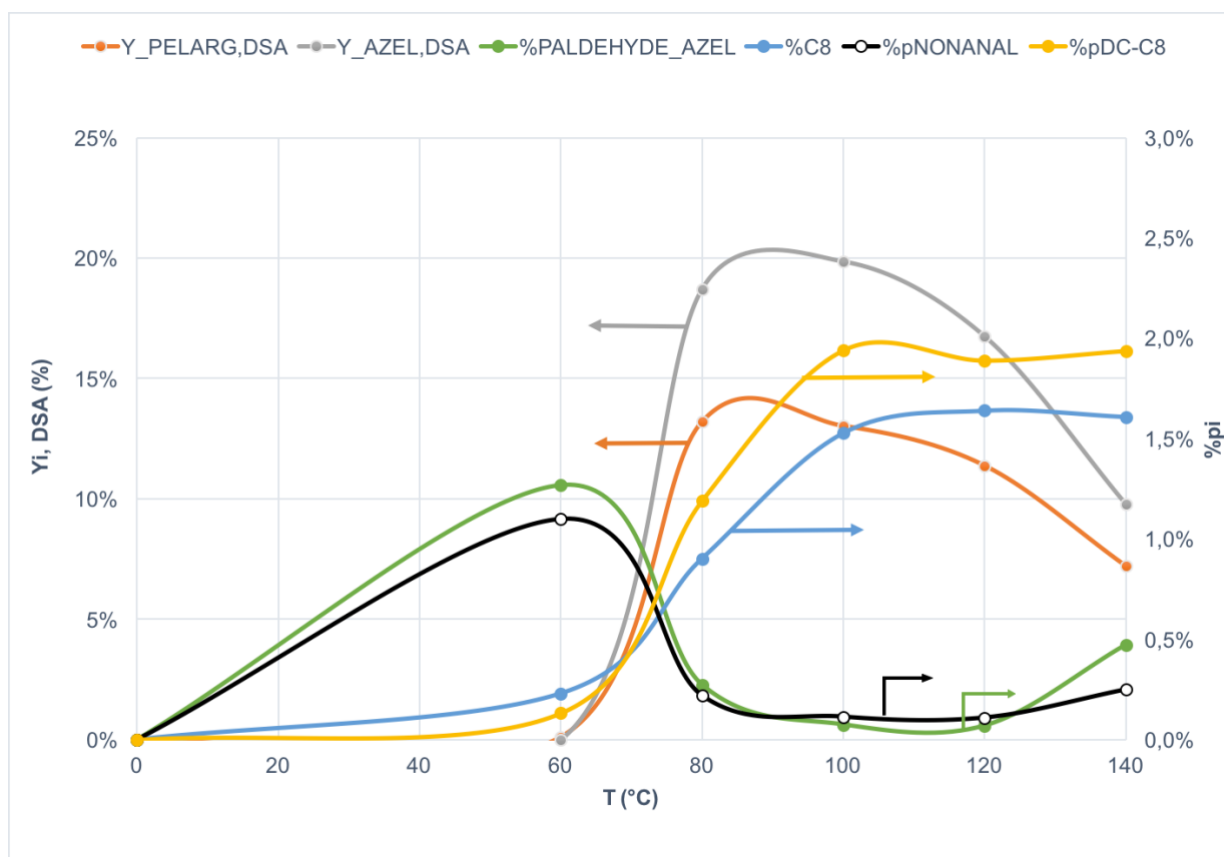


**Figure 6.26.** Oxidative cleavage of DSA in function of reaction temperature. Yields of pelargonic acid (Y\_PELARG,DSA) and azelaic acid (Y\_AZEL,DSA) registered at 80 °C, 25 bar O<sub>2</sub>, stirring 500 rpm; the weight percentage of octanoic ac. (%pC8), nonanal (%pNONANAL), suberic ac. (%pDC-C8) and 9-oxononanoic acid (%pALDEHYDE\_AZEL) is also reported.

The graph above corroborates the assumption of the parallel formation of C<sub>n-1</sub> atom molecules via a parallel pathway, while nonanal and 9-oxononanoic acid are the intermediates of the reaction that brought to the formation of PA and AA, respectively.



**Figure 6.27.** Pictures of reaction mixtures obtained after experiments in function of temperature: (in order from left to right) 60 °C, 80 °C, 100 °C, 120 °C, 140 °C, at 5 h, 25 bar O<sub>2</sub>, stirring 500 rpm.

The results demonstrated that the optimal temperature range was 80 - 100°C, at which not only the PA and AA yields were the highest but also the reaction mixture appeared to be clear and free from heavier (dark) by-products. Indeed, at lower temperature the colour of the mixture suggested a partial dissolution (*leaching*) of Cu from the catalyst; this might be caused by the poor mixing and breaking of catalyst particles, due to the high solution viscosity, the latter being due to the low DSA conversion achieved. On the contrary, at higher temperature the solution was dark possibly because of the decomposition of acids and formation of heavy compounds.

### 6.3.3.3. On the effect of stirring rate

The influence of the stirring rate was also investigated.

This parameter could be very important for this type of reaction because of the presence of three different phases during the reaction: the oxidant gas, the liquid diol and the solid catalyst.

In this context, the stirring rate may affect the diffusion of the reagents inside the catalyst pores enhancing the performance of the catalyst itself.

The catalyst used for these experiment was still the commercial CuO over alumina; beside the tests previously described, the catalyst was milled in order to obtain a powder. This choice was made after the results obtained with experiments in function of the temperature (chapter 6.3.3.2): at low conversion of DSA, the high viscosity of the reaction system combined with the impeller movement caused the pellets breaking and consequently the increase of the copper leaching.

Therefore, the used conditions were:

- 100 mL autoclave with magnetic drive and PTFE vessel;
- 15 g of starting material (dihydroxylated oil) and 0,15 g of **powder** catalyst (1%<sub>wt.</sub> of catalyst with respect to the amount of s.m.);
- T = 80 °C;
- stirring rate = 300 – 500 – 700\* rpm;
- P<sub>O2</sub> = 25 bar;

- reaction time = 5 h.

\***Note:** 700 rpm is the maximum stirring rate for the apparatus described in chapter 5.3.1.2.

After the reaction, the catalyst was recovered by means of centrifugation (4500 rpm for 15 min). The reaction products were analysed by GC-FID after derivatization with  $\text{BF}_3/\text{MeOH}$  as previously described.

The results in terms of yields of the desired acids, PA and AA (see equation (5)) are compiled in Table 6-18 and presented in Figure 6.28.

**Table 6-18. Oxidative cleavage of DSA (9,10-dihydroxystearic acid) catalysed by  $\text{CuO}/\text{Al}_2\text{O}_3$  (Sigma-Aldrich) in function of the stirring rate.**

Catalyst	Stirring rate	T (°C)	pO <sub>2</sub> (bar)	t (h)	%wt. Cat.	Y <sub>PELARG,DSA</sub> (%)	Y <sub>AZEL,DSA</sub> (%)
$\text{CuO}/\text{Al}_2\text{O}_3$ (Sigma-Aldrich) (powder from commercial pellets)	300	80	25	5	1,0%	12%	16%
	500	80	25	5	1,0%	20%	31%
	700	80	25	5	1,0%	15%	23%

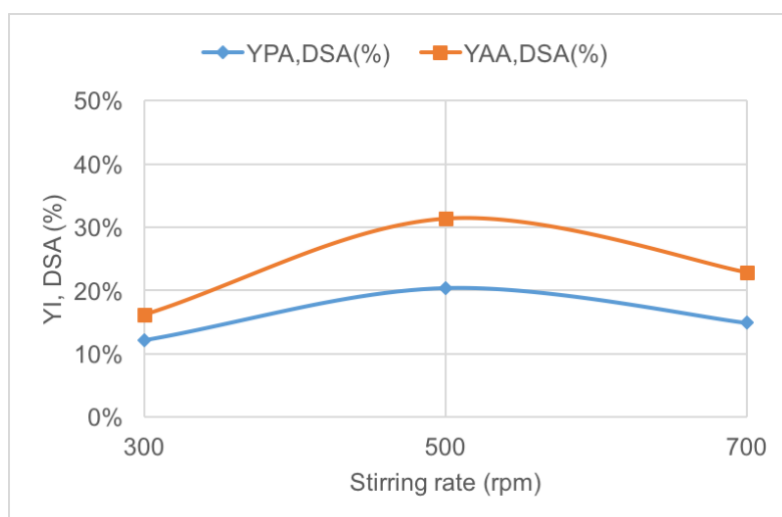


**Figure 6.28. Yields of azelaic ac. (AA) and pelargonic ac.(PA) obtained by changing the stirring rate using  $\text{CuO}/\text{Al}_2\text{O}_3$  Sigma (powder) 1%<sub>wt.</sub> catalyst. Yields are calculated with respect to DSA, reaction conditions 80°C for 5h, 25 bar O<sub>2</sub>, 300 – 500 - 700 rpm.**

The stirring rate slightly affected the yields of the two desired acids and the best result was achieved at 500 rpm.

#### 6.3.3.4. On the effect of catalyst amount

Additionally, reactivity tests were carried out by changing the catalyst amount using the commercial  $\text{CuO}/\text{Al}_2\text{O}_3$  in powder form.

The catalytic tests were carried out with the modality described in chapter 5.3.1.2 under the following conditions:

- 100mL autoclave with magnetic drive and PTFE vessel;
- 15 g of starting material (dihydroxylated oil) and 0,5%<sub>wt.</sub> – 1,0 %<sub>wt.</sub>- 1,5%<sub>wt.</sub> of catalyst respect to the amount of s.m.;
- temperature of reaction = 80 °C;
- stirring rate = 500 rpm;
- pure molecular oxygen as oxidant;
- pressure of oxidant = 25 bar;
- time of reaction = 5 h.

The reaction products were analysed by means of GC-FID after a derivatization process (described in chapter 5.3.2) and catalyst was recovered by centrifugation.

**Table 6-19. Oxidative cleavage of DSA (9,10-dihydroxystearic acid) catalysed by  $\text{CuO}/\text{Al}_2\text{O}_3$  (Sigma-Aldrich) in function of the amount of catalyst (referred to the starting material).**

Catalyst	T (°C)	pO <sub>2</sub> (bar)	t (h)	% <sub>wt.</sub> Cat.	Y <sub>PELARG, DSA</sub> (%)	Y <sub>AZEL, DSA</sub> (%)
CuO/Al <sub>2</sub> O <sub>3</sub>	80	25	5	0,5%	15%	25%
(Sigma-Aldrich)	80	25	5	1,0%	20%	31%
(powder from commercial pellets)	80	25	5	1,5%	13%	23%

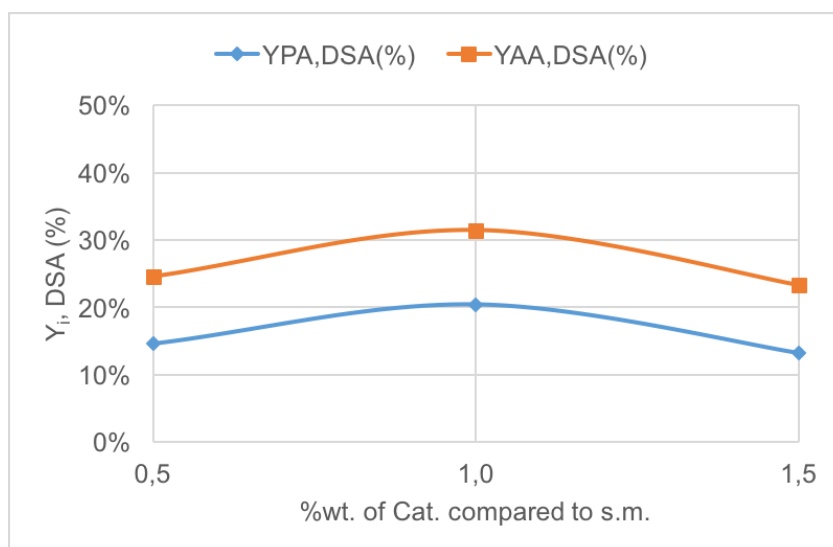


**Figure 6.29. Results obtained by changing the catalyst amount (referred to the starting material) with CuO/Al<sub>2</sub>O<sub>3</sub> Sigma (powder); catalyst amount compared DSA = 0,5%wt., 1,0%wt., 1,5%wt. @ 80°C for 5h, 25 bar O<sub>2</sub>, 500 rpm.**

Results (shown in Figure 6.29) demonstrated that this parameter only slightly affected catalyst performance. Surprisingly, the yields of AA and PA decreased by increasing the amount of catalyst. This could be related to the increased formation of by-products. However, the GC analysis did not reveal the formation of any unexpected compound product.

#### 6.3.3.5. On the effect of oxidant gas pressure

The last parameter investigated was the effect of the oxidant gas pressure.

The reaction conditions used were:

- 100 mL autoclave with magnetic drive and PTFE vessel;
- 15 g of starting material (dihydroxylated oil) and 0,15 g of **powder** catalyst (1%<sub>wt.</sub> of catalyst with respect to the amount of s.m.);
- T = 80 °C;
- stirring rate = 500 rpm;
- P<sub>O<sub>2</sub></sub> = 10 - 15 - 30 bar;
- reaction time = 3 h.

After the reaction, the catalyst was recovered by means of centrifugation (4500 rpm for 15 min). The reaction products were analysed by means of GC-FID after derivatization with  $\text{BF}_3/\text{MeOH}$  as previously described.

It is important to note that in these experiments the reaction time was 3h, calculated starting at the moment when the desired temperature was reached. This because in the experiment with the lowest pressure (10 bar) all the oxygen loaded was consumed already after 4 hours.

Results are presented in Table 6-20 and Figure 6.30.

**Table 6-20. Oxidative cleavage of DSA (9,10-dihydroxystearic acid) catalysed by  $\text{CuO}/\text{Al}_2\text{O}_3$  (Sigma-Aldrich) in function of the oxidant gas pressure (molecular oxygen).**

Catalyst	$p\text{O}_2$ (bar)	T (°C)	t (h)	%wt. Cat.	$Y_{\text{PELARG, DSA}}$ (%)	$Y_{\text{AZEL, DSA}}$ (%)
$\text{CuO}/\text{Al}_2\text{O}_3$ (Sigma-Aldrich) (powder from commercial pellets)	10	80	3	1,0%	11%	14%
	15	80	3	1,0%	11%	14%
	30	80	3	1,0%	13%	16%

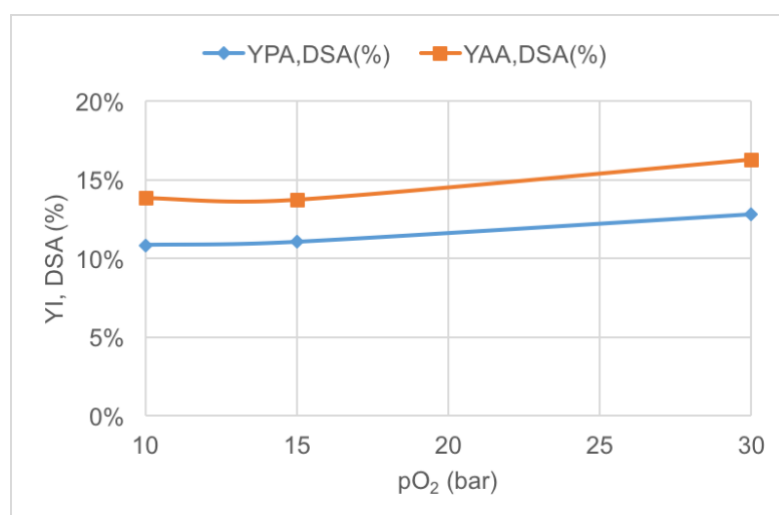


**Figure 6.30. Results in terms of yields of azelaic ac. (AA) and pelargonic ac.(PA) obtained by changing oxidant gas pressure, using 1%<sub>wt.</sub> of  $\text{CuO}/\text{Al}_2\text{O}_3$  Sigma (powder) compared to DSA at 80°C for 3h, 10 – 15 - 30 bar  $\text{O}_2$ , 500 rpm.**

It is shown that the oxygen pressure only slightly affected catalytic performance.

This probably means that already at 10 bar the concentration of the oxygen in diol was enough to sustain the catalytic reaction. Only a small increase of AA and PA yields were



registered with the increase of pressure from 15 to 30 bar. An alternative explanation is that the rate-determining step of the reaction does not include oxygen; this may happen when the adsorption of the diol on active sites is limiting the overall oxidation process.

#### **6.3.3.6. On the reusability of the catalyst**

One of the most important catalyst properties is its recyclability. Therefore, the reusability of CuO/Al<sub>2</sub>O<sub>3</sub> Sigma (powder) was also investigated.

The catalytic tests were carried out with the modality described in chapter 5.3.1.2 at the following conditions:

- 100 mL autoclave with magnetic drive and PTFE vessel;
- 15 g of starting material (dihydroxylated oil) and 0,15 g of catalyst (1%<sub>wt.</sub> of catalyst with respect to the amount of s.m.);
- temperature of reaction = 80 °C;
- stirring rate = 500 rpm;
- pure molecular oxygen as oxidant gas;
- pressure of oxidant gas = 25 bar;
- time of reaction = 0, 2, 4, 6, 8 h.

The reaction products were analysed by means of GC-FID after a derivatization process (described in chapter 5.3.2).

After the reaction, the catalyst recovered (by centrifugation at 4500 rpm for 15 min) was washed with acetone (3 x 15 mL) and then re-used for a new reaction at the same conditions as reported above.

Figure 6.31 compiles DSA conversion and PA and AA yields with respect to the initial oil (see equation (7)). A dramatic decrease of the catalyst performance for the re-used system was shown.

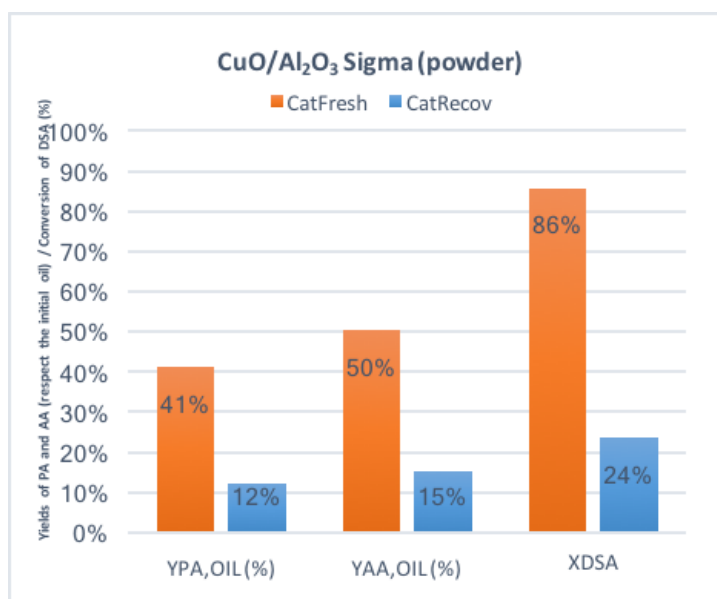


**Figure 6.31. Results obtained by re-usability test using fresh and recovered CuO/Al<sub>2</sub>O<sub>3</sub> Sigma (powder); 1%wt. of catalyst with respect to DSA at 80°C for 5h, 25 bar O<sub>2</sub>, 500 rpm.**

In order to investigate the reason for this deactivation, some characterization analysis of the used catalyst was done. Figure 6-32 and Figure 6-33 report the results obtained by thermogravimetric (T.G.A.) and attenuated total reflection (A.T.R.) analysis, respectively.

From the T.G.A., it is possible to observe a huge loss of weight for the recovered catalyst that was not present in the “fresh” catalyst. This suggests the presence of organic residues that were not removed by washing with acetone.

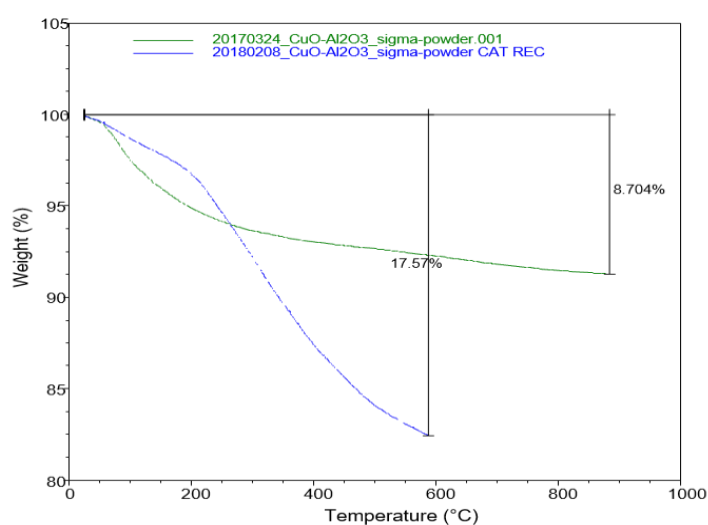


**Figure 6-32. TGA analysis over CuO/Al<sub>2</sub>O<sub>3</sub> (Sigma, powder) after recovering and washing with 3x15 mL of acetone.**

The IR spectra of the catalyst recovered and washed three times with 15 mL of acetone presents some characteristic IR band of specific chemical groups:

- $\nu = 1800 - 1680 \text{ cm}^{-1} \rightarrow$  Carboxylic Acid group;
- $\nu = 1740 - 1660 \text{ cm}^{-1} \rightarrow$  Aldehyde;
- $\nu = 2900 - 2680 \text{ cm}^{-1} \rightarrow$  Aldehyde;
- $\nu = 1230 - 1000 \text{ cm}^{-1} \rightarrow$  Alcohol.

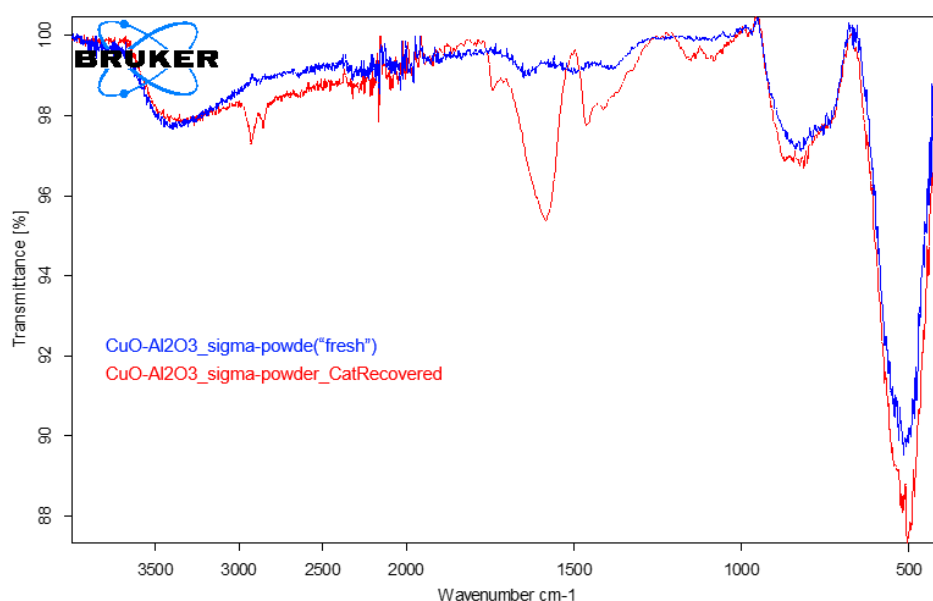


**Figure 6-33.** IR spectra obtained with A.T.R. analysis on CuO/Al<sub>2</sub>O<sub>3</sub> (Sigma, powder) after recovering and washing with 3x15 mL of acetone.

These results demonstrate the presence of organic compounds that were formed during reaction and that were strongly bound to the catalyst surface. This could be the reason for catalyst deactivation.

Therefore, we decided to calcine the used catalyst at high temperature, aimed at the removal of the organic residues. For sake of comparison, also the “fresh” catalyst was calcined at high temperature.

Therefore, two systems were examined: CuO/Al<sub>2</sub>O<sub>3</sub> Sigma (powder) and *IWI*\_CuO/Al<sub>2</sub>O<sub>3</sub> (prepared with *incipient wetness impregnation* of the support calcined at 500 °C, CuO loading = 10%wt.), both calcined at 500 °C for 3h. Table 6-21 shows the

results obtained: CuO/Al<sub>2</sub>O<sub>3</sub> Sigma (powder) and *IWI*\_CuO/Al<sub>2</sub>O<sub>3</sub> both as such and calcined at 500 °C for 3h (3 °C/min\*).

\*Note: this temperature ramp was chosen in order to keep the same T ramp. used for the *IWI* synthesis (see chapter 5.1.4)

**Table 6-21. Results in terms of yields of azelaic ac. (AA) and pelargonic ac.(PA) obtained in DSA oxidative cleavage using CuO/Al<sub>2</sub>O<sub>3</sub> (Sigma, powder) and CuO/Al<sub>2</sub>O<sub>3</sub> (*IWI* CuO loading = 10 %wt.) as such and calcined at 500°C.**

Catalyst	T (°C)	pO <sub>2</sub> (bar)	t (h)	Stirring rate (rpm)	%wt. Cat.	Y <sub>PELARG,DSA</sub> (%)	Y <sub>AZEL,DSA</sub> (%)
CuO/Al <sub>2</sub> O <sub>3</sub> Sigma	80	25	5	500	1,0%	20%	31%
CuO/Al <sub>2</sub> O <sub>3</sub> Sigma Calc500°C	80	25	5	500	1,0%	21%	31%
CuO/Al <sub>2</sub> O <sub>3</sub> <i>IWI</i> _10%wt.	80	25	5	500	1,0%	13%	20%
CuO/Al <sub>2</sub> O <sub>3</sub> <i>IWI</i> _10%wt. Calc500°C	80	25	5	500	1,0%	21%	30%

As it is possible to note from the table above, the calcination treatment caused an increase of the yields of PA and AA only with the catalyst synthesized with *IWI* method. These results can be explained by comparing T.P.R./O. (Figure 6.34) and B.E.T. (Table 6-22) analysis of the samples as such and calcined at 500°C for 3 h.

The T.P.R. profiles of the samples were similar despite the different thermal treatment. However, the TPR<sub>2</sub> peak area shown by CuO/Al<sub>2</sub>O<sub>3</sub> *IWI*\_10%wt. calcined at 500 °C was greater than the area of the material calcined at 300 °C. Therefore, the amount of reducible species obtained after oxidation was higher than that one obtained by calcination at 300 °C.

As far as the commercial material is concerned, the calcination step caused an increase of surface area (see Table 6-22) probably because of the decomposition of some additive used by the producer in order to form the pellets. The increase of surface area was registered together with a small increase of the yield of PA and AA. Moreover, the

temperature at which the TPR<sub>1</sub> occurred was lower for the calcined sample, suggesting an easier reducibility of the Cu compared to the same catalyst calcined at 300 °C only.

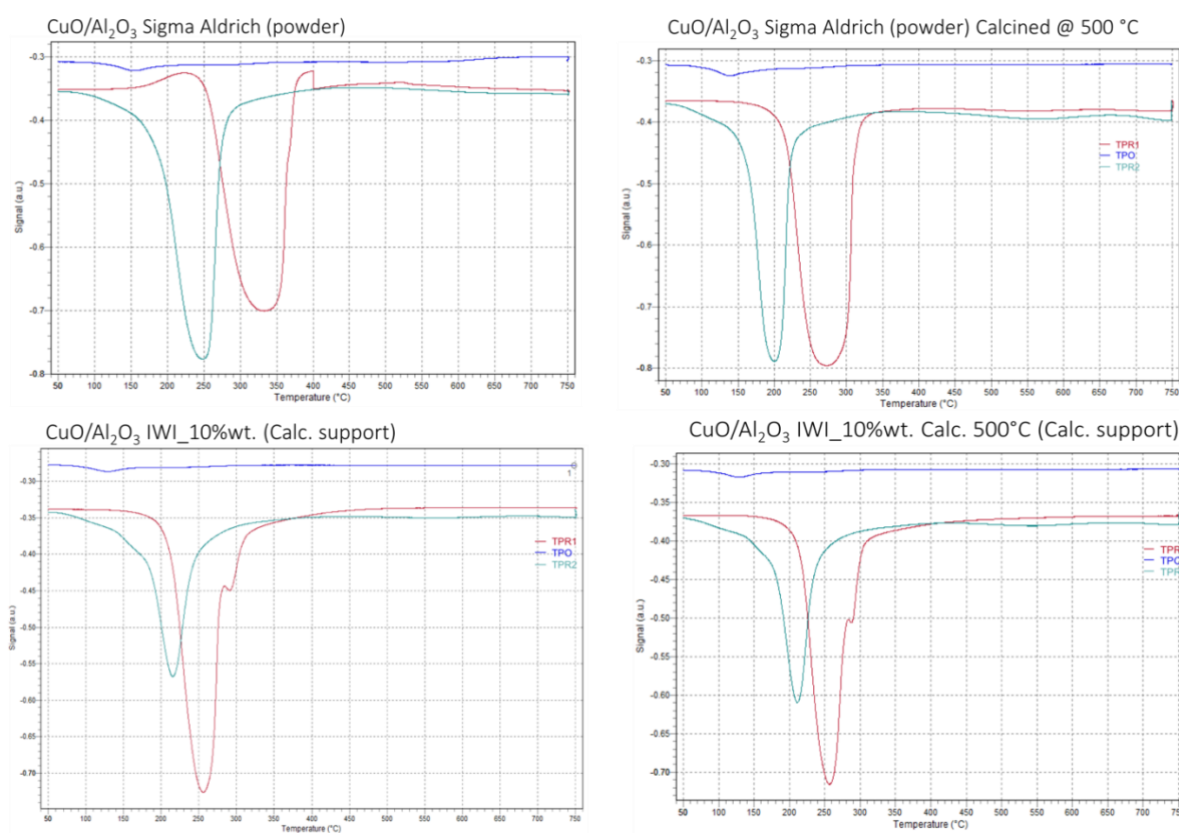


**Figure 6.34.** TPR<sub>1</sub>-O-R<sub>2</sub> profile of CuO supported on alumina: commercial CuO/Al<sub>2</sub>O<sub>3</sub> Sigma-Aldrich (powder from pellets) and synthesized CuO/Al<sub>2</sub>O<sub>3</sub> (support calc.@500°C) with two different thermal treatments.

**Table 6-22.** B.E.T. surface area of commercial copper oxide supported over alumina as it and calcined at 500 °C.

SAMPLE	Thermal treatment	ASS <sub>B.E.T.</sub> m <sup>2</sup> /g
CuO/Al <sub>2</sub> O <sub>3</sub> Sigma (Powder)	None	179
	Calc. 500°C for 3h (3°C/min)	185

Thereafter, the two materials calcined at 500°C were tested in the oxidative cleavage after their recovery from the reaction mixture and then regenerated with a calcination

step at 500 °C for 3h. As it is possible to note from the graph in Figure 6.35, the regeneration procedure was successful.

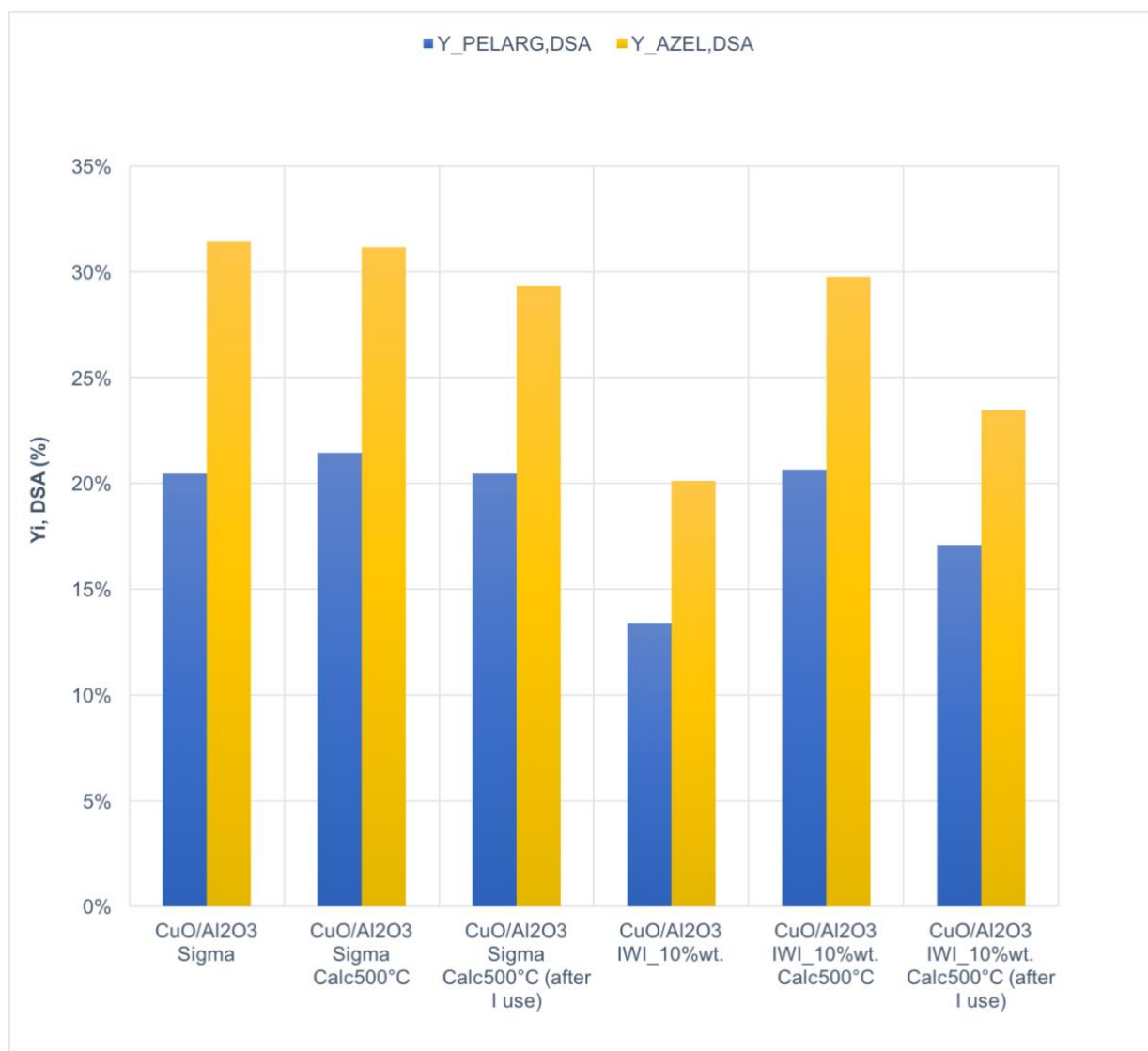


**Figure 6.35.** Results in terms of yields of azelaic ac. (AA) and pelargonic ac.(PA) obtained in the oxidative cleavage of DSA using CuO/Al<sub>2</sub>O<sub>3</sub> (Sigma, powder) and CuO/Al<sub>2</sub>O<sub>3</sub> (IWI CuO loading = 10 %wt.) as such, calcined at 500 °C and after a regeneration step (calc. at 500 °C for 3 h).

### **6.3.3.7. Conclusions on Catalytic tests with CuO over alumina**

The reactivity tests carried out by using CuO/Al<sub>2</sub>O<sub>3</sub> underlined the possibility of exploitation of copper oxide as active phase for the oxidative cleavage of vicinal glycols derived from unsaturated fatty acids. The commercial catalyst showed an enhancement of the performance compared to the unsupported bulk active phase especially in regard to the recovery and stability of the catalytic system. Moreover, it was demonstrated the possibility of the re-use of the recovered catalyst just through an easy regeneration step consisting in calcination.

Thanks to the experiments carried out by changing time and temperature it was demonstrated that the best performance in terms of yield to AA and PA was obtained with the commercial CuO/Al<sub>2</sub>O<sub>3</sub> between 80-100°C and after 6-8 hours of reaction.

Furthermore, this commercial catalyst was successfully reproduced in our lab with a very easy technique commonly used for the synthesis of supported catalysts.

### 6.3.4. Copper oxide over different supports

As reported in chapter 6.2.2, copper based catalysts showed a very good activity in the oxidative cleavage of 9,10-dihydroxystearic acid.

We then focussed the investigation on the active phase-support interaction.

The synthesis of the selected materials was performed with the *incipient wetness impregnation* of the desired support, as described in chapter 5.1.4.

#### 6.3.4.1. Characterization of catalysts

The synthesized materials were characterized by means of several techniques, described in the chapter 5.2.

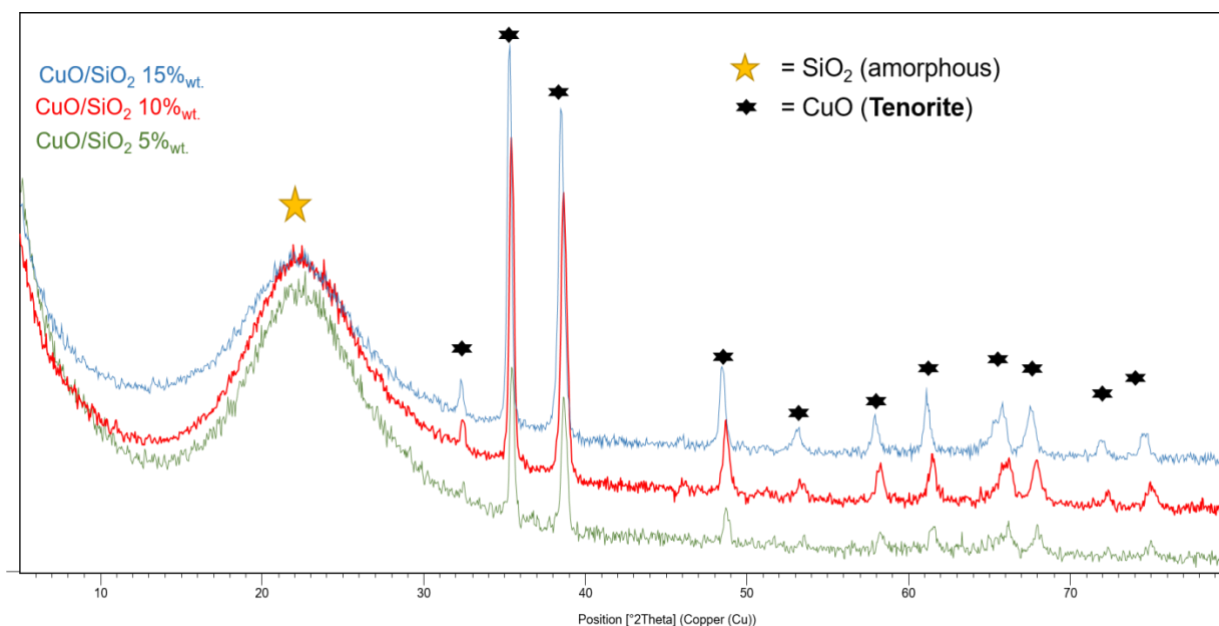


Figure 6.36. X.R.D. pattern of CuO over SiO<sub>2</sub>.

Figure 6.36 shows the X.R.D. patterns of CuO/SiO<sub>2</sub> catalysts. Diffraction lines attributable to CuO (tenorite) were very clear due to the amorphous nature of the support. The broad reflection at 22° 2θ was attributed to SiO<sub>2</sub>.

Furthermore, X.R.D. patterns of CuO over CeO<sub>2</sub> and TiO<sub>2</sub> (Figure 6.37 and Figure 6.38, respectively) showed the typical reflections of CuO only for the sample with CuO loading of 10% wt. and 15% wt. for CuO/TiO<sub>2</sub> samples, and of 15% wt. for CuO/CeO<sub>2</sub> samples.



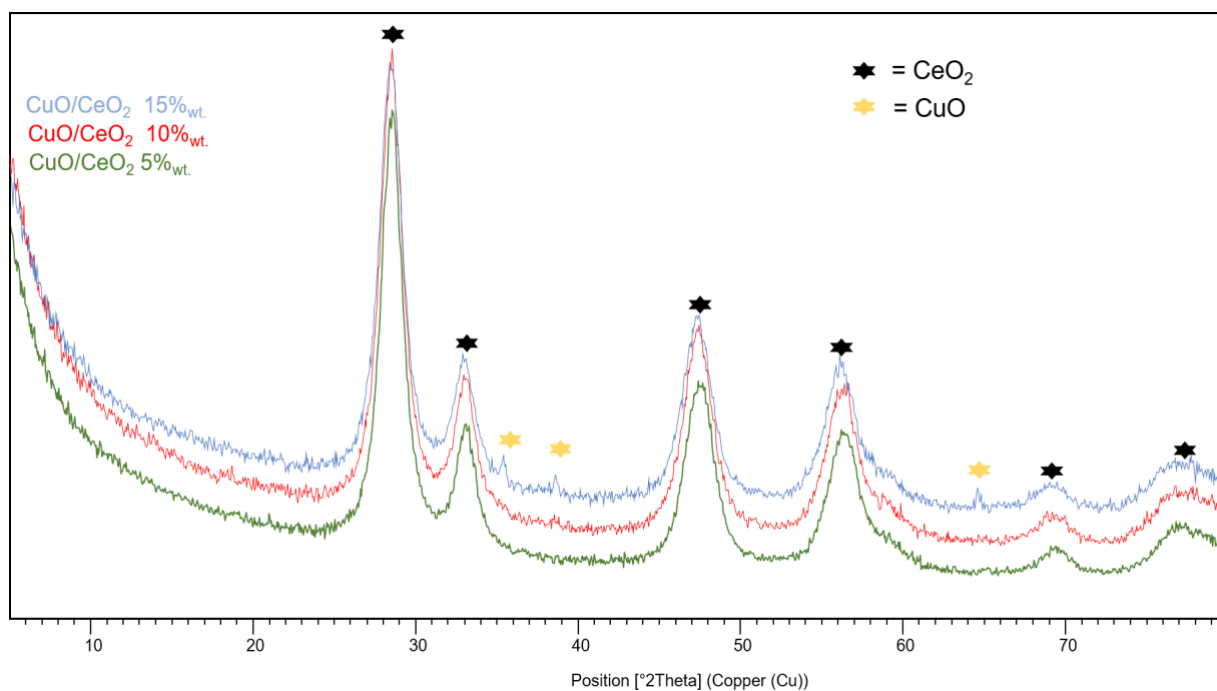


Figure 6.37. X.R.D. pattern of CuO over Ce<sub>2</sub>O.

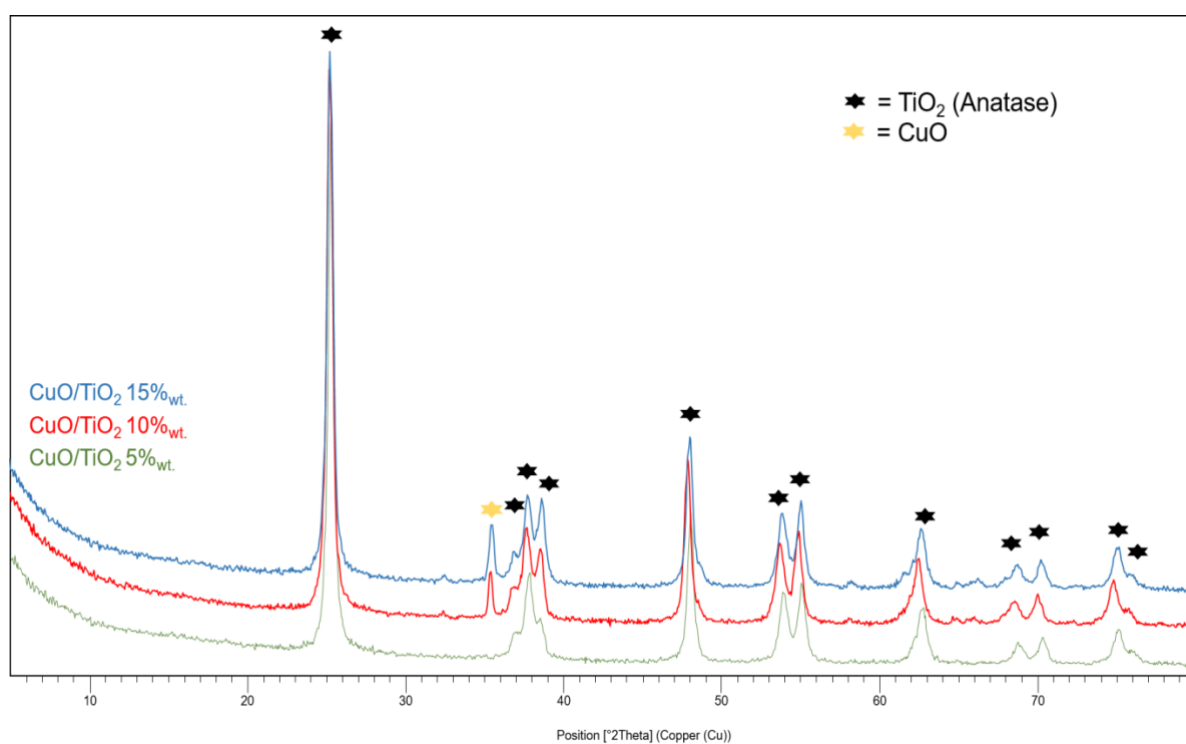


Figure 6.38. X.R.D. pattern of CuO over TiO<sub>2</sub>.

The results of surface area and porosity measurements are presented in Table 6-23:

**Table 6-23. Results of the surface area and porosity analysis of CuO over different supports.**

SAMPLE	S <sub>B.E.T.</sub>	V <sub>pore</sub>	Pore average diameter
	m <sup>2</sup> /g	cm <sup>3</sup> /g	nm
TiO <sub>2</sub> - DT51	90	0,32	14,6
CuO/TiO <sub>2</sub> 5% <sub>wt.</sub>	75	0,31	13,8
CuO/TiO <sub>2</sub> 10% <sub>wt.</sub>	76	0,31	13,8
CuO/TiO <sub>2</sub> 15% <sub>wt.</sub>	76	0,31	13,6
CeO <sub>2</sub> Solvay	264	0,16	3,0
CuO/CeO <sub>2</sub> 5% <sub>wt.</sub>	214	0,17	3,2
CuO/CeO <sub>2</sub> 10% <sub>wt.</sub>	195	0,15	3,3
CuO/CeO <sub>2</sub> 15% <sub>wt.</sub>	198	0,15	3,0
SiO <sub>2</sub> - 360 GRACE	543	1,09	8,1
CuO/SiO <sub>2</sub> 5% <sub>wt.</sub>	487	0,99	8,2
CuO/SiO <sub>2</sub> 10% <sub>wt.</sub>	475	0,97	8,2
CuO/SiO <sub>2</sub> 15% <sub>wt.</sub>	442	0,91	8,3

It is possible to note that the surface area changed from catalyst to catalyst, together with the pores diameter and volume. This could have significant effects on catalysts reactivity.

Results of X-ray Fluorescence spectroscopy (X.R.F.) analysis are shown in Table 6-24.

It is possible to conclude that the amount of active phase deposited was in all cases close to the expected one.

Table 6-24. X.R.F. analysis of CuO over different inorganic supports.

Sample	% <sub>wt.</sub> CuO
CuO/TiO <sub>2</sub> 5% <sub>wt.</sub>	5,3
CuO/TiO <sub>2</sub> 10% <sub>wt.</sub>	9,9
CuO/TiO <sub>2</sub> 15% <sub>wt.</sub>	13,5
CuO/CeO <sub>2</sub> 5% <sub>wt.</sub>	5,1
CuO/CeO <sub>2</sub> 10% <sub>wt.</sub>	10,7
CuO/CeO <sub>2</sub> 15% <sub>wt.</sub>	15,2
CuO/SiO <sub>2</sub> 5% <sub>wt.</sub>	6,3
CuO/SiO <sub>2</sub> 10% <sub>wt.</sub>	10,5
CuO/SiO <sub>2</sub> 15% <sub>wt.</sub>	14,6

The morphology and structure of catalysts with CuO loading of 5%<sub>wt.</sub> were investigated by means of S.E.M-E.D.X. analysis. Figure 6.36 shows the images obtained, while Table 6-25 collects the results of E.D.X. analysis.

Table 6-25. Results obtained with E.D.X. analysis of CuO over different supports.

Catalyst	Cu % <sub>wt.</sub>	Si % <sub>wt.</sub>	Ti % <sub>wt.</sub>	Ce % <sub>wt.</sub>	O % <sub>wt.</sub>	Calculated % <sub>wt.</sub>
<b>CuO/SiO<sub>2</sub></b> IWI_5% <sub>wt.</sub>	4,5	44,0	-	-	51,5	5,7
<b>CuO/CeO<sub>2</sub></b> IWI_5% <sub>wt.</sub>	3,8	-	-	78,6	32,6	4,7
<b>CuO/TiO<sub>2</sub></b> IWI_5% <sub>wt.</sub>	3,7	-	50,3	-	45,9	4,7

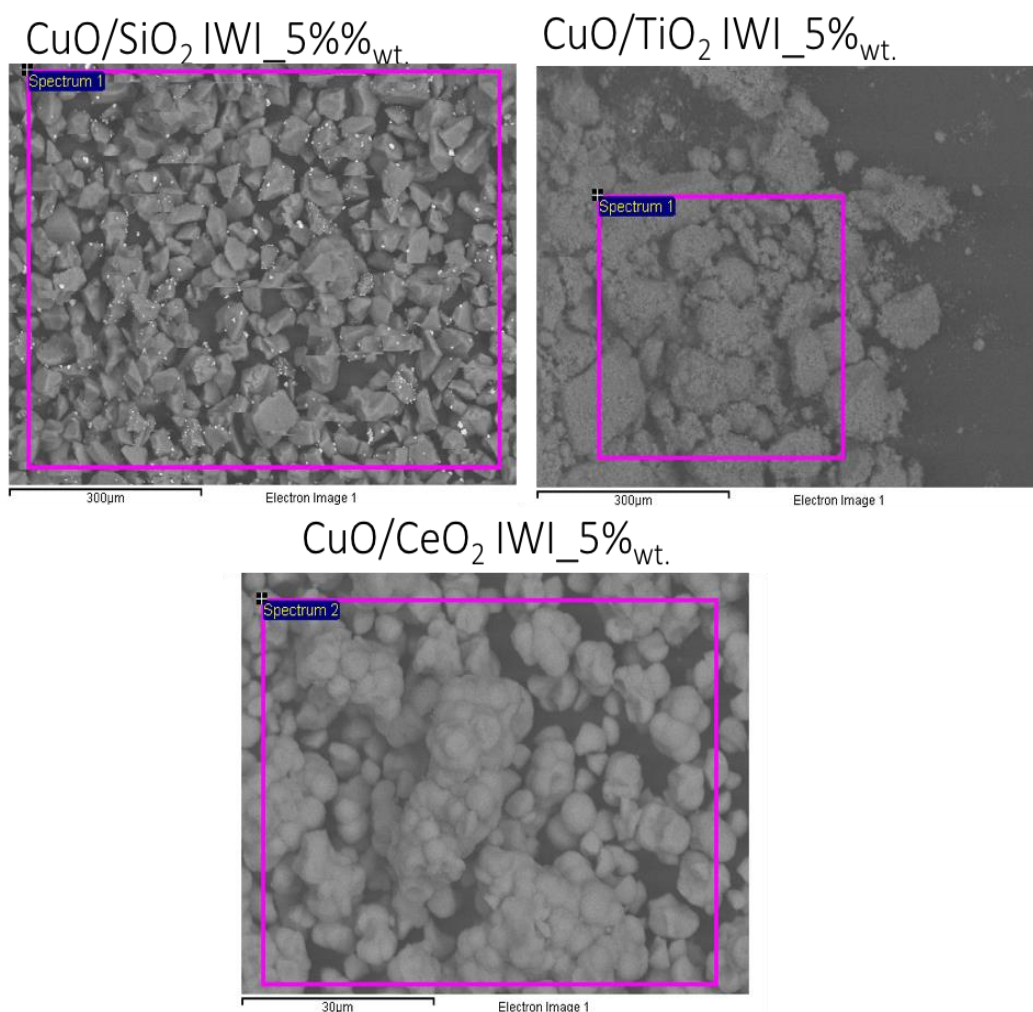


**Figure 6.39. S.E.M. images of CuO over different supports.**

S.E.M.-E.D.X. analysis confirmed the results of X.R.F. Therefore, *IWI* was a reliable method to obtain the amount of the supported phase.

Catalysts appeared very different both in terms of morphology and dispersion of the active phase. With CuO/SiO<sub>2</sub>, it is possible to see clearly the active phase (white dots) with a very good dispersion, while with the other catalysts CuO was not detectable, maybe because of the extremely low particles dimension.

The temperature programmed reduction-oxidation-reduction (TPR<sub>1</sub>-O-R<sub>2</sub>) analysis was performed in order to evaluate the redox properties of CuO in supported materials, with the aim of correlating with catalytic performance.

The conditions used for analysis were the same as those used for the copper oxide over alumina, as reported in chapter 5.2.4

Temperature programmed reduction/oxidation/reduction profiles for catalysts with 5%<sub>wt.</sub> CuO loading of are shown in Figure 6.40.

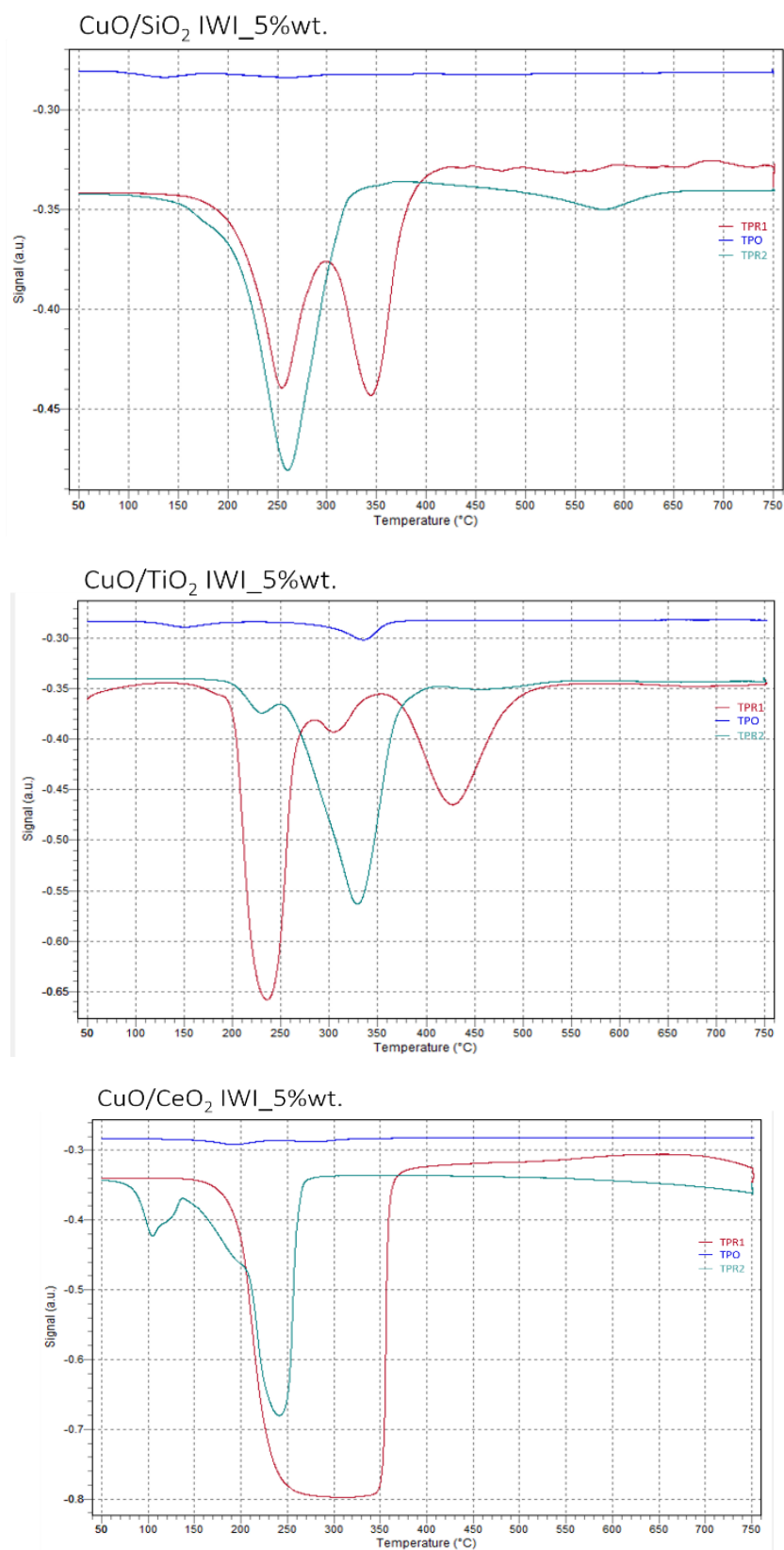


Figure 6.40. TPR<sub>1</sub>-O-R<sub>2</sub> profiles of supported CuO catalysts.

It was very interesting to observe different TPR/O profiles for the materials synthesized despite the fact that they contained the same amount of active phase.

For each sample, TPR<sub>1</sub> showed a peak that can be ascribed to the reduction of CuO into Cu<sup>(0)</sup>.

Another important parameter is the temperature at which peaks occurred, that gives an idea of the easiness of the reduction/oxidation process: if the temperature of the peak is low, the energy required for the reaction (red/ox) is lower. Different peaks at different temperatures could mean either the presence of different particles or the formation of different species. Table 6-26 compiles the temperature of peaks of each catalyst.

**Table 6-26. Temperature maxima of the peaks obtained from the TPR<sub>1</sub>-O-R<sub>2</sub> analysis with supported CuO.**

CATALYST	Temperature of (First) Reduction peak maxima (°C)			Temperature of Oxidation peak maxima (°C)				Temperature of (Second) Reduction peak maxima (°C)			
	$\alpha 1$	$\alpha 2$	$\alpha 3$	$\beta 1$	$\beta 2$	$\beta 3$	$\beta 4$	$\gamma 1$	$\gamma 2$	$\gamma 3$	$\gamma 4$
<b>CuO (Merck)</b>		300					690			350	
<b>CuO/TiO<sub>2</sub></b> <b>IWI_5%<sub>wt.</sub></b>	235	310	430	150		335			230	330	460
<b>CuO/CeO<sub>2</sub></b> <b>IWI_5%<sub>wt.</sub></b>		280		190	290			105	240		
<b>CuO/SiO<sub>2</sub></b> <b>IWI_5%<sub>wt.</sub></b> (pellets)	255	350		135	260				260		

Thermogravimetric analysis was performed in order to fully characterize the materials synthesized.

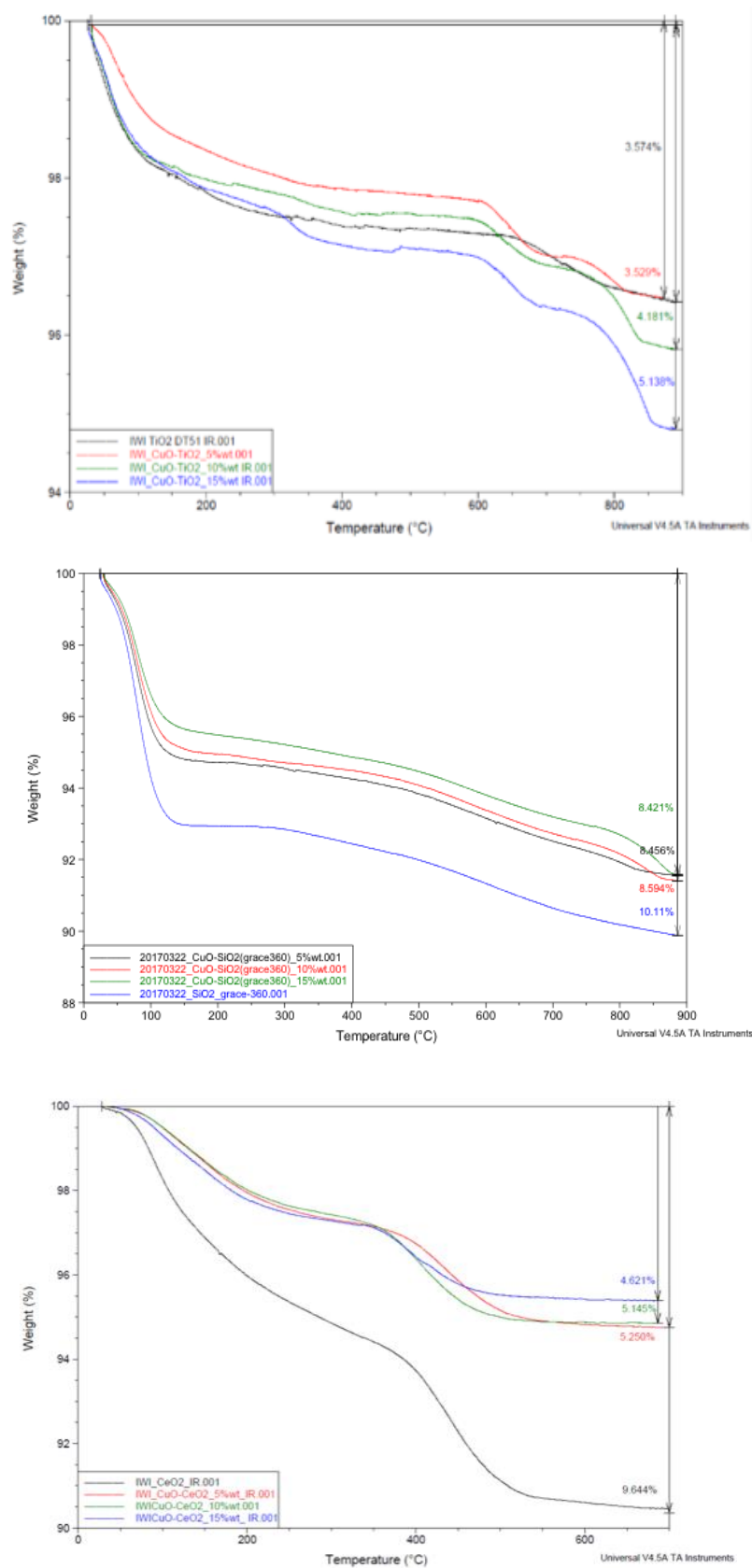
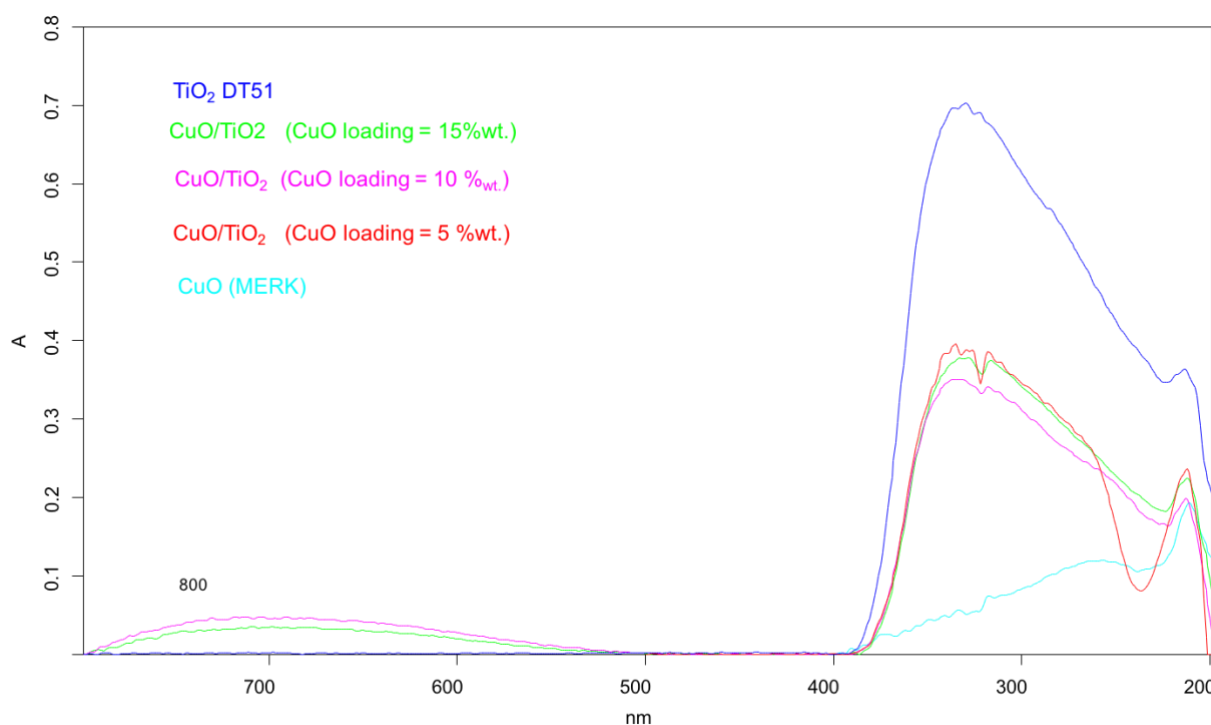


Figure 6.41. Results of T.G.A. analysis of copper oxide over (from the top-left image) TiO<sub>2</sub>, SiO<sub>2</sub> and CeO<sub>2</sub>.



In the case of CuO/TiO<sub>2</sub>, materials synthesized showed different colours. Therefore, Diffuse Reflectance UV-vis spectroscopy analysis was performed in order to explain this experimental evidence. The coordination of Ti into the materials can be determined by means of DR-UV spectroscopy; spectra are reported in Figure 6.42



**Figure 6.42. UV-Vis DRS spectra of CuO over titania (DT-51).**

It was possible to distinguish the band at 210 nm attributed to framework a tetrahedral Ti, and the broad band between 290 nm and 320 nm that was attributed to bulk Ti in the anatase form.

Differences in spectra can be attributed to the different condensation degree of copper species: CuO was dispersed on titania surface in the form of monomeric species with high dispersion only at low concentration 5%wt. while more aggregated species were formed upon increasing CuO loading.

Accordingly, the different dispersion of the active phase could explain the different colour shown by samples.

In conclusion, CuO when dispersed over different supports showed different redox proprieties. This difference could be related to two reasons: first, the chemical

interaction between the active phase and the support was different; second, supporting CuO over materials with dissimilar morphology caused different dispersion and uniformity in the active phase particle size, as confirmed by S.E.M. and UV-vis DRS analysis.

#### **6.3.4.2. Catalysts screening with multiple reactor system**

The materials synthesized with the *IWI*-method were tested in the multiple reactor system described in chapter 5.3.1.1. With this apparatus it was possible to quickly test all the catalysts under the same reaction conditions.

The catalysts used in the screening were:

- CuO/SiO<sub>2</sub> (CuO loading: 5%<sub>wt.</sub>, 10%<sub>wt.</sub>, 15%<sub>wt.</sub>);
- CuO/TiO<sub>2</sub> (CuO loading: 5%<sub>wt.</sub>, 10%<sub>wt.</sub>, 15%<sub>wt.</sub>);
- CuO/CeO<sub>2</sub> (CuO loading: 5%<sub>wt.</sub>, 10%<sub>wt.</sub>, 15%<sub>wt.</sub>).

The catalyst screening was carried out using the 9,10-dihydroxystearic acid as the starting material (see chapter 6.1.2).

The reactions were performed in a six independent autoclaves system of 25 cm<sup>3</sup> each, equipped with bottom magnetic stirrers.

The catalysts screening were carried out with the modality described in chapter 5.3.1.1, while conditions used were those taken from the previous catalytic tests:

- 10 g of starting material (dihydroxylated oil) and 0,10 g of catalyst (1%<sub>wt.</sub> of catalyst with respect to the amount of s.m.);
- temperature of reaction = 80 °C;
- stirring rate = 500 rpm;
- pure molecular oxygen as oxidant;
- pressure of oxidant = 25 bar;
- reaction time = 5 h.

For the catalysts screening, attention was focused on the production of the two desired products: pelargonic acid and azelaic acid. Yields were calculated with equation (7) reported in chapter 5.3.5.2.

Results are reported in Figure 6.43, while the pictures of the different final reaction mixtures are presented in Figure 6.44:

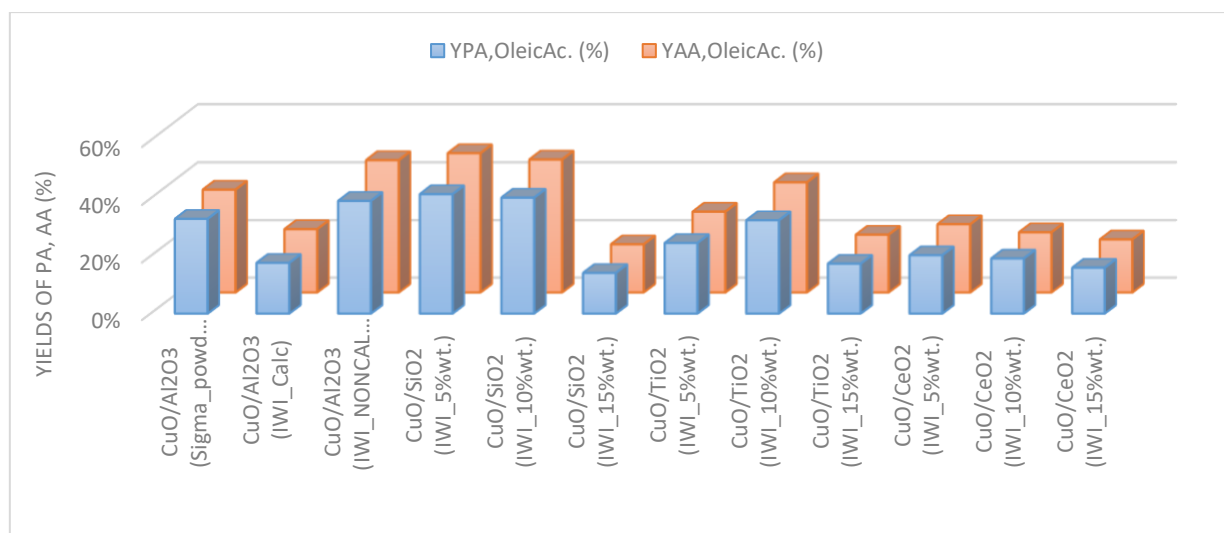


**Figure 6.43.** Catalytic performance in terms of yields of PA and AA obtained using CuO over different supports, at 80 °C, 5 h, 25 bar O<sub>2</sub>, stirring 1000 rpm.

It is clear that copper oxide over silica presented a good activity in the oxidative scission, similar to that one shown by CuO/Al<sub>2</sub>O<sub>3</sub>.



**Figure 6.44.** Reaction mixture obtained with all catalysts screened in the multiple reactor system at 80 °C, 5h, 25 bar O<sub>2</sub>, bottom stirring 1000 rpm.

As already described in conclusions of chap. 6.2.3, the reaction mixture obtained with the inactive catalysts continued to be solid at room temperature. On the contrary, active catalysts produced a fluid reaction mixture with a viscosity more or less inversely proportional to the degree of conversion.

Another very important feature was the colour of the final reaction mixture: in some cases, the reaction mixture appeared green, suggesting the occurrence of leaching phenomenon. Copper oxide over silica showed a very pale yellow colour indicating no important leaching phenomenon.

#### **6.3.4.3. *Conclusions about supported catalysts screening***

Based on results achieved with the catalytic screening, CuO/SiO<sub>2</sub> was chosen as candidate for subsequent investigation in batch reactor, in order to compare the results with those achieved with the commercial CuO/Al<sub>2</sub>O<sub>3</sub>.

### 6.3.5. Catalyst tests with copper oxide supported over silica

Based on results achieved by the screening of different supports, another promising candidate was selected: CuO/SiO<sub>2</sub>.

With this material, it was possible to obtain a final reaction mixture looking like those obtained with CuO/Al<sub>2</sub>O<sub>3</sub>, besides a good yield of the two desired products (i.e. AA and PA).

Furthermore, silica presented some advantages compared to alumina. On the one hand, silica has high surface area compared to alumina, second it is less expensive.

**Table 6-27. B.E.T. surface area of different materials chose as support.**

MATERIAL	ASS <sub>B.E.T.</sub> (m <sup>2</sup> /g)
Al <sub>2</sub> O <sub>3</sub> (Aldrich)	292
Al <sub>2</sub> O <sub>3</sub> (Aldrich) calcined at 500°C	256
SiO <sub>2</sub> 360-Grace	544

On the other hand, the main drawback of the industrial use of silica could be the erosion of some mechanical parts of the reactor because of its abrasive properties.

Nevertheless, the catalyst made of copper oxide over silica was tested in batch reactor (see chap.5.3.1.2) with the following conditions:

- 100 mL autoclave with magnetic drive and PTFE vessel;
- 15 g of starting material (dihydroxylated oil) and 0,15 g of catalyst (1%<sub>wt.</sub> of catalyst with respect to the amount of s.m.);
- temperature of reaction = 80 °C;
- stirring rate = 500 rpm;
- pure molecular oxygen as oxidant;

- pressure of oxidant = 25 bar;
- time of reaction = 5 h.

The reaction products were analysed by means of GC-FID after a derivatization process (described in chapter 5.3.2) and the catalyst was recovered by means of centrifugation.

Results in terms of maximum yields of PA and AA (see equation (7)) are shown in Figure 6.45.

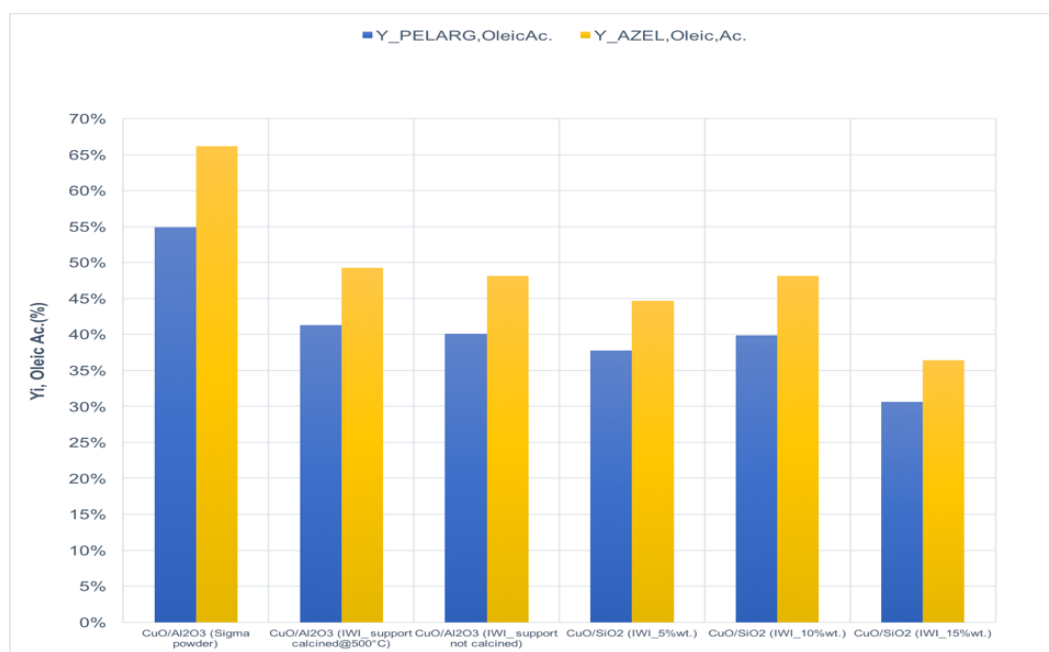


**Figure 6.45.** Maximum yields of PA and AA in the oxidative cleavage of DSA with CuO over different supports in batch reactor at 80 °C, 5 h, 25 bar O<sub>2</sub>, stirring 500 rpm.

The final reaction mixture obtained with CuO over alumina and silica are compared in Figure 6.46.

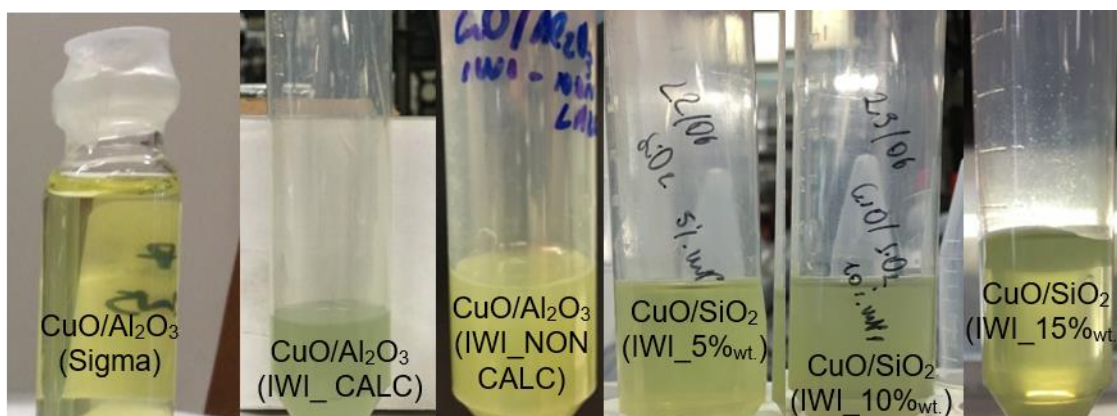


**Figure 6.46.** Reaction mixture obtained with all catalyst tested in batch reactor at 80 °C, 5h, 25 bar O<sub>2</sub>, stirring 500 rpm.

The mixture obtained with CuO/SiO<sub>2</sub> looked more or less the same as those obtained with CuO/Al<sub>2</sub>O<sub>3</sub>, suggesting that no leaching occurred, as already discussed in chap. 6.3.4.

Interesting results were obtained by evaluating the “turnover” for each catalyst, using the following formula:

$$(4) \text{TON} = \frac{Y_{i,\text{Oil}}}{\%p_{\text{CuO}}} \times 100$$

(With %*p*<sub>CuO</sub> the amount (expressed in percentage by weight) of CuO over the support.)

This parameter is representative of the activity of the catalyst: a higher *TON* means a higher amount of substrate that is converted into the desired products per unit time.

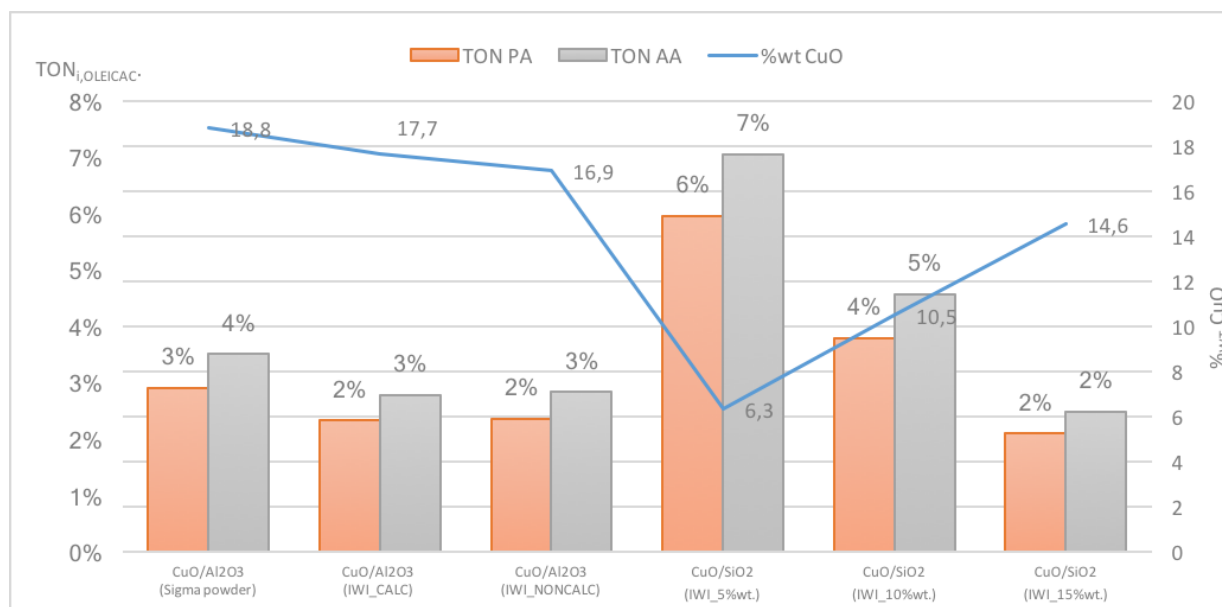


**Figure 6.47. “Turnover” related to pelargonic and azelaic ac. %wt. CuO loading of each catalyst tested in batch reactor at 80 °C, 5h, 25 bar O<sub>2</sub>, stirring 500 rpm**

According to these results, it was clear that CuO/SiO<sub>2</sub> (CuO loading = 5%wt.) was able to convert a higher amount of DSA into AA and PA compared to the other catalysts.

Therefore, the CuO/SiO<sub>2</sub> (CuO loading = 5%wt.) system was studied more in detail in the aim of correlating its chemical-physical properties with reactivity results.

#### **6.3.5.1. On the effect of reaction time**

The synthesized CuO/SiO<sub>2</sub> (CuO loading = 5%<sub>wt.</sub>) was employed for the kinetic investigation of DSA oxidative cleavage. The experiments were carried out by changing the reaction time from 0 to 8 hours.

The catalytic tests were carried out with the modality described in chapter 5.3.1.2 with the following conditions:

- 100 mL autoclave with magnetic drive and PTFE vessel;
- 15 g of starting material (dihydroxylated oil) and 0,15 g of catalyst (1%<sub>wt.</sub> of catalyst with respect to the s.m. amount);
- temperature of reaction = 80 °C;
- stirring rate = 500 rpm;
- pure molecular oxygen as oxidant;
- pressure of oxidant = 25 bar;
- time of reaction = 0, 2, 5, 6, 8 h.

The reaction products were analysed by GC-FID after derivatization (described in chapter 5.3.2), and the catalyst was recovered by means of centrifugation.

DSA conversion and yields to AA and PA are shown in Table 6-15. In this case, results were calculated by applying equations (4) and (5).



**Table 6-28. DSA Oxidative cleavage catalysed by CuO/SiO<sub>2</sub> (IWI\_5%<sub>wt.</sub>) in function of reaction time.**

Catalyst	t (h)	pO <sub>2</sub> (bar)	T (°C)	% <sub>wt.</sub> Cat.	X <sub>DSA</sub> (%)	Y <sub>PELARG,DSA</sub> (%)	Y <sub>AZEL,DSA</sub> (%)
CuO/SiO <sub>2</sub> (IWI_5% <sub>wt.</sub> )	2	25	80	1,0	11	2	2
	4	25	80	1,0	57	2	18
	5	25	80	1,0	65	12	17
	8	25	80	1,0	58	14	19

Experiments were carried out by changing the reaction time and results are reported in Figure 6.48. Even in this case, yields of PA and AA were calculated with equation (5).

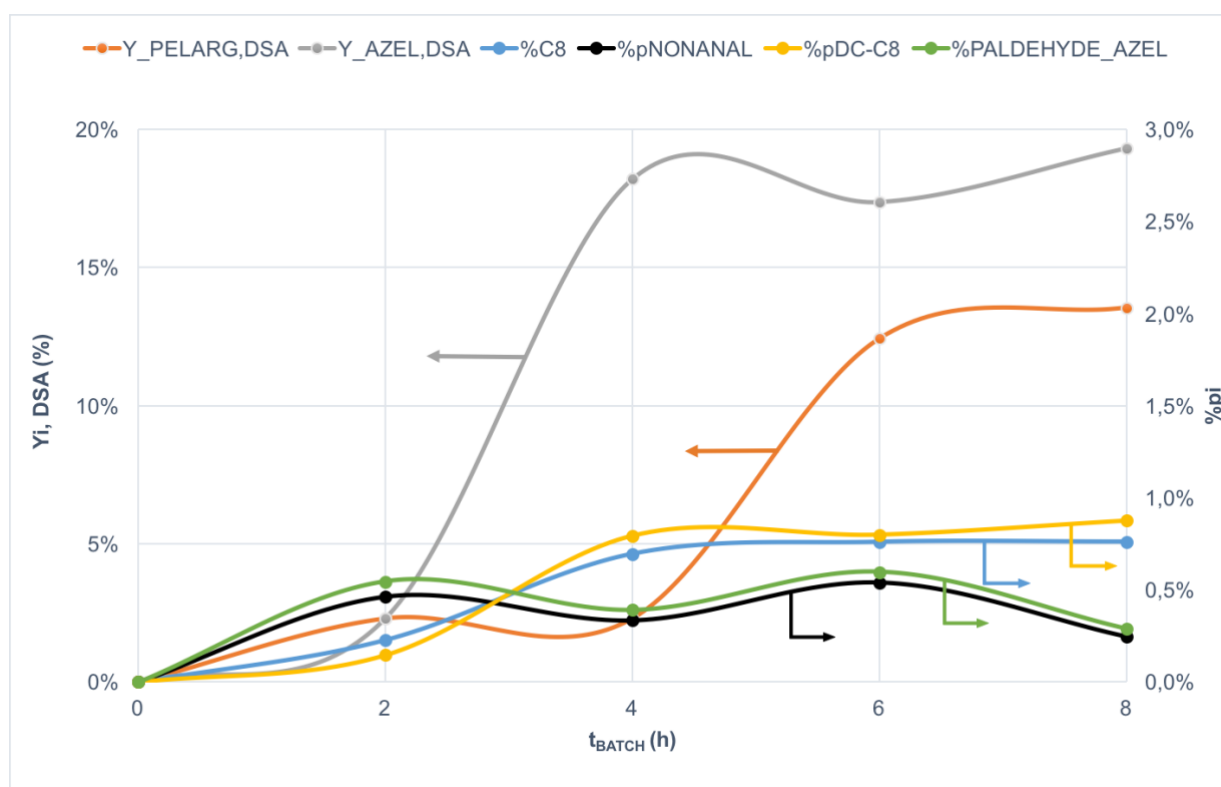


**Figure 6.48. Oxidative cleavage of DSA with CuO/SiO<sub>2</sub> (CuO loading = 5%<sub>wt.</sub>) by changing the reaction time with 1%<sub>wt</sub> CuO/SiO<sub>2</sub> (CuO loading: 5%<sub>wt.</sub>). Yields of pelargonic acid (Y<sub>PELARG,DSA</sub>) and azelaic acid (Y<sub>AZEL,DSA</sub>) registered at 80 °C, 25 bar O<sub>2</sub>, stirring 500 rpm; it is also reported the weight percentage of octanoic ac. (%pC8), nonanal (%pNONANAL), suberic ac. (%pDC-C8) and 9-oxononanoic acid (%pALDEHYDE\_AZEL).**

An increase of yields of the two targeted products (i.e. PA and AA) were shown by increasing the reaction time until a constant value at around 4-5 hours of reaction time.

The picture shows the %p<sub>i</sub> (see eq. (6)) of the main by-products. The amount of suberic and octanoic acids followed the same profile as that one shown in the case of the CuO/Al<sub>2</sub>O<sub>3</sub> catalyst. Conversely, the two aldehydes were formed at the very beginning the reaction, but their consecutive conversion was lower and almost constant compared to the one registered with CuO/Al<sub>2</sub>O<sub>3</sub>.

The final reaction mixtures are shown in Figure 6-51; they appeared of pale yellow colour for all tests and this effect could be attributed to a negligible catalyst leaching.

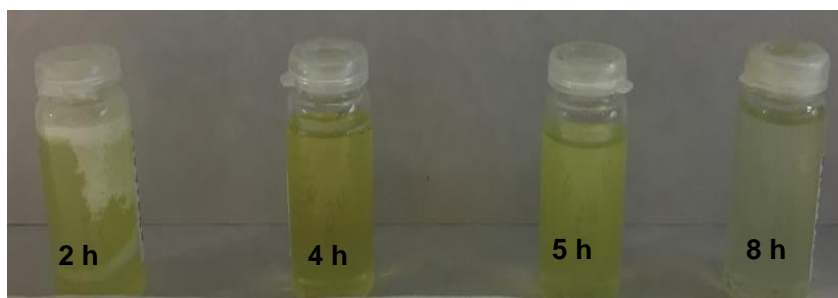


**Figure 6-49.** Pictures of reaction mixtures obtained after experiments with CuO/SiO<sub>2</sub> (CuO loading = 5%wt.) in function of temperature: (in order from left to right) 2, 4, 6, 8 h at 80 °C, 25 bar O<sub>2</sub>, stirring 500 rpm.

### 6.3.5.2. On the effect of reaction temperature

Oxidative scission of DSA was carried out in function of temperature using CuO/SiO<sub>2</sub> (CuO loading = 5%<sub>wt.</sub>). The experiments were carried out by changing the temperature from 60 °C until 140 °C; 60 °C was the lowest T because below it the starting material is solid, while 140 °C was the upper T limit for the PTFE vessel, as explained in chap. 6.3.3.2.

The catalytic tests were carried out with the modality described in chapter 5.3.1.2 using the following conditions:

- 100mL autoclave with magnetic drive and PTFE vessel;
- 15 g of starting material (dihydroxylated oil) and 0,15 g of catalyst (1%wt. of catalyst respect to the amount of s.m.);
- temperature of reaction = 60, 80, 100, 120, 140 °C;
- stirring rate = 500 rpm;
- pure molecular oxygen as oxidant;
- pressure of oxidant = 25 bar;
- reaction time = 5 h.

The reaction products were analysed by means of GC-FID after derivatization (described in chapter 5.3.2) and the catalyst was recovered by means of centrifugation.

Results are summarized in Table 6-29 and Figure 6.50.

**Table 6-29. Oxidative cleavage of DSA (9,10-dihydroxystearic acid) catalysed by CuO/SiO<sub>2</sub> (IWI\_5%wt.) in function of reaction temperature.**

Catalyst	T (°C)	pO <sub>2</sub> (bar)	t (h)	% <sub>wt.</sub> Cat.	X <sub>DSA</sub> (%)	Y <sub>PELARG,DSA</sub> (%)	Y <sub>AZEL,DSA</sub> (%)
CuO/SiO <sub>2</sub> (IWI_5%wt.)	60	25	5	1,0%	11%	0%	0%
	80	25	5	1,0%	80%	13%	19%
	100	25	5	1,0%	81%	13%	20%
	120	25	5	1,0%	82%	7%	12%
	140	25	5	1,0%	86%	1%	1%

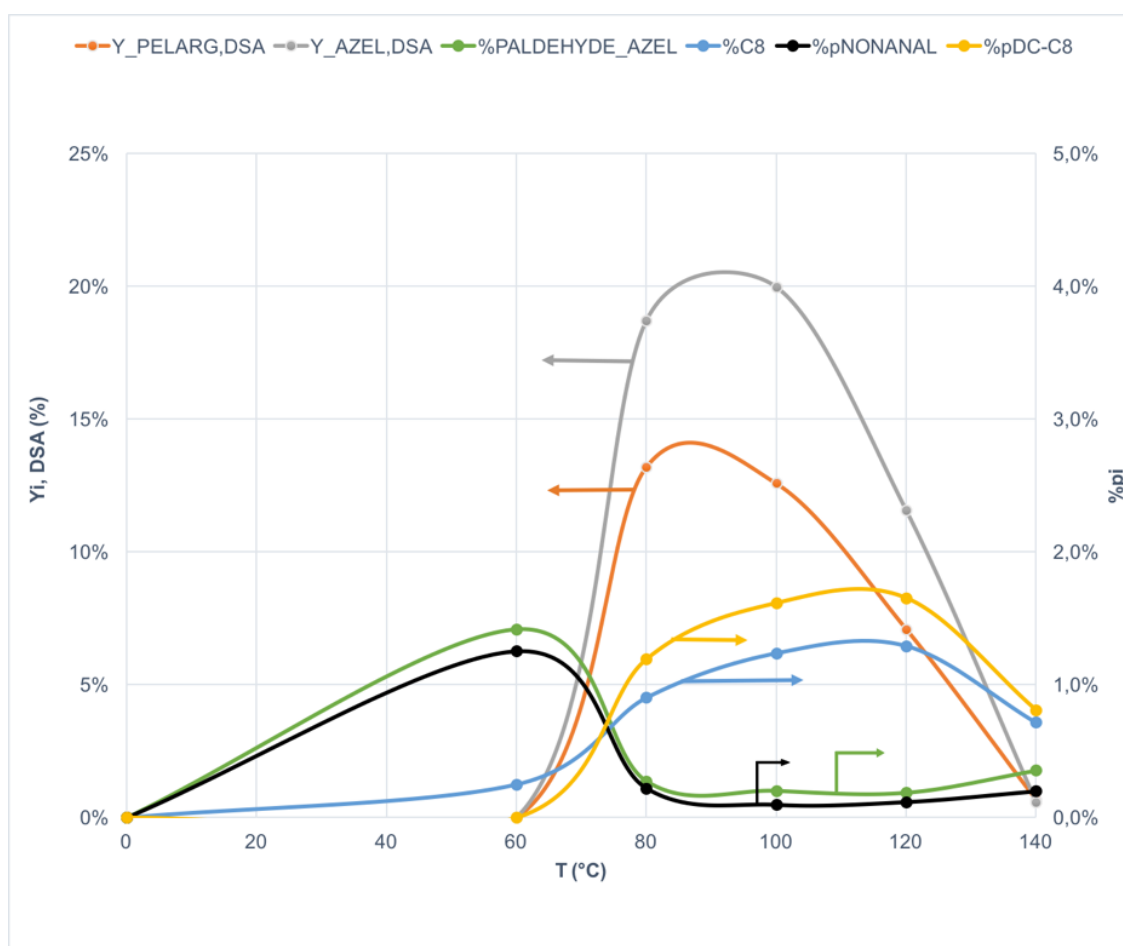


**Figure 6.50. Oxidative cleavage of DSA with CuO/SiO<sub>2</sub> (CuO loading = 5%wt.) obtained by changing the reaction temperature with 1%wt CuO/SiO<sub>2</sub> (CuO loading: 5%wt.); yields of pelargonic acid (Y<sub>PELARG,DSA</sub>) and azelaic acid (Y<sub>AZEL,DSA</sub>) registered at 80 °C, 25 bar O<sub>2</sub>, stirring 500 rpm; it is also reported the weight percentage of octanoic ac. (%pC8), nonanal (%pNONANAL), suberic ac. (%pDC-C8) and 9-oxononanoic acid (%pALDEHYDE\_AZEL).**

It is shown that DSA conversion of increased in concomitance with the increase of the reaction temperature. Conversely, the yields of AA and PA reached a maximum value

at 100 °C, after which the drop shown was probably due to a thermal degradation. This hypothesis was confirmed by data shown in Figure 6.36: the final reaction mixture became darker due to the formation of heavier by-products already at 100 °C.

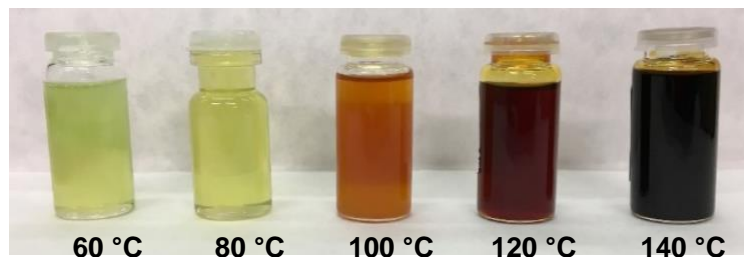


**Figure 6-51. Pictures of reaction mixtures obtained with CuO/SiO<sub>2</sub> (CuO loading = 5%wt.) after experiments in function of temperature: (in order from left to right) 60 °C, 80 °C, 100 °C, 120 °C, 140 °C, at 5 h, 25 bar O<sub>2</sub>, stirring 500 rpm.**

Moreover, the mixture obtained at lower temperature appeared slightly greenish, suggesting a partial dissolution (leaching) of Cu from the catalyst, possibly due to the high viscous solution generated because of the low DSA conversion achieved.

### **6.3.5.3. On the effect of stirring rate**

The influence of the stirring rate was investigated also for CuO/SiO<sub>2</sub> (CuO loading = 5%<sub>wt.</sub>).

As already mentioned in chap. 6.3.3.3, this parameter could be very important for this type of reaction because of the presence of three different phases during the reaction: the oxidant gas, the liquid diol and the solid catalyst. Therefore, the stirring rate may affect the diffusion of the reagents inside the catalyst pores finally influencing the performance of the catalyst itself.

The conditions used for the experiments were:

- 100 mL autoclave with magnetic drive and PTFE vessel;
- 15 g of starting material (dihydroxylated oil) and 0,15 g of catalyst (1%<sub>wt.</sub> of catalyst respect to the amount of s.m.);
- T = 80 °C;
- stirring rate = 300 – 500 – 700\* rpm;
- P<sub>O<sub>2</sub></sub> = 25 bar;
- reaction time = 5 h.

\*Note: 700 rpm represents the maximum stirring rate for the apparatus described in chapter 5.3.1.2.

After the reaction, the catalyst was recovered by means of centrifugation (4500 rpm for 15 min). The reaction products were analysed by means of GC-FID after derivatization with BF<sub>3</sub>/MeOH, as previously described.

Yields of PA and AA (see the equation (5)) are presented in Table 6-18 and Figure 6.28.

**Table 6-30. Oxidative cleavage of DSA (9,10-dihydroxystearic acid) catalysed by CuO/SiO<sub>2</sub> (CuO loading = 5%wt.) in function of the stirring rate.**

Catalyst	Stirring rate	T (°C)	pO <sub>2</sub> (bar)	t (h)	% <sub>wt.</sub> Cat.	Y <sub>PELARG,DSA</sub> (%)	Y <sub>AZEL,DSA</sub> (%)
CuO/SiO <sub>2</sub> (IWI_5%wt.)	300	80	25	5	1,0%	12%	16%
	500	80	25	5	1,0%	20%	31%
	700	80	25	5	1,0%	15%	23%

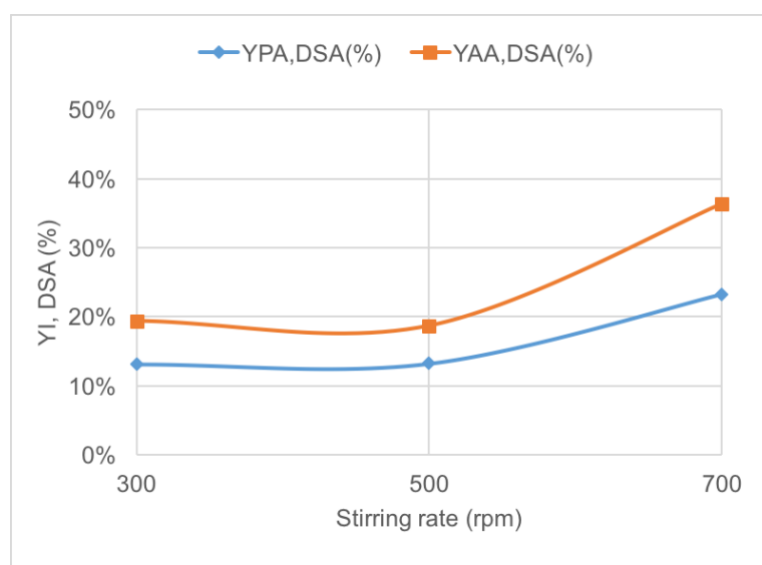


**Figure 6.52. Results obtained by changing the stirring rate using CuO/SiO<sub>2</sub> (CuO loading = 5%wt.); 1%wt. of catalyst compared to DSA at 80°C for 5h, 25 bar O<sub>2</sub>, 300 – 500 - 700 rpm.**

The yields of the two desired products increased drastically when the stirring rate increased, at variance with what observed with CuO/Al<sub>2</sub>O<sub>3</sub> (see chap. 6.3.3.3). This could be due to the large difference of porosity between the two supports, as shown in Figure 6.53.

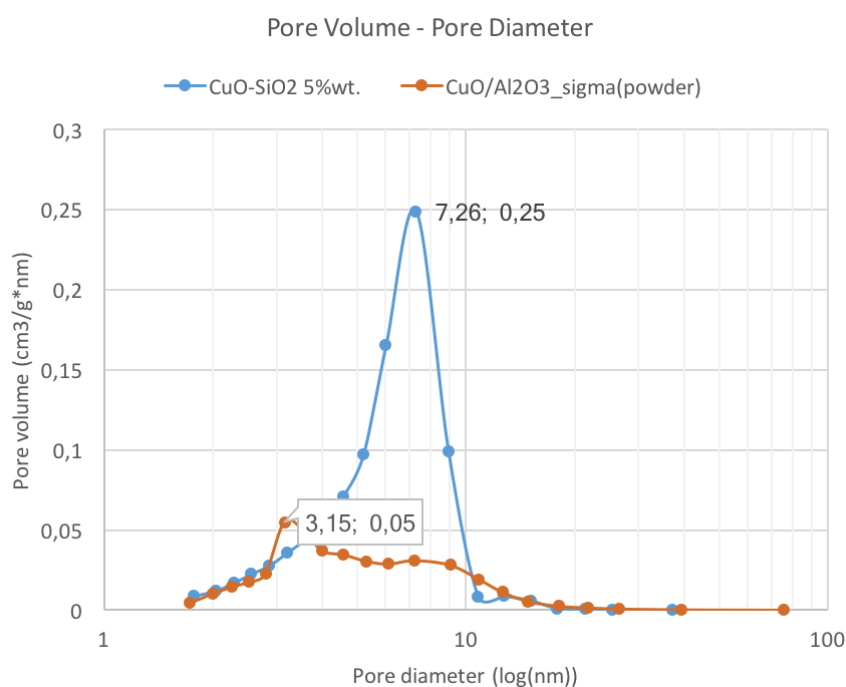


**Figure 6.53. Pores distribution of CuO/SiO<sub>2</sub> (CuO loading = 5%<sub>wt.</sub>) obtained with *IWI* method and commercial CuO/Al<sub>2</sub>O<sub>3</sub>.**

Accordingly, by increasing the stirring rate it was possible to exploit all the surface of the silica pores enhancing the performance of the catalyst.

#### **6.3.5.4. On the effect of catalyst amount**

Reactivity tests were carried out by changing the catalyst amount with the CuO/SiO<sub>2</sub> (silica 360-Grace with 5%<sub>wt.</sub> active phase loading).

The catalytic tests were carried out as described in chapter 5.3.1.2 with the following conditions:

- 100mL autoclave with magnetic drive and PTFE vessel;
- 15 g of starting material (dihydroxylated oil) and 0,5%<sub>wt.</sub> – 1,0 %<sub>wt.</sub>- 1,5%<sub>wt.</sub> of catalyst respect to the amount of s.m.);
- temperature of reaction = 80 °C;
- stirring rate = 500 rpm;
- pure molecular oxygen as oxidant;



- pressure of oxidant = 25 bar;
- reaction time = 5 h.

The reaction products were analysed by GC-FID after derivatization (as described in chapter 5.3.2); catalyst was recovered by means of centrifugation.

**Table 6-31. Oxidative cleavage of DSA (9,10-dihydroxystearic acid) catalysed by CuO/SiO<sub>2</sub> (IWI-method, CuO loading = 5%<sub>wt.</sub>) in function of the amount of catalyst**

Catalyst	T (°C)	pO <sub>2</sub> (bar)	t (h)	% <sub>wt.</sub> Cat.	Y <sub>PELARG,DSA</sub> (%)	Y <sub>AZEL,DSA</sub> (%)
CuO/SiO <sub>2</sub> (IWI_5% <sub>wt.</sub> )	80	25	5	0,5%	0%	1%
	80	25	5	1,0%	13%	19%
	80	25	5	1,5%	14%	23%

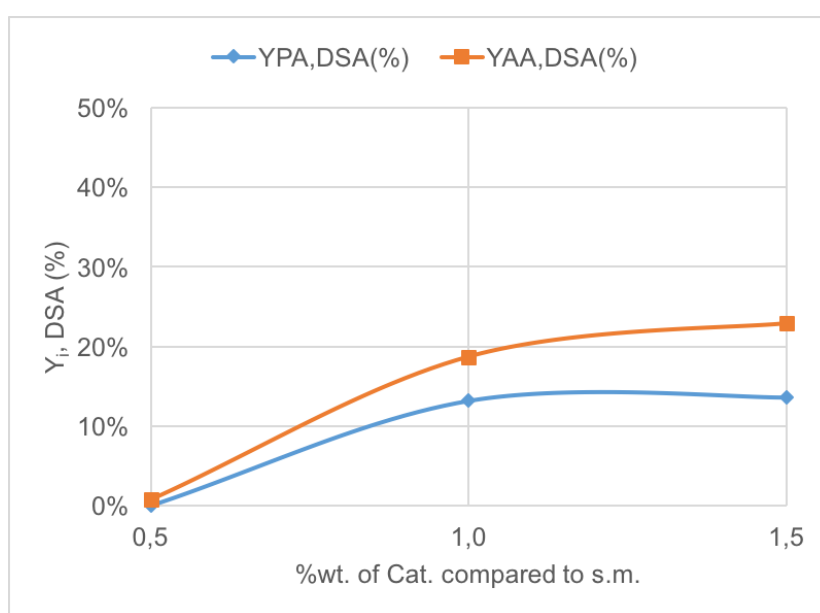


**Figure 6.54. Effect of catalyst amount with CuO/SiO<sub>2</sub> (CuO loading = 5%<sub>wt.</sub>); catalyst amount compared to DSA = 0,5%<sub>wt.</sub>, 1,0%<sub>wt.</sub>, 1,5%<sub>wt.</sub>. @ 80°C for 5h, 25 bar O<sub>2</sub>, 500 rpm.**

Yields of AA and PA increased together with an increase of the catalyst amount from 0,5%<sub>wt.</sub> to 1%<sub>wt.</sub> and then remained almost constant.

### 6.3.5.5. On the effect of type of oxidant

CuO over silica 360-Grace with 5%<sub>wt.</sub> active phase loading was used for a kinetic study of DSA oxidative cleavage by changing the reaction temperature and using air as the oxidant.

The reaction conditions are reported below:

- 100 mL autoclave with magnetic drive and PTFE vessel;
- 15 g of starting material (dihydroxylated oil) and 0,15 g of **powder** catalyst (1%<sub>wt.</sub> of catalyst respect to the amount of s.m.);
- T = 60–80-100 °C;
- stirring rate = 700 rpm;
- oxidant: AIR;
- P<sub>AIR</sub> = 25 bar;
- reaction time = 5 h.

After reaction, the catalyst was recovered by means of centrifugation (4500 rpm for 15 min). The reaction products were analysed by means of GC-FID after derivatization with BF<sub>3</sub>/MeOH, as previously described.

Results are presented in Table 6-20 and Figure 6.55

**Table 6-32. Oxidative cleavage of DSA (9,10-dihydroxystearic acid) catalysed by CuO/SiO<sub>2</sub> (IWI\_5%<sub>wt.</sub>) in function of reaction temperature by using AIR as oxidant and 700 rpm as stirring rate.**

Catalyst	T (°C)	pAIR (bar)	t (h)	% <sub>wt.</sub> Cat.	X <sub>DSA</sub> (%)	Y <sub>PELARG,DSA</sub> (%)	Y <sub>AZEL,DSA</sub> (%)
CuO/SiO <sub>2</sub> (IWI_5% <sub>wt.</sub> )	60	25	5	1,0%	21%	0%	0%
	80	25	5	1,0%	49%	4%	4%
	100	25	5	1,0%	42%	3%	2%

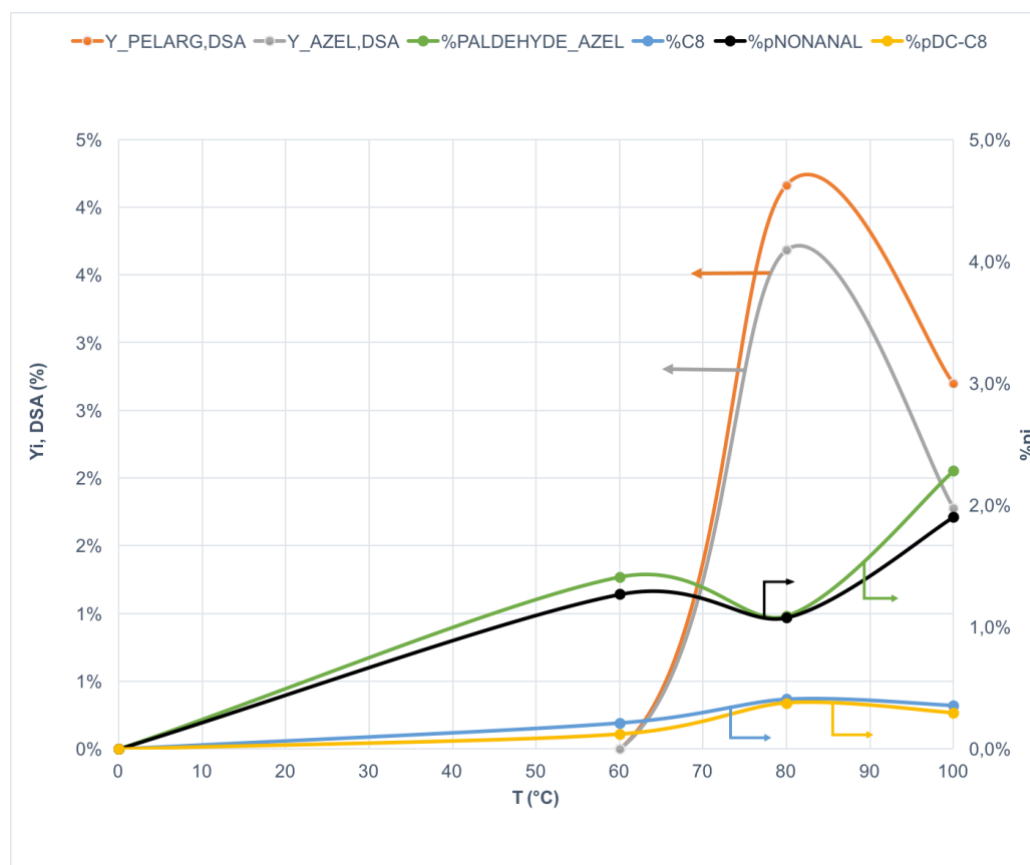


**Figure 6.55.** Oxidative cleavage of DSA with CuO/SiO<sub>2</sub> (CuO loading = 5%wt.) obtained by changing the reaction temperature with 1%wt CuO/SiO<sub>2</sub> (CuO loading: 5%wt.); yields of pelargonic acid (Y\_PELARG,DSA) and azelaic acid (Y\_AZEL,DSA) registered at 80 °C, 25 bar AIR, stirring 700 rpm; it is also reported the weight percentage of octanoic ac. (%pC8), nonanal (%pNONANAL), suberic ac. (%pDC-C8) and 9-oxononanoic acid (%pALDEHYDE\_AZEL).

As shown in Figure 6.55, these results perfectly reproduced those obtained using oxygen.

The results achieved with these experiments permitted to verify the possibility of using a safer oxidant such as air.

#### 6.3.5.6. Conclusions on the catalytic test with CuO/SiO<sub>2</sub>

The use of Silica as the support for the active phase offered some advantages; it is readily available on the market at very low price compared to other supports commonly used in catalysis. Moreover, it guarantees a high surface area compared to the other supported catalysts synthesized in this work.

The copper oxide over silica with 5%<sub>wt.</sub> loading was the catalytic system that showed the best turnover number; therefore, it was used for reactivity tests carried out by changing some reaction parameters. The maximum yields of AA and PA were obtained at 80 °C after 5 hours, that is, at lower temperature and shorter time compared to the commercial CuO/Al<sub>2</sub>O<sub>3</sub>. Furthermore, reactivity tests done by changing the stirring rate highlighted some diffusional problem with CuO/SiO<sub>2</sub> (5%<sub>wt.</sub>). Finally, it was demonstrated that air could be as a possible oxidant instead of pure oxygen.

## 6.4. Copper – ferrites

From the previous catalysts screening, it was observed that copper ferrites are a valid alternative to more conventional systems already used in industry.

The following chapters describe in details the different steps made with the aim of investigating the use of these materials as catalysts for the production of AA and PA.

### 6.4.1. Copper ferrites with different Cu/Fe ratio

The first step was the study of the influence of the amount of copper inside the magnetite structure and its effect on the overall physical and chemical properties of catalysts.

Due to the different ionic radius of the  $\text{Cu}^{2+}$  ion compared to  $\text{Fe}^{2+}$ , the synthesis carried out using a high molar content of copper led to the non-incorporation of the copper into the ferrite structure (see Table 6-5).

In fact, the segregation of a large amount of  $\text{CuO}$  (~ 21% by weight) was observed during the synthesis of a copper-ferrite with Cu/Fe molar ratio of about  $\frac{1}{2}$ . Therefore, the higher Cu/Fe used was  $\text{Cu/Fe} = \frac{1}{2}$ .

#### 6.4.1.1. Synthesis

**Copper ferrites ( $\text{Cu}_x\text{Fe}_{3-x}\text{O}_y$ ) with spinel structure** and different Cu/Fe atomic ratio were prepared by the co-precipitation method described in chapter 5.1.1.

Table 6-33 summarizes the details of the synthesis and the final composition of the material synthesized:

Table 6-33. Synthesis details and nominal composition of the Copper ferrites synthesized.

Name	M <sub>Cu</sub> (mol/L)	M <sub>Fe</sub> (mol/L)	V <sub>precursors</sub> solution (mL)	Atomic ratio Cu/Fe	Thermal treatment*	Nominal Composition
<b>CuFeO12</b>	0,17	0,33	376	1/2	450°C for 8h (10°C/min)	<b>CuFe<sub>2</sub>O<sub>4</sub></b>
<b>CuFeO14</b>	0,13	0,50	301	1/4	450°C for 8h (10°C/min)	<b>Cu<sub>0,6</sub>Fe<sub>2,4</sub>O<sub>4,2</sub></b>
<b>CuFeO16</b>	0,10	0,60	269	1/6	450°C for 8h (10°C/min)	<b>Cu<sub>0,43</sub>Fe<sub>2,57</sub>O<sub>4,2</sub></b>
<b>CuFeO18</b>	0,08	0,67	251	1/8	450°C for 8h (10°C/min)	<b>Cu<sub>0,33</sub>Fe<sub>2,67</sub>O<sub>4,3</sub></b>

\*See chap. 6.2.1.1 for details on the effect of thermal treatment on the bulk feature of the materials.

All the materials obtained with this co-precipitation synthesis looked like a black powder, as shown in Figure 6.56:



Figure 6.56. CuFeO12 obtained with co-precipitation method using Fe(NO<sub>3</sub>)<sub>3</sub>·9H<sub>2</sub>O and Cu(NO<sub>3</sub>)<sub>2</sub>·2,5H<sub>2</sub>O as precursors.

#### 6.4.1.2. Characterization

X-Ray diffraction patterns of the materials calcined at 450 °C for 8h are shown in Figure 6.57.

All the ferrites displayed the typical pattern of the “spinel” phase of magnetite (Fe<sub>3</sub>O<sub>4</sub>), as evidenced from reflections at 2θ: 18°, 31°, 36°, 44°, 58°, 63°, 74°, 75°. However, when the amount of copper incorporated in the crystalline structure of the material decreased, crystallinity declined and some characteristic reflections disappeared. The decrease of crystallinity was confirmed by the surface area analysis (see Table 6-34);,

which increased when the Cu-content was decreased until the maximum value shown by CuFeO16.

In the case of CuFeO18, the disappearance of some peaks could be attributed to different reasons: first, the decrease of crystallite size (see Table 6-34) which caused peak broadening; secondly, the sample with a high amount of iron showed fluorescence of the Cu-K $\alpha$  radiation that caused the increase of the background signal and the disappearing of peaks at low  $2\theta$ .

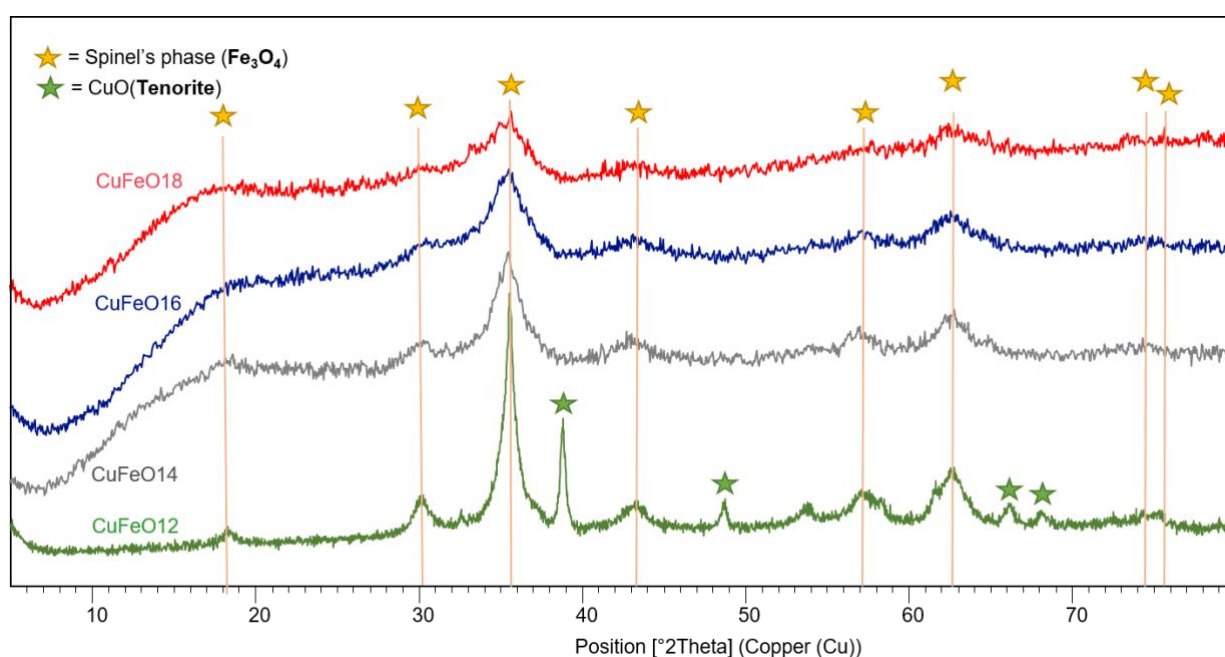


**Figure 6.57.** X.R.D. patterns of Cu-ferrites with different Cu/Fe atomic ratio: CuFeO12 (Cu/Fe =  $\frac{1}{2}$ ), CuFeO14 (Cu/Fe =  $\frac{1}{4}$ ), CuFeO16 (Cu/Fe =  $\frac{1}{6}$ ), CuFeO18 (Cu/Fe =  $\frac{1}{8}$ ) calcined at 450 °C for 8 hours.

Therefore, a large amount of CuO segregated during the synthesis of CuFeO12. For this reason, a treatment with NH<sub>3</sub> and re-calcination at 450 °C for 8 h was performed in order to remove CuO.

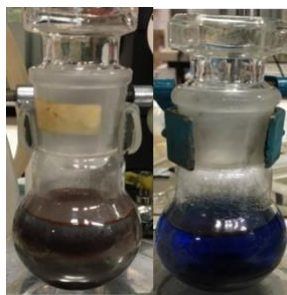


**Figure 6.58.  $\text{NH}_3$  treatment of  $\text{CuFeO}_{12}$ .**

Figure 6.58 shows the final mixture obtained after the  $\text{NH}_3$  treatment of  $\text{CuFeO}_{12}$ : it is clear the presence of the complex  $\text{Cu}(\text{NH}_3)_4^{2+}(\text{aq})$  caused by the dissolution of  $\text{CuO}$ .

X.R.D. analysis of the  $\text{NH}_3$ -treated ferrite was performed. It is possible to observe (Figure 6.59), that the treated sample did not present the characteristic peaks of  $\text{CuO}$  at  $2\theta$ :  $39^\circ$ ,  $49^\circ$ ,  $62^\circ$ ,  $66^\circ$  and  $68^\circ$ . This result suggests the complete elimination of  $\text{CuO}$  from  $\text{CuFeO}_{12}$ .

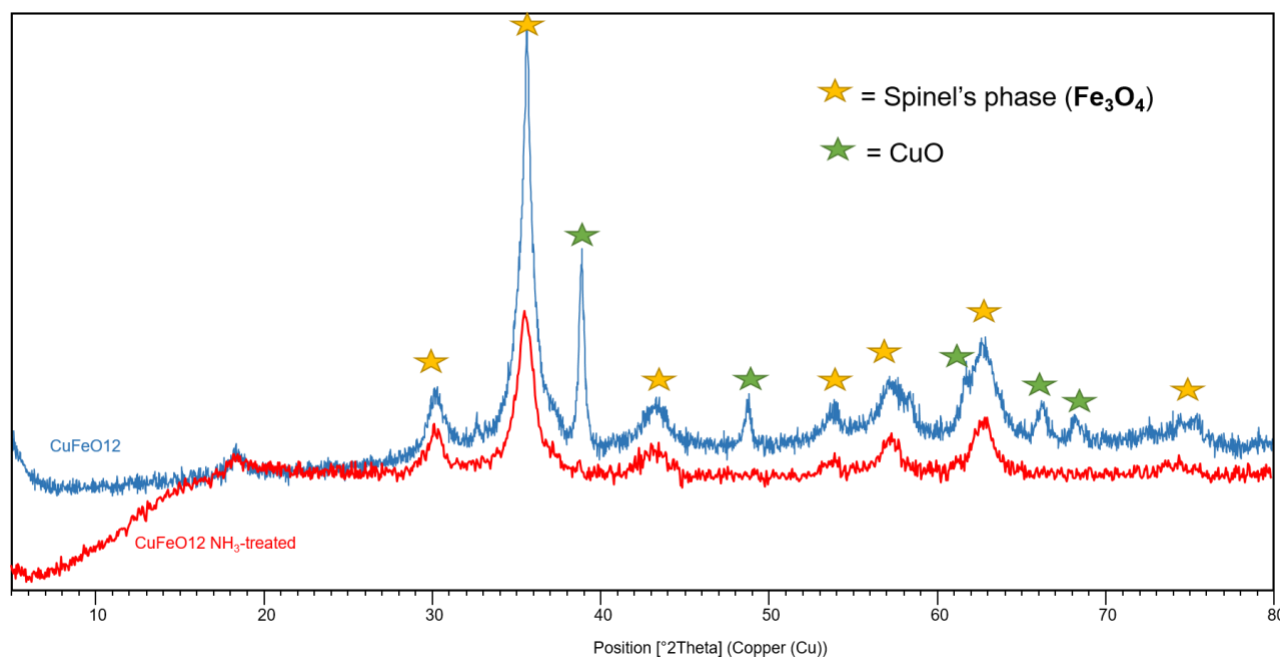


**Figure 6.59. X.R.D. patterns of Cu-ferrites:  $\text{CuFeO}_{12}$  calcined at  $450^\circ\text{C}$  (for 8h) and  $\text{CuFeO}_{12}$  treated with an ammonia solution (30%) and re-calcined at  $450^\circ\text{C}$  (for 8h).**

The porosity and surface area of Cu-ferrites were measured with physisorption of  $\text{N}_2$  at 77K (see chap.5.2.1); results obtained are shown in Table 6-34:



**Table 6-34. Results of the surface area and porosity analysis of Copper ferrites with spinel structure and different Cu/Fe atomic ratio. Crystallite size evaluated with the Scherrer equation**

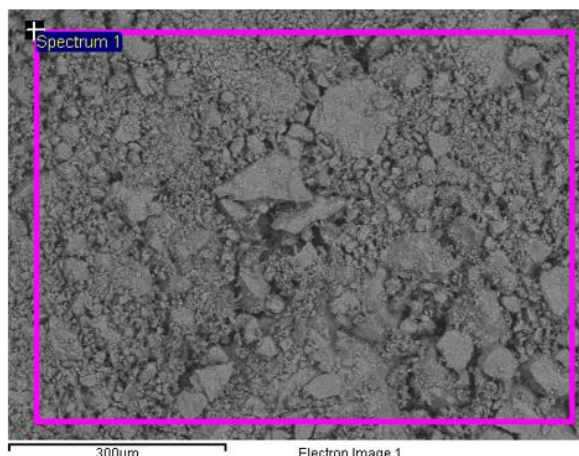
SAMPLE	S <sub>B.E.T.</sub>	V <sub>pore</sub>	Pore average diameter	Crystallite size
	m <sup>2</sup> /g	cm <sup>3</sup> /g	Nm	Å
<b>CuFeO12</b>	67	0,17	7,2	59*
<b>CuFeO14</b>	86	0,14	5,2	55
<b>CuFeO16</b>	98	0,18	6,1	35
<b>CuFeO18</b>	64	0,12	5,2	29

(\*evaluated after the treatment with NH<sub>3</sub>).

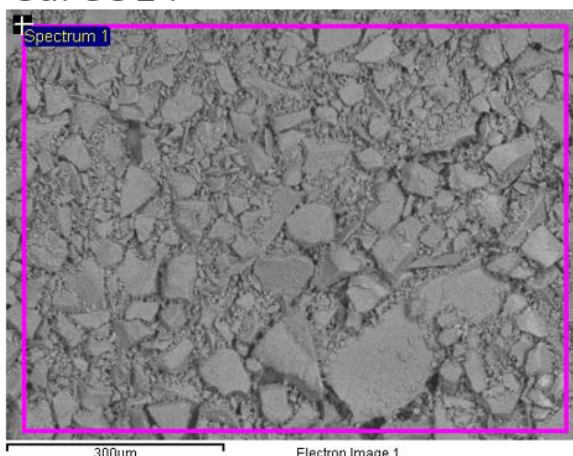
When the copper amount in the material was decreased, the surface area increased up to a maximum value of 98 m<sup>2</sup>/g for CuFeO16 (Cu/Fe = 1/6). At the same time, there was a considerable decrease of the surface area and pore volume together with the reduction of the crystallite size in the case of CuFeO18.

The morphology and structure of Cu-ferrites were studied also by means of S.E.M. analysis. Figure 6.60 shows the images:

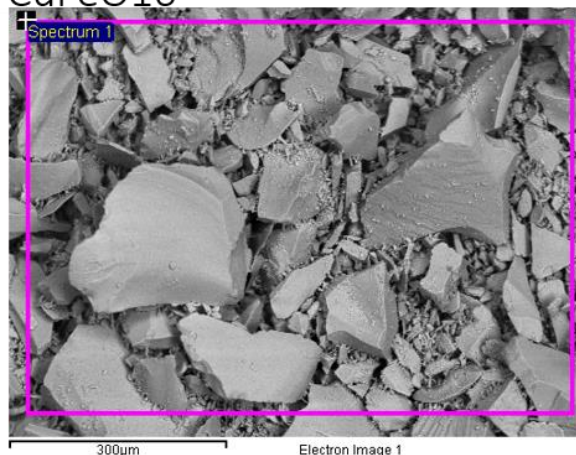
CuFeO12



CuFeO14



CuFeO16



CuFeO18

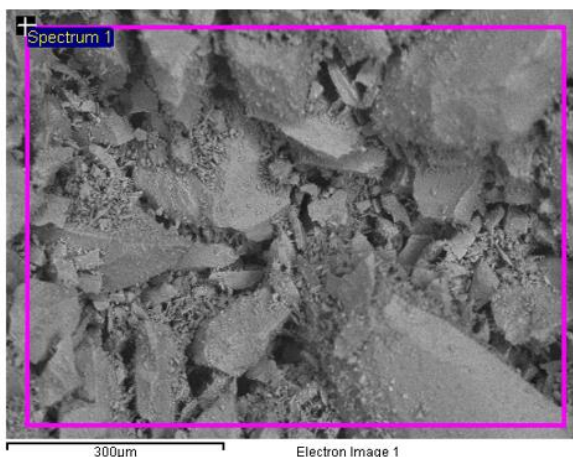


**Figure 6.60. S.E.M. images of copper ferrites with spinel structure and different Cu/Fe atomic ratio.**

Results showed that samples with high copper content had particles smaller than ferrites with low Cu-content. Furthermore, CuFeO14 was the sample showing the best uniformity in terms of morphology and particle size.

The temperature programmed reduction-oxidation-reduction (TPR<sub>1</sub>-O-R<sub>2</sub>) analysis was used in order to investigate the effect of the different Cu content on the redox properties of the materials. The analysis involved the reduction-oxidation-reduction cycle of the catalyst under controlled temperature and H<sub>2</sub>/O<sub>2</sub> concentration.

The conditions used for the redox cycle were the same as those reported in chap. 5.2.4.

The profiles obtained with this technique are shown in Figure 6.61:

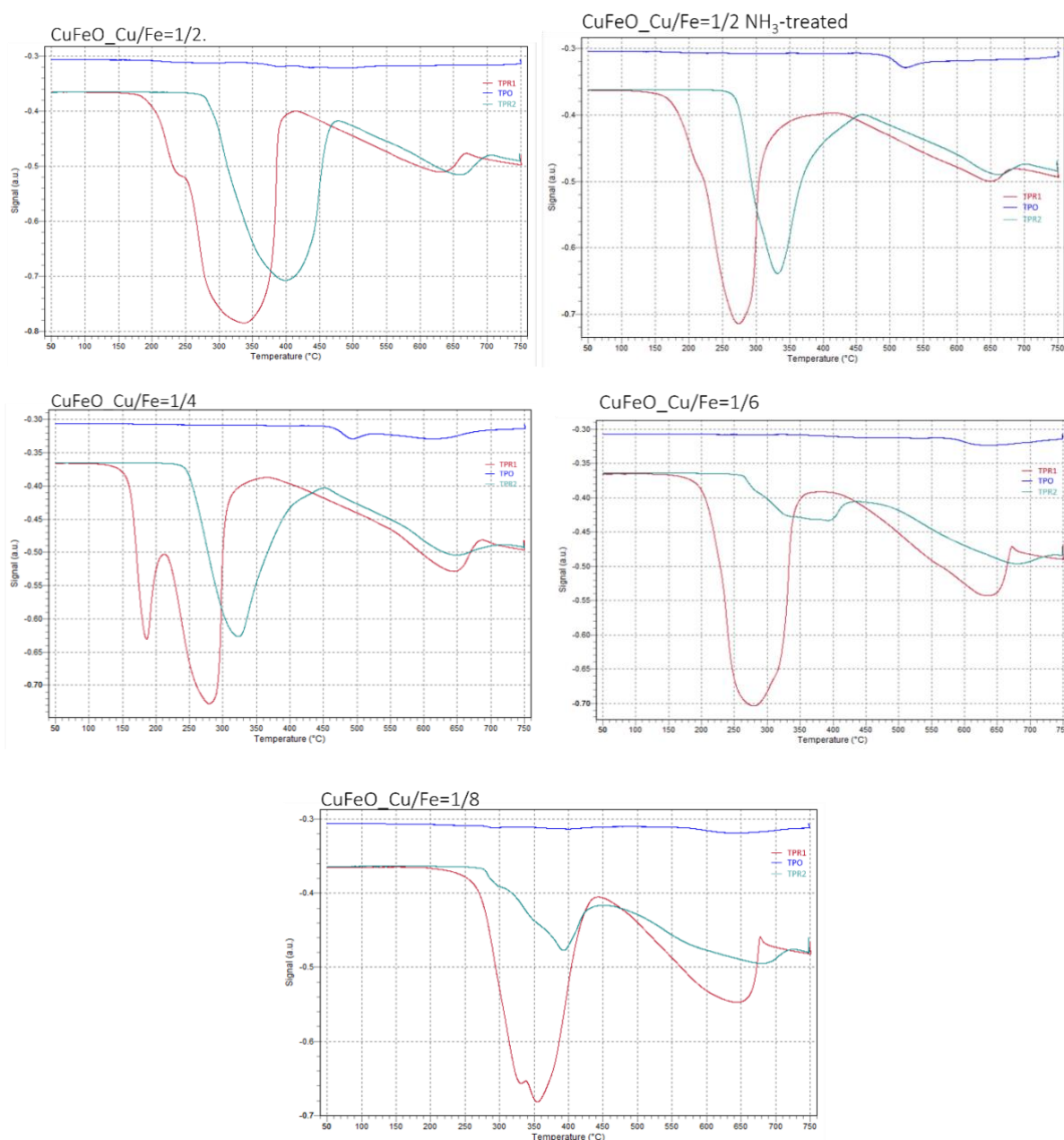


**Figure 6.61. TPR<sub>1</sub>-O-R<sub>2</sub> profiles of Cu-ferrites with different Cu/Fe atomic ratio.**

Many parameters were evaluated with this technique:

- the number of peaks, that represent the number of reducible/oxidizable species;
- the temperature at which the peaks shows the maximum value
- the shape of the peaks

The temperature at which the peaks occur may vary from sample to sample depending on several features, for example the particle size.

For Cu/Fe/O spinels the reduction peaks at 250 °C are attributable to the reduction of Cu and Fe<sub>3</sub>O<sub>4</sub><sup>195, 196</sup>:



The large peaks between 350 °C and 650 °C were attributed to the reduction of Fe<sub>3</sub>O<sub>4</sub> to Fe which should occur in two steps with the intermediate formation of Fe<sup>2+</sup><sup>197</sup>. It can be observed that the relative intensity of the first peak for CuFeO12 sample was greater than for the other catalysts because of the presence of CuO (as shown in XRD analysis), which should be reduced at 250 °C.

Moreover, it is important to note that sample CuFeO14 presented a very sharp peak compared to the other materials. This could be related to the high dispersion and uniformity of the particle dimension, as highlighted from S.E.M. analysis.

In Table 6-35, the temperatures at which peaks showed the maximum value, for each catalyst, is summarized.

**Table 6-35. Temperature maxima of the peaks obtained from the TPR<sub>1</sub>-O-R<sub>2</sub> analysis of Cu-ferrites with different Cu/Fe atomic ratio.**

CATALYST	Temperature of First Reduction peak maxima (°C)		Temperature of Oxidation peak maxima (°C)					Temperature of Second Reduction peak maxima (°C)			
	$\alpha 1$	$\alpha 2$	$\beta 1$	$\beta 2$	$\beta 3$	$\beta 4$	$\beta 5$	$\gamma 1$	$\gamma 2$	$\gamma 3$	$\gamma 4$
CuFeO12	230	335	230	280	390	435	490	395	655		
CuFeO12 NH3-treated	210	275					520	330	655		
CuFeO14	185	280				495	615	320	650		
CuFeO16	280	635					625	330	675		
CuFeO18	330	355	290			400	640	300	350	390	675

Therefore, from TPR<sub>1</sub>-O-R<sub>2</sub> measurements it was possible to conclude that the replacement of ferrous ion with different amount of copper affects the oxygen mobility in the solid, thus modifies the reducibility/oxidability of the material.

#### 6.4.1.3. Reactivity tests using Cu/Fe/O ferros spinels

Cu-ferrites with spinel structure and different Cu:Fe molar ratios were tested in DSA oxidative cleavage.

The catalysts examined were:

- **CuFe<sub>2</sub>O<sub>4</sub>** (Cu/Fe = 1/2; code CuFeO12)
- **Cu<sub>0,6</sub>Fe<sub>2,4</sub>O<sub>4,2</sub>** (Cu/Fe = 1/4; code CuFeO14)
- **Cu<sub>0,43</sub>Fe<sub>2,57</sub>O<sub>4,28</sub>** (Cu/Fe = 1/6; code CuFeO16)

- **$\text{Cu}_{0,33}\text{Fe}_{2,67}\text{O}_{4,33}$**  (Cu/Fe = 1/8; code CuFeO18)

All these catalysts were investigated as described in chapter 5.3.1.2 with the following conditions:

- batch autoclave with PTFE vessel of 100 mL;
- 15 g of starting material (dihydroxylated oil) and 0,15 g of catalyst (1%<sub>wt.</sub> of catalyst respect to the amount of s.m.);
- T = 80 °C;
- stirring rate = 500 rpm;
- P<sub>O<sub>2</sub></sub> = 25 bar;
- reaction time = 5 h.

The reaction products were analysed by GC-FID after derivatization (described in chapter 5.3.2); the catalyst was recovered by means of centrifugation.

The results obtained from the catalytic tests using Cu-ferrites with different composition are shown in Figure 6.62.



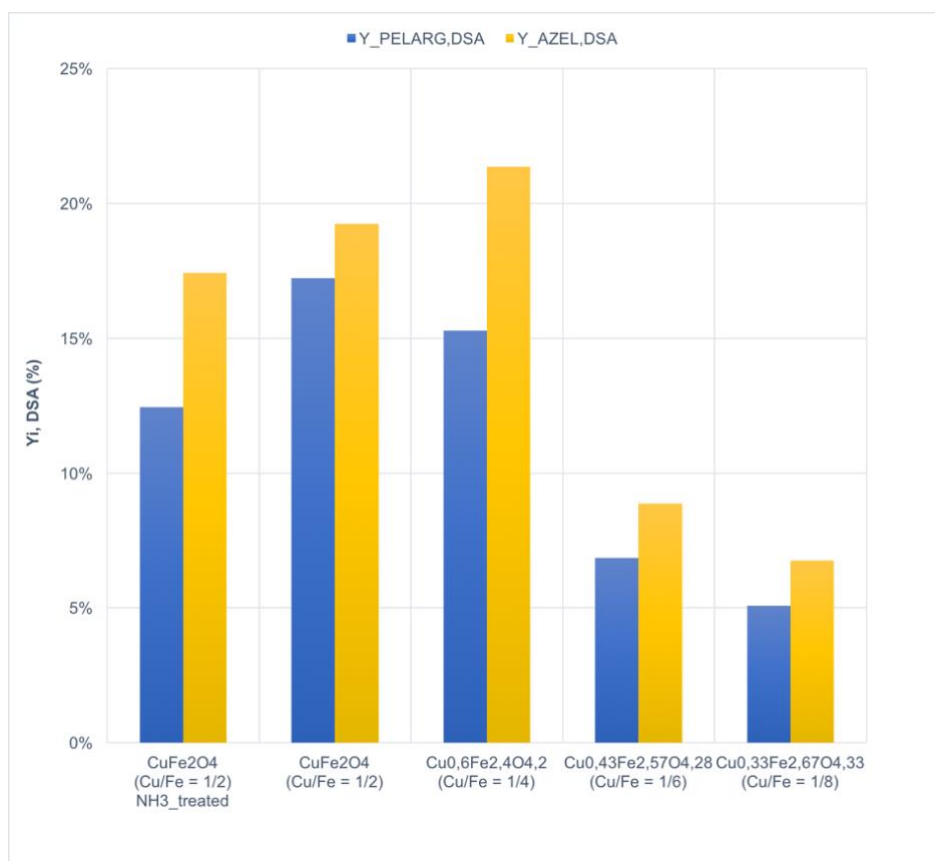


**Figure 6.62.** Yields of azelaic ac. (AA) and pelargonic ac.(PA) obtained in DSA oxidative cleavage using different spinel-type Cu-ferrites in batch reactor at 80 °C, 5h, 25 bar O<sub>2</sub>, 500 rpm.

The two catalysts showing best performance were CuFeO<sub>1/2</sub> and CuFeO<sub>1/4</sub>.

However, CuFeO<sub>1/2</sub> presented an impurity of CuO on its surface. For this reason, we also tested the reactivity of CuFeO<sub>1/2</sub> treated with ammonia. Catalytic tests were performed using the same conditions mentioned above.

Results (calculated with equation (7)) are presented in Figure 6.63. As far as the treated Cu-ferrite is concerned, a decrease of AA and PA yields was registered (compared to the non-treated Cu-ferrite). However, still the catalyst showed better performance than samples CuFeO<sub>1/6</sub> and CuFeO<sub>1/8</sub>.

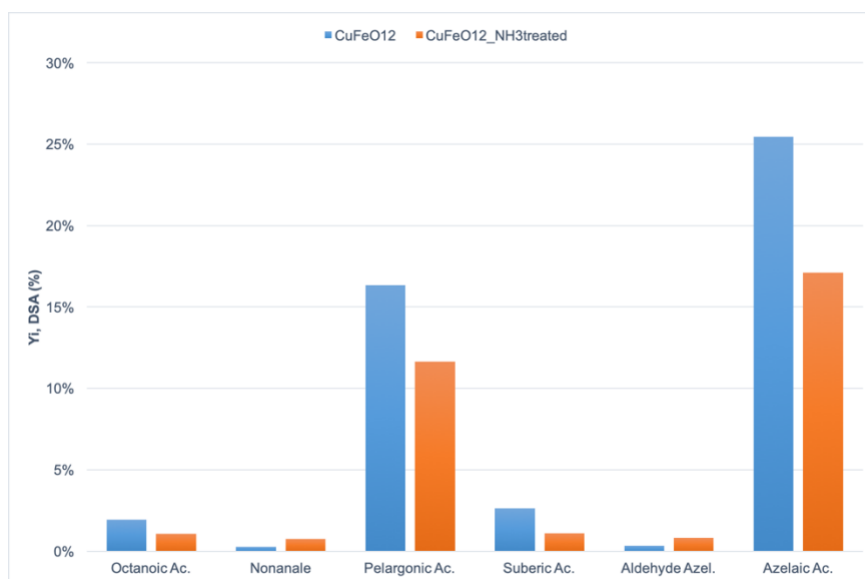


Figure 6.63. Oxidative cleavage of DSA with CuFeO1/2 calcined at 450 °C (for 8h) and CuFeO12 treated with  $\text{NH}_3(\text{aq})$  and re-calcined at 450 °C (for 8h), in batch reactor at 80 °C, 5 h, 25 bar  $\text{O}_2$ , stirring 500 rpm.

### 6.4.2. *Cu/Fe/O (Cu/Fe = 1/4) ferrospinel catalyst*

According to the results obtained, CuFeO14 was the best candidate for the conversion of DSA into azelaic and pelargonic acids.

Therefore, the research was focussed on the study of this catalyst; we investigated the effect of some reaction parameters.

#### 6.4.2.1. *Effect on thermal annealing on catalytic performance*

As already reported in chapter 6.2.1.1, the thermal annealing of the ferrospinel significantly affect the structure of the material. This effect was evident from the X.R.D. patterns of the samples annealed at different temperature, reported in Figure 6.6.

The materials annealed at different temperature were then tested in DSA oxidative scission. The catalytic tests were carried out as described in the chapter 5.3.1.2, using the following conditions:

- 100 mL autoclave with magnetic drive and PTFE vessel;



- 15 g of starting material (dihydroxylated oil) and 0,15 g of catalyst (1%<sub>wt.</sub> of catalyst respect to the amount of s.m.);
- temperature of reaction = 80 °C;
- stirring rate = 500 rpm;
- pure molecular oxygen as oxidant;
- pressure of oxidant = 25 bar;
- reaction time = 5 h.

The reaction products were analysed by GC-FID after derivatization (described in chapter 5.3.2); the catalyst was recovered by means of centrifugation.

Results are shown in Figure 6.64 (they were obtained applying the equation (5)).

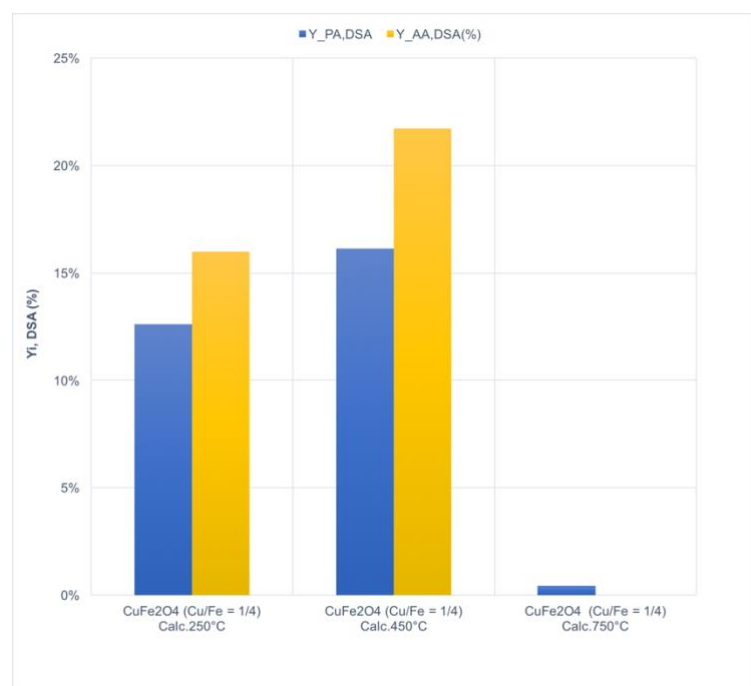


**Figure 6.64. DSA Oxidative cleavage with CuFeO<sub>14</sub> annealed at different T (250 °C, 450 °C, 750 °C) in batch reactor at 80 °C, 5 h, 25 bar O<sub>2</sub>, stirring 500 rpm.**

The reasons behind these results are probably related to the different structural properties of the material. CuFeO<sub>14</sub> calcined at 750 °C was completely inactive due to the formation of a material with features completely different from the desired one (see XRD pattern in Figure 6.6). Also CuFeO<sub>14</sub> calc. at 250 °C showed lower activity

compared to the material calcined at 450 °C. Also in this case, the reason could be ascribed to a non-complete formation of the spinel phase, as highlighted in Figure 6.6.

#### **6.4.2.2. On the effect of reaction time**

The CuFeO<sub>14</sub> catalyst calcined at 450 °C was employed for the kinetic investigation of DSA oxidative cleavage. The experiments were carried out by changing the reaction time from 0 to 8 hours.

The catalytic tests were carried out as described in chapter 5.3.1.2 using the following conditions:

- 100 mL autoclave with magnetic drive and PTFE vessel;
- 15 g of starting material (dihydroxylated oil) and 0,15 g of catalyst (1%<sub>wt.</sub> of catalyst respect to the amount of s.m.);
- temperature of reaction = 80 °C;
- stirring rate = 500 rpm;
- pure molecular oxygen as oxidant;
- pressure of oxidant = 25 bar;
- reaction time = 0, 2, 4, 6, 8 h.

The reaction products were analysed by GC-FID after derivatization (described in chapter 5.3.2); the catalyst was recovered by means of centrifugation.

Results, obtained applying equations (4) and (5), are shown in Table 6-36 and Figure 6.65..

**Table 6-36. . Oxidative cleavage of DSA (9,10-dihydroxystearic acid) catalysed by CuFeO14 (calcined at 450 °C) in function of reaction time.**

Catalyst	t (h)	pO <sub>2</sub> (bar)	T (°C)	% <sub>wt.</sub> Cat.	X <sub>DSA</sub> (%)	Y <sub>PELARG,DSA</sub> (%)	Y <sub>AZEL,DSA</sub> (%)
CuFeO14 (calcined at 450 °C)	2	25	80	1,0%	38%	2%	2%
	4	25	80	1,0%	63%	11%	14%
	6	25	80	1,0%	72%	16%	23%
	8	25	80	1,0%	76%	16%	25%

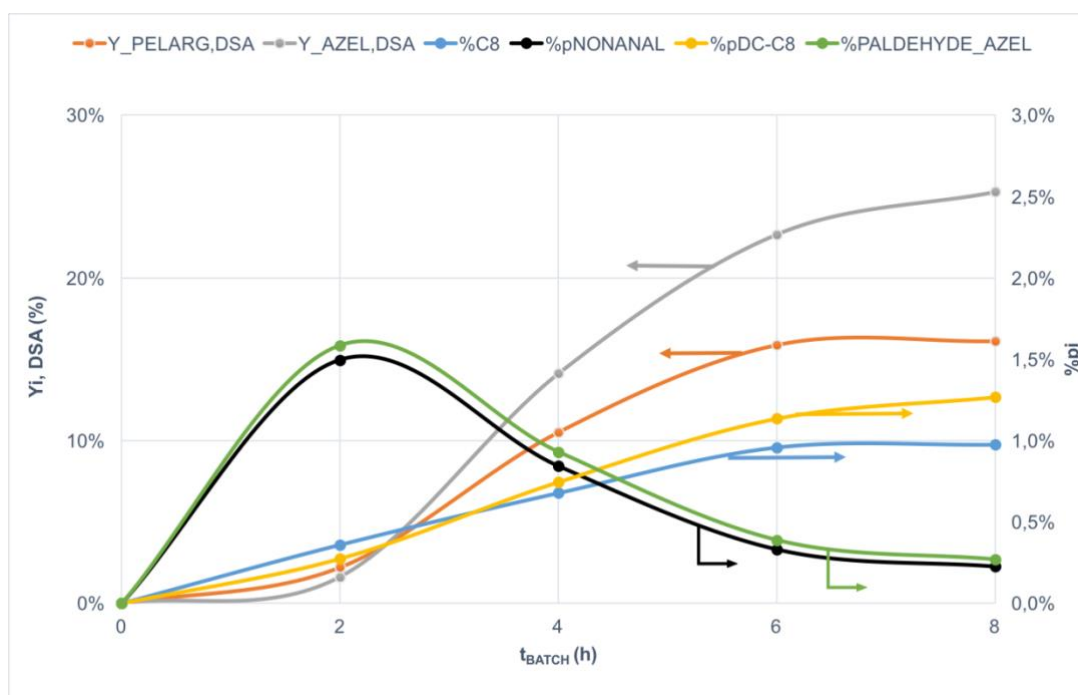


**Figure 6.65. Effect of reaction time with 1%<sub>wt.</sub> CuFeO14 (Calc. @450°C) in DSA oxidative cleavage. Yields of pelargonic acid (Y\_PELARG,DSA) and azelaic acid (Y\_AZEL,DSA) registered at 80 °C, 25 bar O<sub>2</sub>, stirring 500 rpm; it is also reported the weight percentage of octanoic ac. (%pC8), nonanal (%pNONANAL), suberic ac. (%pDC-C8) and 9-oxononanoic acid (%pALDEHYDE\_AZEL).**

Results demonstrate the increase of PA and AA yields along with the increase of reaction time. The main by-products showed similar trends as for CuO/Al<sub>2</sub>O<sub>3</sub> (chap. 6.3.3.1): C8 products showed the typical trend of parallel reaction, while the two aldehydes formed at the beginning of the reaction and their yields decreased during the progress of the reaction, as usually shown by intermediate products. Moreover, AA and PA formed by transformation of the two aldehydes.

The final reaction mixture, after filtration with PTFE filter of 0,45  $\mu\text{m}$ , appeared of a pale yellow colour only after tests at short time of reaction, as shown in Figure 6.66.

At 6 hours of reaction, it was possible to obtain a very clear and colourless mixture, presumably because of an excellent catalyst recovery. The formation of coloured compounds began after 8 h of reaction.

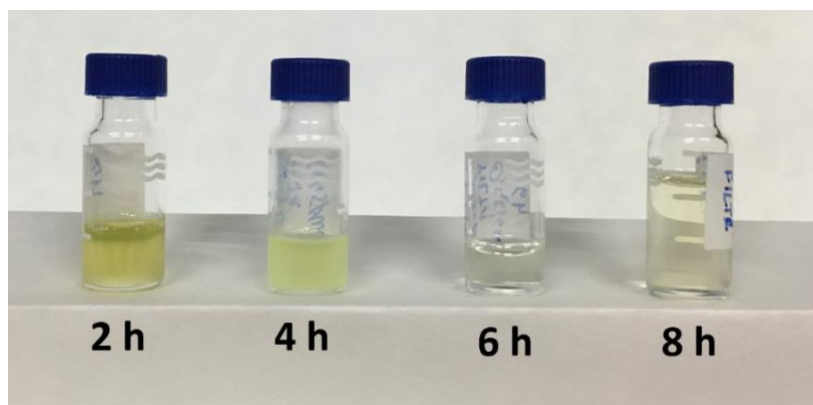


**Figure 6.66.** Pictures of reaction mixtures obtained with CuFeO1/4 after experiments in function of reaction time: (in order from left to right) 2h, 4h, 6h, 8h, at 80 °C, 25 bar O<sub>2</sub>, stirring 500 rpm.

### **6.4.2.3. On the effect of reaction temperature**

The reactivity experiments in function of temperature were carried out by using CuFeO1/4 calc. at 450 °C, from 60 °C to 100 °C; 60 °C represented the lower T limit because under this temperature the starting diol is solid. The maximum temperature used for these experiments was 100 °C because the other catalysts previously tested (CuO over alumina and over silica) at this temperature produced some heavier (dark) by-products.

Catalytic tests were carried out as described in chapter 5.3.1.2 with the following conditions:

- 100mL autoclave with magnetic drive and PTFE vessel;
- 15 g of starting material (dihydroxylated oil) and 0,15 g of catalyst (1%<sub>wt.</sub> of catalyst respect to the amount of s.m.);
- temperature of reaction = 60, 80, 100 °C;
- stirring rate = 500 rpm;

- pure molecular oxygen as oxidant;
- pressure of oxidant = 25 bar;
- reaction time = 5 h.

The reaction products were analysed by GC-FID after derivatization (described in chapter 5.3.2) and the catalyst was recovered by means of centrifugation.

Results are summarized in Table 6-37 and Figure 6.67.

**Table 6-37. Oxidative cleavage of DSA (9,10-dihydroxystearic acid) catalysed by CuFeO14 (Calc. @450°C) in function of the reaction temperature.**

Catalyst	T (°C)	pO <sub>2</sub> (bar)	t (h)	% <sub>wt.</sub> Cat.	X <sub>DSA</sub> (%)	Y <sub>PELARG, DSA</sub> (%)	Y <sub>AZEL, DSA</sub> (%)
CuFeO14 (Calcined at 450°C)	60	25	5	1,0%	0%	0%	0%
	80	25	5	1,0%	2%	0%	0%
	100	25	5	1,0%	65%	13%	18%
	120	25	5	1,0%	87%	14%	21%
	140	25	5	1,0%	0%	0%	0%

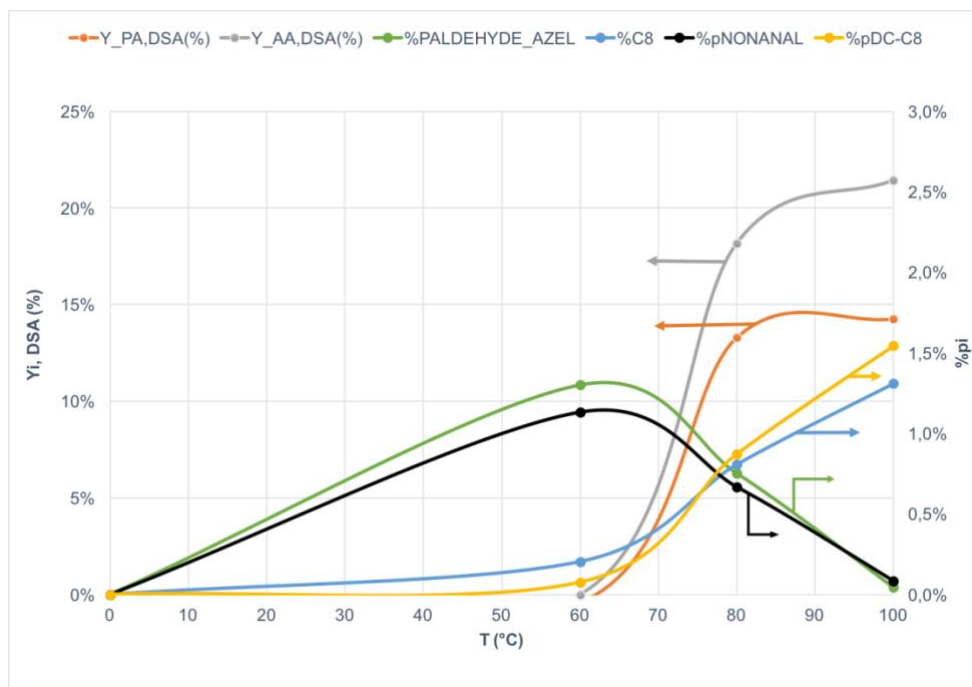


Figure 6.67. Oxidative cleavage of DSA in function of reaction temperature employing CuFeO14 (Calc.@450°C) as catalyst. Yields of pelargonic acid (Y\_PELARG,DSA) and azelaic acid (Y\_AZEL,DSA) registered at 80 °C, 25 bar O<sub>2</sub>, stirring 500 rpm; it is also reported the weight percentage of octanoic ac. (%pC8), nonanal (%pNONANAL), suberic ac. (%pDC-C8) and 9-oxononanoic acid (%pALDEHYDE\_AZEL). Yield of pelargonic acid.

Figure 6.68 shows the final reaction mixture obtained with CuFeO14 by changing the reaction temperature. It is very important to underline that in this case it was possible to achieve the recovery of the catalyst simply by filtration with a PTFE filter of 0,45 µm (see the reaction mixture obtained at 80 °C). Therefore, it is possible to conclude that the most suitable temperature for the process is 80 °C.

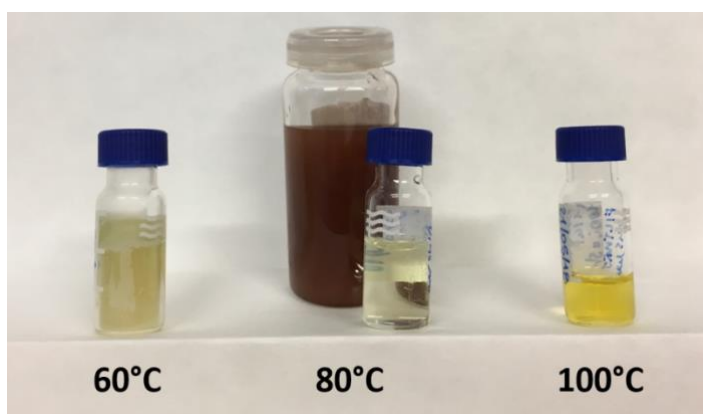


Figure 6.68. Pictures of reaction mixtures obtained after experiments with CuFeO14 in function of temperature: (in order from left to right) 60, 80 (filtrated before and not filtrated behind) and 100 °C, 25 bar O<sub>2</sub>, stirring 500 rpm.

#### 6.4.2.4. On the effect of stirring rate

The influence of the stirring rate was also investigated with CuFeO<sub>14</sub> calc. at 450 °C.

As already mentioned, this parameter could be very important for this type of reaction because of the presence of three different phases during the reaction.

The used conditions were:

- 100 mL autoclave with magnetic drive and PTFE vessel;
- 15 g of starting material (dihydroxylated oil) and 0,15 g of catalyst (1%<sub>wt.</sub> of catalyst respect to the amount of s.m.);
- T = 80 °C;
- stirring rate = 300 – 500 – 700\* rpm;
- P<sub>O<sub>2</sub></sub> = 25 bar;
- reaction time = 5 h.

\*Note: 700 rpm represent the maximum stirring rate for the apparatus described in chapter 5.3.1.2.

After the reaction, the catalyst was recovered by means of centrifugation (4500 rpm for 15 min). The reaction products were analysed by means of GC-FID after derivatization with BF<sub>3</sub>/MeOH as previously described.

Results (calculated with equation (5)) are reported in Table 6-18 and Figure 6.28.

**Table 6-38. Oxidative cleavage of DSA (9,10-dihydroxystearic acid) catalysed by CuFeO<sub>14</sub> (calc. at 450°C) in function of the stirring rate.**

Catalyst	Stirring rate	T (°C)	pO <sub>2</sub> (bar)	t (h)	% <sub>wt.</sub> Cat.	Y <sub>PELARG,DSA</sub> (%)	Y <sub>AZEL,DSA</sub> (%)
CuFeO <sub>14</sub> (Calc. @ 450°C)	300	80	25	5	1,0%	12%	16%
	500	80	25	5	1,0%	20%	31%
	700	80	25	5	1,0%	15%	23%

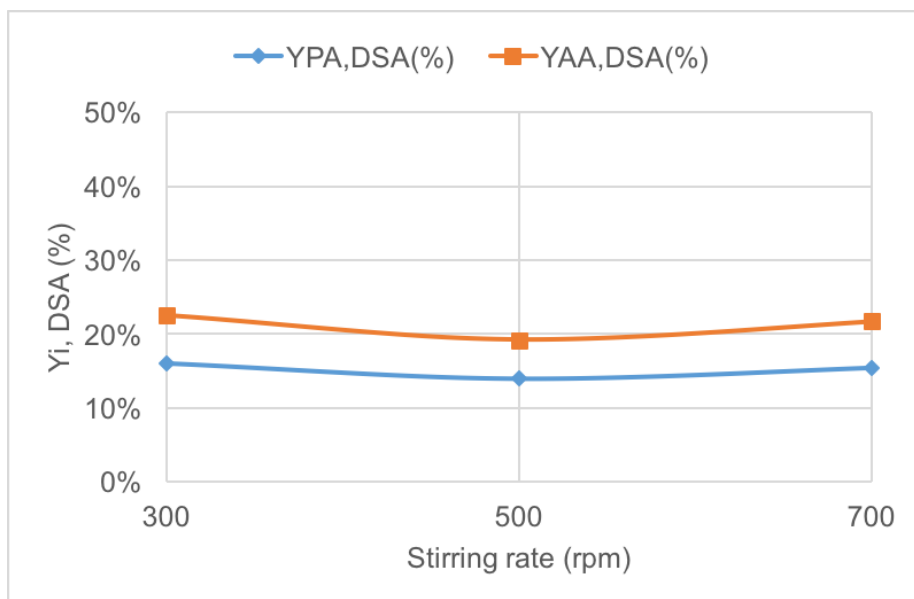


**Figure 6.69. Results obtained by changing the stirring rate using CuFeO14 (Calc. @450°C); 1%<sub>wt.</sub> of catalyst compared to DSA at 80°C for 5h, 25 bar O<sub>2</sub>, 300 – 500 - 700 rpm.**

No effect of the stirring rate was registered, evidencing that no diffusional limitation occurred during these experiments.

#### **6.4.2.5. On the effect of catalyst amount**

Additionally, the reactivity tests were carried out using CuFeO14 calc. at 450 °C by changing the catalyst amount.

The catalytic tests were carried out as described in chapter 5.3.1.2 at the following conditions:

- 100mL autoclave with magnetic drive and PTFE vessel;
- 15 g of starting material (dihydroxylated oil) and 0,5%<sub>wt.</sub> – 1,0 %<sub>wt.</sub>- 1,5%<sub>wt.</sub> of catalyst with respect to the amount of s.m.);
- temperature of reaction = 80 °C;
- stirring rate = 500 rpm;
- pure molecular oxygen as oxidant;
- pressure of oxidant = 25 bar;
- reaction time = 5 h.



The reaction products were analysed by GC-FID after derivatization (described in chapter 5.3.2) and catalyst was recovered by means centrifugation.

Results of the experiments are reported in Table 6-39.

**Table 6-39. DSA oxidative cleavage catalysed by CuFeO14 (calc. at 450°C) in function of the amount of catalyst (calculated with respect to DSA).**

Catalyst	T (°C)	pO <sub>2</sub> (bar)	T (h)	%wt. Cat.	Y <sub>PELARG,DSA</sub> (%)	Y <sub>AZEL,DSA</sub> (%)
CuFeO14	80	25	5	0,5%	9%	12%
(calc. @ 450°C)	80	25	5	1,0%	14%	19%
	80	25	5	1,5%	16%	23%

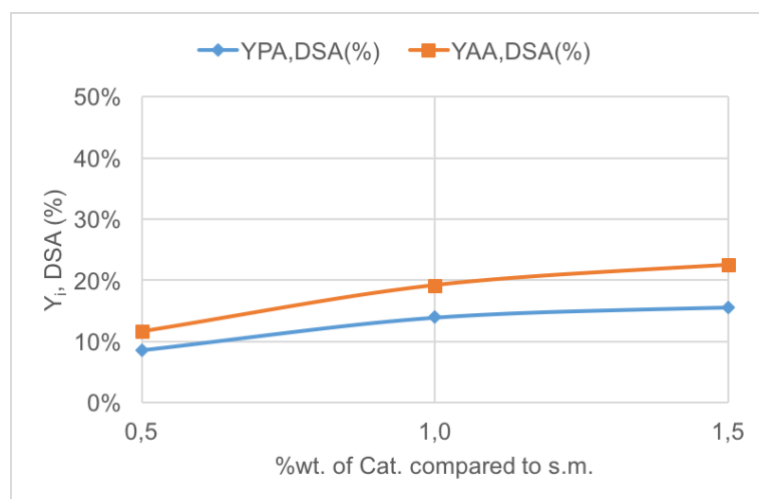


**Figure 6.70. Results obtained by changing the catalyst amount with CuFeO14 calc. at 450°C; catalyst amount compared to DSA = 0,5%wt., 1,0%wt., 1,5%wt. @ 80°C for 5h, 25 bar O<sub>2</sub>, 500 rpm.**

As it is possible to predict from these experiments, upon increasing the amount of catalyst the yield of the desired products slightly increased.

#### 6.4.2.6. On the effect of oxidant pressure

The last parameter investigated with the CuFeO14 calc. at 450 °C was the effect of the oxidant gas pressure.

The reaction conditions used are reported below:

- 100 mL autoclave with magnetic drive and PTFE vessel;

- 15 g of starting material (dihydroxylated oil) and 0,15 g of catalyst (1%<sub>wt.</sub> of catalyst respect to the amount of s.m.);
- T = 80 °C;
- stirring rate = 500 rpm;
- P<sub>O2</sub> = 10 - 15 - 30 bar;
- reaction time = 3 h.

After the reaction, the catalyst was recovered by means of centrifugation (4500 rpm for 15 min). The reaction products were analysed by means of GC-FID after derivatization with BF<sub>3</sub>/MeOH as previously described.

It is important to note that the time of reaction used for these tests was about 3h, calculated after the desired temperature had been reached. The reaction conditions were modified in this way because in the experiment with the lowest pressure (10 bar) all the oxygen was consumed already after 4 hours of reaction.

Results are presented in Table 6-40 and Figure 6.71.

**Table 6-40. Oxidative cleavage of DSA (9,10-dihydroxystearic acid) catalysed by CuFeO14 calcined at 450 °C in function of the oxidant gas pressure (molecular oxygen).**

Catalyst	pO <sub>2</sub> (bar)	T (°C)	t (h)	% <sub>wt.</sub> Cat.	Y <sub>PELARG,DSA</sub> (%)	Y <sub>AZEL,DSA</sub> (%)
CuFeO14 (calc. @ 450°C)	10	80	3	1,0%	12%	16%
	15	80	3	1,0%	17%	24%
	30	80	3	1,0%	3%	4%

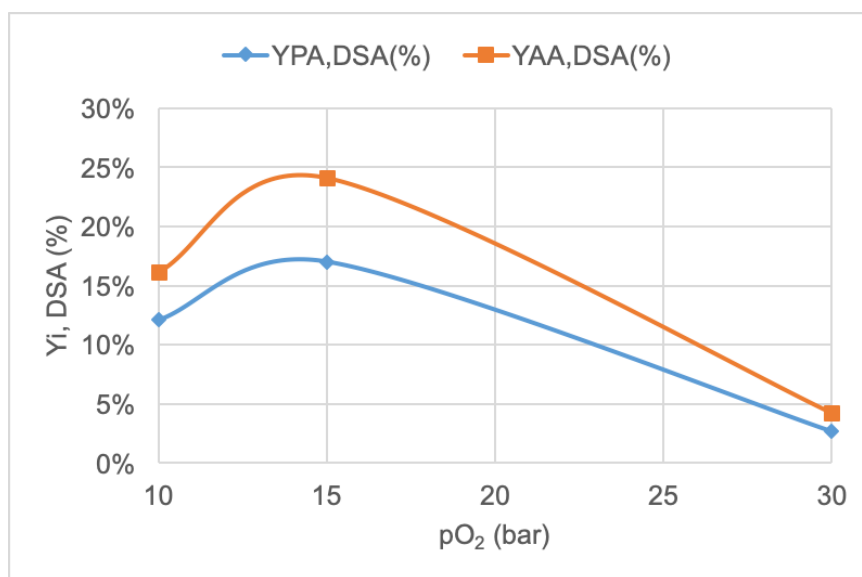


**Figure 6.71. Results in terms of yields of azelaic ac. (AA) and pelargonic ac.(PA) obtained by changing oxidant gas pressure, using 1%<sub>wt.</sub> of CuFeO14 calc. at 450 °C compared to DSA at 80°C for 3h, 10 – 15 - 30 bar O<sub>2</sub>, 500 rpm.**

In this case, the increase in the pressure of the oxidant gas caused a dramatic decline in the performance of the catalyst: the material exhibited a very low activity at 30 bar of pressure and the formation of the products was disfavoured. This could be probably attributed to the formation of an oxygen interlayer that prevents the substrate to reach the active sites of the catalyst.

#### **6.4.2.7. On the reusability of the catalyst**

One of the most important features for a catalyst is the possibility of being reused. Therefore, the reusability of CuFeO14 was investigated. As already underlined in chap. 6.3.3.6 for CuO/Al<sub>2</sub>O<sub>3</sub>, the catalyst could be reused only if it was subjected to a regeneration step.

Based on the synthesis protocol developed in our lab, the catalyst could be regenerated by a re-calcination at the same temperature used for the synthesis, that is 450 °C for 8 h (10 °C/min).

The catalytic tests were carried out as described in chapter 5.3.1.2 at following conditions:

- 100 mL autoclave with magnetic drive and PTFE vessel;

- 15 g of starting material (dihydroxylated oil) and 0,15 g of catalyst (1%<sub>wt.</sub> of catalyst respect to the amount of s.m.);
- temperature of reaction = 80 °C;
- stirring rate = 500 rpm;
- pure molecular oxygen as oxidant;
- pressure of oxidant = 25 bar;
- reaction time = 5 h.

The reaction products were analysed by GC-FID after derivatization (described in chapter 5.3.2).

The catalyst was recovered by means of centrifugation (4500 rpm for 15 min) and then regenerated by means of calcination at 450 °C for 8 h (10 °C/min).

The regenerated catalyst was employed in another oxidative scission at the reaction conditions reported above.

Results are reported in Figure 6.72.; it is shown that the performance of the re-used catalyst was similar to that one of the “fresh” catalyst.

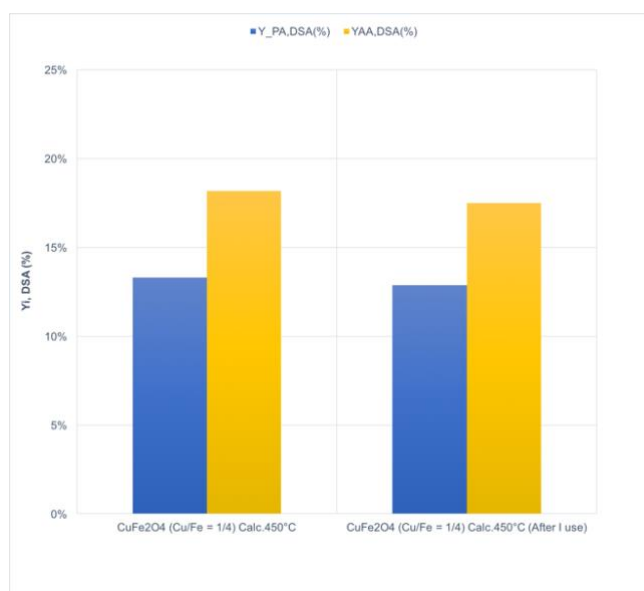


**Figure 6.72. Results in terms of yields of azelaic ac. (AA) and pelargonic ac.(PA) obtained in the oxidative cleavage of DSA using CuFeO14 (Calc. @450°C) and as such and after a regeneration step (calc. at 450 °C for 8 h).**

#### **6.4.2.8. Conclusions on the reactivity tests with copper ferrite with Cu/Fe ratio =1/4**

The Cu ferrite used for the oxidative cleavage of 9,10-dihydroxystearic acid into AA and PA showed performance similar to that one of the supported material used in the first part of this study; for example, the best performance was obtained at about 80-100 °C in 5 hours of reaction.

The main difference compared to supported CuO was obtained with reactivity tests by changing the pressure of the oxidant gas: the materials showed a very low activity at 30 bar of oxygen pressure. This phenomenon suggested a different catalytic mechanism compared to the supported materials that have to be further investigated.

This catalyst could be easily recovered by means of filtration and regenerated by calcination.

## 6.5. *Leaching experiments*

The catalyst tested in the oxidative cleavage of DSA were also used for some leaching tests.

These tests were important because it is necessary to check the stability of the catalyst under reaction conditions.

The catalytic tests were carried out as described in chapter 5.3.1.2 using the following conditions:

- 100 mL autoclave with magnetic drive and PTFE vessel;
- 15 g of starting material (dihydroxylated oil) and 0,15 g of catalyst (1%<sub>wt.</sub> of catalyst respect to the amount of s.m.);
- T = 80 °C;
- stirring rate = 500 rpm;
- P<sub>O2</sub> = 25 bar;
- reaction time = 5 h.

After the reaction, the catalyst was recovered by means of centrifugation (4500 rpm for 15 min) and the reaction mixture obtained was transferred into the autoclave in order to perform the reaction at the same conditions (as above), but in the absence of the solid catalyst.

The products obtained during the reactions with the catalyst and with the same reaction mixture after the successive reaction without catalyst, were analysed by means of GC-FID (after derivatization with BF<sub>3</sub>/MeOH, as described in chapter 5.3.2).

Any difference between the two reactions in terms of DSA conversion could be due to the active phase dissolved during the first reaction.

The results obtained for each catalyst tested in terms of DSA conversion are presented in the Figure 6.73:

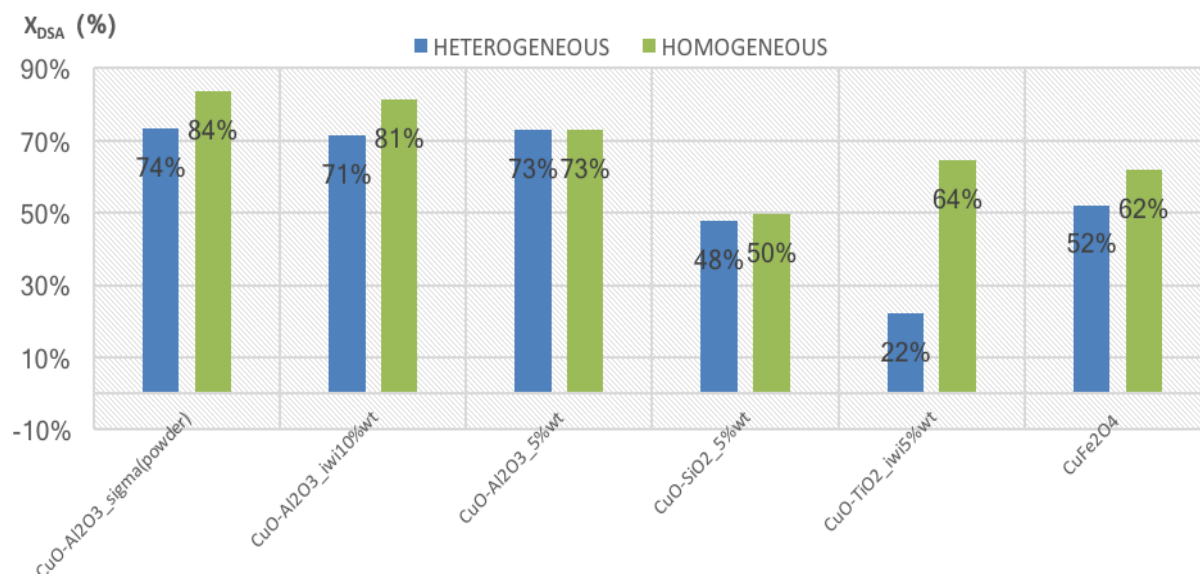


**Figure 6.73. Results obtained from the leaching tests of copper-based catalysts (HETEROGENEOUS: 1%<sub>wt.</sub> catalyst respect DSA, 80 °C for 5h, 25 bar O<sub>2</sub>, stirring rate 500 rpm; HOMOGENEOUS: reaction mixture obtained from “HETEROGENEOUS” without catalyst, 80 °C for 5h, 25 bar O<sub>2</sub>, stirring rate 500 rpm).**

For most of the catalysts tested there was no certainty that the slight differences in terms of DSA conversion were caused by the leached active phase. The only case where it was possible to observe a big difference between the “heterogeneous” and “homogeneous” conditions was with CuO over TiO<sub>2</sub> (CuO loading = 5 %<sub>wt.</sub>).

Figure 6.74 shows that, while the amount of certain compounds decreased (e.g. 9,10 – dihydroxystearic ac.) the amount of other species (for instance, azelaic and pelargonic acid) increased. This could be attributed to the catalytic effect of the active phase leached and still present in the reaction mixture.

Furthermore, the final reaction mixture resulting from the leaching tests with CuO/SiO<sub>2</sub> (CuO loading = 5%<sub>wt.</sub>) and CuO/TiO<sub>2</sub> (CuO loading = 5%<sub>wt.</sub>) were very dissimilar (see Figure 6.74): in the former case the mixture appeared to be limpid and clear compared to that one obtained with CuO/TiO<sub>2</sub>. This difference may be due to a considerable leaching of the Cu active phase from titania.



**Figure 6.74.** Final reaction mixture obtained from leaching test with (on the left)  $\text{CuO}/\text{SiO}_2$  (CuO loading = 5%wt.) and (on the right)  $\text{CuO}/\text{TiO}_2$  (CuO loading = 5%wt.).

Figure 6.75 shows another important difference; the brownish colour of the final reaction mixture using copper-ferrites as catalyst could be attributed to the solid particle held inside the oily phase. As far as the copper-supported catalysts are concerned, the leaching could be ascribed to a dissolution of copper inside the reaction mixture, probably due to its coordination with the carboxylic acid formed during the reaction. This is the reason of why the final reaction mixture appeared greenish also after filtration with the PTFE-filter (0,45  $\mu\text{m}$ ).

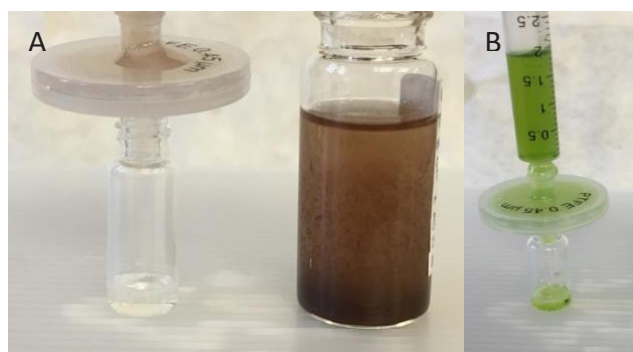


**Figure 6.75.** Final reaction mixture obtained from leaching test with (on the left)  $\text{CuO}/\text{SiO}_2$  (CuO loading = 5%wt.) and (on the right)  $\text{CuO}/\text{TiO}_2$  (CuO loading = 5%wt.).

Therefore, it is possible to conclude that cu-ferrites synthetized with co-precipitation method and CuO supported on alumina and silica and prepared by incipient wetness impregnation present a very good stability at the reaction conditions.



## 7. CONCLUSIONS

The three years of my PhD work described in the present thesis have been focused on the oxidative cleavage of vicinal glycols derived from unsaturated fatty acid using a sustainable oxidant (i.e. oxygen) in the presence of a heterogeneous catalyst.

At the very beginning of this research, several catalytic systems were synthesized (M-modified ferros spinels, supported gold nanoparticles, iron-substituted polyoxometalate), characterized (i.e. powder-X.R.D., N<sub>2</sub>-physisorption, D.L.S., A.T.R.-IR, etc.) and screened in the oxidative scission with oxygen as benign oxidant in order to identify an active phase alternative to the catalysts proposed in literature and industry.

These preliminary tests gave promising results which permitted us to focus the study on copper-based materials, also developing different systems by changing some aspects of the synthetic methodology.

From this research, it was possible to discover three efficient catalytic systems in terms of both efficiency and cost: copper oxide over alumina and silica, and Cu-modified ferros spinels. These catalysts were used for further tests in order to evaluate any possible effect of the reaction parameters on performance. Specifically, these materials were employed by changing the temperature, the time of reaction, the stirring rate, the catalyst amount and the oxidant pressure. Finally, the reusability (after a regeneration step consisting of calcination) and the stability of the materials (e.g. with leaching tests) were verified.

Different results were achieved with these systems suggesting significant differences in their chemical behaviour. Moreover, from catalytic tests it was possible to hypothesize a possible reaction network for the catalytic oxidative cleavage of 9,10-dihydroxystearic (Figure 7.1).

Concluding, after the large number of tests carried out during these years it was possible to obtain important results which could lead to a new heterogeneous process for oxidative cleavage. The work presented in this Thesis may represent a breakthrough in the sustainable production of valuable bio-chemicals starting from renewable feedstocks, such as vegetable oils.

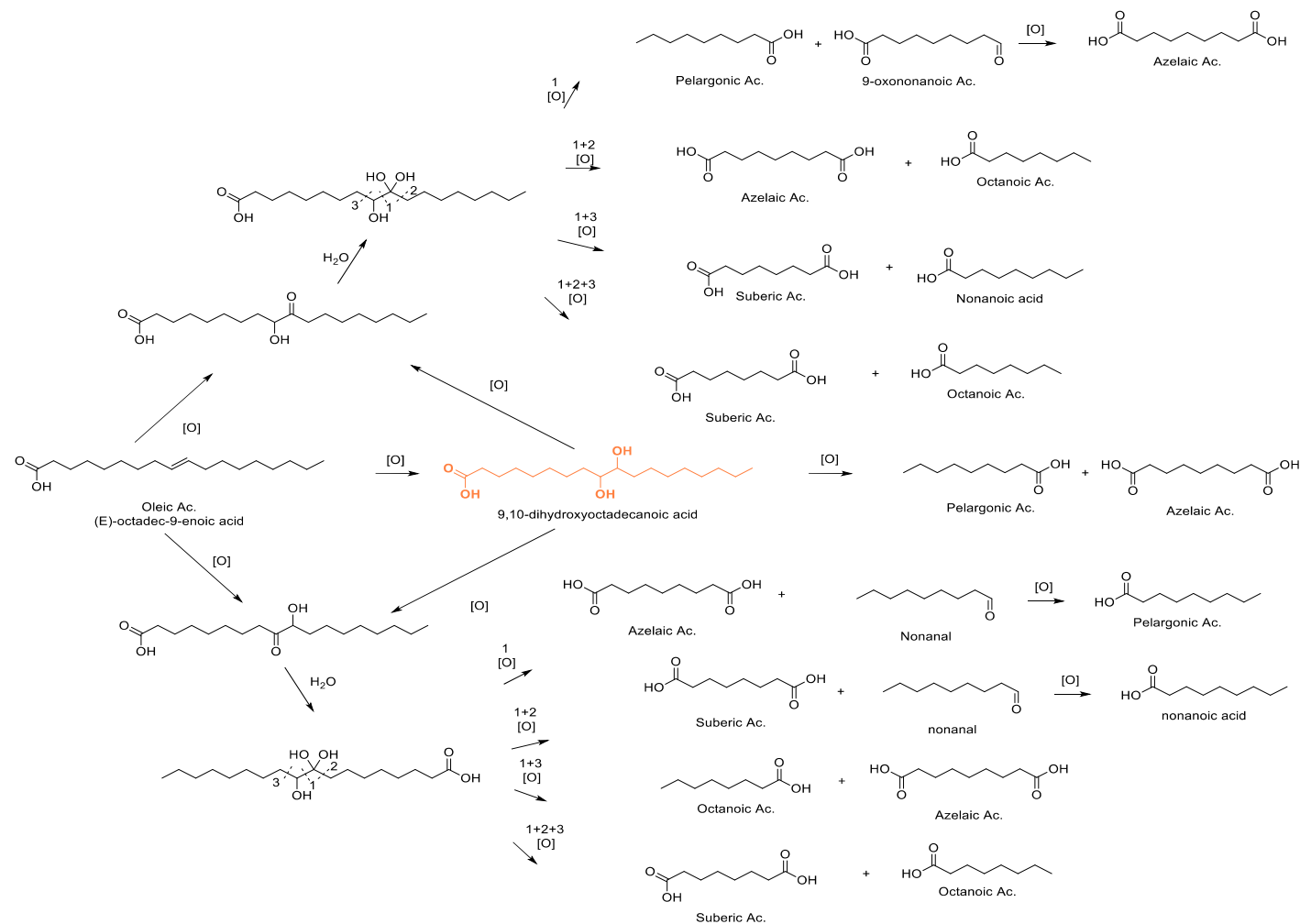


Figure 7.1. Possible reaction network of the oxidative cleavage of 9,10-dihydroxystearic acid advanced by the reactivity tests.

# Appendix I - Nomenclature

**AA:** azelaic acid;

**Cu/Fe/O:** copper and iron mixed oxide;

**DSA:** 9,10 – dihydroxystearic acid;

**FAME:** fatty acid methyl ester;

**FFA:** free fatty acid;

**FT-IR:** Fourier Transform Infra-Red spectroscopy analysis;

**GHG:** greenhouse gas;

**IWI:** incipient wetness impregnation;

**Mn/Fe/O:** manganese and iron mixed oxide;

**PA:** pelargonic acid;

**TGA:** thermogravimetric Analysis;

**UFA:** unsaturated fatty acid;

**X:** conversion;

**X.R.D.:** x-ray Diffraction analysis;

**Y:** yield;

# Appendix II - Fatty acids

## Saturated fat

Common Name	Systematic Name	Structural Formula	Lipid Numbers
<b>Propionic acid</b>	Propanoic acid	$\text{CH}_3\text{CH}_2\text{COOH}$	C3:0
<b>Butyric acid</b>	Butanoic acid	$\text{CH}_3(\text{CH}_2)_2\text{COOH}$	C4:0
<b>Valeric acid</b>	Pentanoic acid	$\text{CH}_3(\text{CH}_2)_3\text{COOH}$	C5:0
<b>Caproic acid</b>	Hexanoic acid	$\text{CH}_3(\text{CH}_2)_4\text{COOH}$	C6:0
<b>Enanthic acid</b>	Heptanoic acid	$\text{CH}_3(\text{CH}_2)_5\text{COOH}$	C7:0
<b>Caprylic acid</b>	Octanoic acid	$\text{CH}_3(\text{CH}_2)_6\text{COOH}$	C8:0
<b>Pelargonic acid</b>	Nonanoic acid	$\text{CH}_3(\text{CH}_2)_7\text{COOH}$	C9:0
<b>Capric acid</b>	Decanoic acid	$\text{CH}_3(\text{CH}_2)_8\text{COOH}$	C10:0
<b>Undecylic acid</b>	Undecanoic acid	$\text{CH}_3(\text{CH}_2)_9\text{COOH}$	C11:0
<b>Lauric acid</b>	Dodecanoic acid	$\text{CH}_3(\text{CH}_2)_{10}\text{COOH}$	C12:0
<b>Tridecylic acid</b>	Tridecanoic acid	$\text{CH}_3(\text{CH}_2)_{11}\text{COOH}$	C13:0
<b>Myristic acid</b>	Tetradecanoic acid	$\text{CH}_3(\text{CH}_2)_{12}\text{COOH}$	C14:0
<b>Pentadecylic acid</b>	Pentadecanoic acid	$\text{CH}_3(\text{CH}_2)_{13}\text{COOH}$	C15:0
<b>Palmitic acid</b>	Hexadecanoic acid	$\text{CH}_3(\text{CH}_2)_{14}\text{COOH}$	C16:0
<b>Margaric acid</b>	Heptadecanoic acid	$\text{CH}_3(\text{CH}_2)_{15}\text{COOH}$	C17:0
<b>Stearic acid</b>	Octadecanoic acid	$\text{CH}_3(\text{CH}_2)_{16}\text{COOH}$	C18:0
<b>Nonadecylic acid</b>	Nonadecanoic acid	$\text{CH}_3(\text{CH}_2)_{17}\text{COOH}$	C19:0
<b>Arachidic acid</b>	Eicosanoic acid	$\text{CH}_3(\text{CH}_2)_{18}\text{COOH}$	C20:0
<b>Heneicosylic acid</b>	Heneicosanoic acid	$\text{CH}_3(\text{CH}_2)_{19}\text{COOH}$	C21:0
<b>Behenic acid</b>	Docosanoic acid	$\text{CH}_3(\text{CH}_2)_{20}\text{COOH}$	C22:0
<b>Tricosylic acid</b>	Tricosanoic acid	$\text{CH}_3(\text{CH}_2)_{21}\text{COOH}$	C23:0
<b>Lignoceric acid</b>	Tetracosanoic acid	$\text{CH}_3(\text{CH}_2)_{22}\text{COOH}$	C24:0
<b>Pentacosylic acid</b>	Pentacosanoic acid	$\text{CH}_3(\text{CH}_2)_{23}\text{COOH}$	C25:0
<b>Cerotic acid</b>	Hexacosanoic acid	$\text{CH}_3(\text{CH}_2)_{24}\text{COOH}$	C26:0
<b>Heptacosylic acid</b>	Heptacosanoic acid	$\text{CH}_3(\text{CH}_2)_{25}\text{COOH}$	C27:0
<b>Montanic acid</b>	Octacosanoic acid	$\text{CH}_3(\text{CH}_2)_{26}\text{COOH}$	C28:0
<b>Nonacosylic acid</b>	Nonacosanoic acid	$\text{CH}_3(\text{CH}_2)_{27}\text{COOH}$	C29:0
<b>Melissic acid</b>	Triacontanoic acid	$\text{CH}_3(\text{CH}_2)_{28}\text{COOH}$	C30:0

<b>Henatriacontylic acid</b>	Henatriacontanoic acid	$\text{CH}_3(\text{CH}_2)_{29}\text{COOH}$	C31:0
<b>Lacceroic acid</b>	Dotriacontanoic acid	$\text{CH}_3(\text{CH}_2)_{30}\text{COOH}$	C32:0
<b>Psyllic acid</b>	Tritriacontanoic acid	$\text{CH}_3(\text{CH}_2)_{31}\text{COOH}$	C33:0
<b>Geddic acid</b>	Tettriacontanoic acid	$\text{CH}_3(\text{CH}_2)_{32}\text{COOH}$	C34:0
<b>Ceroplactic acid</b>	Pentatriacontanoic acid	$\text{CH}_3(\text{CH}_2)_{33}\text{COOH}$	C35:0
<b>Hexatriacontylic acid</b>	Hexatriacontanoic acid	$\text{CH}_3(\text{CH}_2)_{34}\text{COOH}$	C36:0
<b>Heptatriacontanoic acid</b>	Heptatriacontanoic acid	$\text{CH}_3(\text{CH}_2)_{35}\text{COOH}$	C37:0
<b>Octatriacontanoic acid</b>	Octatriacontanoic acid	$\text{CH}_3(\text{CH}_2)_{36}\text{COOH}$	C38:0

## Unsaturated fat

$\omega$ -n	Common Name	Lipid Numbers	$\Delta^n$	Structural Formula	Trans or Cis
$\omega$ -3	$\alpha$ -Linolenic acid	C18:3	$\Delta^{9,12,15}$	$\text{CH}_3\text{CH}_2\text{CH}=\text{CHCH}_2\text{CH}=\text{CHCH}_2\text{CH}=\text{CH}(\text{CH}_2)_7\text{COOH}$	cis
$\omega$ -3	Stearidonic acid	C18:4	$\Delta^{6,9,12,15}$	$\text{CH}_3\text{CH}_2\text{CH}=\text{CHCH}_2\text{CH}=\text{CHCH}_2\text{CH}=\text{CHCH}_2\text{CH}=\text{CH}(\text{CH}_2)_4\text{COOH}$	cis
$\omega$ -3	Eicosapentaenoic acid	C20:5	$\Delta^{5,8,11,14,17}$	$\text{CH}_3\text{CH}_2\text{CH}=\text{CHCH}_2\text{CH}=\text{CHCH}_2\text{CH}=\text{CHCH}_2\text{CH}=\text{CH}(\text{CH}_2)_3\text{COOH}$	cis
$\omega$ -3	Docosahexaenoic acid	C22:6	$\Delta^{4,7,10,13,16,19}$	$\text{CH}_3\text{CH}_2\text{CH}=\text{CHCH}_2\text{CH}=\text{CHCH}_2\text{CH}=\text{CHCH}_2\text{CH}=\text{CHCH}_2\text{CH}=\text{CH}(\text{CH}_2)_2\text{COOH}$	cis
$\omega$ -6	Linoleic acid	C18:2	$\Delta^{9,12}$	$\text{CH}_3(\text{CH}_2)_4\text{CH}=\text{CHCH}_2\text{CH}=\text{CH}(\text{CH}_2)_7\text{COOH}$	cis
$\omega$ -6	Linolelaidic acid	C18:2		$\text{CH}_3(\text{CH}_2)_4\text{CH}=\text{CHCH}_2\text{CH}=\text{CH}(\text{CH}_2)_7\text{COOH}$	trans
$\omega$ -6	$\gamma$ -Linolenic acid	C18:3	$\Delta^{6,9,12}$	$\text{CH}_3(\text{CH}_2)_4\text{CH}=\text{CHCH}_2\text{CH}=\text{CHCH}_2\text{CH}=\text{CH}(\text{CH}_2)_4\text{COOH}$	cis
$\omega$ -6	Dihomo- $\gamma$ -linolenic acid	C20:3	$\Delta^{8,11,14}$	$\text{CH}_3(\text{CH}_2)_4\text{CH}=\text{CHCH}_2\text{CH}=\text{CHCH}_2\text{CH}=\text{CH}(\text{CH}_2)_6\text{COOH}$	cis
$\omega$ -6	Arachidonic acid	C20:4	$\Delta^{5,8,11,14}$	$\text{CH}_3(\text{CH}_2)_4\text{CH}=\text{CHCH}_2\text{CH}=\text{CHCH}_2\text{CH}=\text{CHCH}_2\text{CH}=\text{CH}(\text{CH}_2)_3\text{COOH}$	cis
$\omega$ -6	Docosatetraenoic acid	C22:4	$\Delta^{7,10,13,16}$	$\text{CH}_3(\text{CH}_2)_4\text{CH}=\text{CHCH}_2\text{CH}=\text{CHCH}_2\text{CH}=\text{CHCH}_2\text{CH}=\text{CH}(\text{CH}_2)_5\text{COOH}$	cis
$\omega$ -7	Palmitoleic acid	C16:1	$\Delta^9$	$\text{CH}_3(\text{CH}_2)_5\text{CH}=\text{CH}(\text{CH}_2)_7\text{COOH}$	cis

$\omega$ -7	Vaccenic acid	C18:1	$\Delta^{11}$	$\text{CH}_3(\text{CH}_2)_5\text{CH}=\text{CH}(\text{CH}_2)_9\text{COOH}$	Trans
$\omega$ -7	Paullinic acid	C20:1	$\Delta^{13}$	$\text{CH}_3(\text{CH}_2)_5\text{CH}=\text{CH}(\text{CH}_2)_{11}\text{COOH}$	Cis
$\omega$ -9	Oleic acid	C18:1	$\Delta^9$	$\text{CH}_3(\text{CH}_2)_7\text{CH}=\text{CH}(\text{CH}_2)_7\text{COOH}$	Cis
$\omega$ -9	Elaidic acid	C18:1	$\Delta^9$	$\text{CH}_3(\text{CH}_2)_7\text{CH}=\text{CH}(\text{CH}_2)_7\text{COOH}$	Trans
$\omega$ -9	Gondoic acid	C20:1	$\Delta^{11}$	$\text{CH}_3(\text{CH}_2)_7\text{CH}=\text{CH}(\text{CH}_2)_9\text{COOH}$	Cis
$\omega$ -9	Erucic acid	C22:1	$\Delta^{13}$	$\text{CH}_3(\text{CH}_2)_7\text{CH}=\text{CH}(\text{CH}_2)_{11}\text{COOH}$	Cis
$\omega$ -9	Nervonic acid	C24:1	$\Delta^{15}$	$\text{CH}_3(\text{CH}_2)_7\text{CH}=\text{CH}(\text{CH}_2)_{13}\text{COOH}$	Cis
$\omega$ -9	Mead acid	C20:3	$\Delta^{5,8,11}$	$\text{CH}_3(\text{CH}_2)_7\text{CH}=\text{CHCH}_2\text{CH}=\text{CHCH}_2\text{CH}=\text{CH}(\text{CH}_2)_3\text{COOH}$	Cis

**Note:**  $\omega$ - $n$  and  $\Delta^n$  notation is commonly used for two different notations for the double bond's position:

- $\omega$ , is the last letter of the Greek alphabet and it is used to indicate the “last” carbon atom in the fatty acid chain;  $\omega$ - $n$  specifies the position of the unsaturation close to the final  $-\text{CH}_3$ . If there is more than one unsaturation, the double bond closer to the final carbon is the only one indicated.
- $\Delta^n$ , “ $\Delta$ ” is the Greek letter “delta”, which translates into “D” (as **D**ouble bond), specifies the double bonds’ position starting from the  $-\text{COOH}$  (or  $-\text{COOR}$ , for fatty esters) group. In the case of several unsaturation, all the double bonds present into the fatty acid are included specifying only the carbon closer to the carboxylic group.

The Greek letter presents at the beginning of the “common name”,  $\gamma$ -Linolenic acid for instance, represents a specific isomer of that acid.

Example:

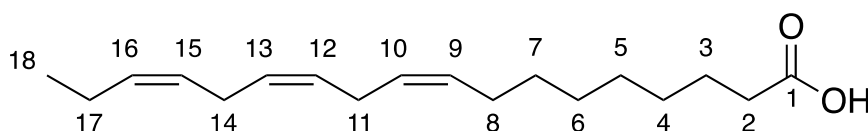


**Figure 7.2.  $\alpha$ -Linolenic acid**

$\omega$ - $n$  nomenclature:  $\omega$ -3

$\Delta^n$  nomenclature:  $\Delta^{9,12,15}$

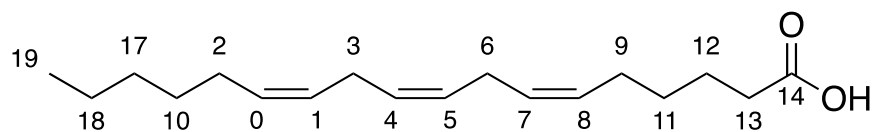


**Figure 7.3.  $\gamma$ -linolenic acid**

$\omega$ - $n$  nomenclature:  $\omega$ -6

$\Delta^n$  nomenclature:  $\Delta^{6,9,12}$

## 8. REFERENCES

---

- <sup>1</sup> Science Advances: <http://advances.sciencemag.org/content/3/7/e1700782>.
- <sup>2</sup> The Guardian: <https://www.theguardian.com/environment/2017/jun/28/a-million-a-minute-worlds-plastic-bottle-binge-as-dangerous-as-climate-change>
- <sup>3</sup> UNEP, Marine plastic debris and microplastics – Global lessons and research to inspire action and guide policy change. Nairobi, Kenya: United Nations Environment Programme, **2016**.
- <sup>4</sup> P. T. Anastas; J. C. Warner, Green Chemistry: Theory and Practice, Oxford University, **1998**, 30.
- <sup>5</sup> P. T. Anastas; M.M. Kirchhoff Acc. Chem. Res., **2002**, 35, 686.
- <sup>6</sup> <https://www.acs.org/content/acs/en/greenchemistry/principles/12-principles-of-green-chemistry.html>
- <sup>7</sup> P. T. Anastas, Green Chem., **2003**, 5, 29.
- <sup>8</sup> [http://unfccc.int/meetings/paris\\_nov\\_2015/items/9445.php](http://unfccc.int/meetings/paris_nov_2015/items/9445.php)
- <sup>9</sup> IEA Bioenergy Task 42 Biorefinery, **2009**. Brochure: [http://www.biorefinery.nl/fileadmin/biorefinery/docs/Brochure\\_Totaal\\_definitief\\_HR\\_opt.pdf](http://www.biorefinery.nl/fileadmin/biorefinery/docs/Brochure_Totaal_definitief_HR_opt.pdf)
- <sup>10</sup> P. Fornasiero, M. Graziani, Renewable Resources and Renewable Energy, CRC press, **2012**.
- <sup>11</sup> F. Cavani, S. Albonetti, F. Basile, A. Gandini, Chemicals and Fuels from Bio-based Building Blocks, Wiley-VCH, **2016**.
- <sup>12</sup> Kamm, B., Gruber, P.R., and Kamm, M., Biorefineries-Industrial Processes and Products: Status Quo and Future Directions, Wiley-VCH, **2010**.
- <sup>13</sup> R. Luque, Curr. Green Chem., **2015**, 2, 90.
- <sup>14</sup> S. Rama Mohan, Biores. Technol., **2016**, 215, 76.
- <sup>15</sup> J. C. Serrano-Ruiz, R. Luque, Chem. Soc. Rev., **2011**, 40, 5266.
- <sup>16</sup> S. G. Wettstein, D. M. Alonso, E. I. Gürbüz, J. A. Dumesic, Curr. Opt. Chem. Eng., **2012**, 1, 218.
- <sup>17</sup> K. Shimizu, A. Satsuma, Ener. Environ. Sci., **2011**, 4, 3140.
- <sup>18</sup> Haword, H.J., Chem. Rev., **1962**, 62, 99.
- <sup>19</sup> Salimon, J., Salih, N., and Yousif, E., Eur. J. Lipid Sci. Technol., **2010**, 112, 519.
- <sup>20</sup> Baranowsky, K., Beyer, W., Billek, G., Buchold, H., Gertz, C., Grothues, B., Sen Gupta, A.K., Holtmeier, W., Knuth, M., Lau, J., Mukherjee, K.W., Münch, E.-W., Saft, H., Schneider, Tiebach, R., Transfeld, P., Unterberg, C., Weber, K., and Zschau, W., Eur. J. Lipid Sci. Technol., **2001**, 103, 519.
- <sup>21</sup> Star colibri, Joint European Biorefinery Vision for 2030 Star-coliBri, **2011**, 1.
- <sup>22</sup> Kamm, B., Gruber, P.R., and Kamm, M. (eds), Biorefineries – Industrial Processes and Products, Wiley-VHC Verlag GmbH, Weinheim, **2005**.
- <sup>23</sup> F. Cavani, G. Centi, S. Perathoner and F. Trifirò, Sustainable Industrial Chemistry: Principles, Tools and Industrial Examples, Wiley-VCH, **2009**.
- <sup>24</sup> Centi, G., Lanzafame, P., and Perathoner, S., Chem. Soc. Rev., **2014**, 43, 7562.
- <sup>25</sup> Aresta, M., Dibenedetto, A., and Dumeignil, F., Biorefinery: From Biomass to Chemicals and Fuels, **2012**.



- <sup>26</sup> Matrica's website: <http://www.matrica.it/>
- <sup>27</sup> Baumann, H.; Bühler, M.; Fochem, H.; Hirsinger, F.; Zoebelein, H.; Falbe, J. Natural Fats and Oils—Renewable Raw Materials for the Chemical Industry. *Angew. Chemie Int. Ed. English* **1988**, 27, 41.
- <sup>28</sup> Baumann, H.; Bühler, M.; Fochem, H.; Hirsinger, F.; Zoebelein, H.; Falbe, J. Natural Fats and Oils—Renewable Raw Materials for the Chemical Industry. *Angew. Chemie Int. Ed. English* **1988**, 27, 41.
- <sup>29</sup> Lanzafame, P., Centi, G., and Perathoner, S., *Catal. Today*, **2014**, 234, 2.
- <sup>30</sup> Novamont's website: <https://www.novamont.com/>
- <sup>31</sup> Cavani, F., Albonetti, S., Basile, F., Gandini, A., Chemicals and Fuels from Bio-Based Building Blocks, **2016**.
- <sup>32</sup> Swern, D., *Bailey's Industrial Oil and Fat Products*, **1979**.
- <sup>33</sup> Martinenghi, G.B., *Tecnologia Chimica industriale di oli, grassi e derivati*, **1963**.
- <sup>34</sup> Zschau, W. Bleaching of Edible Fats and Oils. *Eur. J. Lipid Sci. Technol.* **2001**, 103, 505.
- <sup>35</sup> Oil World Monthly, ISTA Mielke GmbH, **2015**.
- <sup>36</sup> Mielke, T. Global Supply, Demand and Price Outlook for Vegetable Oils as Well as for Palm Oil. ISTA Mielke GmbH, OIL WORLD, Hambg. **2017**.
- <sup>37</sup> Malveda, M.P., Blagoev, M., and Funada, C., CEH Industry Overview. IHS Report 220.5000, **2015**.
- <sup>38</sup> Mielke, T. Global Supply, Demand and Price Outlook for Vegetable Oils as Well as for Palm Oil. ISTA Mielke GmbH, OIL WORLD, Hambg. **2017**.
- <sup>39</sup> Barnwal, B.K., and Sharma, M.P., *renewable Sustainable Energy Rev.*, **2005**, 9, 363.
- <sup>40</sup> Dyer, J.M. and Mullen, R.T., *Physiol. Plant.*, **2008**, 132, 11.
- <sup>41</sup> Carlsson, A.S., *Biochimie*, **2009**, 91, 665.
- <sup>42</sup> Salimon, J.; Salih, N.; Yousif, E. Biolubricants: Raw Materials, Chemical Modifications and Environmental Benefits. *Eur. J. Lipid Sci. Technol.* **2010**, 112, 519.
- <sup>43</sup> Meier, M. A. R.; Metzger, J. O.; Schubert, U. S. Plant Oil Renewable Resources as Green Alternatives in Polymer Science. *Chem. Soc. Rev.* **2007**, 36, 1788.
- <sup>44</sup> Hill, K. Fats and Oils as Oleochemical Raw Materials. *Pure Appl. Chem.* **2000**, 72, 1255.
- <sup>45</sup> Alam, M.; Akram, D.; Sharmin, E.; Zafar, F.; Ahmad, S. Vegetable Oil Based Eco-Friendly Coating Materials: A Review Article. *Arab. J. Chem.* **2014**, 7, 469.
- <sup>46</sup> Schneider, M. P. Plant-Oil-Based Lubricants and Hydraulic Fluids. *Journal of the Science of Food and Agriculture*, **2006**, 86, 1769.
- <sup>47</sup> Pagliaro, M.; Ciriminna, R.; Kimura, H.; Rossi, M.; Della Pina, C. From Glycerol to Value-Added Products. *Angewandte Chemie - International Edition*. **2007**, 46, 4434.
- <sup>48</sup> Yang, F.; Hanna, M. A.; Sun, R. Value-Added Uses for Crude Glycerol - A Byproduct of Biodiesel Production. *Biotechnology for Biofuels*, **2012**, 5, 13.
- <sup>49</sup> Malveda, M.P., Blagoev, M., and Funada, C., CEH Industry Overview. HIS Report, **2018**.
- <sup>50</sup> Harwood, H. J. Reactions of the Hydrocarbon Chain of Fatty Acids. *Chem. Rev.* **1962**, 62, 99.

- <sup>51</sup> Jie, M.; Pasha, M.; Syed-Rahmatullah, M. Fatty Acids, Fatty Acid Analogues and Their Derivatives. *Nat. Prod. Rep.* **1997**, 2, 163.
- <sup>52</sup> "Nuts, macadamia nuts, raw", website: <https://nutritiondata.self.com/facts/nut-and-seed-products/3123/2>
- <sup>53</sup> "Natural trans fats may be good for you", **2008**.
- <sup>54</sup> Villarreal-Lozoya, Jose E.; Lombardini, Leonardo; Cisneros-Zevallos, Luis, *Food Chemistry*, **2007**, 102, 1241.
- <sup>55</sup> Canola Council of Canada, **2008**.
- <sup>56</sup> Carvalho, Isabel Saraiva de, I. Miranda, and H. Pereira, *Industrial Crops and Products*, **2006**, 24, 75.
- <sup>57</sup> Fernández-Moya, V., Martínez-Force, E., Garces, R., *Agric. Food Chem*, **2005**, 53, 5326.
- <sup>58</sup> F. C. Palazzo & A. Tamburello, "Atti della Accademia Nazionale die Lincei", **1914**, 5, 352.
- <sup>59</sup> B. Breuer; T. Stuhlfauth; H. Fock; H. Huber, *Phytochemistry*, **1987**, 26, 1441.
- <sup>60</sup> R. Kleiman & G. Spencer, *J. of the American Oil Chemists' Society*, **1982**, 59, 29
- <sup>61</sup> Oil, peanut, salad or cooking: search for peanut oil on "Archived copy". Archived from the original on **2015**.
- <sup>62</sup> M. K. Nutter, E. E. Lockhart and R. S. Harris, *J. of the American Oil Chemists' Society*, **1943**, 20, 231.
- <sup>63</sup> "Olive Oil: Chemical Characteristics".
- <sup>64</sup> Beltran; Del Rio, C; Sánchez, S; Martínez, L; et al., "Influence of Harvest Date and Crop Yield on the Fatty Acid Composition of Virgin Olive Oils from Cv. Picual", **2004**.
- <sup>65</sup> Simopoulos, Artemis P., *Asia Pacific Journal of Clinical Nutrition*, **2002**, 11, S163.
- <sup>66</sup> <http://www.med.nyu.edu/content?ChunkIID=21587>
- <sup>67</sup> Flider, Frank J., *Lipid Technology*, **2013**, 25, 227.
- <sup>68</sup> Miner, C. S. and Dalton, N. N., Editors. *Glycerol*, American Chemical Society Monograph Series. Reinhold Publishing Company, New York. **1953**, 1.
- <sup>69</sup> A. Behr, J. Eilting, K. Irawadi, J. Lechinski and F. Lindner, *Green Chem.*, **2008**, 10, 13.
- <sup>70</sup> M. Ayoub and A. Z. Abdullah, *Renewable Sustainable Energy Rev.*, **2012**, 16, 2671.
- <sup>71</sup> J. J. Bozell and G. R. Petersen. *Green Chem.*, **2010**, 12, 539.
- <sup>72</sup> D. Cespi, F. Passarini and F. Cavani. *Green Chem.*, **2015**, 17, 343.
- <sup>73</sup> Meier, M. A. R.; Metzger, J. O.; Schubert, U. S. *Chem. Soc. Rev.*, **2007**, 36, 1788.
- <sup>74</sup> Nieschlag, H. J.; Rothfus, J. A.; Sohns, V. E.; Perkins, R. B. *Ind. Eng. Chem. Prod. Res. Dev.*, **1977**, 16, 101.
- <sup>75</sup> Hill, J. W.; McEwen, W. L. *Org. Synth.*, **1933**, 13, 4.
- <sup>76</sup> Ayorinde, F. O.; Osman, G.; Shepard, R. L.; Powers, F. T. *J. Am. Oil Chem. Soc.*, **1988**, 65, 1774
- <sup>77</sup> *Sustainable industrial processes*; Cavani, F., Ed.; Wiley-VCH: Weinheim, **2009**.
- <sup>78</sup> Cavani, F.; Teles, J. H. *ChemSusChem* **2009**, 2, 508.
- <sup>79</sup> Rothenberg, G. *Kirk-Othmer Encycl. Chem. Technol.* **2010**.
- <sup>80</sup> Suresh, A. K.; Sharma, M. M.; Sridhar, T., *Ind. Eng. Chem. Res.*, **2000**, 39, 3958.

- <sup>81</sup> Teles, J. H.; Hermans, I.; Franz, G.; Sheldon, R. A. In *Ullmann's Encyclopedia of Industrial Chemistry*; Wiley-VCH Verlag GmbH & Co. KGaA, Ed.; Wiley-VCH Verlag GmbH & Co. KGaA: Weinheim, Germany, **2015**, 1.
- <sup>82</sup> Cavani, F. J. *Chem. Technol. Biotechnol.*, **2010**, 85, 1175.
- <sup>83</sup> Wang, M.; Ma, J.; Liu, H.; Luo, N.; Zhao, Z.; and Wang, F., *ACS Catal.*, **2018**, 8, 2129.
- <sup>84</sup> Köckritz, A.; Martin, A. *Eur. J. Lipid Sci. Technol.*, **2011**, 113, 83.
- <sup>85</sup> Hoffmann-Ostenhof, O.; Cohn, W. E.; Braunstein, A. E.; Dixon, H. B. F.; Horecker, B. L.; Jakoby, W. B.; Karlson, P.; Klyne, W.; Liebecq, C.; Webb, E. C. *Eur. J. Biochem.*, **1977**, 79, 11.
- <sup>86</sup> Santacesaria, E.; Sorrentino, A.; Rainone, F.; Di Serio, M.; Speranza, F. *Ind. Eng. Chem. Res.*, **2000**, 39, 2766.
- <sup>87</sup> Spannring, P.; Bruijninx, P. C. A.; Weckhuysen, B. M.; Gebbink, R. J. M. K. *RSC Adv.* **2013**, 3, 6606.
- <sup>88</sup> Zimmermann, F. O.; Meux, E.; Mieloszynski, J. L.; Lecuire, J. M.; Oget, N. *Tetrahedron Lett.* **2005**, 46, 3201.
- <sup>89</sup> Rup, S.; Zimmermann, F.; Meux, E.; Schneider, M.; Sindt, M.; Oget, N. *Ultrason. Sonochem.*, **2009**, 16, 266.
- <sup>90</sup> Rup, S.; Sindt, M.; Oget, N. *Tetrahedron Lett.*, **2010**, 51, 3123.
- <sup>91</sup> Turnwald, S. E.; Lorier, M. A.; Wright, L. J.; Mucalo, M. R. J. *Mater. Sci. Lett.*, **1998**, 17, 1305.
- <sup>92</sup> Spannring, P.; Prat, I.; Costas, M.; Lutz, M.; Bruijninx, P. C. A.; Weckhuysen, B. M.; Gebbink, R. J. M. K. *Catal. Sci. Technol.*, **2014**, 4, 708.
- <sup>93</sup> Santacesaria, E.; Sorrentino, A.; Rainone, F.; Di Serio, M.; Speranza, F. *Ind. Eng. Chem. Res.*, **2000**, 39, 2766.
- <sup>94</sup> Behr, A.; Tenhumberg, N.; Wintzer, A. *RSC Adv.*, **2013**, 3, 172.
- <sup>95</sup> Oakley, M. A.; Woodward, S.; Coupland, K.; Parker, D.; Temple-Heald, C. J. *Mol. Catal. A: Chem.*, **1999**, 150, 105.
- <sup>96</sup> Turnwald, S. E.; Lorier, M. A.; Wright, L. J.; Mucalo, M. R. J. *Mater. Sci. Lett.*, **1998**, 17, 1305.
- <sup>97</sup> Pai, Z. P.; Tolstikov, A. G.; Berdnikova, P. V.; Kustova, G. N.; Khlebnikova, T. B.; Selivanova, N. V.; Shangina, A. B.; Kostrovskii, V. G. *Russ. Chem. Bull.*, **2005**, 54, 1847.
- <sup>98</sup> Antonelli, E.; D'Aloisio, R.; Gambaro, M.; Fiorani, T.; Venturello, C. J. *Org. Chem.*, **1998**, 63, 7190.
- <sup>99</sup> Godard, A.; De Caro, P.; Thiebaud-Roux, S.; Vedrenne, E.; Mouloungui, Z. J. *Am. Oil Chem. Soc.*, **2013**, 90, 133.
- <sup>100</sup> Nouredini, H.; Kanabur, M. J. *Am. Oil Chem. Soc.*, **1999**, 76, 305.
- <sup>101</sup> Ello, A. S.; Enferadi-kerenkan, A.; Trokourey, A.; Do, T.-O., J. *Am. Oil Chem. Soc.*, **2017**, 94, 1451.
- <sup>102</sup> Dapurkar, S. E.; Kawanami, H.; Yokoyama, T.; Ikushima, Y., *Top. Catal.*, **2009**, 52, 707.
- <sup>103</sup> Köckritz, A.; Blumenstein, M.; Martin, A. *Eur. J. Lipid Sci. Technol.*, **2010**, 112, 58.
- <sup>104</sup> Fujitani, K.; Manami, H.; Nakazawa, M.; Oida, T.; Kawase, T. J. *Oleo Sci.*, **2009**, 58, 629.
- <sup>105</sup> Travis, B. R.; Narayan, R. S.; Borhan, B. J. *Am. Chem. Soc.*, **2002**, 124, 3824.

- <sup>106</sup> Spannring, P.; Bruijninx, P. C. A.; Weckhuysen, B. M.; Gebbink, R. J. M. K. *RSC Adv.*, **2013**, 3, 6606.
- <sup>107</sup> Behr, A.; Tenhumberg, N.; Wintzer, A., *Eur. J. Lipid Sci. Technol.*, **2012**, 114, 905.
- <sup>108</sup> Pai, Z. P.; Tolstikov, A. G.; Berdnikova, P. V.; Kustova, G. N.; Khlebnikova, T. B.; Selivanova, N. V.; Shangina, A. B.; Kostrovskii, V. G. *Russ. Chem. Bull.*, **2005**, 54, 1847.
- <sup>109</sup> Oakley, M. A.; Woodward, S.; Coupland, K.; Parker, D.; Temple-Heald, C. J. *Mol. Catal. A: Chem.*, **1999**, 150, 105.
- <sup>110</sup> Kulik, A.; Janz, A.; Pohl, M.-M.; Martin, A.; Köckritz, A. *Eur. J. Lipid Sci. Technol.*, **2012**, 114, 1327.
- <sup>111</sup> Fujitani, K.; Manami, H.; Nakazawa, M.; Oida, T.; Kawase, T. *J. Oleo Sci.*, **2009**, 58, 629
- <sup>112</sup> Oakley, M. A.; Woodward, S.; Coupland, K.; Parker, D.; Temple-Heald, C. J. *Mol. Catal. A: Chem.*, **1999**, 150, 105.
- <sup>113</sup> Khlebnikova, T. B.; Pai, Z. P.; Fedoseeva, L. A.; Mattsat, Y. V. *React. Kinet. Catal. Lett.*, **2009**, 98, 9.
- <sup>114</sup> Criegee, R. *Angew. Chem., Int. Ed. Engl.*, **1975**, 14, 745.
- <sup>115</sup> Goebel, C. G. U.S. Patent No. US2813113A, **1957**.
- <sup>116</sup> Carlson, K. D.; Sohns, V. E.; Perkins, R. B.; Huffman, E. L. *Ind.Eng. Chem. Prod. Res. Dev.*, **1977**, 16, 95.
- <sup>117</sup> Sawut, A., Eli, W., Nurulla, I.,Jingxi Shiyou Huagong, **2009**, 26, 43.
- <sup>118</sup> Monson, K. D.; Hayes, J. M. *Geochim. Cosmochim. Acta*, **1982**, 46, 139.
- <sup>119</sup> Borka, L.; Privett, O. S. *J. Am. Oil Chem. Soc.*, **1965**, 42, 1070.
- <sup>120</sup> Witthaus, M.; Heins, A.; Carduck, F. J.; Majmudar, S. *Fette Seifen Anstrichmittel* **1984**, 86, 424.
- <sup>121</sup> Ackman, R. G.; Retson, M. E.; Gallay, L. R.; Vandenheuvel, F. A. *Can. J. Chem.*, **1961**, 39, 1956.
- <sup>122</sup> Castell, J. D.; Ackman, R. G. *Can. J. Chem.* **1967**, 45, 1405.
- <sup>123</sup> Kadhum, A. A. H.; Wasmi, B. A.; Mohamad, A.; Al-Amiery, A. A.; Takriff, M. S. *Res. Chem. Intermed.*, **2012**, 38, 659.
- <sup>124</sup> Hung, H.-M.; Ariya, P. J. *Phys. Chem. A.*, **2007**, 111, 620.
- <sup>125</sup> Izumi, G., Preparation of azelaic acid from oleic acid by ozonization in glacial acetic acid. *Kogyo Kagaku Zasshi*, **1958**, 61, 1475.
- <sup>126</sup> Shi, C., Yan, Y., Yin, W., Study on synthesis and reaction mechanism of azelaic acid by united oxidation. *Huagong Keji*, **2009**, 17, 16.
- <sup>127</sup> Sun, Z.-C., Zhang, Y.-G., Eli, W., Hu, S.-M., Gao, J.-J., Production of azelaic acid by the compound solvent-ozonization-catalytic oxidation process from oleic acid. *Zhongguo Youzhi*, **2006**, 31, 40.
- <sup>128</sup> Sun, Z.-C., Wumanjiang, E., Xu, T.-Y., Zhang, Y.-G., Catalysts for oxidation of the ozonolysis product of oleic acid with oxygen to make azelaic acid. *Yingyong Huaxue*, **2006**, 23, 161.
- <sup>129</sup> Li, Y., Song, Z., Preparation of azelaic acid from ozonolysis of oleic acid. *Jingxi Shiyou Huagong*, **2003**, 37.
- <sup>130</sup> Chen, Y., Cao, S.-G., Synthesis of azelaic acid by oxidative ozonolysis using microwave. *Fujian Shifan Daxue Xuebao, Ziran Kexueban*, **2008**, 24, 58.
- <sup>131</sup> Ackman, R. G., Retson, M. E., Gallay, L. R., Vandenheuvel, F. A., *Can. J. Chem.*, **1961**, 39, 1956.
- <sup>132</sup> Ayorinde, F. O.; Osman, G.; Shepard, R. L.; Powers, F. T. *J. Am.Oil Chem. Soc.*, **1988**, 65, 1774.

- <sup>133</sup> Garti, N., Avni, E., Coll. Surf., **1982**, *4*, 33.
- <sup>134</sup> Gao, Z., Catalytic oxidation of oleic acid. Huagong Shikan, **2000**, *14*, 26.
- <sup>135</sup> Kobayashi, T., Miyazaki, S., , Tokyo Kogyo Shikensho Hokoku, **1954**, *49*, 73.
- <sup>136</sup> Kobayashi, T., Miyazaki, S., Tokyo Kogyo Shikensho Hokoku, **1954**, *49*, 78.
- <sup>137</sup> Ansell, M. F., Shepherd, I. S., Weedon, B. C. L., J. Chem. Soc. C, **1971**, 1840.
- <sup>138</sup> Mallat, T.; Baiker, A. Chem. Rev., **2004**, *104*, 3037.
- <sup>139</sup> Murahashi, S.-I.; Imada, Y. In, Transition Metals for Organic Synthesis: Building Blocks and Fine Chemicals, Second Revised and Enlarged Edition; Beller, M.; Bolm, C., Eds.; Wiley-VCH Verlag GmbH: Weinheim, **2008**, *2.15*, 497.
- <sup>140</sup> Punniyamurthy, T.; Velusamy, S.; Iqbal, J. Chem. Rev., **2005**, *105*, 2329.
- <sup>141</sup> Taube, Henry, The Journal of general physiology, **1965**, *49.1*, 29.
- <sup>142</sup> Swern, D.; Knight, H. B.; Scanlan, J. T.; Ault, W. C. J. Am. Chem.Soc., **1945**, *67*, 1132.
- <sup>143</sup> Satyarthi, J. K.; Srinivas, D. Appl. Catal., A, **2011**, *401*, 189.
- <sup>144</sup> Cecchini, M. M.; De Angelis, F.; Iacobucci, C.; Reale, S.; Crucianelli, M. Appl. Catal. A, **2016**, *517*, 120.
- <sup>145</sup> Tiozzo, C.; Bisio, C.; Carniato, F.; Marchese, L.; Gallo, A.; Ravasio, N.; Psaro, R.; Guidotti, M. Eur. J. Lipid Sci. Technol., **2013**, *115*, 86.
- <sup>146</sup> Santacesaria, E.; Sorrentino, A.; Rainone, F.; Di Serio, M.; Speranza, F. Ind. Eng. Chem. Res., **2000**, *39*, 2766.
- <sup>147</sup> Santacesaria, E.; Ambrosio, M.; Sorrentino, A.; Tesser, R.; Di Serio, M. Catal. Today, **2003**, *79*, 59.
- <sup>148</sup> Kulik, A.; Martin, A.; Pohl, M.-M.; Fischer, C.; Kockritz, A. Green Chem., **2014**, *16*, 1799.
- <sup>149</sup> Laszlo, P.; Levart, M. Tetrahedron Lett., **1993**, *34*, 1127.
- <sup>150</sup> Dell'Anna, M. M.; Mastorilli, P.; Nobile, C. F. J. Mol. Catal. A: Chem., **1998**, *130*, 65.
- <sup>151</sup> Marteau, C.; Ruyffelaere, F.; Aubry, J. M.; Penverne, C.; Favier, D.; Nardello-Rataj, V. Tetrahedron, **2013**, *69*, 2268.
- <sup>152</sup> Kockritz, A.; Blumenstein, M.; Martin, A. Eur. J. Lipid Sci. Technol., **2008**, *110*, 581.
- <sup>153</sup> Warwel, S.; Sojka, M.; Klaas, M. R. G. Top. Curr. Chem., **1993**, *164*, 79.
- <sup>154</sup> Sato, M., Sasaki, Y., Komatsu, M., Japanese Patent 2009155320, **2009**.
- <sup>155</sup> R.Padilla, M.Benito, L. Rodriguez, A.Serrano, G. Munoz, L. Daza, *Int. j.l of Hydrogen energy*, **2010**, *35*, 8921.
- <sup>156</sup> Ballarini, N.; Cavani, F.; Passeri, S.; Pesaresi, L.; Lee, A. F.; Wilson, K., *Applied Catalysis A: General* **2009**, *366*, 184.
- <sup>157</sup> U. Muller, Inorganic structural chemistry, Wiley, **2001**, *2*, 40.
- <sup>158</sup> Hosterman, Brian D. "Raman spectroscopic study of solid solution spinel oxides." **2011**.
- <sup>159</sup> M. E. Melinda Darby Dyar and Gunter, Mineralogy and Optical Mineralogy, Mineralogical Society of America, **2008**.

- <sup>160</sup> M. Blosi, S. Albonetti, M. Dondi, G. Bardi, A. Barzanri, T. Pasini, M. Piccinini, M. Blosi, R. Bonelli, S. Albonetti, N. Dimitratos, J.A. Lopez-Sanchez, M. Sankar, Q. He, C.J. Kiely, G.J. Hutchings, F. Cavani, *Green Chem.*, **2011**, 13, 2091.
- <sup>161</sup> M. Ammam, *J. Mater. Chem.*, **2013**, A1, 6291.
- <sup>162</sup> V.F. Odyakov, E.G. Zhizhina, R.I. Maksimovskaya, K.I. Matveev, *Kinet. Catal.*, **1995**, 36, 733.
- <sup>163</sup> K. Oberlander, *Applied Industrial Catalysis* (Ed.: B. E. Leach), Academic Press, New York, **1984**, 63.
- <sup>164</sup> K. Wefers, *Alumina Chemicals: Science and Technology Hand-book* (Ed.: L. D. Hart), The American Ceramic Society, **1990**, 13.
- <sup>165</sup> Konstantin I. Hadjiivanov, Dimitar G. Klissurski, *Chem. Soc. Rev.*, **1996**, 25, 61.
- <sup>166</sup> S Matsuda and A Kato, *Appl Catal*, **1983**, 8, 149.
- <sup>167</sup> T. Bunluesin, E. S. Putna, R. J. Gorte, *Catal. Lett.*, **1996**, 41, 1.
- <sup>168</sup> M Campanati, G Fornasari, A Vaccari, *Catalysis Today*, **2003**, 77, 299.
- <sup>169</sup> W. L. Bragg, "The Diffraction of Short Electromagnetic Waves by a Crystal," *Proc. Camb. Philol. Soc.*, **1913**, 17, 43.
- <sup>170</sup> Cavani, F., *Sustainable industrial processes*; Ed.; Wiley-VCH: Weinheim, **2009**.
- <sup>171</sup> C.G Ramankutty, S Sugunan, Bejoy Thomas, *Journal of Molecular Catalysis A: Chemical*, **2002**, 187, 105.
- <sup>172</sup> YOUSEFI, M.; KAMEL ATTAR KAR, M. H.; KAMEL ATTAR KAR, M., *Main Group Chemistry*, **2013**, 12, 177.
- <sup>173</sup> Neațu F., Marin R.S., Florea M., Petrea N., Pavel O.D., Pârvulescu, *Applied Catalysis B*, **2016**, 180, 751.
- <sup>174</sup> Dugal, M., Sankar, G., Raja, R., & Thomas, J. M., *Angewandte Chemie International Edition*, **2000**, 39, 2310.
- <sup>175</sup> Solmi, S., Rozhko, E., Malmusi, A., Tabanelli, T., Albonetti, S., Basile, F., Cavani, F., *Applied Catalysis A: General*, **2018**, 557, 89.
- <sup>176</sup> Cavani, F., *Catalysis Today*, **1998**, 41, 73.
- <sup>177</sup> I. Weinstock, *Chem. Rev.*, **1998**, 98, 289.
- <sup>178</sup> El Ali, J.-M. Bregeault, J. Martin, C. Martin, *New J. Chem.*, **1989**, 13, 173.
- <sup>179</sup> A. Atlamsani, J.-M. Bregeault, M. Ziyad, *J. Org. Chem.*, **1993**, 58, 5663.
- <sup>180</sup> L. El Aakel, F. Launay, A. Atlamsani, J.-M. Bregeault, *Chem. Commun.*, **2001**, 21, 2218.
- <sup>181</sup> J.-M. Brégeault, *Dalton Trans.*, **2003**, 3289.
- <sup>182</sup> Larsson, Per-Olof, and Arne Andersson., *Journal of Catalysis*, **1998**, 179, 72.
- <sup>183</sup> S. Cocchi, M. Mari, F. Cavani, and J.-M. M. Millet, *Appl. Catal. B Environ.*, **2014**, 152, 250.
- <sup>184</sup> S. Cocchi, "A chemical loop approach for methanol reforming," *Università di Bologna*, **2012**.
- <sup>185</sup> RRUFFTM," University of Arizona. [Online]. Available: <http://rruff.info/magnetite/display=default/R061111>.
- <sup>186</sup> G.B. McGarvey, J.B. Moffat, *Journal of Molecular Catalysis*, **1991**, 69, 137.



- 
- <sup>187</sup> K. Nowinska, A. Wacław, W. Masierak, A. Gutsze, *Catalysis Letters*, **2004**, 92, 157.
- <sup>188</sup> K.M. Parida, D. Rath, *J. of M. Catalysis A: Chemical*, **2006**, 258, 381.
- <sup>189</sup> Surjakanta Rana, Sujata Mallick, Lagnamayee Mohapatra, G. Bishwa Bidita Varadwaj, K.M. Parida, *Catalysis Today*, **2012**, 198, 52.
- <sup>190</sup> Takayuki Tsukada, Hideo Segawa, Atsuo Yasumori and Kiyoshi Okada *J. Mater. Chem.*, **1999**, 9, 549.
- <sup>191</sup> G. C. Bond, S. N. Namijo and J. S. Wakeman, *J. Mol. Catal.*, **1991**, 64, 305.
- <sup>192</sup> G. S. Jeon and J. S. Chung, *Appl. Catal.*, **1994**, 115, 29.
- <sup>193</sup> F.-H. Chang, W.-Y. Kuo and K.-C. Lee, *Appl. Catal., A*, **2003**, 246, 253.
- <sup>194</sup> Anna Kulik, Andreas Martin, Marga-Martina Pohl, Christine Fischera and Angela Köckritz, *Green Chem.*, **2014**, 16, 1799.
- <sup>195</sup> S. Kameoka, T. Tanabe, and A. P. Tsai, *Appl. Catal. A Gen.*, **2010**, 375, 163.
- <sup>196</sup> X. Tan, G. Li, Y. Zhao, and C. Hu, *J. Alloys Compd.*, **2010**, 493, 55.
- <sup>197</sup> W. Ramadan, M. I. Zaki, N. E. Fouad, and G. A. H. Mekhemer, *J. Magn. Mater.*, **2014**, 355, 246.